

THE UNIVERSITY OF HULL

Ensemble-characterisation of Satellite Rainfall Uncertainty and its Impacts
on the Hydrological Modelling of a Sparsely Gauged Basin in Western
Africa

being a Thesis submitted for the Degree of Doctor of Philosophy

in the University of Hull

by

Christopher James Skinner MPhys Geog

March 2013

Declaration

I confirm that this is my own work and the use of all material from other sources has been properly and fully acknowledged.

Christopher James Skinner

Acknowledgements

My first thank you, of course, goes to my supervisor, Tim Bellerby; I can only aspire to your intelligence and I am grateful for the many patient hours of support, guidance and assistance, without which I would have been lost. Thank you also to David Grimes, whose inspiration and many years of work provided the foundations on which this research is built on – David's feedback on this thesis was sorely missed. Thank you to those who have also offered guidance throughout this thesis – Graham, Dave and Tom.

A thank you to the TAMSAT team at the University of Reading, whose work informed this thesis. A special thank you to Helen Greatrex for her support and assistance – thank you for answering all my emails!

A thank you to Alison Hook for finding the advert for the studentship, and making me promise to mention you in the acknowledgements when I wrote them. Thank you to Thorwald Stein for guidance with the application, and the sofa to sleep on when I was visiting Reading.

It has been a privilege to be a part of the Department of Geography, Environment and Earth Sciences, University of Hull. Thank you to all of those who have made my time thoroughly enjoyable – Karen, Tim, Carl, Baoli, Michelle, Steve, Joe, Chris, Leiping, Jordan, Sarah, Lucy, Sally, plus the many other participants of 'Pub Wednesday' over the years.

Thank you to my church family at Hull Vineyard, especially Jeremy and Elaine, and the members of my small group, whose love, prayers and encouragement have been invaluable. Thank you to my family for their love and support, and for given me plenty of excuses to meet you at Krispie Kreme. Finally, a huge thank you and much love to my amazing wife, Amy. Thank you for being you, for being my rock through my PhD, encouraging me, proof reading and bringing me crisps and liquorice.

Abstract

Many areas of the planet lack the infrastructure required to make accurate and timely estimations of rainfall. This problem is especially acute in sub-Saharan Africa, where a paucity of rain recording radar and sufficiently dense raingauge networks combine with highly variable rainfall, a reliance on agriculture that is predominantly rain fed and systems that are prone to flooding and drought. Satellite Rainfall Estimates (SRFE) are useful as they can provide additional spatial and temporal information to drive various downstream environmental models and early warning systems (EWS). However, when operating at higher spatial and temporal resolutions SRFE contain large uncertainties which propagate through the downstream models.

This thesis uses the TAMSAT1 SRFE algorithm developed by Teo (2006) to estimate the rainfall over a large, data sparse and heterogenous catchment in the Senegal Basin. The uncertainty within the TAMSAT1 SRFE is represented using a set of ensemble estimates, each unique but equiprobable based on the full conditional distribution of the recorded rainfall, produced using the TAMSIM algorithm, also developed by Teo (2006). The ensemble rainfall estimates were then used in turn to drive a Pitman Rainfall-Runoff model of the catchment hydrology.

The use of ensemble rainfall estimates was shown to be incompatible with the pre-calibrated parameter values for the hydrological model. A novel approach, the EnsAll method, was developed to calibrate the hydrological model which incorporated each individual ensemble member. The EnsAll calibrated model

showed the greatest skill when driven by the ensemble rainfall estimates and little bias. A comparison of the hydrographs produced from TAMSIM ensemble rainfall estimates and that from an ensemble of perturbed TAMSAT1 estimates showed that the full spatio-temporally distributed method used by TAMSIM is superior to a simpler perturbation method for characterizing SRFE uncertainty.

Overall, the SRFE used were shown to outperform the rainfall estimates produced from the sparse raingauge network as a hydrological model driver. However, they did demonstrate a lack of ability to represent the large interseasonal variations in rainfall resulting in large systematic biases. These biases were observed propagating directly to the modelled hydrological output.

Contents

	Chapter 1 - Introduction	1
1.1	Satellite Rainfall Estimation and Hydrological Modelling	1
1.2	Using Satellites to Estimate Rainfall in Africa	9
1.3	Thesis Aims	11
1.4	Experimental Process and Thesis Plan	12
	Chapter 2 - Satellite Rainfall Applications in Hydrological Modelling	18
2.1	Introduction	18
2.2	Dealing with Input Uncertainty in Hydrological Models	18
2.3	Satellite Rainfall Estimation	24
2.4	Satellite Rainfall Uncertainty Characterisation	31
2.5	Hydrological Modelling and Calibration	37
2.6	Summary	49
	Chapter 3 - Study Area and Context	51
3.1	Introduction	51
3.2	The Problem in Context	52
3.3	Description of the Study Area	67
3.4	Previous Studies Relating to the Bakoye Catchment	82
3.5	Available Data	86
3.6	Summary	103
	Chapter 4 - Methodology - Spatial Interpolation	105
4.1	Introduction	105
4.2	Spatial Interpolation and the Double Kriging (DK) Method	105
4.3	Implementation of the DK Method	111
4.3.1	Introduction	111
4.3.2	Calibration	112
4.3.3	Validation	119
4.4	Summary	129
	Chapter 5 - Methodology - Ensemble Representation of Satellite Rainfall Uncertainty	131
5.1	Introduction	131
5.2	TAMSAT1	131
5.3	TAMSIM	136
5.4	Implementation	141
5.4.1	Introduction	141
5.4.2	Calibration	142

5.4.3	Validation of the TAMSAT1 SRFE	148
5.4.4	Implementation of TAMSIM	152
5.5	Summary	155
Chapter 6 - Methodology - Hydrological Modelling		156
6.1	Introduction	156
6.2	The Pitman Model	156
6.3	The Shuffled Complex Evolution method implemented at the University of Arizona (SCE-UA)	160
6.4	Calibration of the Pitman Model using SCE-UA	166
6.5	Summary	170
Chapter 7 - Validation of the Ensemble Representation of the Daily Senegal Basin Rain Field		171
7.1	Introduction	171
7.2	Daily Senegal Basin Rain Field	172
7.3	Influence of Uncertainty on the Estimates	187
7.4	Conclusions	198
Chapter 8 - The Influence of SRFE Uncertainty on Hydrological Model Output		202
8.1	Introduction	202
8.2	Ensemble Parameterisation of the Pitman Model	204
8.3	The Propagation of Input Uncertainty through the Pitman Model	208
8.4	Comparison with a Perturbation Method	227
8.5	Conclusions	239
Chapter 9 - The Influence of Ensemble Rainfall Input on the Calibration of the Pitman Model		243
9.1	Introduction	243
9.2	Pitman Model Behaviours	244
9.3	Variability of Parameter Values for an Ensemble Driven Pitman Model	250
9.4	Conclusions	278
Chapter 10 - Discussions		281
10.1	Key Results	281
10.2	Issues and Recommendations	286
Chapter 11 - Conclusions		300
Bibliography		304

1

Introduction

1.1 - Satellite Rainfall Estimation and Hydrological Modelling

Rainfall estimation is most accurately and timely performed using ground instrumentation - such as raingauges or radar – however, in many areas of the planet – such as sub-Saharan Africa – large regions are covered only by sparse raingauge networks and often with no rain recording radar. Satellite Rainfall Estimates (SRFE) offer a substitute for the ground instrumentation, able to estimate rainfall at a high spatial and temporal resolution at real-time or near real-time, but these estimates contain high uncertainties that need to be measured and characterised. The use of ensemble estimates of rainfall provides a useful method of representing the uncertainty in the SRFE which can then be used as a direct input for downstream applications, such as crop yield or hydrological models. When using a deterministic hydrological model, driven by an ensemble input, an appropriate calibration of the parameters needs to be established.

Gebremichael and Hossain (2010) described how the terms “satellite rainfall” and “surface hydrology” have been well established over decades of research, yet the combination of the two, which was termed “satellite rainfall applications

for surface hydrology”, was a relatively new topic. Although Gebremichael and Hossain (2010) acknowledged that SRFE have been used to drive models representing surface hydrology processes, the two fields have only marginally intersected during their development.

The connection of the two fields and the development of the new topic led Gebremichael and Hossain (2010) to propose a series of questions pertinent to this new discipline:

1. Which SRFE is best for a specific application?
2. What is the optimum SRFE resolution for a specific application?
3. How much uncertainty is there within the SRFE and how does this propagate to the surface hydrology application?
4. Where can data be acquired for research and operational applications?
5. How are SRFE developed and how do they vary from one another?

While each of the five questions posed are important to this field, the focus of this thesis is an attempt to address the third question: the issue of quantifying SRFE uncertainty and the impact it has on modelling the hydrology of a river basin.

SRFE contain significant uncertainties, principally because they rely upon an indirect relationship between rainfall and the data recorded by the satellite, most often thermal infrared imagery of cloud top temperature, or microwave back scatter. This leads to three main uncertainties in any SRFE:

1. When it is raining
2. Where it is raining
3. How much it is raining – i.e., the rain rate

The full extent and implications of SRFE uncertainty are discussed in Chapters 2 and 3, but the Tropical Applications of Meteorology using SATellites (TAMSAT) method provides an example of how the three types of uncertainty emerge within a SRFE. Dugdale *et al.* (1991) described how TAMSAT estimates rainfall using a calibrated relationship between the temperatures of cloud tops – as recorded by Meteosat thermal infrared (TIR) sensors – and rainfall – as recorded by ground raingauges. In order to do so it has to make two assumptions:

1. All clouds are convective
2. All convective clouds are raining

These assumptions come from the area-time integral (ATI) method that informs the TAMSAT rainfall estimation, which relies on a statistical relationship between cold cloud duration, coverage and areal rainfall (Kebe *et al.* 2004).

The use of ensemble estimates provides an effective way of characterising and representing the uncertainty in rain fields. A notable experiment in this area is the Hydrological Ensemble Prediction Experiment (HEPEX), led by the National Oceanic and Atmospheric Administration (NOAA) (Schaafe *et al.*, 2007). The

goal of HEPEX is to produce an end-to-end system that accounts for all the uncertainties inherent within streamflow forecasting. A conceptual diagram of one possible system is shown in Figure 1.1.

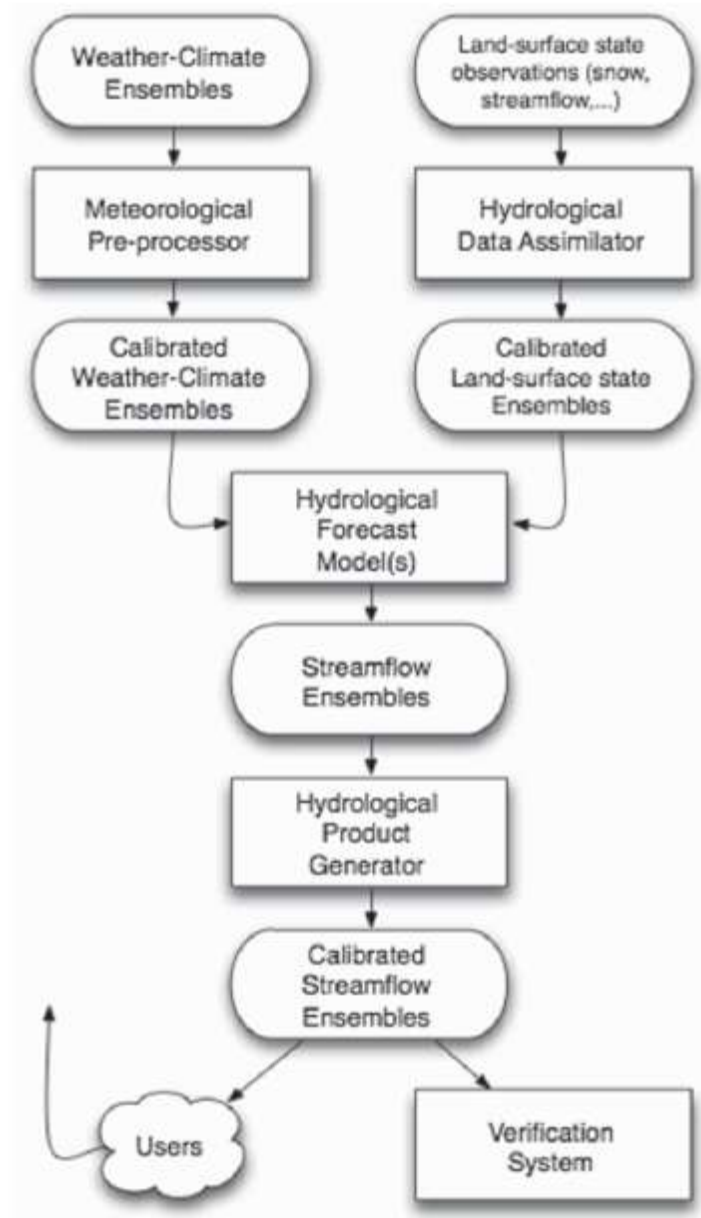


Figure 1.1 – A conceptual diagram of a possible end-to-end meteorological-hydrological ensemble streamflow system. The system allows for all sources of uncertainty to be accounted for (from Schaake *et al.*, 2007).

Although HEPEX is not explicitly aimed at the use of SRFE - the weather-climate ensembles shown in Figure 1.1 are derived from forecasts using satellite and radar data, amongst other sets of data which include SRFE (Schaake *et al.*, 2007) – the principles and the processes shown in Figure 1.1 are useful for informing research into the use of SRFE in hydrological modelling and accounting for uncertainties.

The production of an ensemble estimate requires the use of a stochastic element, where for a rainfall estimate the uncertainty is measured and a random element is used to produce a multitude of estimates from within these bounds of uncertainty. A major advantage of the ensemble approach is that it produces estimates of rainfall that resemble a deterministic estimate allowing for an almost direct application to a downstream model, often designed to operate using a single, deterministic input. Ensemble inputs provide an easy and useful method of demonstrating the propagation of input uncertainty in a hydrological model, as each can be applied as a separate input and an ensemble of model outputs can be extracted (Bellerby and Sun, 2005, Germann *et al.*, 2007).

The simplest method of producing an ensemble estimate of rainfall is to perturb the estimation at each timestep by an amount drawn from a distribution reflecting the uncertainty. This can be achieved by using either an additive method, and/or a multiplicative method, where the deterministic estimate is altered by randomly applying the perturbing factor. For the purpose of this thesis, all such methods are referred to as perturbation methods.

The major issue with perturbation methods is that they are only capable of representing the third facet of the main sources of uncertainty previously detailed for SRFE – the rain rate – and a perturbation method is unable to account for intermittencies in the rainfall field. In addition, an ensemble estimate produced using a perturbation estimate is dependent on a deterministic estimate. An alternative approach for producing ensemble SRFE is the use of a fully spatio-temporally distributed stochastic approach, such as Bellerby and Sun (2005), Teo (2006) and Teo and Grimes (2007), which allow for a full representation of the spatial and temporal intermittencies in the rainfall field as well as uncertainty about the rainfall rate. These methods are based on the full conditional distribution of the rainfall in respect to the input data, and therefore are independent on the deterministic SRFE.

Although there have been previous studies into the impacts of input uncertainty on hydrological models, many have been limited to stochastic perturbations, of a given magnitude, of the input, without attempting to fully characterise the error (McMillan *et al.*, 2011). Given the complex, non-linear, nature of rainfall and hydrological models, such an approach is not sufficiently detailed, and a critical research priority must be for a full analysis of rainfall input uncertainty (McMillan *et al.*, 2011).

Vrugt *et al.* (2008) provide a good example of how past attempts to bridge the gaps between SRFE and hydrological modelling have fallen short, despite best intentions. The Differential Evolution Adaptive Metropolis (DREAM) method was used to determine Bayesian statistics about the model parameters when being

driven by rainfall inputs that characterised the input error. The input error was characterised using multipliers on individual storm events.

Hong *et al.* (2006) used the Precipitation Estimation from Remote Sensed Information using Artificial Neural Network – Cloud Classification System (PERSIANN-CSS) algorithm to drive the HyMod hydrological model. The input uncertainty was characterised by calculating error bounds at 10 rainfall intensity bands, and producing ensemble members from within these bounds. Although the rain intensity-dependent error approach employed is an improvement on a simpler multiplier method, such as Vrugt *et al.* (2008), it still does not adequately reflect the uncertainty within SRFE as it only addresses rainfall rate uncertainty.

The approach of using perturbation methods to try and characterise input uncertainty, as used by Vrugt *et al.* (2008) and Hong *et al.* (2006), is, as suggested by McMillan *et al.* (2011), not adequate. Although it simulates possible uncertainty inherent in estimating rainfall rate, and total input volume, it cannot simulate the uncertainties inherent in estimating both the timing of rainfall and its location.

Bellerby and Sun (2005) presented a fully spatio-temporally distributed stochastic ensemble approach for characterising uncertainty in a multi-platform SRFE but, although suitable for such a use, the ensemble outputs were never used to drive a downstream application. Using a similar method, Teo (2006) and Teo and Grimes (2007) demonstrated that the TAMSIM algorithm could

successfully characterise the full range of uncertainties within a SFRE. The approach produced ensemble representations of the rainfall field at daily timesteps which represented uncertainty around the location, timing and rate of rainfall. The ensemble outputs were used to drive a crop yield model, demonstrating the influence of the propagation of input uncertainty. This thesis proposes the use of the TAMSIM algorithm to produce ensemble rainfall input to drive a hydrological model, and assess how this full characterisation of uncertainty propagates through the model.

As highlighted by Gebremichael and Hossain (2010) studies have often focussed on one aspect of the field when looking at satellite rainfall applications for surface hydrology. For example, Hossain *et al.* (2004) characterised the retrieval and sampling errors within passive microwave (PM) derived products, and applied this to the TOPMODEL hydrological model which was only calibrated using a basin average of the rainfall recorded by raingauges. Although this approach demonstrates how SRFE uncertainty can be characterised and applied to a surface hydrology model, it does not consider the surface hydrology facet of the field as the study did not attempt to separate the sensitivity of TOPMODEL to the error, from its sensitivity to its input-parameter interactions.

The key issue that continues to separate the two fields of satellite rainfall estimation and hydrology is a matter of assumptions. Vrugt *et al.* (2008) suggested that a traditional approach to hydrological model calibration makes the assumption that both input and output data are free from uncertainty, and

that any errors are due to parameter set selection. Similar assumptions are made in the approach to hydrometeorology, with the assumption being that all uncertainty is within the SRFE, and any error in the hydrological model is negligible.

The use of ensemble inputs for the same temporal period is likely to have an influence on the calibration of a hydrological model, with input uncertainties potentially interacting with model structure and parameter uncertainty in complex and non-Gaussian ways. The traditional approach to calibration of a hydrological model uses the minimisation of one or more error scores (objective functions), against a single deterministic input, and for the use with ensemble inputs there remains an unanswered question of what constitutes an appropriate calibration. This thesis demonstrates how calibration against deterministic estimates of rainfall, for the study period, produce parameterisations of the Pitman model that are not suitable for use with ensemble inputs, and proposes the EnsAll parameterisation that incorporates each individual ensemble member – this parameterisation showed superior performance to the alternative methods and little bias.

1.2 – Using Satellites to Estimate Rainfall in Africa

SRFEs are becoming increasingly important in rainfall monitoring and prediction in Africa. The African continent poses a particular problem to many fields, in that many regions face severe insecurity in regards to food provision and water resources - which are likely to increase with predicted climatic changes

(Commission for Africa, 2010) – and driven by variations in rainfall. Such extreme events in rainfall can lead to devastating floods and droughts, such as the ‘Horn of Africa’ drought which struck the eastern Sahel region in 2011 (Hillier and Dempsey, 2012).

Although Early Warning Systems (EWS) are in place to help predict and manage potential humanitarian disasters resulting from the extreme variations in rainfall, such as the Famine Early Warning Systems Network (FEWSNET) (Hillier and Dempsey, 2012), they rely on timely and accurate rainfall estimation. This second issue, one of data availability, is another significant challenge facing those working in Africa, with Washington *et al.* (2006) describing the provision of ground instrumentation recording rainfall in Africa as historically poor, with few radar and sparse raingauge networks.

To fill this void many researchers have turned to using SRFE, as these can provide increased spatial and temporal resolution, and can be provided in near real-time. Examples of services that provide daily or dekadal (10-day total) rainfall estimates for the whole of Africa are the Climate Prediction Centre (CPC) and TAMSAT, both of which are freely accessible on the internet (Teo, 2006).

1.3 – Thesis Aims

The main aims of this thesis can be summarised as:

1. Characterising the SRFE uncertainty over a large, data sparse, heterogenous area, using a fully spatio-temporally distributed stochastic ensemble method.
2. Investigating how this uncertainty in the SRFE propagates through as uncertainty in a hydrological model.
3. Investigating how the use of ensemble rainfall inputs interacts with the calibration of a hydrological model.

In addressing the three aims above, there exists a number of research questions that require addressing in order to inform the research. Principal amongst these are:

- a) *To what extent do the ensemble SRFE reproduce the characteristics of the rainfall fields for the study area?*
- b) *How does the uncertainty in the SRFE manifest – error, spatial bias, temporal bias?*
- c) *How can a hydrological model be best calibrated for use with ensemble rainfall inputs?*

- d) *With an appropriate calibration, which of the sources of uncertainty are evident in the hydrological model output when driven by the ensemble rainfall inputs?*
- e) *How does the use of a fully spatio-temporally distributed method of uncertainty characterisation compare to a perturbation method for modelling input uncertainty in a hydrological model?*
- f) *What influence does using ensemble rainfall inputs have on the hydrological model calibration and behaviour?*

1.4 – Experimental Process and Thesis Plan

The choice of study area, data and methods that are used in this thesis position the experimentation directly in their operational context. The double Kriging, TAMSAT1 and TAMSIM methods have been tested and validated, experimentally and for the Gambian catchment, in Teo (2006) and this thesis does not seek to reproduce this, rather it seeks to use those methods in an area where they might be used operationally. The study area chosen is large, heterogeneous and very sparsely covered by ground instrumentation used to measure rainfall, which will produce an abundance of uncertainties that can be measured. It should be noted that the data used will not provide the best representation of the methods employed – this has been the domain of previous studies – the aim of this thesis is to characterise the uncertainty in a SRFE and investigate how it propagates through a downstream application, not to show

how well a SRFE performs as a driver for the model, which has been previously shown (see Chapter 2). The choice of study area and data will deliberately stretch the methods adopted to the limits of their performance, as they might be when used operationally in sub-Saharan Africa.

Chapter 3 will detail the sources of raw data and these are summarised below:

- Raingauge data from 81 gauges across the Senegal Basin area for the period covering 1986-1996.
- Discharge data from seven discharge stations, providing mixed coverage for the period 1986-2005.
- Cold Cloud Duration (CCD) data covering the study area for the periods above, extracted from Meteosat thermal infrared (TIR) data, at a daily timestep with a spatial resolution of 0.05°.

The experimental process of this thesis can be seen summarised in Figure 1.2. This details the stages from the collection of the raw raingauge data, and its interpolation into a grid that is compatible with the satellite CCD data collected. The satellite data is calibrated using the interpolated raingauge data to produce a TAMSAT1 deterministic estimate of rainfall, and a TAMSIM (using the SIMU programme) stochastic ensemble estimate of rainfall. The rainfall estimates, from the raingauge and satellite data, are used as an input for a lumped hydrological model, both to drive it and to calibrate it.

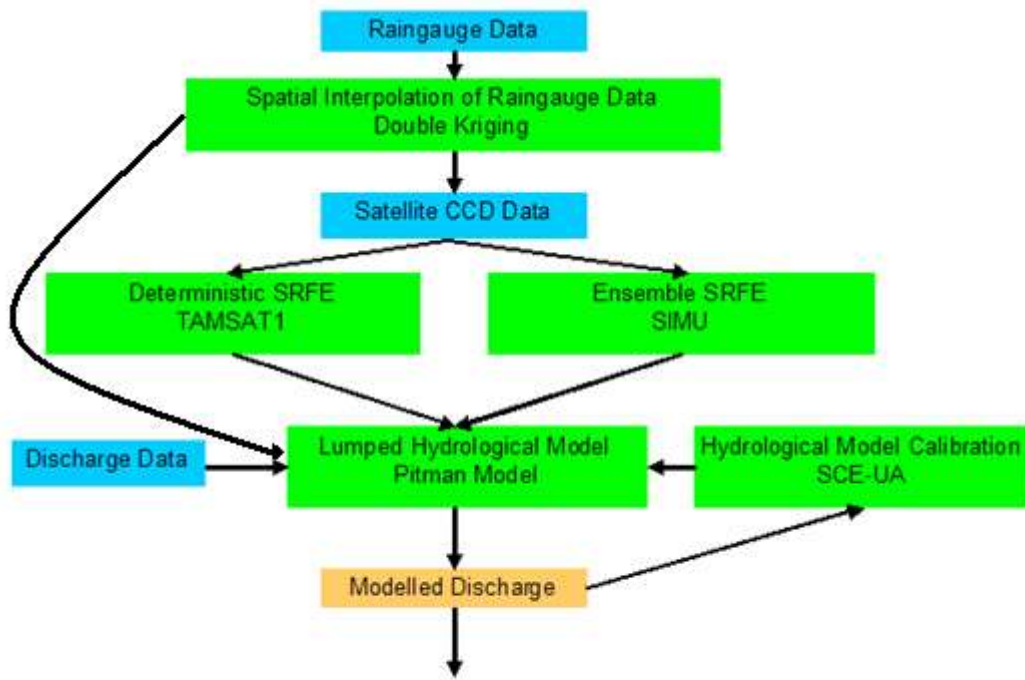


Figure 1.2 – Flow chart demonstrating the process used in this thesis, the main steps, and the methods employed. Blue boxes indicate the input data, green boxes the main steps and methods, whilst the brown box indicates the output.

The remainder of this thesis demonstrates the fulfilment of the process above. Chapter 2 investigates the literature associated with the emerging field of satellite rainfall applications for surface hydrology (Gebremichael and Hossain, 2010), focussing particularly on issues regarding the influence and propagation of input uncertainty on hydrological modelling when using SRFE.

Chapter 3 discusses the issues raised in this thesis in their geographical context and the Sahel region. The chapter looks broadly at the pressing need for accurate environmental models in the area, and in turn the requirement for timely rainfall estimations to drive these models – the role of uncertainty is

explored, highlighting the importance of accurate and proper uncertainty characterisation, its clear communication and the implications for risk management. The Senegal Basin study area, and the Bakoye catchment within it, are explored focussing on the physical attributes and climate of the area, and discussing previous relevant studies in the region. Finally the raw data available to the thesis is described, showing how it reflects the physical characteristics previously detailed.

Chapter 4 focuses on the spatial interpolation of the raingauge data and the double Kriging (DK) method used to do this, demonstrating how the method is superior to ordinary Kriging (OK), both in its ability to account for fractional rainfall fields but also in its ability to better match the initial raingauge data at individual gauge locations, and also as an average for the Bakoye catchment.

Chapter 5 highlights the SRFE methods used, showing the calibration of the both the TAMSAT1 and TAMSIM methods and their use in generating daily rainfall fields for the Senegal Basin, and the Bakoye catchment average rainfall estimates.

Chapter 6 demonstrates the hydrological modelling methods used for the thesis, describing the Pitman lumped conceptual rainfall-runoff (CRR) model and the Shuffled Complex Evolution (SCE-UA) method used to automatically calibrate it. It is shown how the automatic calibration method significantly increases the performance of the Pitman model using a rainfall estimate produced from the raingauge data.

Chapter 7 describes TAMSIM's ability to reproduce the underlying spatio-temporal distributions of the rainfall (as described by the DK raingauge fields) by observing the 200 ensemble members produced. Its performance is described at both gauge-pixel (pixels that contain at least one raingauge) and Bakoye catchment scale. The performance of the TAMSIM ensemble SRFE is compared against the TAMSAT1 deterministic SRFE, finding that not only is it able to demonstrate the full bounds of uncertainty, but also when taken as a whole the ensembles perform better at modelling the underlying rainfall field. The main sources of uncertainty within the SRFE are explored, showing that the estimates display significant spatial and temporal biases.

Chapter 8 demonstrates the outcome from the process shown in Figure 1.2, using the TAMSIM ensemble SRFE to drive an optimised Pitman model of the Bakoye catchment: the ensemble output discharge data used to produce hydrographs that show the bounds of the 95% confidence envelope for discharge which fully reflects the influence of the input uncertainty on the Pitman model. It is seen that the spatial biases in the TAMSIM ensemble estimates have been compensated for by the calibration, but significant temporal biases have been directly propagated into the Pitman model output. The discharge envelopes are compared to those produced by a simpler perturbation method on the TAMSAT1 data, highlighting the inadequacy of this method in fully characterising the propagation of input uncertainty. The chapter introduces the EnsAll method for calibrating a lumped CRR hydrological model

for use with an ensemble input, demonstrated how the method outperforms all the alternatives and shows little overall bias.

Chapter 9 focuses specifically on the influence of the input uncertainty on the calibration of the variable parameters in the Pitman model, and on the resulting behaviour of the model. The individual calibrations from the TAMSIM ensemble SRFE are investigated closely, observing the relationships between the spread of parameter values on model behaviour and performance. It was found that the uncertainty within the input had little influence on the calibration of the parameter values, but there was some evidence for equifinality in the model behaviours.

Chapter 10 discusses the key issues encountered by this thesis, critically evaluating the analyses undertaken and highlighting the key results and their implications on the research field. Suggestions are made for appropriate avenues of future research.

Finally, Chapter 11 concludes the thesis, discussing the major findings.

2

Satellite Rainfall Applications in Hydrological Modelling

2.1 – Introduction

In Chapter 1, the field of satellite rainfall applications for surface hydrology was introduced along with a demonstration for the need for a holistic approach to research into the influence of uncertainty, as highlighted by Gebremichael and Hossain (2010). This chapter breaks the field down into its component features and investigates the current state of uncertainty research in each facet.

2.2 – Dealing with Input Uncertainty in Hydrological Models

The issue of observation uncertainty, in particular input uncertainty, is an often neglected element of hydrological model uncertainty analysis (Vrugt *et al.*, 2008, Baldassarre and Montanari, 2009). Vrugt *et al.* (2008) described this issue within the field of hydrology where the common approach to modelling assumes that the primary source of uncertainty is associated with parameter values, and the model calibration, resulting in neglecting the influence of uncertainty within the rainfall input. Baldassarre and Montanari (2009) agreed with the sentiments

of Vrugt *et al.* (2008), suggesting that few attempts have been made to assess the influence of observation uncertainty as it is often regarded as negligible compared to model structure or parameter uncertainty. Moradkhani *et al.* (2005) stated that often the uncertainties associated with inputs, outputs and model structure are ignored, and assumed to be associated with model parameter uncertainty.

Michaud and Sorooshian (1994b) suggested that the influence of rainfall error on hydrological models is undetermined, with some studies showing very little significance and others showing very marked effects on the modelled output – although by reducing the raingauge density over a catchment, it was found that spatial sampling error alone could contribute up to 50% of the difference between the observed and modelled discharges.

Hughes (1995) suggested the sources of uncertainties in hydrological models are:

- Erroneous data inputs
- Poor interpretation of model results
- Inadequate or inappropriate modelling of catchment processes
- Inadequate modelling of the spatial variability of runoff generation from rainfall
- Inadequate representation of the spatial variability of the rainfall input
- Inadequate representation of the temporal variability of the rainfall input
- Inadequate representation of the parameter values.

From the list provided by Hughes (1995), three of the potential sources of uncertainty in hydrological models can be attributed to the rainfall input, and these can be grouped as input uncertainty, composed of three components:

1. Temporal – differentiating between when it is raining and when it is not
2. Spatial – differentiating between areas where it is raining and where it is not
3. Rate – the intensity of rainfall where raining

A common approach to representing the input uncertainty in hydrological models is to use a perturbation method, where the rainfall estimated at each timestep is perturbed within set bounds, usually a multiplier or an additive factor. Examples of studies that have employed a perturbation method can be seen in Butts *et al.* (2004), Vrugt *et al.* (2008) and Montanari and Baldassarre (2013).

The studies listed above vary in nature, for example Butts *et al.* (2004) randomly perturbed each estimate by the addition of a value chosen from a normal distribution with a mean of zero and a standard deviation equal to 50% of the rainfall estimate for that timestep, producing an ensemble of 200 estimates. Montanari and Baldassarre (2013) perturbed the estimates obtained by the average of raingauge measurements by adjusting the weighting given to each gauge in the production of the estimate. The method demonstrated by Vrugt *et al.* (2008) was more complex, instead applying multipliers based on the identification of individual storm events. Both Butts *et al.* (2004) and Montanari

and Baldasarre (2013) found the representation of input uncertainty showed little influence on simulated discharges, yet Vrugt *et al.* (2008) showed their method acted to remove systematic biases in the rainfall estimates.

Butts *et al.* (2004) highlighted that there was a requirement for a more complete representation of the uncertainty within the radar rainfall estimate used, with a full characterisation of the spatial and temporal uncertainties. This can be said of each of the methods above, and for all conventional perturbation methods that can only characterise the rainfall rate aspect of rainfall input uncertainty. When using areal averages of rainfall it is tempting to do this, as ultimately all three components of the rainfall uncertainty will be expressed as a rainfall rate for the timestep over that area, but the methods are limited by their inability to fully represent the complex nature of rainfall. This was highlighted in McMillan *et al.* (2011) who described the requirement for a comprehensive analysis of the uncertainty due to the complex, non-linear nature of rainfall as a critical research need. In reference to SRFE, Hossain and Anagnostou (2004) suggested that simple additive methods of characterising input uncertainty are insufficient to understand the propagation of the uncertainty through a hydrological model.

The spatial distribution of rainfall has been shown to be important to hydrological modelling, with Azimi-Zonooz *et al.* (1989) arguing that the accurate determination of storm locations within a watershed is necessary for hydrological modelling, particularly in the case of localised storm and flood forecasting. Using a lumped model, Sivaplan *et al.* (1997) showed that

heterogeneity in rainfall inputs has a significant influence on modelled discharges. The spatial and temporal variability of rainfall was also highlighted as an issue needing to be properly addressed by hydrological modellers by O'Connell and Todini (1996). In a study observing the influence of spatial resolution and sampling error in the MIKE SHE distributed hydrological model, Shah *et al.* (1996) found that the spatial variability of rainfall was particularly influential on the modelled discharge during dry periods, as soil moisture was sensitive to the spatial distribution of precipitation.

A study by Xuan *et al.* (2009) directly applied rainfall forecasts produced by a numerical weather prediction (NWP) model to a distributed hydrological model. They used data from a raingauge network to correct storm locations in the ensembles and found that this improved the modelling of the discharge. Lee *et al.* (2012) also observed the importance of spatial distributions of rainfall on hydrological modelling, by modelling scenarios displaying different temporal and spatial distributions of the rainfall field and applying them to a distributed hydrological model.

Tsai *et al.* (in press 2012) noted that the requirement to account for the spatial distribution of convective rainfall, which displays a high degree of spatio-temporal heterogeneity and uncertainty, is particularly acute when it is the key driver for runoff. They also added that the majority of studies focus on the impacts of temporal variations to the detriment of the impacts of the spatial variations of model inputs. Using a reservoir model they demonstrated how the

inclusion of spatial distributions of rainfall improved the performance of a semi-distributed model, when modelling the impacts of typhoons in Taiwan.

Hong *et al.* (2006) demonstrated a spatio-temporal method of characterising rainfall uncertainty within a SRFE. The method worked by binning data from the PERSIAN-CSS SRFE into spatial aggregation, temporal aggregation and rainfall rate categories, and providing a reference error value in a contingency table for each bin – the contingency table was then used to produce ensemble rainfall estimates. The method was adopted by Moradkhani *et al.* (2006) to further investigate the propagation of the input uncertainty on the conceptual Hydrological MODel (HyMOD), using a sequential data assimilation (SDA) method to account for all sources of error in hydrological modelling – in comparison to parameter, the input uncertainty showed a wider range of uncertainty.

Although the method employed by Hong *et al.* (2006) and Moradkhani *et al.* (2006) does make account of some spatial and temporal details of rainfall uncertainty and better represents the uncertainty of the input over the fixed perturbation approach, ultimately it still amounts to applying a multiplier to the estimates. This method cannot fully represent the uncertainty within the input – for example, it is unable to predict rainfall where the original SRFE predicts none and vice versa.

There remains a pressing research requirement for a study into the influence of the full spectrum of uncertainties within SRFEs on the modelling of hydrological

systems (McMillan *et al.*, 2011). The TAMSIM algorithm introduced by Teo (2006) and Teo and Grimes (2007) provides the opportunity to do this as it fulfils the requirements specified, in that it allows for the characterisation of temporal, spatial and rainfall rate uncertainties, both in rainfall retrieval and sampling.

2.3 – Satellite Rainfall Estimation

The study area, like much of sub-Saharan Africa and especially the Sahel region, lacks extensive coverage of ground instrumentation for the estimation of rainfall in real-time. As part of the World Meteorology Organisation's (WMO) World Weather Watch (WWW) raingauge network, Africa has 1,152 stations, giving a raingauge density of 1 per 26,000km² – eight times lower than the WMO's own specified minimum recommendation (Washington *et al.*, 2006).

Washington *et al.* (2006) also suggested that the actual situation is worse than this as many of the stations are intermittent in transmitting data, especially in central Africa where large areas are essentially unmonitored. This is supported by NOAA (2010), where out of 1,000 raingauges available to the African Rainfall Estimation (RFE 2.0) project, usually less than 500 are used on any single day due to lack of transmission or erroneous data. It has been found that the situation in sub-Saharan Africa regarding raingauge coverage has deteriorated over recent decades (Ali *et al.*, 2005).

The probable reason for this lack of ground instrumentation, in the form of raingauge and weather radar systems, is the considerable financial and

technological investment that is required to install and operate these networks (Anagnostou *et al.*, 2010).

The Senegal Basin study area is not atypical to the situation described above. As is shown in Chapter 3, the Bakoye catchment part of the study area has a raingauge density of 1 gauge per 7,000km² – relatively high given the African average provided by Washington *et al.* (2006). In contrast, Teo and Grimes (2007) studying the Gambia region close to the Senegal Basin used a gauge network averaging 1 gauge per 500km².

Given this lack of ground instrumentation, satellite data has been increasingly used to fill the data gap and currently constitutes the only viable method of providing data for use in hydrological studies for many areas of the Earth (Anagnostou *et al.*, 2010).

SRFEs have been made since the 1970s, with observations made in either the visible (VIS), thermal infrared (TIR) and passive microwave (PM) spectrums (Anagnostou *et al.*, 2010). VIS sensors are able to provide information of the density of droplets in a cloud by measuring the cloud albedo. TIR sensors measure the temperature of cloud tops and this can be used to infer rainfall using a statistical relationship between the cloud top temperature and rainfall, exploiting the fact that tropical rainfall is dominated by convective storms comprising of high-top cumulonimbus clouds. PM sensors measure the long-wave radiation re-emitted from water droplets and the shortwave radiation scattered by ice crystals – direct indicators of rainfall. Due to the nature of the

sensors PM retrieval is restricted to low polar orbits, which provide limited areal coverage but high spatial resolution. TIR and VIS sensors can be mounted on satellites in geostationary orbits, which are higher and provide greater spatial coverage over a fixed point but often sacrifice the spatial resolution available at lower orbits. Table 3.1 shows a list of current satellites that contribute towards the WMO's Global Observing System (GOS).

There are efforts to improve the satellite coverage for rainfall retrieval, for example the Global Precipitation Measurement (GPM) will significantly decrease the sampling intermittencies from PM sensors. GPM is an international mission that will involve a large constellation of PM sensors in Low-Earth orbits (LEO), giving global coverage at a temporal resolution of 3-6 hours and a spatial resolution of 100km (Hossain and Anagnostou, 2004). At the centre of the constellation is a core satellite which will carry the first space-borne Dual-frequency Precipitation Radar (DPR) which will monitor precipitation in 3-dimensions – it is due for launch in 2014 (NASA, 2013).

Chapter 2 – Satellite Rainfall Applications in Hydrological Modelling

Geostationary	Operator	Sensors	Sector
GOES-15	NOAA	VIS/TIR	East Pacific
GOES-14	NOAA	VIS/TIR	West Atlantic
GOES-13	NOAA	VIS/TIR	West Atlantic
GOES-12	NOAA	VIS/TIR	West Atlantic
Meteosat-10	EUMETSAT	VIS/TIR	East Atlantic
Meteosat-9	EUMETSAT	VIS/TIR	East Atlantic
Meteosat-8	EUMETSAT	VIS/TIR	East Atlantic
INSAT-3E	ISRO	VIS/TIR	Indian Ocean
Meteosat-7	EUMETSAT	VIS/TIR	Indian Ocean
INSAT-3C	ISRO	VIS/TIR	Indian Ocean
Kalpana-1	ISRO	VIS/TIR	Indian Ocean
Electro-L N1	RosHydroMet	VIS/TIR	Indian Ocean
FY-2D	CMA	VIS/TIR	Indian Ocean
INSAT-3A	ISRO	VIS/TIR	Indian Ocean
FY-2E	CMA	VIS/TIR	Indian Ocean
FY-2F	CMA	VIS/TIR	West Pacific
COMS-1	KMA	VIS/TIR	West Pacific
Himawari-6	JMA	VIS/TIR	West Pacific
Himawari-7	JMA	VIS/TIR	West Pacific

Low Earth Orbits	Operator	Sensors	Sector
DMSP-F15	DoD	VIS/TIR/PM	Early Morning Orbit
DMSP-F17	DoD	VIS/TIR/PM	Early Morning Orbit
DMSP-F13	DoD	VIS/TIR/PM	Early Morning Orbit
DMSP-F16	DoD	VIS/TIR/PM	Early Morning Orbit
NOAA-17	NOAA	VIS/TIR/PM	Morning Orbit
DMSP-F18	DoD	VIS/TIR/PM	Morning Orbit
NOAA-16	NOAA	VIS/TIR/PM	Morning Orbit
Meteor-M N1	RosHydroMet	VIS/TIR/PM	Morning Orbit
MetOp-A	EUMETSAT	VIS/TIR/PM	Morning Orbit
MetOp-B	EUMETSAT	VIS/TIR/PM	Morning Orbit
FY-3A	CMA	VIS/TIR/PM	Morning Orbit
Soumi-NPP	NASA	VIS/TIR/PM	Afternoon Orbit
NOAA-19	NOAA	VIS/TIR/PM	Afternoon Orbit
FY-3B	CMA	VIS/TIR/PM	Afternoon Orbit
NOAA-18	NOAA	VIS/TIR/PM	Afternoon Orbit
DMSP-F14	DoD	VIS/TIR/PM	Afternoon Orbit
NOAA-15	NOAA	VIS/TIR/PM	Afternoon Orbit

Table 3.1 – Table showing current meteorological satellites that contribute towards the WMO’s GOS, their types of orbits, operators, types of sensors carried and sectors covered. For satellites in low earth orbits, the sector refers to the time the platform crosses the equator during daylight in a sun-synchronous orbit (WMO, 2013).

Of the principal sensors used for rainfall retrieval, PM data is more desirable as it provides physical observation of rain areas as related hydrometeors interact with the upwelling microwave radiation, however, these sensors need to be positioned in polar LEO and thus only a few observations (6-10) of a limited region can be obtained each day (Tadesse and Anagnostou, 2009, Dinku *et al.*, 2010). Even if the rainfall retrieval error was zero, the intermittence in coverage leads to sampling error which is the dominate source of uncertainty in low orbit SRFE (Bell *et al.*, 1990). The ability of PM sensors to accurately measure rainfall is influenced by the land surface of the observation region, with certain land surfaces interfering with the signals (Dinku *et al.* 2007). Amongst these are land surfaces associated with arid and semi-arid regions (Morland *et al.* 2001), which is of particular importance to this thesis - Chapter 3 argues that a significant proportion of the study area can be classified as arid and/or semi-arid.

TIR data can be collected from a geosynchronous orbit able to make continuous observation of a wide area, but cannot directly observe rainfall, rather collecting information on storms based on the temperature of cloud tops – with the assumption that colder cloud tops are most likely to be representative of areas of rainfall (Tadesse and Anagnostou, 2009, Dinku *et al.*, 2010). As TIR data is available at higher spatial (4km) and temporal (1/2 hourly) intervals, it can be used to fill the spatial and temporal gaps in PM rainfall retrieval (Tadesse and Anagnostou, 2009).

Many modern SRFE algorithms take advantage of the different types of sensors available, combining the data to cover the shortfalls in each. An example is the Tropical Rainfall Measuring System (TRMM) Multisatellite Precipitation Analysis (TMPA) which merges PM and TIR data where available, and covers the sampling intermittencies from PM sensors using a PM calibrated TIR estimate of rainfall (Huffman *et al.*, 2010).

SRFEs are utilised for many purposes, including providing driving inputs for hydrological and crop yield models (Teo, 2006, Teo and Grimes, 2007), and informing global atmospheric circulation models (Arkin and Meisner, 1987) and Early Warning Systems (EWS) – drought, famine and disease (Verdin *et al.* 2005). Skees and Collier (2008) highlighted the use of satellite weather data as a useful check for weather indexes, used to inform microinsurance schemes for the data poor regions of the Sahel.

For many applications of hydrological modelling it is desirable to have rainfall estimates provided in fine temporal timesteps, and for distributed models a reasonably high spatial resolution is required. There is also a desire for the capability of providing real-time, or near real-time estimates. Bellerby *et al.* (2000) suggest that for meteorological and hydrology purposes, a product at a temporal scale of one day or less and a spatial scale of 25km or less would be invaluable.

Examples of methods of SRFE that fulfil these criteria above are:

- **The Tropical Rainfall Measuring System (TRMM) – The Multi-Satellite Precipitation Analysis (TMPA)** - TMPA can produce global rainfall estimates at 3-hour timesteps at a spatial resolution of $0.25^{\circ} \times 0.25^{\circ}$. For real-time TMPA estimates, rainfall estimates derived from several PM and TIR measuring platforms are combined by using PM estimates where available, and using PM calibrated TIR estimates to fill in gaps (Huffman *et al.*, 2010).
- **The African Rainfall Estimation (RFE 2.0)** – The RFE 2.0 combines rainfall estimates from three satellite platforms (two PM making four passes each a day, and one TIR taking half-hour measurements), weighted to ground raingauge data to produce a daily rainfall estimate for Africa at $0.1^{\circ} \times 0.1^{\circ}$ pixel resolution (NOAA, 2010).
- **The Climate Prediction Centre morphing method (CMORPH)** – This method produces global estimates of rainfall at half-hour resolution, using a combination of PM and geostationary TIR satellite data. The method uses the temporal resolution of the TIR data to calculate the passage of rainfall for the period between LEO satellite passes collecting PM data, producing a rainfall estimation derived from the higher-quality PM alone (Joyce *et al.*, 2004).

- **Precipitation Estimation from Remotely Sensed Information using Neural Networks (PERSIANN)** – The PERSIANN method processes TIR and ground data through an artificial neural network to produce rainfall estimates. The relationships can be updated using spatio-temporally limited ground-based data as it becomes available (Hsu *et al.*, 1996). A Cloud Classification System (CSS) has been added to the PERSIANN method to improve rainfall estimates (Hong *et al.*, 2004).
- **Tropical Applications of Meteorology from SATellites (TAMSAT)** – The TAMSAT method has a long operational history in sub-Saharan Africa and has proven successful in this context (Teo and Grimes, 2007). The method produces estimates of rainfall for sub-Saharan Africa at $0.05^{\circ} \times 0.05^{\circ}$ pixel resolution. The only satellite input is TIR cloud top brightness and rainfall is derived by calibrating a simple linear relationship between cloud top temperature and rain, locally (Dugdale, 1991). Although the publically available TAMSAT products, produced by the TAMSAT team, University of Reading, are only in dekadal time-steps, the methodology provided by Teo and Grimes (2007) expanded the algorithm to produce daily rainfall estimates.

2.4 – Satellite Rainfall Uncertainty Characterisation

The previous section detailed the necessity for producing SRFE and highlighted some of the techniques and the existing products available. However, SRFE contain uncertainties inherent in their generation and often these uncertainties

are large. Any uncertainty in the rainfall input for a hydrological model is likely to propagate through to its output and to assess the impact of this it is necessary to quantify and represent the scale of these uncertainties. This section looks at some of the major sources of uncertainty in SRFE, with a focus on the TAMSAT method in particular, and explores the methods that have been previously employed to measure and represent them.

Rainfall generators have been developed to generate ensemble products from single inputs - either single satellite sensors or satellite rainfall estimates themselves (using a delta approach). The full conditional simulation from multiple satellite sensors requires the implementation of techniques to cater for discontinuities at sensor coverage boundaries, but these are still in development (Bellerby, 2012). However, methods have been demonstrated for use with SRFE derived from single sensors, such as TAMSAT. TAMSAT is ideal for use with this study area as it has a long operational history in sub-Saharan Africa and has previously been used with a full spatio-temporally distributed uncertainty characterisation method, in TAMSIM (Teo, 2006).

The only satellite information required by TAMSAT is the Meteosat TIR cloud brightness data, processed into CCD values at given cloud top temperature thresholds. To estimate rainfall from this data TAMSAT uses an area-time integral (ATI) that assumes that the areal rainfall is proportional to the CCD and cloud coverage over the observation area, when a sufficient number of storms are aggregated over space and time (Kebe *et al.* 2004). The method therefore has to make two assumptions about the relationship between it and real rainfall:

1. All cold clouds are convective
2. All convective clouds are raining

This works well for areas where the dominant rainfall type is convective – which is the case for the study area and the wider Sahel region, as detailed in Chapter

3. The TAMSAT1 method, introduced by Teo (2006) and Teo and Grimes (2007) for daily SRFE estimation, maintains these assumptions in its operation and as a result this will lead into two major sources of uncertainty in the resulting SRFE. First, not all cold clouds are convective, for example high altitude cirrus clouds can be recorded as raining. Second, the method will miss low level storms that have warm clouds. In addition, the calibrated relationship is non-stationary, both spatially and temporally, and likely to be non-linear, all contributing to the uncertainty in the SRFE (Nikolopolous *et al.*, 2010). Vicente *et al.* (1998) states that the relationship between cloud-top temperature and rainfall rates can vary between storm types, the season, location and the land-surface, amongst many other contributory factors.

A review by Hossain and Anagnostou (2006) found that due to the variety of methods for producing SRFE, using different sensor platforms and algorithms, the methods developed to quantify and characterise the uncertainty within them were just as varied, adding that many were limited to the errors involved in large spatio-temporal resolutions. An example is Hong *et al.* (2006), which modelled the uncertainty in an aggregated estimate based on the resolution of the aggregation used.

If SRFE are to be used effectively as rainfall inputs in hydrological models then the errors inherent need to be accurately characterised, but that characterisation also needs to fully reflect the complexity of the error structure of rainfall fields at a scale useful for dynamic surface hydrological processes (Hossain and Anagnostou, 2006, Nikolopoulos *et al.*, 2010). Bellerby and Sun (2005) highlighted how SRFE were often aggregated to lower spatio-temporal resolutions to avoid the large uncertainties associated with using the higher resolutions, but this means that much of the spatial information cannot be used. For use with modelling dynamic surface hydrological processes, such as runoff or flood forecasting, the more uncertain higher resolution data is more desirable as it provides the spatio-temporal information required (Bellerby and Sun, 2005), but to ensure that these uncertain products are useful to the downstream applications, the uncertainties need to be modelled fully, accurately and in a way where they can be translated to the downstream applications and propagation of the uncertainties can be measured (Bellerby and Sun, 2005, Hossain and Anagnostou, 2006, and Nikolopoulos *et al.*, 2010).

Probabilistic Ensembles

The use of probabilistic ensemble weather forecasts was shaped by the work of Lorenz (1963, 1969), whose research informed the meteorological community about the concept of chaos theory – the atmosphere is a complex, non-linear system and subject to small perturbations that over time cause forecasts to diverge, and to cover the possible divergences ensemble sets of forecasts are

produced, each unique but equally plausible within the bounds of possibilities (Slingo and Palmer, 2011). For use with a rainfall estimate, a stochastic weather generator is used to produce an ensemble set of rain fields, each consistent with the statistics of the observed rain field and containing a random element based on measured uncertainty. This makes each ensemble representation of the rain field unique yet equiprobable.

The use of ensemble estimates is a useful and relatively recent method of characterising the uncertainty within a rainfall estimation. Examples of their use can be found for interpolated raingauge estimates (Clark and Slater, 2006), estimates from weather radar stations (Germann *et al.*, 2007) and for SRFE (Bellerby and Sun, 2005, Teo, 2006, Hossain and Anagnostou, 2006, Teo and Grimes, 2007). Germann *et al.* (2007) highlighted how probabilistic ensemble approaches allowed the propagation of the input uncertainty to be effectively examined and, possibly most importantly, in a way that is easy to understand for end users.

There have been several studies into the stochastic generation of the spatial and temporal variation of rainfall which could be applied to SRFE. Notably, amongst these are the Modified Turning Bands (MTB) model in the trilogy of papers Mellor (1996), Mellor and O’Connell (1996) and Mellor and Metcalfe (1996), and in the model presented by Lanza (2000).

Three methods have been developed for characterising the uncertainty in high-resolution SRFEs using probabilistic ensemble approaches:

- **The method of Bellerby and Sun, 2005 (BS05)** – The method described by Bellerby and Sun (2005) produced equiprobable ensemble realisations of the rainfall field, by combining a pixel by pixel derived conditional distribution with a modelled spatio-temporal covariance structure. The technique was tested on a multiplatform, TIR/PM, TRMM product (Bellerby and Sun, 2005).
- **SREM2D** – SREM2D is a multi-dimensional error model that produced ensemble representations of rain fields. The method uses nine parameters of error to produce the equiprobable ensembles and was tested on a TIR only, and a multiplatform, TIR/PM, SRFE. SREM2D also used high resolution radar data to simulate satellite data with errors rather than simulating the errors from satellite data themselves (Hossain and Anagnostou, 2006).
- **TAMSIM** - The TAMSIM method operates by combining two stochastically generated fields, a rain/no-rain 'indicator' field, and a no-zeros' rainfall field, to produce equiprobable ensemble rainfall fields that allow for spatial intermittency of rainfall. The underlying spatial correlation of the raingauge rain field is determined and maintained in each ensemble using a variogram approach (Teo, 2006, Teo and Grimes, 2007).

Of the methods above, BS05 and TAMSIM both function in similar ways incorporating a full conditional distribution in regards to the input. SREM2D instead uses a delta method.

Each of the methods detailed above uses a stochastic ensemble generation approach for characterisation of the rainfall field. This allows the ensembles to be used as inputs in a deterministic hydrological model, in turn producing an ensemble of model discharges that characterise the propagation of the SRFE input uncertainty (Bellerby and Sun, 2005). The use of ensembles also allows for the upscaling of uncertainties to lower spatial resolution, which is useful for inputs in lumped or semi-distributed hydrological models (Teo and Grimes, 2007).

2.5 – Hydrological Modelling and Calibration

The list of types of uncertainty in hydrological models, provided by Hughes (1995) and shown in Section 2.2, suggested that input uncertainty, as composed of three components, is a major contributing factor to the overall uncertainty in the modelling of catchment discharge. Section 2.2 investigated the literature regarding input uncertainties in hydrological models, but this is not the only significant form of uncertainty that needs to be addressed – Hughes (1995) also suggested that model structure and model calibrations are significant contributing factors.

There are numerous types of hydrological models and calibration methods. An in-depth review of the current state of the field can be found in Wheater (2002), and more recently in Pechlivanidis *et al.* (2011) - both describing different model structures, classifications, calibration methods, sensitivity analyses and uncertainty measurements. Pechlivanidis *et al.* (2011) describes four main types of hydrological models:

- Metric Models (based on physically recorded data from the catchment)
- Conceptual Models (with parameters calibrated against input-output data)
- Physics-based Models (based on experimentally determined relationships)
- Hybrid Models (elements of at least two of the above)

The ideal hydrological model would be a fully physically based model - which Pechlivanidis *et al.* (2011) refers to as a metric model - with parameters defined by data collected in the field or observed remotely (Wagener *et al.*, 2001).

However, such data is often limited and even when available the model would still not be able to represent the heterogeneity of the study catchment (Beven, 1989).

A physics-based model, using largely known definite physical relationships, is also limited by the requirement to make assumptions, and simplified averages, of largely unknown boundary conditions and the use of simplified empirical relationships (Nash and Sutcliffe, 1970).

As such the majority of hydrological models used can be defined as conceptual rainfall-runoff (CRR) models, which Wagener *et al.* (2003) described as complying to two criteria:

1. The structure of the model is determined before the modelling is conducted (i.e., the data does not define the model structure).
2. Some, if not all, of the parameters in the model are not based on direct measurement of the study catchment.

As CRR models have parameters that are not able to be defined by actual measurements they must be calibrated against observed data (Wheater *et al.*, 1993, Wheeler, 2002). Chapter 3 details the data available for the study catchment, the Bakoye catchment, and it is clear that there is insufficient data available to operate a physical-based model. Therefore a CRR model would be the most suitable choice for the catchment and will be the focus of this section.

A hydrological model can be defined as the combination of its structure and the calibration of its parameters (Wagener *et al.*, 2003), and this thesis uses this definition. The remainder of this section is split into first reviewing the structures of hydrological models and second, reviewing some of the ways to calibrate the variable parameters.

Hydrological Model Structure

In the broadest sense there are three main types of CRR structure - lumped, distributed and semi-distributed. Beven (2008) defined a lumped model as one that treats the catchment as a whole, averaging the values and variables over the whole area, whilst a distributed model is one that allows for spatial variations of the values and variables. A semi-distributed model operates by combining a series of lumped models to operate as a single model covering a larger area (Boyle *et al.*, 2001).

Of the three basic structures, distributed models are the most sophisticated and closer to the idealised 'physics-based' models. However these models require significant spatial data to be calibrated at a distributed level and this is often not possible (Stisen *et al.*, 2008). Ajami *et al.* (2004) described some of the issues with distributed models, highlighting that their use is likely to cause a significant increase in the amount of parameters needing to be calibrated – this not only increases the computational time of modelling, but also the uncertainty as little, if not no, distributed discharge data is available for calibration at that scale. This has led to the argument that despite their ambitions, distributed models are complex CRR models rather than the physically based models they are designed to be (Refsgaard and Abbott, 1996, Grayson and Blöschl, 2001). The lack of ground spatial data available for this study means that the use of a distributed hydrological model is likely to produce significant uncertainties because of the paucity of calibration and validation data, although Stisen *et al.* (2008) demonstrated how the distributed MIKE SHE model could be used

effectively for modelling discharge of the Bakoye catchment, using multiple sources of remotely sensed spatial data.

Semi-distributed models have previously been used successfully in semi-arid and African contexts (Ajami *et al.*, 2004, Hughes *et al.*, 2006, Wilk *et al.*, 2006). Boyle *et al.* (2001) described semi-distributed models as an attractive alternative to both lumped models and fully distributed models, as they utilise the strengths of both whilst bypassing some of the weaknesses. Ajami *et al.* (2004) found that a semi-distributed model offered marginal improvement in final outlet discharge modelling, over a lumped model, but not enough to justify the additional complexity and resulting increase of uncertainty – although it did allow for the modelling of the interior of the catchment.

The goal of this thesis is to show how the uncertainty of SRFE inputs propagates through the hydrological model. As such a distributed model would not be suitable as it would introduce additional complexity that would require extensive measurement to separate the uncertainty from the hydrological modelling from the uncertainty in the SRFE. A semi-distributed model is also not suitable as the discharge data which is unaffected by dam processes is unavailable for the extra level of modelling. Given the limitations in spatial data available, and the need to minimise uncertainty associated with the hydrological model itself, the best structure to use is a lumped one. This is a similar view to that taken by Perrin *et al.* (2003), where it is seen as a logical first step to monitor how processes work at a catchment scale before trying to model in more detail.

Lumped Model Structure

There are numerous lumped hydrological models in common use, each representing the conceptual relationship between rainfall and runoff in different ways, and in varying degrees of complexity. There have been hundreds of hydrological response models developed due to the complexity of the rainfall-runoff process, and each has merits and flaws (Choi and Beven, 2007).

A study by Seiller *et al.* (2012) produced ensemble runoff to represent model structure uncertainty by using the same rainfall input through twenty different lumped hydrological models with different structures. The complexity of the models varied widely, with numbers of parameters between 4 and 10, and stores between 2 and 7.

Some examples of lumped models are:

- TOPMODEL (Beven and Kirkby, 1979) – a lumped model with 3 stores and 7 variable parameters, but incorporates a distributed element for flow routing.
- The TANK model (Sugawara, 1979) – a model with 4 stores (“tanks”) and 7 variable parameters.
- IHACRES (Jakeman *et al.*, 1990) – a model with 7 variable parameters and three stores.

- MODHYDROLOG (Chiew and McMahon, 1994) – full model has 19 variable parameters and 5 stores but can be simplified.
- PE-P (Abulohom *et al.*, 2001) – a single store, 5 parameter model run at a monthly timestep.
- HyMOD (Wagener *et al.*, 2001) – a model with 4-buckets, split between fast-flow route with 3 stores and a single slow-flow bucket, and 6 variable parameters.
- GR4J (Perrin *et al.*, 2003) – a 2-bucket model with 4 variable parameters.
- Pitman Model (Grimes and Diop, 2003) – a 2-bucket model with 11 variable parameters (originally a monthly discharge model by Pitman (1973), and adapted for daily discharge by Grimes and Diop (2003)).

Perrin *et al.* (2003) suggested that increasing the model complexity through increasing the number of variable parameters could lead to overparameterisation, resulting in a loss of model efficiency, demonstrating that 4 variable parameters were optimum for the GR4J model. Chiew and McMahon (1994), studying a model with a possible 19 variable parameters, found that 9 or fewer variable parameters were required for accurate daily streamflow prediction, and even less for temperate catchments.

Additional information can be incorporated into a lumped model to improve its performance, for example Beven and Kirkby (1979) developed the TOPMODEL that incorporates a distributed representation of channel routing using measurement of the catchment topography.

The Pitman lumped CRR model (Pitman, 1973) has been successfully used across Africa, in areas similar to the study area, climatically and in land cover (Wilk *et al.*, 2006, Hughes *et al.*, 2006, and Andersson *et al.*, 2006), and has also been used to model the Bakoye Catchment (Hardy *et al.*, 1989, and Grimes and Diop, 2003). Further discussion regarding the Pitman model can be found in Chapter 6.

Hydrological Model Calibration

As stated by Wagener *et al.* (2003), a hydrological model is the sum of its structure and the calibration of its variable parameters. As discussed earlier, ideally the parameter values would be set through direct measurement in the field of the processes they represent (Wagener *et al.*, 2003). The data for this is most often lacking, and although it can be substituted to some extent by remote sensing (Stisen *et al.*, 2008), almost all models require some parameters to be calibrated against observed data (Wheater *et al.*, 1993).

The methods of calibration are wide ranging and often dependent on the desired outcome, or the role of a particular model e.g. floods forecasting. A full and comprehensive review of hydrological modelling calibration can be found in Beven (2008), particularly in Chapter 6.

There are two principal approaches to hydrological model calibration – manual and automatic (Wagener *et al.*, 2003). Manual calibration can be favoured by

hydrologists, where an expert with extensive working knowledge of a catchment can manipulate the model parameters to produce a satisfactory hydrograph (Boyle *et al.*, 2001). However, such extensive ground knowledge of the Bakoye catchment is not available, and a manual approach would be too subjective to be suitable for a quantitative study of uncertainty propagation.

An automatic calibration approach typically works by minimising an objective function, which is an error score produced when comparing the modelled output data with recorded data. The parameter set that produces the lowest score from the objective function is said to be the 'optimal' set. Gan *et al.* (1997) suggested that the parameter sets produced by an automatic calibration procedure performed on a CRR are unlikely to be uniquely optimal and depend on:

1. The optimisation method/algorithm used
2. The objective function chosen to minimise
3. The calibration data – length and quality
4. The model structure

At the heart of hydrological model calibration is a philosophical debate that it would be inappropriate not to acknowledge at this stage – as it should be at the heart of further research in this area. It is borne out of the issues raised above, such that whilst an automatic and deterministic calibration approach will produce a set of parameters and a hydrograph that statistically fits the data better, an experienced hydrologist may wish to reject the approach as they believe the fitted hydrograph is not the best (Boyle *et al.*, 2001). This argument

led Beven (2006) to propose the 'equifinality' approach to model calibration through the Generalised Likelihood Uncertainty Estimation (GLUE) method (see Freer *et al.* 1996, Beven, 2006, Beven, 2008, amongst others).

The philosophical debate discussed by Beven (2006) is one at odds with the traditional scientific approach of discovering the best description of reality possible, and in hydrological modelling this is the goal to find the 'optimal' model. Equifinality on the other hand does not implicitly reject the idea of an optimal model, but rather accepts a reality where with the current state of the art the discovery of one, single, best model might not be possible. Beven (2006) claims it takes a post-modern approach which acknowledges that there may exist several model structures and several parameters sets that will equally represent the catchment response. As all model structures are extreme simplifications of natural systems (Beven, 1989), then all model structures will be subject to error and, as an extension, any parameter set will also be subject to errors (Beven and Binley, 1992). This is a view supported by Sevenjje (2001), that the hydrological laws are simply laws of averaging and that any parameters are a function of that averaging.

In response to this, the GLUE methodology was developed and introduced by Beven (1989) and also Beven and Binley (1992). GLUE uses a sensitivity analysis of the variable parameters of a defined model structure to produce multiple sets of parameter values, each of which has survived a set 'behavioural threshold' likelihood rejection levels based on its representation of the catchment. The surviving parameter sets are then assigned a new, relative

likelihood score. This ‘fuzzy’ approach allows for the use of hydrological models (structure and calibration) which previously were rejected for not being optimal, despite their error score being close to the optimal model – these may represent the catchment behaviours in a different way (Beven, 2006).

An example of the criticism aimed at GLUE can be found in Thiemann *et al.* (2001), specifically highlighting the elements of “user defined” values, for example the ‘behavioural threshold’. Thiemann *et al.* (2001) argued that such values are subjective, proposing that a Bayesian based approach is superior and more rigorous. Beven (2006) acknowledges these criticisms and suggests that it is, again, a matter of philosophy.

Given the goals of this thesis, and the significant additional complexity that a GLUE method would introduce, an optimal model based approach is the most suitable. However, the merits of the equifinality thesis should be acknowledged and should form the composition of further research in this field. A further discussion of automatic calibration methods and the methodology used in this thesis can be seen in Chapter 6.

Additional sources of uncertainty in hydrological models

In addition to the types of uncertainty discussed previously in this Chapter, there are other sources which influence the accurate modelling of catchment discharge. The influence of observation data uncertainty has been discussed in

Section 2.2 but only in the context of precipitation input uncertainty. However, the driving input is not the only source of observation data.

As discussed previously, the calibration of parameters is often performed by minimising an objective function when comparing recorded output and modelled output data, commonly discharge. Di Baldassarre and Montanari (2009) highlighted the influence that uncertainty within the recorded discharge may have on hydrological modelling – these uncertainties emerge from inaccuracy in the measuring instruments and unsteady flows during measurements, when using a traditional velocity-area method.

Many hydrological models, including the Pitman model, incorporate evapotranspiration data as part of the modelling process. This too is a potential source of uncertainty. A discussion of the sources and value of evapotranspiration data for hydrological modelling can be seen in Chapter 3.

Hughes (1995) also highlighted poor interpretation of output data as a source of uncertainty. This is most likely to be an issue when using a manual calibration technique, but should not be viewed as a source of uncertainty when using an automatic calibration method (any uncertainty here can be classified as parameter or structural uncertainty).

In addition to each of the above, it is also likely that uncertainty within the measurement of rainfall by the raingauges will also have a cascading effect on the modelling process. The uncertainties of raingauge measurements can be

large, with Nespor and Sevruk (1998) suggesting that the influence of wind alone on a raingauge measurement was on average between 2% and 10%. A full analysis of raingauge measurement error is not proposed as part of this thesis, but a conservative estimate of the errors in the order of up to 10% should be considered when observing the data used in this thesis

Although each of these sources of uncertainty discussed are legitimate, they are likely to be minor and any attempts to quantify them and their influence is beyond the scope of this thesis. In essence the uncertainty from each will be regarded as negligible but with a note of caution against such an assumption.

2.6 - Summary

This chapter has argued that when SRFE are used to drive a hydrological model there are a multitude of sources of uncertainty that need to be addressed, principal amongst those being input uncertainty, model parameter uncertainty and model structure uncertainty. It is inappropriate to consider any of these sources of uncertainty as negligible or trivial in regards to the final output, and it should be anticipated that they will interact with each other in complex and non-Gaussian ways.

Whilst model parameter and model structure uncertainties have been widely researched, with established methods of measuring, managing and minimising them, the influence of input uncertainty has often not been investigated in full detail. Previous studies have focussed on representing the uncertainty within a

rainfall input by using perturbation methods which only alter the rainfall rate.

They have not fully characterised the spatio-temporal distribution of uncertainty within the estimates, and this was highlighted by McMillian *et al.* (2011) as a critical research need.

The main aim of this thesis is to demonstrate a methodology for characterising the full spatio-temporal distribution of uncertainty within a SRFE, for use as a driver for a hydrological model, showing how this uncertainty propagates through the model when using traditional hydrological modelling methods for reducing and measuring model parameter and structure uncertainties. The thesis demonstrates not only that this method can be successfully implemented for a sparsely gauged region, but that the method is superior in representing uncertainty compared to simpler perturbation methods.

3

Study Area and Context

3.1 – Introduction

The previous chapter has described the general literature around satellite rainfall estimation and the use of SRFE in hydrological modelling. The need for SRFE was highlighted, especially in areas with a paucity of ground instrumentation recording rainfall – such as radar and raingauges. This chapter will expand upon this with a strong focus on the Sahel region of Africa, within which the Senegal Basin and Bakoye catchment study areas belong. The dire necessity for improved uncertainty characterisation, measurement of propagation and better communication of the uncertainties is also a focus.

The second half of this chapter will take a close look at the Senegal Basin and Bakoye catchment study areas, focussing on the aspects that may have an influence on the experiments in this thesis, as well as looking at the raw data available and how these relate to the study area characteristics ascertained.

3.2 – The Problem in Context

The variability of rainfall in the Sahelian region of Africa is a major factor in food and water resource security for the area. In semi-arid regions, of which the Sahel is typical, rainfall displays great temporal and spatial variability over several temporal periods (Ali *et al.*, 2003). As agriculture is almost completely rain-based crops (Ali *et al.*, 2003), the region is sensitive to this variability and the Commission for Africa report (2005) listed extreme weather events as one of the main reasons why food insecurity is still prevalent, and is potentially a reason why Sultan *et al.* (2005) found that the Sahel was the only region in the world where food production per capita had reduced in the previous twenty years.

The availability of water, and therefore rainfall, is vital to the agriculture of the region. Nicholson (1993) showed how the Sahelian rainfall can vary, with drought conditions prevalent in the 1980s, after two decades of high rainfall, though more recent studies have suggested that rainfall is again increasing and the drought becoming less persistent (Nicholson, 2005).

The Commission for Africa (2010) claimed that climate change is expected to have a particularly damaging effect on the African continent, with the following possibilities:

- Expansion of deserts
- Increase of floods and droughts

- Reduced crop yields and availability of agricultural land
- Increased food insecurity and malnutrition
- Increased prevalence of severity of disease, like Malaria
- Damage to land and property from environmental disasters
- Damage to biodiversity and ecosystems

The Commission for Africa (2010) suggested that a high proportion of Africa's agricultural land is dependent on rainfall alone, largely due to a lack of irrigation, and this is particularly important as many African economies are dependent on agriculture and are therefore vulnerable to impacts of climate change.

The Sahel area of Africa is experiencing climate change that is likely to put strain on the water resources (Andersen *et al.*, 2001). This strain on the water resources could lead to political and humanitarian issues on the area, and Andersen *et al.* (2001) describes the region as a potential conflict area because of attempts to manage the resources, such as large irrigation schemes and dam construction. Climate change, along with urbanisation, poverty and inequality, is listed as a possible reason for future conflict in Africa by the Commission for Africa (2010).

Vorosmarty *et al.* (2010) analysed the potential threats surrounding the world's fresh water resources, using rivers as a focus, in regards to risks to human water security and also the biodiversity of the rivers, from influences of human activities like anthropogenic climate change, land use changes and industrialisation. The potential threats were weighted against nations' ability to

invest in engineering works to maintain or improve the water security, without damaging the biodiversity of the rivers. The study found that the Sahel region was an area with a high risk to its human water security and to its biodiversity.

However, any study into the possible future effects of rainfall variability could never demonstrate the impact it has as effectively as the unfolding disasters that are all too evident, with the real outcomes of people being displaced or dying from thirst, famine or disease. This reality became all too prominent during the Horn of Africa drought that affected Ethiopia, Uganda, Kenya, Somalia and Djibouti in 2011, as low rainfalls resulted in water shortages and crop failures (Water Aid, 2012).

The “A Dangerous Delay” Report

The “A Dangerous Delay” report (Hillier and Dempsey, 2012), jointly published by Save the Children and Oxfam in 2012 (referred to henceforth as ADD12), highlighted the Horn of Africa drought as the worst hunger crisis this century, but one that was utterly avoidable. ADD12 stated that the drought represents the latest in what it described as a systematic failure of the international system, where early warning of the drought was given but not heeded and acted upon.

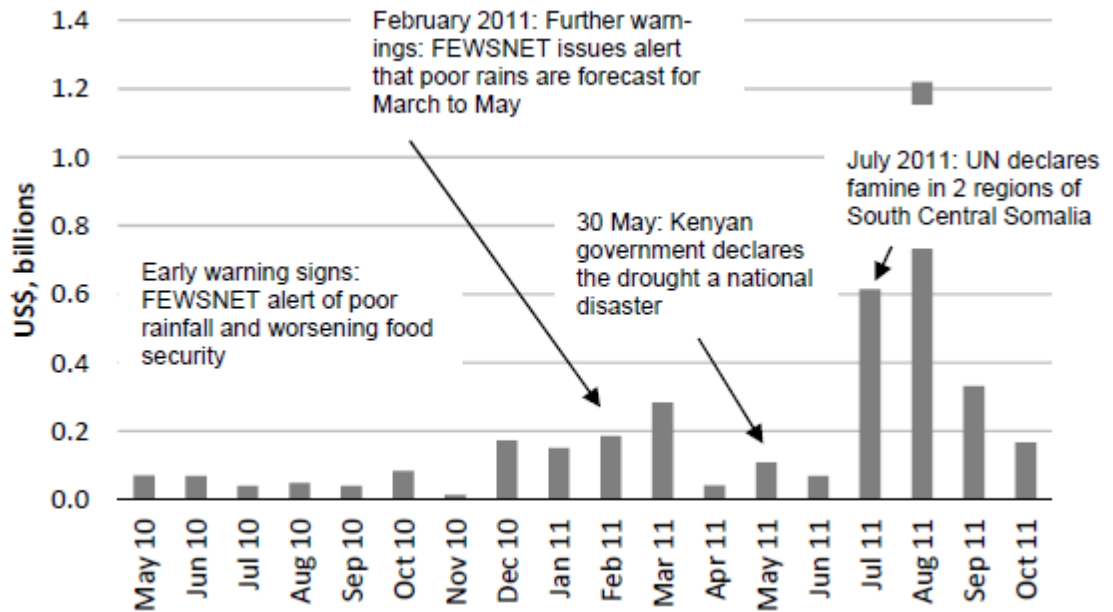


Figure 3.1 – Timeline showing the unfolding of the Horn of Africa drought in 2011, detailing the timing of early warning alerts and the delivery of aid (ADD12, source given as OCHA Financial Tracking Service).

The unfolding of the events of the Horn of Africa drought in 2011 can be seen in Figure 3.1. The early warning alerts for a crisis first came in August 2010, mainly due to the predictions of changing weather patterns linked to La Nina, which were increased in November as the winter rains were predicted to be poor. The predictions were correct and a drought began to unfold, and the early warning systems also warned of a failure of the March to May rains, suggesting that even average rains would result in famine conditions.

It was not until the drought had taken grip, causing famine conditions to develop, that the international community responded. The report shows that a window of opportunity to take preventative action existed between November 2010 and March 2011, but the actual emergency response did not reach

capacity until April 2011, months after several declarations of emergency had been issued.

The conclusion of the report was that the international response to the disaster was too late, and when it did arrive it was still too small. The crisis affected 13 million people and estimates of those who died in the crisis are given between 50,000 and 100,000, with half of those under the age of five. On top of this there was widespread malnutrition, and with a quicker response many of the deaths and displacements could have been avoided.

In short, the report showed that the delay unnecessarily cost lives. A major contributor to this was misunderstanding and miscommunication of the uncertainty when using EWS, and thus failing to convince governments and agencies to act. The solution proposed by ADD12 was to produce a risk matrix of probability of a risk and the impact of that risk, with a specified threshold that would trigger an emergency response – in order to do this the uncertainty of an EWS forecast needs to be quantified to establish the probability of the risk.

Early Warning Systems (EWS) and Uncertainty

The ADD12 report showed how EWS are useful for forecasting possible droughts, famines and other crises. However, although the EWS were found to be wholly correct in their predictions of the Horn of Africa, the uncertainties within the EWS were poorly understood and communicated to governments and agencies responsible for acting upon the warnings.

The EWS that was highlighted in ADD12 was the Famine Early Warning Systems Network (FEWSNET), administered by the United States Agency for International Aid (USAID) and incorporating several private institutions and US government agencies, such as the United States Geological Survey (USGS), the National Aeronautics and Space Administration (NASA), the National Oceanographic and Atmospheric Administration (NOAA) and the United States Department of Agriculture (USDA).

A key component of FEWSNET is drought monitoring, for which it utilises several satellite data products for early detection for indication of drought, including the Normalised Difference Vegetation Index (NDVI) and Satellite Rainfall Estimates (SRFE) (Verdin *et al.*, 2005). Flood risk also poses a threat to food security in Africa and FEWSNET uses SRFE to monitor potential flood hazards, although this has proven more difficult due to a paucity of ground data required to replicate more conventional methods (Verdin *et al.*, 2005).

A major factor in dealing with uncertainties in EWS is communicating them clearly, and putting in place guidelines for action based on uncertain forecasts. A good example of this is demonstrated in Braman *et al.* (2012), which examined the Early Warning, Early Action (EWEA) strategy. EWEA works from medium and long range flood forecasts and puts in place low cost efforts that are not wasted if the forecast proves inaccurate – such as training local volunteers and deploying non-perishable relief items. Braman *et al.* (2012)

showed that the EWEA strategy was effective using the West African floods of 2007 and 2008 as a case study.

The Origin of Uncertainty

To understand why governments and agencies delayed action in response to uncertainty within EWS, the understanding of what is meant by uncertainty must be clearly defined, from the point of view of the scientific field and that more general accepted in the public arena.

The Collins English Dictionary gives the definition of ‘uncertain’ and thus ‘uncertainty’ as:

“not able to be accurately known or predicted; not able to be depended on; changeable” – (Collins, 2012, page 619)

It is hardly surprising that when faced with an ‘uncertain’ EWS alert that a government or agency would be reluctant to act upon it, given the generally accepted definition claims that it cannot be depended upon. However, in the scientific field, this is not what is meant when referring to uncertainty. Beven (2008) briefly defines uncertainty in the context of an environmental model simply as the risk of it being wrong.

This is a problem that permeates the public perception of science that goes beyond the field of hydrometeorology, and the issue of uncertainty in

environmental models. May (2011) described how, due in part to the way science is communicated or used in education, it is often seen to be 'certain', yet in reality and within the scientific community it is seen as organised scepticism – the public perception of science does not admit debate or uncertainty.

Palmer and Hardaker (2011) took this further and claimed that any prediction that does not acknowledge the existence of uncertainty has no basis in science at all, highlighting the pressing need for the use of probabilistic methods and for improved ways of communicating uncertainty, especially in terms of decision making. Smith and Stern (2011) suggested that scientists have an important role in the decision making process, where instead of just presenting results the community should engage and converse with policy-makers regarding uncertainty – in this role the most immediate aim of the scientist is not to actually reduce uncertainty, but to quantify it and communicate it more clearly.

Beven (2008) suggested that uncertainty is a concept applicable to environmental models that is often underplayed or misunderstood and highlights the issues of quantifying and communicating this risk - the problem of researchers not adequately communicating the uncertainty of their model predictions derives from the fact that it tends to confuse decision makers, and many go so far as to ignore the uncertainty in their models by not reporting them or even not attempting to calculate them.

Beven and Feyen (2002) noted that identifying ways to best visualise and present uncertainty was a key question to be answered in the field of hydrological modelling. This can be applied to the field of environmental modelling, yet in order to be able to do that the uncertainty needs to be properly defined and quantified beforehand.

Gourley and Vieux (2006) claimed that to calculate the uncertainty in an environmental model prediction, the uncertainty of a number of areas needed to be individually determined. These areas are given as:

- Model inputs
- Boundary and initial conditions
- Model parameters
- Model representations of physical processes
- Model numerical formation, and
- Observations of the system behaviour.

These areas of uncertainty above affirms the view of Beven (2008) that an environmental model's uncertainty comes from the uncertainty within the input, and the model's structure (which encompasses the next four points).

Observations of the system behaviour are used to evaluate the model output, for example in a hydrological model this might be recorded river discharge data – these are often used to calibrate the model parameters so any uncertainty within the observations will contribute to the model structure error. A simplified

schematic of the sources of uncertainty in a hydrological model can be seen in Figure 3.2.

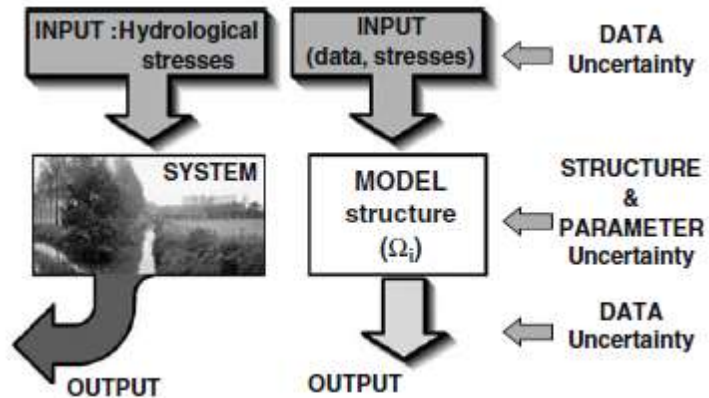


Figure 3.2 – A schematic showing the main sources of uncertainty in a hydrological model (from Vazquez *et al.*, 2009).

It is logical that the more an environmental model is based on reality, derived from the physical properties of the system it purports to represent, the better the output will be. However, such ‘physics’ or ‘physical’ models require a large quantity of high resolution data about the system in order to operate (Wagener *et al.*, 2001). Grayson *et al.* (2002) highlighted the relationship between data availability, model complexity and the performance of an environmental model, suggesting that an optimum model complexity exists which captures the full detail availability but without extrapolating to finer spatio-temporal resolutions. Figure 3.3 shows this relationship.

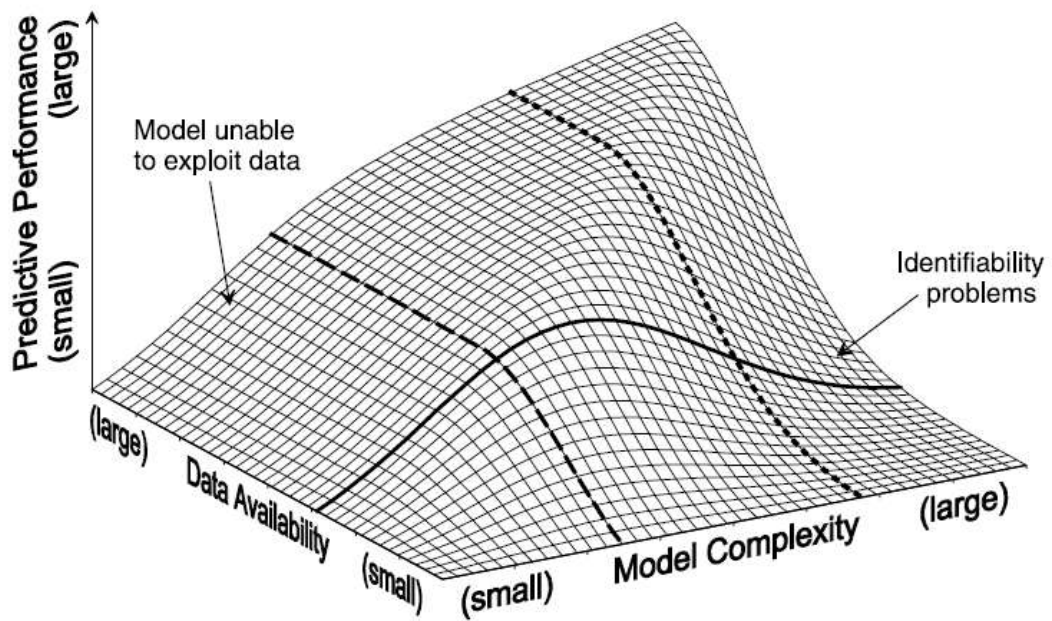


Figure 3.3 – Schematic demonstrating the relationship between data availability, model complexity and the predictive performance of an environmental model, showing where the optimum model complexity exists (from Grayson *et al.*, 2002).

What Grayson *et al.* (2002) and the schematic in Figure 3.3 demonstrate is that the model input is not only a source of uncertainty, but also dictates the complexity that the model structure itself can take. In the context of EWS models for sub-Saharan Africa, their performance and development, including any attempts to quantify and reduce the uncertainty within them, is intrinsically linked the data available to drive them.

The State of Data Availability in Sub-Saharan Africa

Although the EWS models used in sub-Saharan Africa make use of a multitude of data sources, both ground based and remotely sensed, one of the most

important data inputs required, in particular for drought or flood monitoring, is a real time measurement of rainfall.

Ground measurements of rainfall in Africa have historically been very poor, with almost no precipitation radars available and most regions being covered by only sparse networks of raingauges (Washington *et al.*, 2006).

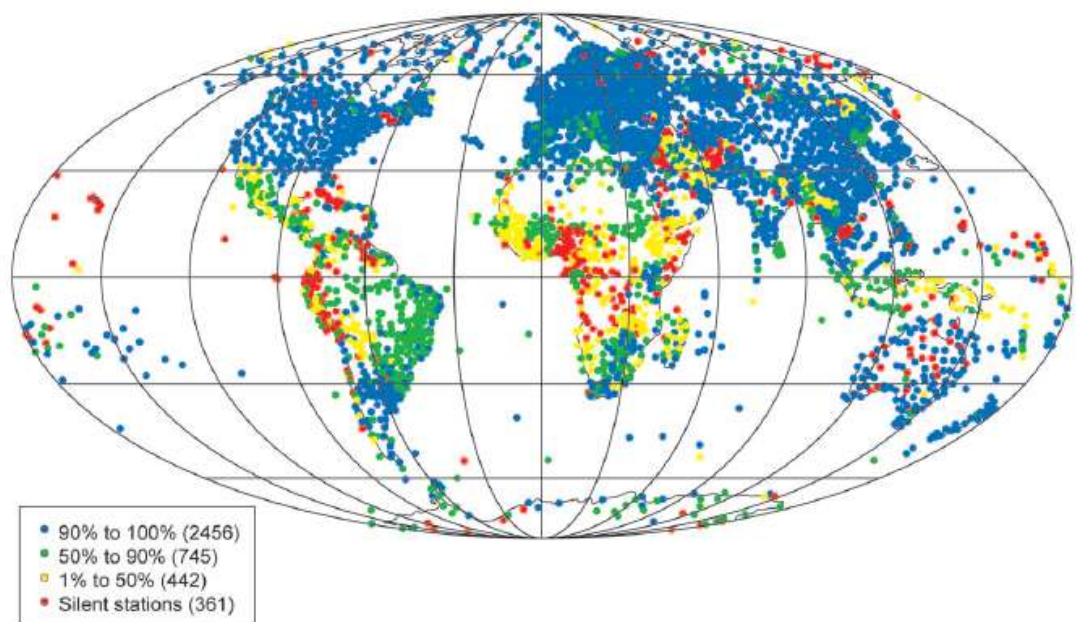


Figure 3.4 – The global distribution of raingauges that are part of the World Meteorological Organisation’s (WMO) World Weather Watch (WWW) Regional Basic Synoptic Network (RSBN) in 2003. Each raingauge station is colour coded dependent upon its reporting rate (from Washington *et al.*, 2006).

Figure 3.4 shows the distribution of raingauge stations that form part of the World Meteorological Organisation’s (WMO) World Weather Watch (WWW) network. It is clear that compared to much of the rest of the world, sub-Saharan Africa is far less densely covered, and of those raingauges covering the region

many report less than 50% of the time. This pattern can also be seen in Latin America.

In 2003 the raingauge density of the Regional Basin Synoptic Network (RBSN) for Africa was just 1 gauge per 26,000km², far below the WMO's own guidelines (Washington *et al.*, 2006).

Washington *et al.* (2006) attributed a lack of investment in both data recording infrastructure, and in the scientists necessary for its operation, as reasons for this situation, stressing that there is a lack of (though increasing) political will to improve data acquisition due to more pressing concerns.

Numerical weather predictions (NWP) could potentially offer an alternative but require ground data in order to be calibrated, with current efforts focussed on mid-latitudes resulting in a loss of predictability for areas in the tropics experiencing convective rainfall (Washington *et al.*, 2006).

Recently the 2002-2008 African Monsoon Multidisciplinary Analyses (AMMA) has increased the density and reliability of the raingauges in Sahelian West Africa (Greatrex, 2012), but there still exists only a sparse network.

The Trans-African Hydro-Meteorological Observatory (TAHMO) is an ambitious project that aims to install 20,000 raingauges across sub-Saharan Africa, increasing the gauge network density to 1 gauge per 30km (Hut and van der Giesen, 2010, TAHMO, 2012). To achieve this each station would cost less

than \$US200, reporting automatically using the mobile telecommunications network and sited in schools, incorporating them into local educational projects. To date the project has produced the acoustic disdrometer, each costing less than \$US10 to produce and records rainfall using a microphone, reporting the data via the mobile telecommunication network: it has been successfully tested in Tanzania (TAHMO, 2012).

Despite the ambitions of the TAHMO project and the progress made via the AMMA project, there still exists a paucity of ground recorded rainfall for sub-Saharan Africa and a requirement for an alternative method of collecting real time rainfall data to drive environmental models and EWS.

Satellite Rainfall Estimates (SRFE)

As discussed earlier in this chapter, the FEWSNET EWS uses SRFE as an input for both its drought monitoring and flood monitoring models (Verdin *et al.*, 2005). The benefit of using SRFEs are that they can be retrieved at real-time, or near real-time, and can show a greater spatial resolution than estimates derived from a sparse raingauge network alone (Hardy *et al.*, 1989).

There are two main sources of satellite data for use in producing SRFE (Dinku *et al.*, 2010) –

- Thermal-Infrared Imagery (TIR)
- Passive Microwave (PM)

TIR imagery is often based on geostationary platforms and SRFE using this data will infer rainfall location and rate based on an indirect statistical relationship between cloud top temperature and rainfall, whilst PM sensors are able to directly record the location and rate of rainfall but are based on platforms in lower, polar orbits resulting in a coarser temporal resolution (Dinku *et al.*, 2010).

SRFE estimates have proven successful as an input in several different types of environmental models, including Malaria EWS monitoring (Grover-Kopec *et al.*, 2005), crop water monitoring (Verdin and Klaver, 2002), crop yield models (Reynolds *et al.*, 2000) and hydrological modelling (Grimes and Diop, 2003, Andersen *et al.*, 2002, Sandholt *et al.*, 2003).

However, when operating at high spatio-temporal resolutions the indirect relationships used by SRFE result in high levels of uncertainty (Bellerby and Sun, 2005). The indirect relationship between rainfall and the satellite data available is often calibrated using ground instrumentation and climatic data, but these relationships are non-stationary – temporally and spatially – and non-linear (Nikolopoulos *et al.*, 2010). As already shown, sub-Saharan Africa has a paucity of ground instrumentation available to calibrate (and validate) SRFE, further increasing the uncertainty.

Teo (2006) and Teo and Grimes (2007) demonstrated how the uncertainty within the TAMSAT SRFE can be characterised using a stochastic ensemble

approach. Each ensemble rainfall estimate was a unique yet equiprobable realisation of the rainfall field, as established using a sparse historic raingauge network for calibration. The full ensemble of SRFEs was used to drive the Generalised Large Area Model (GLAM) crop yield model.

Teo and Grimes (2007) demonstrated that a stochastic ensemble approach could be used to successfully characterise the uncertainty within a SRFE, and showed how this can be applied to a crop yield model, such as those utilised by EWS in sub-Saharan Africa. Hydrological models are a significant component of EWS, for drought and flood monitoring, and also make significant use of SRFE. The TAMSIM method developed by Teo (2006) has yet to be applied to a hydrological modelling context and this is a significant aim of this thesis.

3.3 – Description of the Study Area

The Sahel is a region of sub-Saharan African that lies in a belt across the continent, from the Atlantic Ocean to the Red Sea. The name derives from the Arabic word for coast, or shore, as it appears as a 'coastline' against the expanse of the Saharan desert, a 5,400km stretch across east to west, varying in thickness across the continent. In total it crosses the borders of 12 countries – Senegal, Mauritania, Mali, Burkina Faso, Algeria, Niger, Nigeria, Chad, Sudan, South Sudan, Ethiopia and Eritrea.

The main method for identifying whether a region falls within the Sahel is through observation of physical features, such as the climate, soil types and the

vegetation cover (Koechlin, 1997). Koechlin (1997) describes the principal characteristics Sahelian regions display, and these are summarised below –

Climatic Characteristics

The climate of the Sahel is largely driven by two air currents. The Harmattan is dry and dusty, flowing north-east to east between December and March, whilst the Saint Helen anticyclone flows south-west to west and is humid. The two air flows cause the Intertropical Front (ITF) to fluctuate, driving the transitions between the wet and dry seasons. The wet season usually falls between April and October but varies locally.

Soil Characteristics

The Sahel is dominated by three major soil types:

- Dune Soils
- Soils richer in fine particles, over a bedrock of granite, metamorphic or sandstone geologies
- Soils on a hardpan

Most of the soils in the Sahel are thin and often compact, allowing for little permeability and promoting surface runoff.

Vegetation Characteristics

The vegetation of the region ranges from herbaceous shrubs to steppe or savannah like flora. Only in the southern most regions of the Sahel would woodland and forest plants be found.

Koechlin (1997) also proposed splitting the Sahel into four further sub-regions and these have been summarised in Table 3.1.

Sub-region	Annual Rainfall (mm)	Length of Wet Season (months)	Vegetation
Sub-desert sector	200-250	2 or less	Herbaceous to shrub steppe
Sahelian sector	200-550	2-4	Steppe, shrubby, wooded
Sub-Sahelian sector	550-700	4-5	Steppe to savannah transition
North Sudanese sector	750-1000	5-6	Wooded savannah, hard grasses

Table 3.1 - Characteristics of Sahelian sub-regions (after Koechlin, 1997)

The extent of the West African savannah associated with the Sahel is shown in Figure 3.4. The characteristic shape of the Sahel can be seen, with it forming a band from west to east, with the Sahara forming the northern boundary (taken as the limit of cultivation), and the southern boundary being the start of the forested environment.

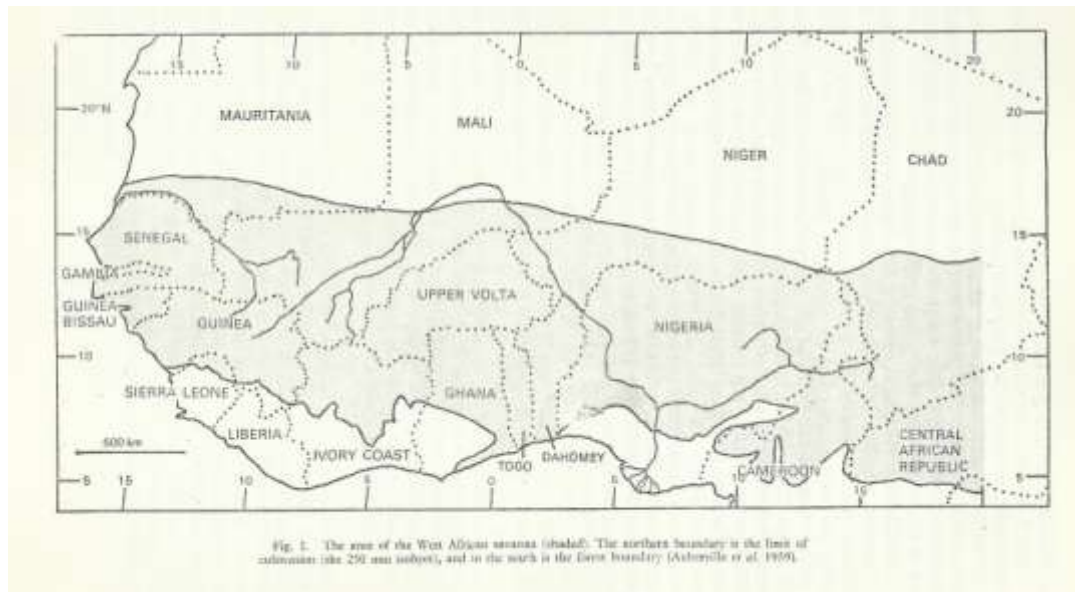


Figure 3.5 - The boundaries of the West African savannah (Jones and Wild, 1975)

Climate

As shown by Koechlin (1997), and in Table 3.1, the Sahel region displays a large gradient in rainfall, with little rainfall towards the north, and far greater rainfall in the south. This distribution of rainfall is shown in Figure 3.6, where the mean annual rainfall at the northern boundaries is as low as 100mm, whilst it exceeds 1600mm in the south.

Jones and Wild (1975) noted that the rainfall in the area is characteristically aggressive, falling in intense storms. This is particularly marked in the northern areas. Various studies have shown high rainfall intensities, including $52\text{mm}\cdot\text{hr}^{-1}$ in Senegal, over $200\text{mm}\cdot\text{hr}^{-1}$ in Ghana and a peak intensity of $290\text{mm}\cdot\text{hr}^{-1}$ in Nigeria (Jones and Wild, 1975).

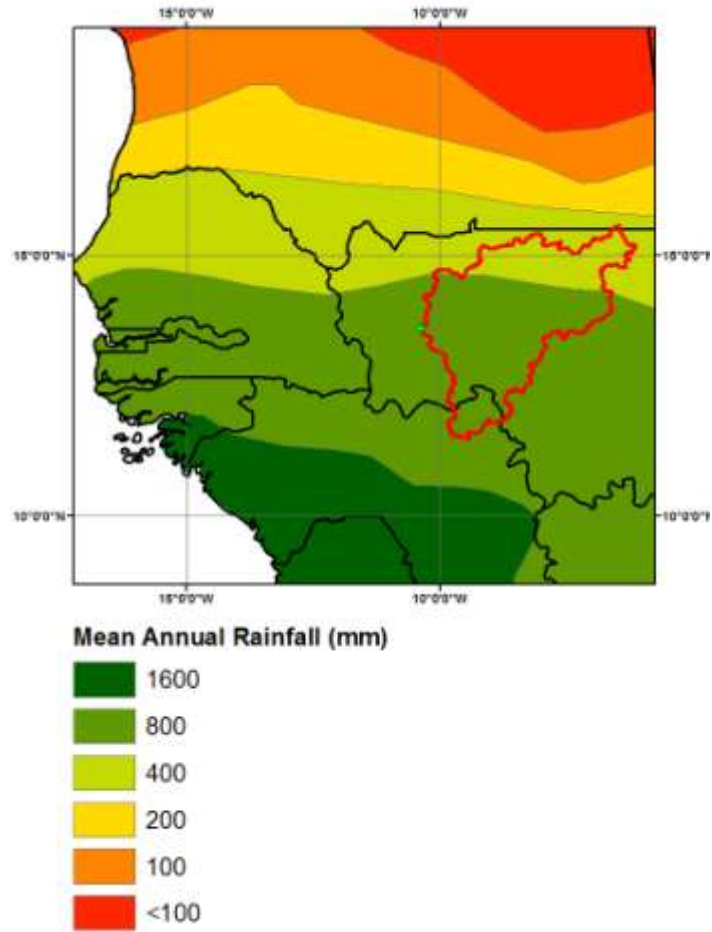


Figure 3.6 - Isohyets of mean annual rainfall (mm) for the Western Sahel (after Jones and Wild, 1975) – The Bakoye catchment is outlined in red and the Oualia gauging station is highlighted by the green dot.

As well as the steep north-south gradient for mean annual rainfall, the same gradient is evident in regards to the initiation and length of the wet season. Figure 3.7 shows the gradient – for the Sahel region, the north has a short, three month wet season beginning in July, and the south largely a 6 month wet season, beginning in April (Jones and Wild, 1975).

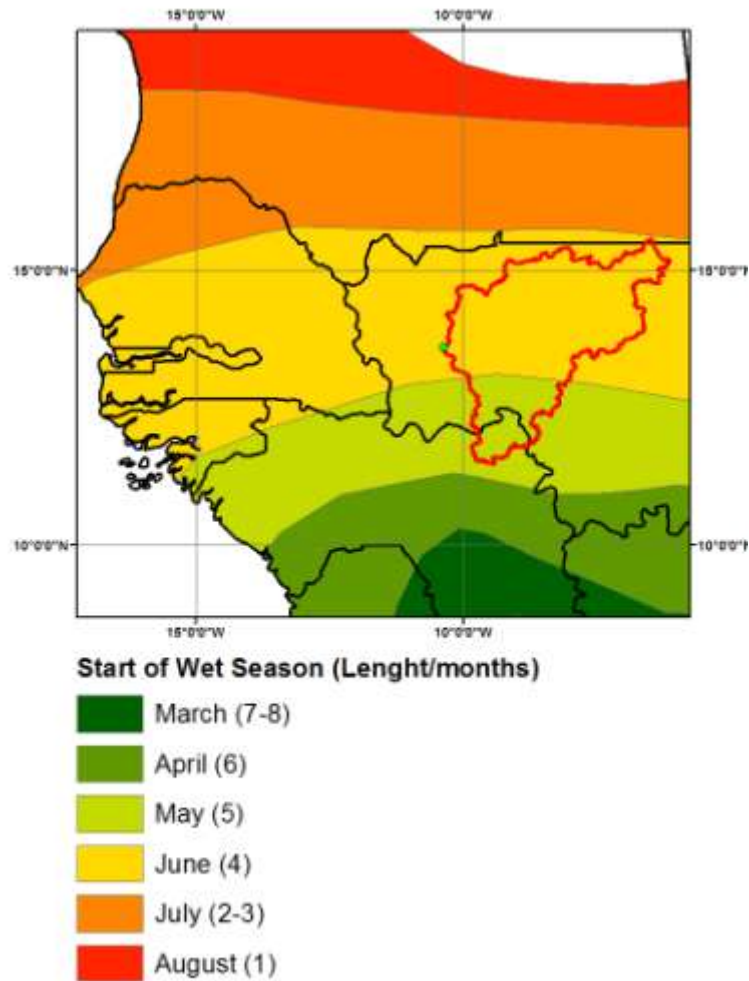


Figure 3.7 – Map showing the extent of the wet season across West Africa, showing the month the wet season begins and the number of months where mean rainfall is >50mm (after Jones and Wild, 1975) – The Bakoye catchment is outlined in red and the Oualia gauging station is highlighted by the green dot.

As would be expected, the mean annual rainfall and length of the wet season has an effect on the ability to grow crops. Figure 3.8 shows the length of the growing season across Western Africa – again this shows a large north-south gradient, rapidly increasing southwards.

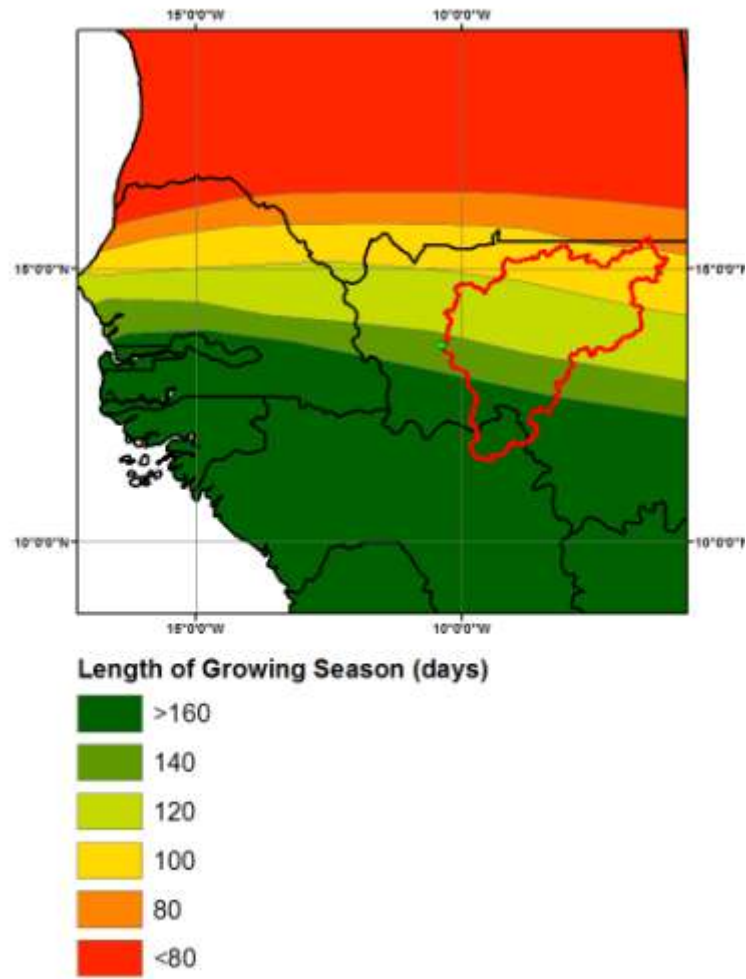


Figure 3.8 - The length of the growing season, in days, across Western Africa (after Jones and Wild, 1975) – The Bakoye catchment is outlined in red and the Oualia gauging station is highlighted by the green dot.

The length of the growing season is linked to the relationship between potential evapotranspiration (PET) and rainfall, where over the entire year in the Sahel the PET exceeds the mean annual rain, but during the growing season the rainfall is intense enough to create an excess (Jones and Wild, 1975).

Jones and Wild (1975) suggested that the Sahelian growing season can be categorised into five distinct periods:

1. Preparatory period – rainfall is below PET but sufficient for cultivation
2. First intermediate period – rainfall close to PET, sufficient for sowing and some growth
3. Humid period – rainfall exceeds PET
4. Second intermediate period – rainfall close to PET
5. Reserve period – PET exceeds rainfall, growth dependent on soil moisture reserves

From north to south the humid period increases in length, along with the overall growing season length, yet the other stages decrease in length (Jones and Wild, 1975).

Similarly the influence of the climate has an input on the natural vegetation of the region, and a generalised map of the vegetation zone across West Africa can be seen in Figure 3.9.

It can be seen from the maps in Figure 3.6 to 3.9 that the Bakoye Catchment straddles many climatic areas, in terms of mean annual rainfall, length of wet season and vegetation zones. The majority of the catchment falls within the area where the wet season can be expected to begin in June and last for four months, and has a mean annual rainfall between 400-800mm. Vegetation is varied across the catchment, with growing seasons lasting 80 days in the north, and over 160 days in the south, and the catchment is almost equally divided between the Northern Guinea, Sudan and Sahel vegetation zones.

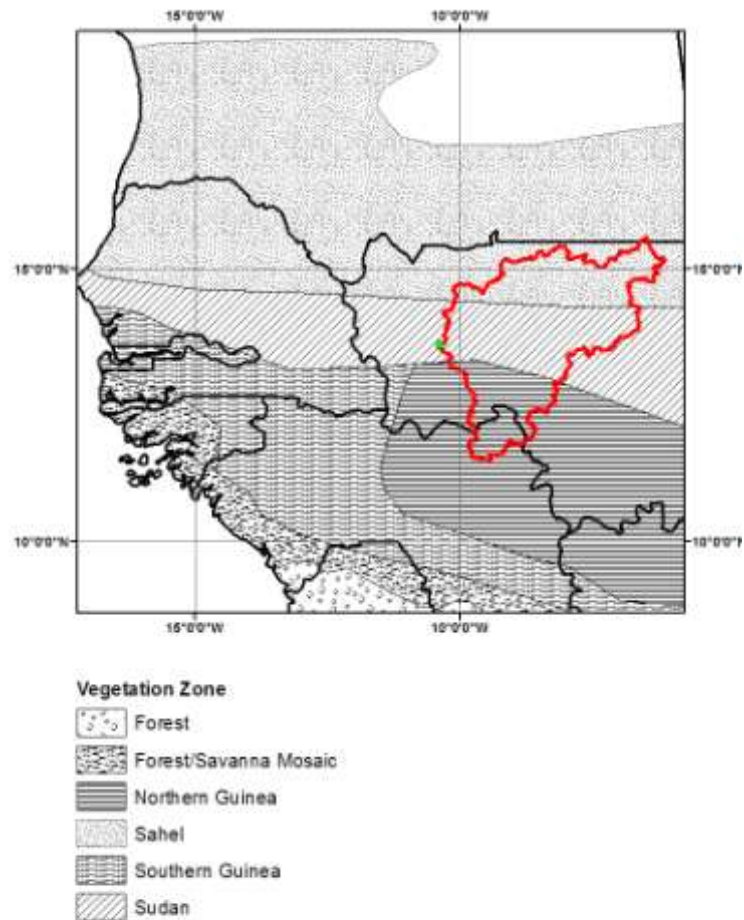


Figure 3.9 – Map showing the generalised vegetation zones across West Africa (after Jones and Wild, 1975) – The Bakoye catchment is outlined in red and the Oualia gauging station is highlighted by the green dot. Northern Guinea – savannah. Sahel – wooded steppe. Southern Guinea – relative moist undifferentiated savannah. Sudan – relatively dry undifferentiated savannah.

Geology and Soil

Jones and Wild (1975) showed there to be a difference between the north and the south in regards to rock types. The rocks of the south are dominated by

granites, and granite-derived metamorphic rocks, yet the north is largely unconsolidated sands. Some areas in Mali, Senegal and Mauritania have large areas of rocks associated with marine conditions, including conglomerates, sandstones and clays. The lack of base-rich primary and volcanic rocks in the region was highlighted.

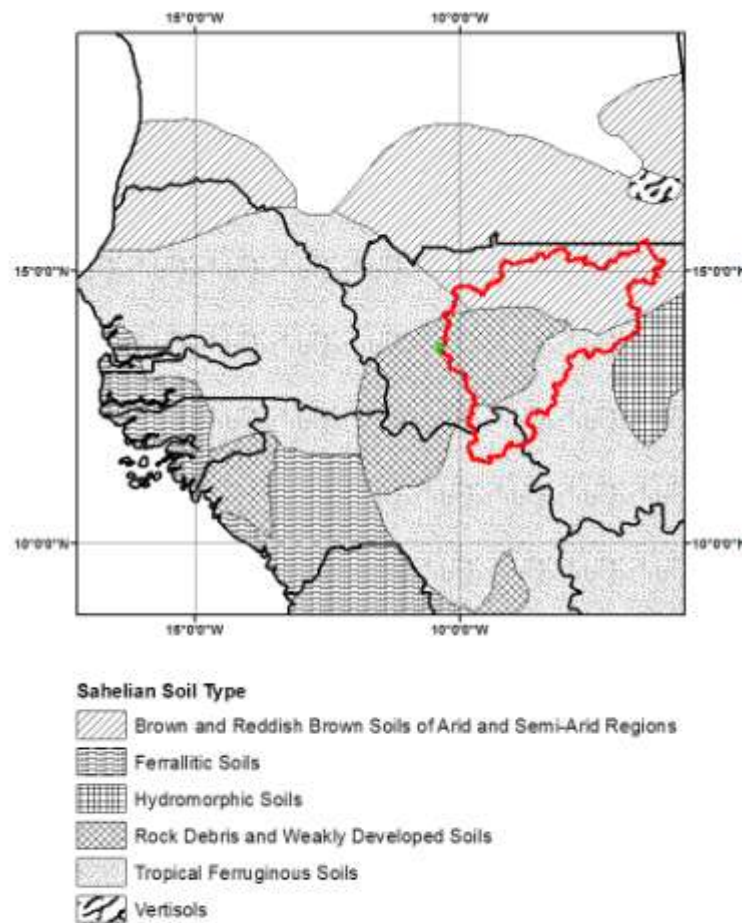


Figure 3.10 - Generalised soil type distributions across the West African savannah (after Jones and Wild, 1975) – The Bakoye catchment is outlined in red and the Oualia gauging station is highlighted by the green dot.

Figure 3.10 shows the generalised soil type distributions across the region. Jones and Wild (1975) suggested that the climate and vegetation have a greater influence on the soil type than the parent material. The land surfaces are predominantly from the late Cenozoic, with some older early Cenozoic areas, with the soils having undergone several cycles of deposition and erosion, resulting in the evidence of significant transportation and mixing. Younger surfaces are restricted to the proximity of major rivers.

It can be seen in Figure 3.10 that the soil distributions broadly shows a north-south gradient in the same way as the mean annual rainfall. Jones and Wild (1975) saw this as a possible relationship, suggesting that the climate drives the leaching and weathering rates, resulting in shallower soil profiles in the north. The lack of vegetation towards the north also exposes the surface to heavier erosion. In addition there is the potential for feedbacks from the land surfaces that can define and/or reinforce the rainfall gradient in the Western Sahel (Taylor and Lebel, 1998).

The Bakoye catchment itself shows significant heterogeneity of soil types across its extent, with red/brown arid type soils in the north (corresponding with the Sahel vegetation zone in Figure 3.9), tropical ferruginous soils in the south and east, and weakly developed rocky soils in the west.

Topography

The Bakoye catchment also displays significant heterogeneity in topography across its extent, as demonstrated in Figure 3.11 which shows the elevation across West Africa as available from the National Geospatial-Intelligence Agency (NGA, 2006).

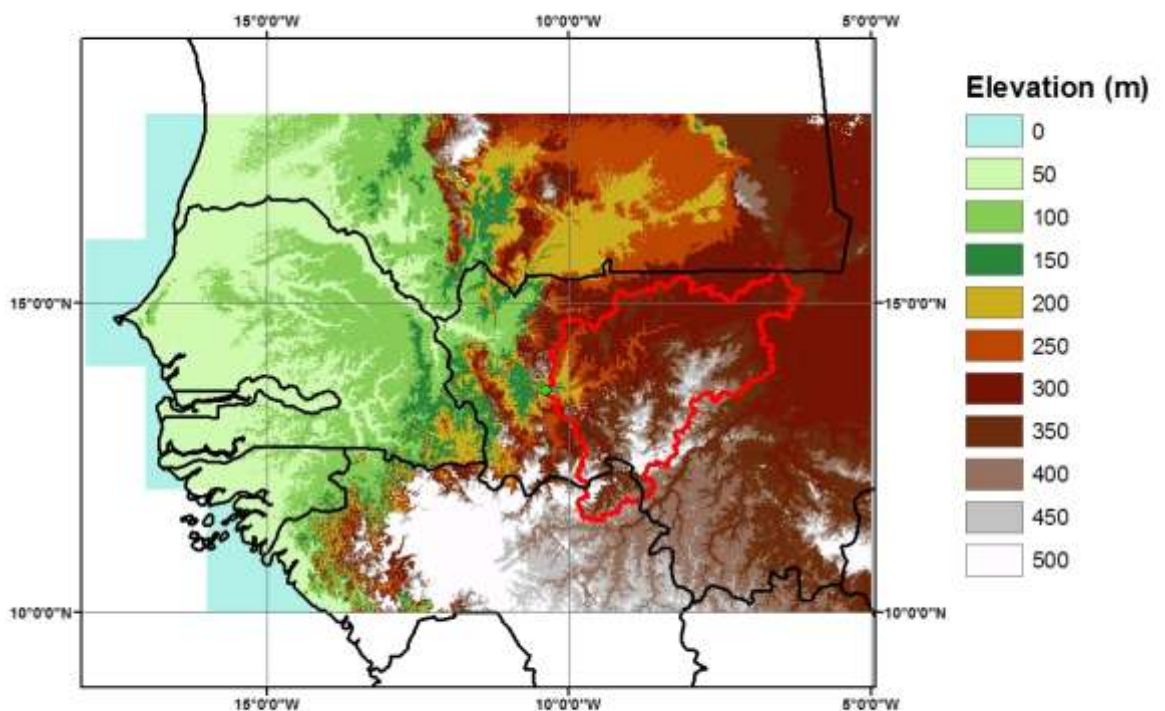


Figure 3.11 – Map showing the topography of West Africa – The Bakoye catchment is outlined in red and the Oualia gauging station is highlighted by the green dot (Elevation data from NGA, cited 2006).

The elevation across the West African region can be seen to vary between highlands in the south, largely within Guinea and Mali, with lowlands to the north and west, particularly along the course of the River Senegal and the Gambia where the elevation is almost wholly below 250m. The Bakoye

catchment shows significant variations, the south and east are mountainous areas, and the height decreases towards the north. Most of the catchment is above 250m elevation, but falls rapidly towards the outlet at the Oualia gauging station.

Natural Hazards

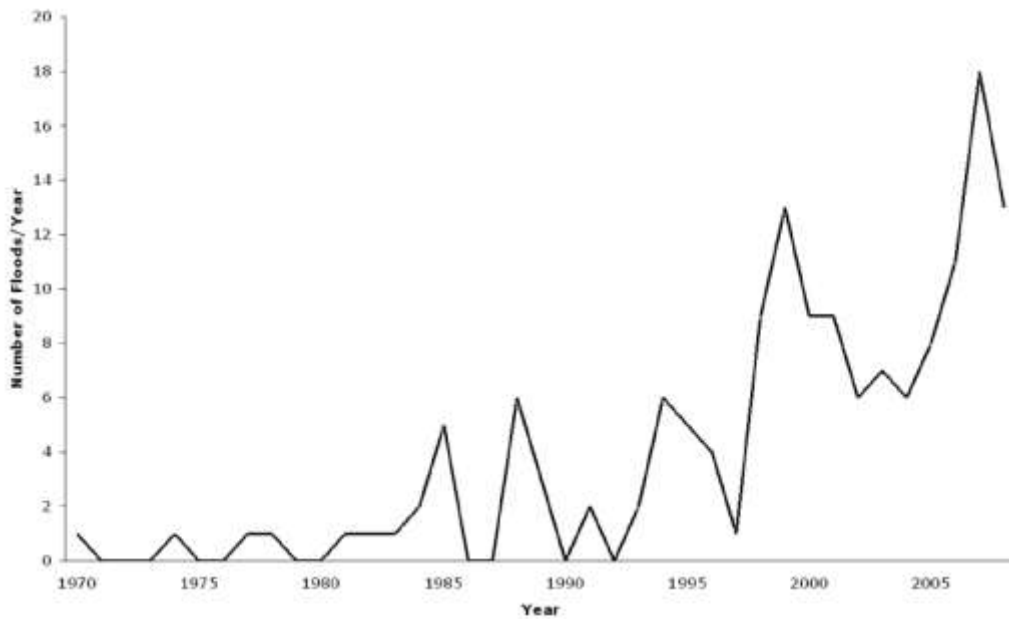
The Sahel region is prone to drought and is often held as an example of the dangers of environmental disaster, especially after the devastating drought that persisted between 1968 and 1974 (Rain, 1999). Berry (1975) showed that during this period, the Agades station in Niger recorded mean annual rainfalls half the amount of the 50 year average between 1922 and 1972.

Similar droughts have occurred prior to the 1968-1974 event, such as in 1913 and 1940 (Berry, 1975). Balme *et al.* (2006) suggested that the Sahel region had actually been in a state of drought from the late 1960s to the mid 1990s, with intense peaks in 1972-1974 and 1983-1985. Most recently, the East African Sahel was gripped by the Horn of Africa drought as described by ADD12 and discussed in Section 3.2.

Overall the 1990-2002 rainfall for the Sahel was 20% below the 1950-1969 average, and 8% below the 1950-1989 average (Balme *et al.*, 2006).

Although the region is prone to drought it is also prone to flooding. The risk of flooding in West Africa is highlighted in Braman *et al.* (2012), showing that the

region is under increased risk because of development upon floodplains during the long drought period, and the International Panel for Climate Change (IPCC) predictions for more intense rainfall events for the region. In recent years there has been an increase in flooding in the West African regions, as shown in Figure 3.12



Note: data covers the following West African countries: Benin, Burkina Faso, Cape Verde Islands, Cote d'Ivoire, Gambia, Ghana, Guinea, Guinea Bissau, Liberia, Mali, Mauritania, Niger, Nigeria, Senegal, Sierra Leone, St Helena, and Togo. 'For a disaster to be entered into the database at least one of the following criteria must be fulfilled: Ten (10) or more people reported killed; Hundred (100) people reported affected; Declaration of a state of emergency; Call for International Assistance'.

Source: Emergency Events Database (EM-DAT), Office of US Foreign Disaster Assistance/ Centre for Research on the Epidemiology of Disasters, Université Catholique de Louvain, Brussels, Belgium (www.emda.net).

Figure 3.12 – Chart showing the increase in the number of annual floods in West Africa between 1970-2008 (from Braman *et al.*, 2012).

The Commission for Africa Report (Commission for Africa, 2010) highlighted the expansion of deserts, or desertification, as a hazard facing the Sahel region. Using a 3,200 year record of dust and proxy precipitation data from West Africa, Mulitza *et al.* (2010) found that the relationship between Sahelian dust

generation and rainfall became decoupled around 1700AD, with the arrival of commercial agriculture in the region, which may be contributing to the observed desertification trend over the last four centuries.

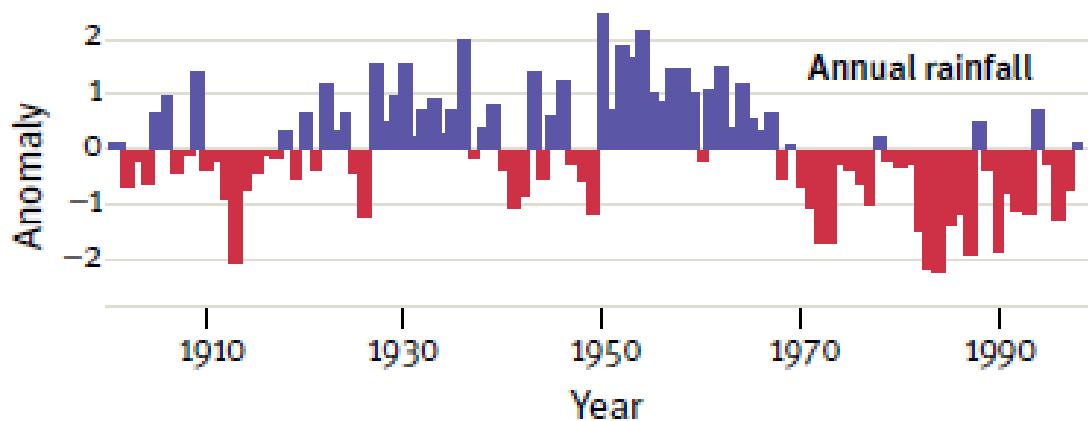


Figure 3.13 – Chart showing the rainfall anomalies across the Sahelian zone (from Conway, 2009).

The Sahelian region is currently in a multidecadal period of drought, which began at the start of the 1970s (Conway, 2009) – this can be seen in the rainfall anomaly chart in Figure 3.13. It is not certain whether this is due to natural cycles – the area has experienced similar periods several times since the last glacial period – or due to anthropogenic climate change (Conway, 2009).

The theory that desertification was occurring in the Sahel emerged from the prolonged drought that afflicted the region after the 1960s, with the prevailing thought being that mismanagement of the land had caused a climatic shift (Giannini *et al.*, 2008). Since the mid 1980s however, there was growing evidence that the droughts were driven by changes in the global pattern of sea

surface temperatures (SST), and the rains have somewhat recovered with 'greening' evident in the region (Giannini *et al.*, 2008).

With strong evidence for a link between warmer ocean temperatures and Sahelian drought (Giannini *et al.*, 2008), it stands to reason that with the predictions for anthropogenic climate change that future warmer oceans will lead to a drier Sahel, and desertification. However, Giannini *et al.* (2008) suggested that recent observation and re-greening in the region contradict this trend and theory, whilst Hein *et al.* (2011) noted that remote sensing techniques have failed to detect wide-spread degradation of vegetation in the Sahel that would be indicative of desertification.

The picture of desertification and possibilities for the future are unclear and highly complex. Land degradation and farming plays a part in complex ways (Conway, 2009), but the evidence points to a stronger link between droughts and SST (Giannini *et al.*, 2008). Conway (2009) shows that the main driver for Sahelian droughts from SST is the difference in temperatures between the cool North Atlantic and a warmer South Atlantic, but it appears that the South Atlantic may have been cooling since the 1990s, and the North warming due to climate change – this would lead to an increase of rainfall in the region.

3.4 – Previous Studies relating to the Bakoye Catchment

There have been five previous studies of the Bakoye Catchment that are relevant to this study, details of which can be found in Hardy *et al.* (1989),

Andersen *et al.* (2002), Grimes and Diop (2003), Diop and Grimes (2003), and Stisen *et al.* (2008). A summary of each is provided below –

Hardy *et al.* (1989)

The study described in Hardy *et al.* (1989) was one of the early applications of the TAMSAT CCD method to drive a manually calibrated Pitman lumped CRR model of the Manantali and Gourbassy catchments, upstream sub-catchments of the Senegal Basin.

The study found that the Pitman model performed comparatively well compared to the model driven by raingauge data, with the benefit of being produced in near real-time. The study acknowledged the requirement for further research, including on other catchments but also acknowledged the implications of hydrological model calibration when using the SRFE.

Andersen *et al.* (2002)

Andersen *et al.* (2001) described the calibration and validation of a MIKE SHE distributed and physically based hydrological model of the Senegal Basin. The same model was used but with remotely sensed data to drive it in Andersen *et al.* (2002), including a TAMSAT CCD estimate of rainfall to fill in areas that were more than 25km away from a recording raingauge station. The study found that the use of the TAMSAT rainfall did not improve the performance of the overall model but there was some improvement at smaller scales, which could be

further improved as the additional spatial information provided by TAMSAT estimates would allow a higher resolution to be used for future modelling.

Grimes and Diop (2003)

The study described in Grimes and Diop (2003) compared the performance of TAMSAT estimates to inputs from a NWP model incorporating satellite data and a mean of the raingauges within the catchment, when used to drive a pre-calibrated Pitman lumped CRR model. Included as part of this study was a modelling of storm types and the influence of the African Eastern Waves (AEWs). The study found that a NWP model utilising satellite data, with a contemporaneous calibration can outperform raingauge data alone for driving a hydrological model, and this can be further improved by including information on storm types and wave phases.

In addition the study also found that inclusion of a relatively complex modelling of PET in the Pitman model - using remotely sensed NDVI data - did not improve the modelling of the catchment.

Diop and Grimes (2003)

The study described by Diop and Grimes (2003), a companion paper to Grimes and Diop (2003) summarised above, investigated the influence of the AEWs on the Bakoye Catchment, and the modelling of rainfall and hydrology.

Produced by instabilities in the African Easterly Jet, AEWs form and travel westwards over North Africa, into the Atlantic and are linked to the formation of tropical cyclones there. For the region of the Senegal Basin and the Bakoye catchment they are significant in that they are key drivers of convection, and the rainfall that results. The study found that the highest levels of rainfall and CCD occurred on the leading edge of the waves, with minima in the trough behind, however the relationship was complex and showed significant inter-annual variation indicating the influence of other meteorological factors. As stated above, Grimes and Diop (2003) showed that the inclusion of wave phase and storm type classification in the modelling process improved performance.

Stisen *et al.* (2008)

The study described by Stisen *et al.* (2008) looked at using remote sensing data to drive a MIKE SHE distributed hydrological model of the Senegal Basin, including six sub-catchments, one of which being the Bakoye catchment. Rainfall data for the study was produced using TAMSAT CCD estimates.

The study concluded that remotely sensed data could provide a valid means of driving a distributed hydrological model for a large river basin, and that by comparing data for a single sub-catchment and previous studies, a distributed approach outperformed less sophisticated lumped methods, especially in the robustness of the calibration.

The Current Picture

It would appear from the studies above that the picture of using SRFE to drive a hydrological model for the Bakoye Catchment is mixed. Hardy *et al.* (1989) and Grimes and Diop (2003) both showed that TAMSAT rainfall estimates can be used effectively to drive a lumped hydrological model of a sub-catchment of the Senegal Basin, and Stisen *et al.* (2008) demonstrated that TAMSAT could also be used effectively with a distributed model of the larger basin area. However, Andersen *et al.* (2002) suggested that the TAMSAT rainfall did not improve the performance of the model at the catchment level.

Diop and Grimes (2003) showed that by introducing the modelling of storm type and wave phases to the modelling of rainfall from satellite data, the performance when driving a lumped model was improved. None of the previous studies have attempted to model the uncertainty within the SRFE and how it influences and propagates through the hydrological model.

3.5 – The Available Data

This section will examine the datasets that have been made available to this thesis, plus the additional sources of data to supplement it. The section will also investigate the data in relation to the climatic conditions discussed earlier in this chapter. The main sources of data available were:

- Historic Raingauge Data

- Historic Discharge Data
- Historic Satellite Data

Additional sources of data available which have been used are:

- Climatic Potential Evaporation Data
- Digital Elevation Model Data

The Raingauge Data

Data from 81 raingauge stations are available, recording the period between 1986 and 1996, at a daily timestep. Figure 3.14 shows the locations of each of the raingauges available, and their percentage of recording coverage between 1986 and 1996.

Coverage of the raingauges is generally good, with an all-over average of 77.71%. 22 stations have data recorded for 100% of the period, 48 stations have over 75% and 67 stations have at least 50% coverage. Only 4 stations record data for less than 25% of the period. Ideally, stations that show such a poor record of coverage would be excluded from the dataset, but due to the already sparse nature of the data all stations were included.

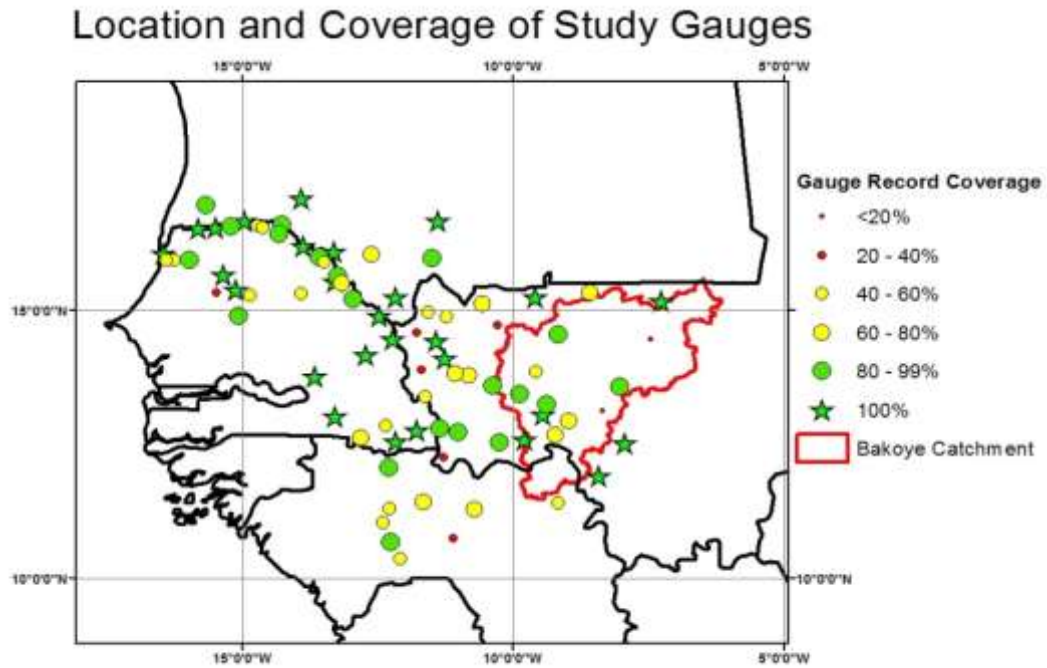


Figure 3.14 – Map showing the extent of the study area and location of the 81 rain gauge stations. The percentage of recording coverage provided by each station is shown for the period between 1986 and 1996, with green stars indicating those stations that provide 100% coverage. The extent of the Bakoye catchment is outlined in red.

Table 3.2 shows the mean annual rainfall for each year of the study taken from all 81 stations, with each station having been weighted depending on the number of days it has recorded data that year. The table also shows the average coverage for each year.

Year	Weighted Mean Rainfall (mm.yr ⁻¹)	Coverage (%)
1986	592.95	88.44
1987	580.63	84.93
1988	689.89	80.13
1989	686.37	76.66
1990	528.82	73.73
1991	549.60	76.86
1992	503.41	68.51
1993	521.41	71.81
1994	715.75	79.61
1995	681.77	78.38
1996	635.54	75.70
Total	6686.14	
Mean	607.83	77.71

Table 3.2 – Mean annual rainfall for each year taken from all the 81 raingauge stations for the period between 1986 and 1996, and the mean recording coverage of the stations for that period.

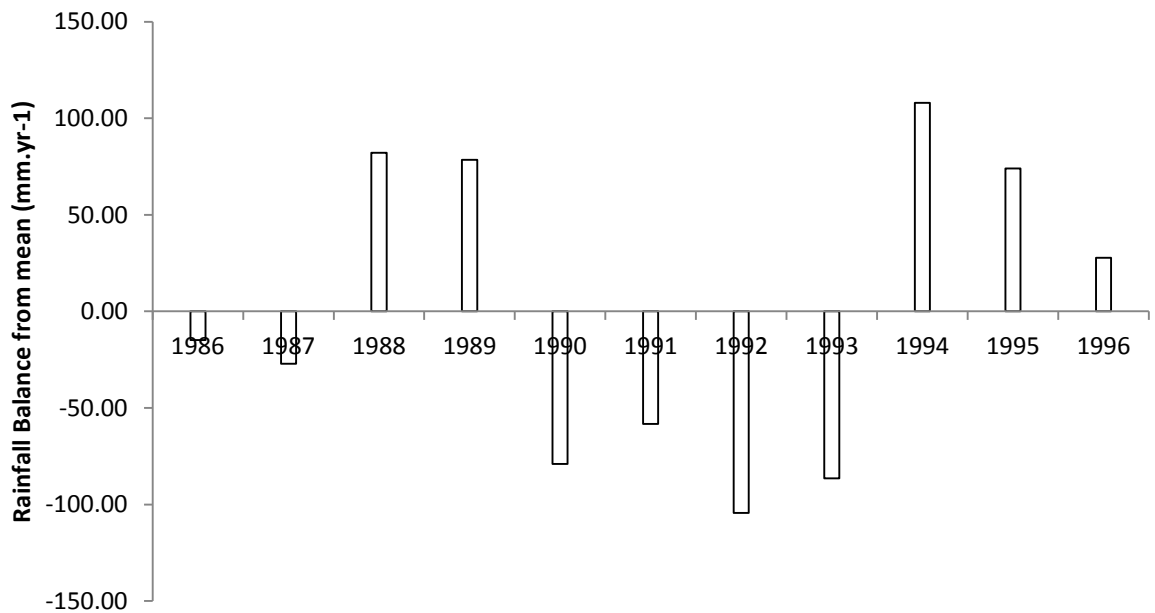


Figure 3.15 – Chart showing the deviation from the 1986-1996 rainfall mean for each year of the study period, for all the raingauge stations.

Table 3.2 and Figure 3.15 show the characteristics of the mean annual rainfalls from all the raingauge stations for the period between 1986 and 1996. The years 1986 and 1987 show average rainfalls that are below the mean for the period, and this could be attributed to a prolonging of the 1983-1985 drought conditions described previously (Balme *et al.*, 2006). There is another prolonged period of below average rainfall between 1990 and 1993, with the rest of the period showing above average rainfall. 1994 is the wettest year from the record, with a mean annual rainfall of 715mm, which is 108mm above the mean.

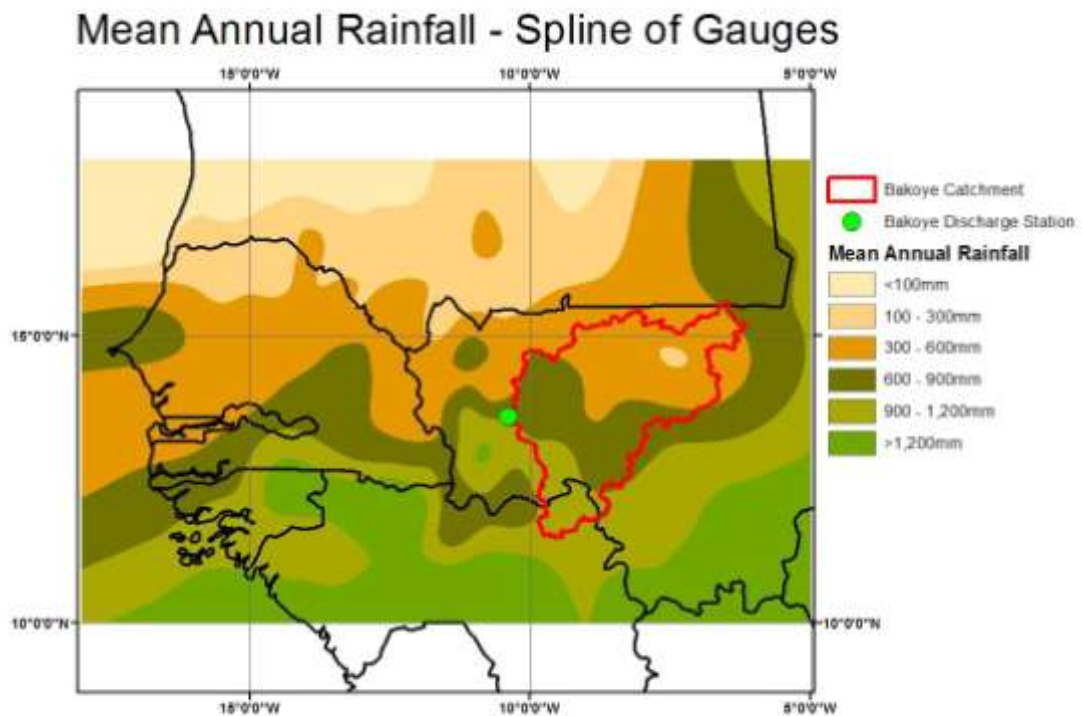


Figure 3.16 – Map showing a spline interpolation of the mean annual rainfall for all the raingauge stations in the Senegal Basin for the period 1986-1996. The extent of the Bakoye catchment is highlighted in red, and the Oualia gauging station is highlighted by the green dot. Although the interpolation contains areas of significant extrapolation and error, it does give a good impression of the rainfall gradient across the region.

Figure 3.16 shows a spline plot of the mean annual rainfall from the gauges across the Senegal Basin area. The mean annual rainfall region (607mm) lies between the dark-brown and dark-green bands.

There are 13 raingauge stations from the record that can be said to be associated with the Bakoye Catchment. These 13 stations will form a sub-set for use in determining the seasonal variations of rainfall over the Bakoye catchment. The mean annual rainfalls for the study period, determined from these stations, are shown in Table 3.3, along with the average recording coverage.

Year	Weighted Mean Rainfall (mm/yr)	Coverage (%)
1986	772.59	100.00
1987	621.84	99.98
1988	892.78	69.23
1989	848.17	76.92
1990	694.74	76.92
1991	760.27	76.92
1992	660.88	59.58
1993	723.25	58.29
1994	940.01	74.35
1995	814.75	75.01
1996	768.36	62.82
Total	8497.64	
Mean	772.51	75.46

Table 3.3 – Mean annual rainfall for each year taken from all the Bakoye catchment sub-set of raingauge stations for the period between 1986 and 1996, and the mean recording coverage of the stations for that period.

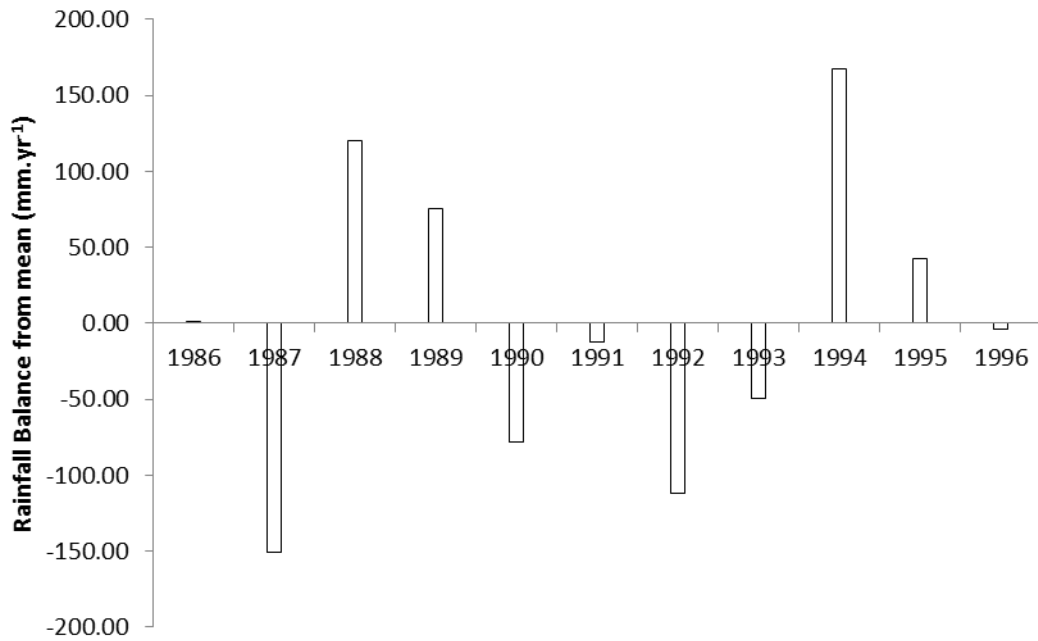


Figure 3.17 – Chart showing the deviation from the 1986-1996 rainfall mean for each year of the study period, for the Bakoye catchment sub-set of raingauge stations.

Table 3.3 and Figure 3.17 show the characteristics of the mean annual rainfall for the Bakoye catchment, based on a sub-set of 13 raingauge stations. The general pattern is similar to that of the wider Senegal Basin, with dry periods between 1986-87 and 1990-93, with 1994 being the wettest year. However, the rainfall in 1986 is slightly more than the mean for the period, and 1996 slightly below – a deviation from the pattern seen for the whole of the Senegal Basin.

Overall the catchment has a higher mean annual rainfall than the Senegal Basin as a whole, which is expected as the Bakoye catchment predominantly lies towards the climatologically wetter, southern end of the Basin. This can be seen in Figure 3.16, with significant areas of the catchment covered by bands of rainfall above the mean annual rainfall for the Senegal Basin (607mm).

However, this might be skewed because the wetter regions of the Bakoye

catchment are more densely gauged than the drier northern areas, which lie in areas of mean annual rainfall below the overall mean, likely to result in overestimation of rainfall for the catchment from the gauges here.

The River Discharge Data

The available river discharge data is from seven discharge stations, with various periods of coverage between 1986 and 2005.

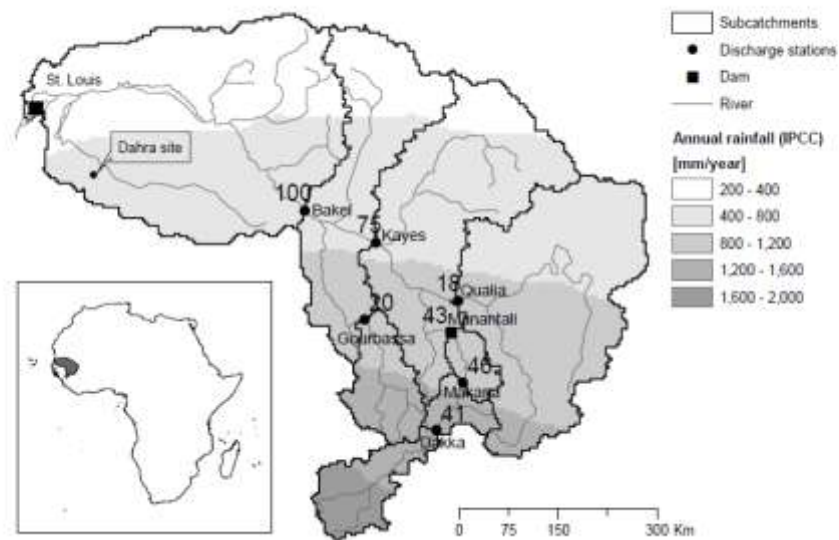


Figure 3.18 – Map showing the locations of the river discharge stations of the Senegal Basin and the associated catchment extents. The Oualia station records the output from the Bakoye catchment. The numbers show the percentage of discharge for each catchment in relation to discharge of the Bakel station (for 1998-2001) (from Stisen *et al.*, 2008).

Figure 3.18 shows the locations of the discharge stations and their associated upstream catchments. From 1987 the discharge from the Manantali outlet is controlled by the dam located there, and the discharge data shows little correlation with rainfall calculated from raingauges within its catchment. As the discharge from Manantali accounts for 43% of that recorded by the Bakel station (Stisen *et al.*, 2008), it would be expected that the output from the dam would have significant impact on the discharge downstream, and this is reflected in the data for Kayes and Bakel.

The sub-catchments of Mankana and Dakka, upstream of Manantali, do not cover enough area to be represented by a sub-set of raingauges, so the influence of the dam at Manantali cannot be assessed, but it is anticipated to be significant.

Of the catchments, the Gourbassa and Bakoye catchments are the best suited for modelling, both being free from the influence of the Manantali dam. Both have a similar output, 20% of the Bakel discharge for Gourbassa, and 18% in the case of Bakoye, yet the Gourbassa catchment is the smaller. This is an issue, as there are five raingauge stations that can be associated with the Gourbassa Catchment (with periods of only two stations recording), and 13 associated with the Bakoye Catchment – this makes the Bakoye catchment the most suitable catchment to model.

Although data is available for the period 1986-2005 for the Oualia station which sits at the outlet of the Bakoye Catchment, raingauge data is only available for

the period 1986-1996. Figures 3.19 and 3.20 show the characteristics of the mean annual discharge for the Bakel and Oualia stations respectively.

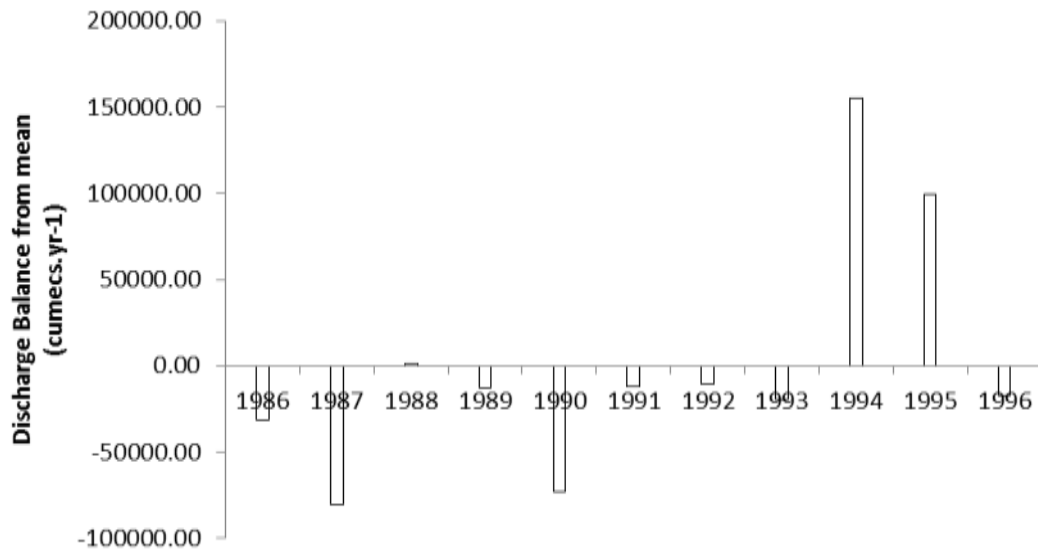


Figure 3.19 – Chart showing deviation of mean annual discharge for the Bakel station from the mean annual discharge for the period 1986-1996.

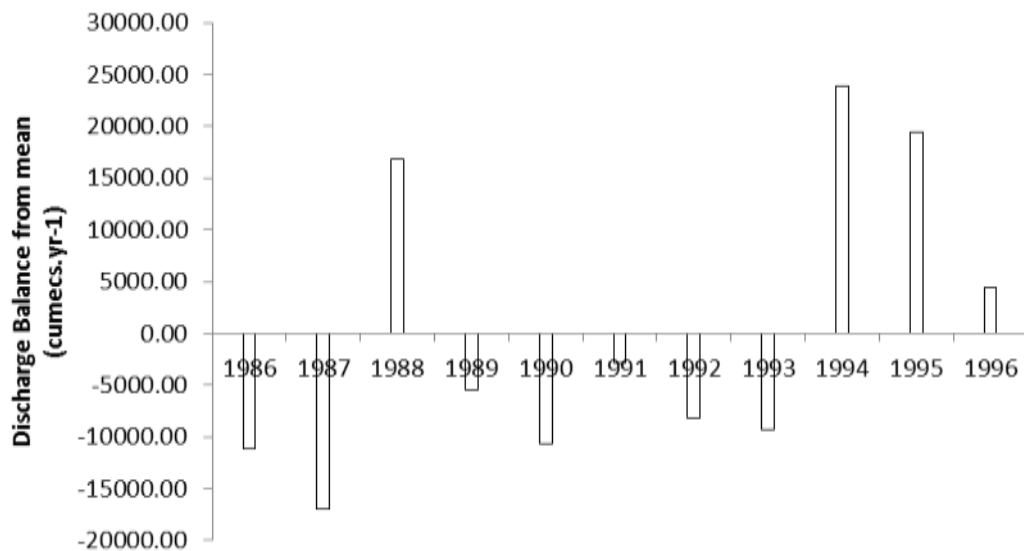


Figure 3.20 – Chart showing deviation of mean annual discharge for the Oualia station from the mean annual discharge for the period 1986-1996.

The patterns shown in Figures 3.19 and 3.20, in the main, resemble the variations from mean annual rainfall shown both for the Senegal Basin area in Figure 3.15, and the Bakoye catchment in Figure 3.17. There are dry periods in 1986-87 and 1990-93, and the discharges for 1994 reflect the fact that the raingauge stations indicated that it was the wettest year of the record. However, 1989, which is a relatively wet year according to the raingauge stations shows below average discharge.

Interestingly, 1996 displayed below average rainfall over the Bakoye catchment yet above average discharge. It is clear that the relationship between a simple average of raingauge measurements and catchment discharge is likely to be non-linear, non-stationary (both temporally and spatially) and uncertain at best. In absence of a more accurate alternative, the raingauge and discharge station data will be assumed to be free of error and uncertainty, although this is clearly not the case.

Satellite Data

The third important dataset available to the study was the satellite data, in the form of 'Cold Cloud Duration' (CCD) data, produced by the Tropical Applications of Meteorology using SATellites (TAMSAT) research group, Department of Meteorology, University of Reading.

The CCD method employed by the TAMSAT group utilises the 10-13 μ m infra-red channel of the Meteosat satellites to capture cloud top temperatures at

quarter-hourly intervals. For each 0.05° pixel a value is produced for the amount of time that pixel records temperatures below specified thresholds for each day. That value is the pixel's daily CCD value.

The database provided includes data for the whole of sub-Saharan Africa for the period of 1983-2010, at daily timesteps at a resolution of 0.05°. It is provided for the temperature thresholds of -20°C, -30°C, -40°C, -50°C and -60°C.

Seasonality in the Data

There is a large seasonality displayed across the region, as described by Jones and Wild (1975), with much of the Senegal Basin area within the region where the wet season can be expected to begin in June and last for four months.

The seasonality expected is seen in the data, as shown in Figure 3.21. The vast majority of the rainfall falls between June and September, with peak rainfalls in August which accounts for 31% of the annual rainfall. The period between June and September accounts for 88% of the annual rainfall. There are still reasonably significant rainfalls in May and October, but these are still only 4% and 7% of the annual total.

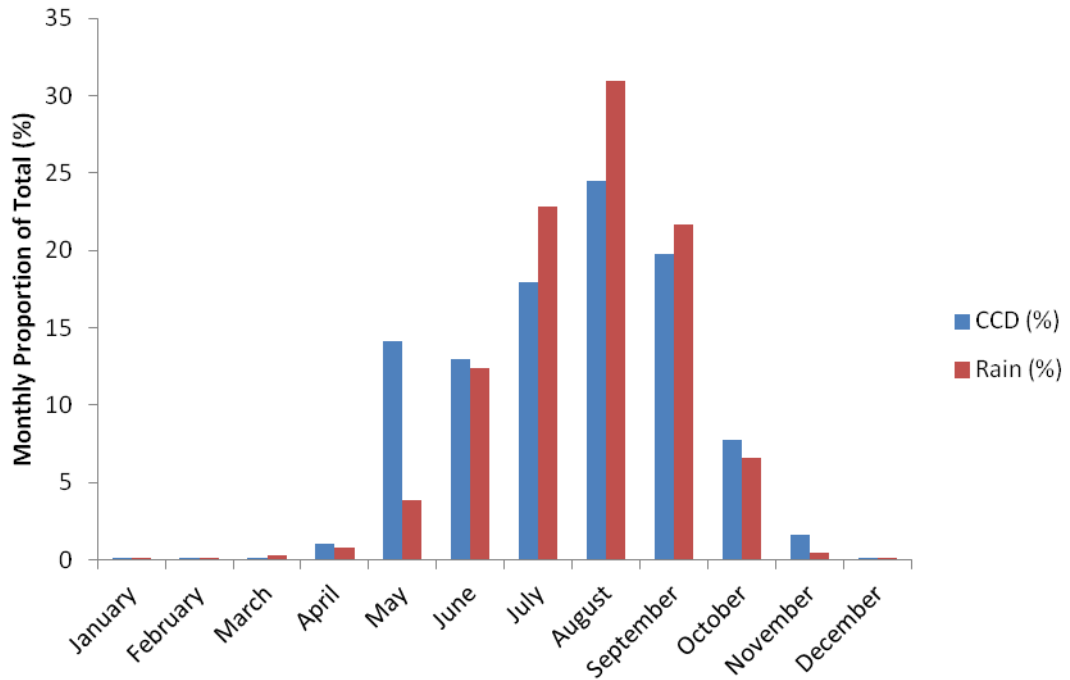


Figure 3.21 – Chart showing the monthly proportions of the yearly total of CCD and rainfall for the period 1986-1996 for the Senegal Basin Area.

The same pattern is seen in the CCD data, although there is a spike of cold cloud in May which does not seem to correspond with rainfall. The June to September period accounts for 75% of the annual CCD total. Figure 3.22 shows the monthly proportions of CCD and rainfall plotted together, showing a good correspondence between the two datasets.

Figures 3.21 and 3.22 show the seasonality displayed by the data, matching the expected climatology for the region, and the close relationship between the CCD and raingauge derived rainfall data. The main rainfall period begins in May and ends in October, with the vast majority of rainfall between June and September. Ideally, the wet season would be taken as May to October, but due to the poor correlation between CCD and rainfall in May this month will be

excluded. Still, the defined wet season of June to October accounts for 95% of the rainfall recorded by the raingauge stations.

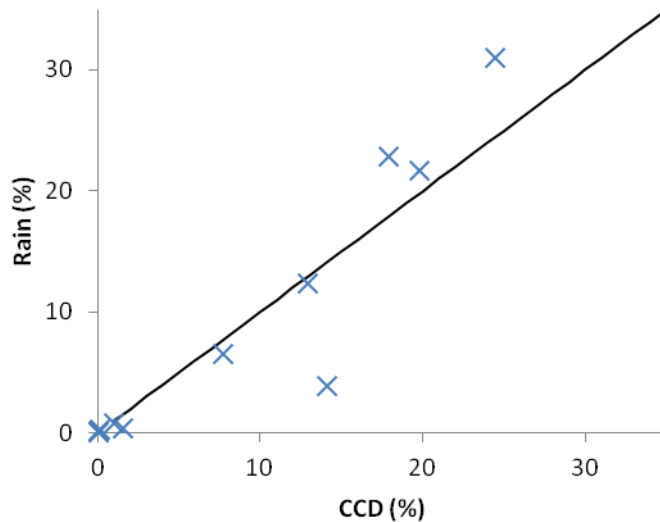


Figure 3.22 – Scatter plot showing the relationship between the monthly CCD and rainfall proportions of the annual total for the period 1986-1996 for the Senegal Basin area.

Climatic Potential Evapotranspiration Data

In a similar way to ground instrumentation for rainfall, the Senegal Basin area does not contain the infrastructure for recording evapotranspiration rates at high spatial or temporal resolution. For use in this thesis, monthly climatic derived values are used, taken from the Food and Agriculture Organisation of the United Nations (FAO), available from FAO (2009) – the values used are from the nearest point available to the Oualia gauging station.

The climatic monthly averages of reference evapotranspiration are determined by the FAO (2009), using the Montieth-Penman method, which is outlined in

Allen et al (1998). In a review of different methods of evaluating climatic evapotranspiration data, the CGIAR-CSI (2009) found that the Monteith-Penman method outperformed the others, the details of which can be seen in Figure 3.23. These findings were similar to Batchelor (1984) which demonstrated that the method was superior in most practical situations. As can be seen in Figure 3.23, the Monteith-Penman does not have the spatial resolution of the other methods but as a lumped value was used this is not relevant. The Monteith-Penman has the additional benefit of being available for download without the need for additional processing.

The Monteith-Penman method makes assumptions that could be a source of uncertainty in hydrological modelling. As a climatic representation of evapotranspiration it lacks the temporal resolution of the model, and cannot account for annual variations from the climatic average. It is also unable to account for antecedent conditions, which Taylor and Lebel (1998) suggested could be significant on the amount of soil moisture, evapotranspiration and feedbacks to rainfall amount. The Monteith-Penman method makes the assumption of global homogeneity in crop types, described as being 0.12m in height, with a surface resistance of 70s.m^{-1} and an albedo of 0.23 (Allen *et al.*, 1998) – obviously this assumption is incorrect and the heterogeneity of vegetation has been shown across the Bakoye catchment in Figures 3.8 and 3.9.

Comparison of Five Methods Used to Estimate PET:											
Mean Difference (mm) and Standard Deviation (mm) between Observed and Predicted Values											
		Holland (Thornthwaite)		Thornthwaite		Hargreaves		Modified Hargreaves		Penman-Montieth FAO	
Region	Month	Mean Diff	Std Dev	Mean Diff	Std Dev	Mean Diff	Std Dev	Mean Diff	Std Dev	Mean Diff	Std Dev
Africa											
	Jan	71.8	40.2	41.6	33.3	22.3	16.1	24.8	20.1	11.1	12.6
	July	84.4	41.7	32.1	23.7	20.0	19.3	21.1	19.3	12.7	16.0
South America											
	Jan	69.9	43.6	50.5	32.9	38.2	19.2	41.6	26.0	34.9	26.7
	July	67.3	35.9	37.2	24.7	27.2	14	30.4	20.1	24.3	15.1
Resolution		1 km		1 km		1 km		1 km		20 km	
Data Requirements											
		Average Temperature		Average Temperature		Average Temperature		Average Temperature		Available online from FAO	
						Average Extraterrestrial Radiation		Average Extraterrestrial Radiation			
						Average Temperature Range		Average Temperature Range			
								Average Precipitation			

Figure 3.23 – Comparison of methodologies for producing reference climatic evapotranspiration data (from CGIAR-CSI, 2009).

Some attempts can be made to mitigate these issues, such as smoothing the data into dekadal time steps, but this is unlikely to significantly improve the quality of the data. Remote sensing has been used to improve the spatial and temporal resolution of evapotranspiration data, and Courault *et al.* (2005) provided an overview of the techniques, broadly categorising them into four types:

1. Direct empirical methods, for example those based on TIR images
2. Residual methods of the energy budget using remotely sensed data with physical parameters
3. Deterministic models such as Soil-Vegetation-Atmosphere-Transfer (SVAT)

4. Vegetation index methods used as adjustments to the initial data

Stisen *et al.* (2008) attempted to improve the temporal resolution of remotely sensed evapotranspiration values by modifying them with satellite derived Normally Distributed Vegetation Index (NDVI) data – the NDVI data was available at daily time steps with a spatial resolution of 6km, and was used as an indicator of Leaf Area Index (LAI). The approach by Stisen *et al.* (2008) was similar to that used by Grimes and Diop (2003) which incorporated daily NDVI data to adjust the FAO climatic estimates, finding no improvement to the model. Baret and Guyot (1991) found that NDVI was highly sensitive to soil optical properties, particularly in areas of low vegetation, showing that other methods outperformed NDVI – it is possible that the approach by Grimes and Diop (2003) was correct but the NDVI data used was not suitable for the Bakoye catchment.

Courault *et al.* (2005) suggested that the methods of perturbing climatic estimates based on remotely sensed data were unlikely to estimate the spatial and temporal variations of evapotranspiration with a high degree of accuracy. Despite this and although Grimes and Diop (2003) found that a more sophisticated method of incorporating PET into the model did not improve performance – and indeed initial tests performed for this thesis found similar results – their use of such methods cannot be excluded from future research and disregarded, especially with the use of a distributed hydrological model and more research is required in this area.

Digital Elevation Data

The digital elevation data used for the thesis is taken from the National Geospatial-Intelligence Agency (NGA, 2006). The elevation data for West Africa can be seen earlier in this Chapter in Figure 3.11.

3.6 – Summary

This chapter has demonstrated how the Sahel region is an area that faces many problems, from food insecurity, drought and famine, to flooding and desertification due to climate change, amongst others. Many agencies have attempted to assist the area's development and help to mitigate and limit the impacts of disasters if they do occur.

A key component to the success of these efforts are the environmental models that are used to inform EWS, but these rely on timely and accurate measurements of precipitations which, when compared to other areas of the globe, are scarce. SRFE have been shown to improve the spatial and temporal resolution of the precipitation data available to environmental models in the Sahel but these can be highly uncertain, and there is a requirement to accurately measure this uncertainty, characterise it in a way that is applicable to an environmental model, and clearly communicate it in a way that can be understood by decision makers.

The Senegal Basin and the Bakoye catchment within it are typical of the Sahel region, and pose a challenge for producing SRFE. The precipitation data from ground recording instrumentation is particularly sparse, and the region displays significant heterogeneity in terms of climate, land cover and geology. This makes the need for accurate uncertainty characterisation even more urgent for SRFE in this area.

The following three chapters detail the methodology adopted for this thesis.

Chapter 4 demonstrates how the point raingauge network was interpolated into a continuous grid. Chapter 5 describes the TAMSAT1 method of producing a deterministic SRFE, and the TAMSIM algorithm for characterising the uncertainty using a fully spatio-temporally distributed stochastic ensemble method. Chapter 6 demonstrates the Pitman lumped CRR model used for the hydrological modelling part of the thesis, and the SCE-UA technique used to optimise the variable parameters.

4

Methodology – Spatial Interpolation

4.1 – Introduction

This chapter is the first of three methodology chapters and details the methods used in the spatial interpolation of the point raingauge data. This is a necessity in order to make the data directly compatible and comparable to the satellite data which is aggregated at 0.5° pixels. The method chosen to perform the spatial interpolation was the double Kriging (DK) method introduced by Barancourt *et al.* (1992).

4.2 – Spatial Interpolation and the Double Kriging (DK) Method

In order to calibrate the satellite data using historical raingauge data one of two approaches must be taken – either calculate point values from the satellite pixel averages, or produce pixel averages of the raingauge data (Grimes *et al.*, 1999). For this thesis, the latter approach has been adopted and therefore it is necessary to produce daily average rainfalls for the Senegal Basin at an appropriate pixel size, and the DK method of Barancourt *et al.* (1992) has been chosen to compute the pixel averages from the raingauge data.

Kriging is a linear interpolation method common to geostatistics, although it has been used widely across many and varied disciplines, for example estimating the proportion of shading across large photovoltaic cells (Di Piazza and Di Piazza, 2009) and even graphical character animation (Courty and Cuzol, 2010), which highlights its versatility.

Kriging is a popular approach for the spatial interpolation of rainfall fields and its usefulness has been demonstrated for a variety of applications, including hydrological modelling (Sun *et al.*, 2000), climate studies (Duchon *et al.*, 1995; Pardo-Iguzquiza, 1998), pollution modelling (Shen *et al.*, 2012), producing large, gridded datasets (Jeffrey *et al.*, 2001; Haylock *et al.*, 2008; Hofstra *et al.*, 2009), designing raingauge networks (Pardo-Iguzquiza, 1998; Campling *et al.*, 2001), producing reference fields for error characterisation (Kirstetter *et al.*, 2010) and calibration of remote sensing techniques (Grimes *et al.*, 1999). It has been found to outperform other methods for spatial interpolation of rainfall, including inverse-distance (Dirks *et al.*, 1998), Thiessen Polygon (Dirks *et al.*, 1998; Goovaerts, 2000) and multi-quadratic interpolation (Syed *et al.*, 2003) – although Dirks *et al.* (1998) and Syed *et al.* (2003) both suggest that for small catchments with a dense network, the benefits of Kriging are negligible compared to simple methods especially when considering the additional computational expense. Dirks *et al.* (1998) added that the benefits of Kriging are more fully realised when the study was sufficiently large to exploit the full extent of the semi-variogram.

Kriging is not without its limitations and Hofstra *et al.* (2009), on spatial interpolation in general, suggested that the network density, spatial characteristics of the variable and the complexity of the terrain all have an effect on the accuracy of the interpolation.

With Kriging there is a tendency for interpolated values to converge upon the mean, described in Haylock *et al.* (2008) as a smoothing of extreme events, where the Kriging interpolation was found to be smoothing the peaks and troughs of the gauge data. Maidment *et al.* (in press 2012) also observed this effect with block Kriging but suggested that in this case it is likely to be physically correct, with high values representing a 'direct hit' over the gauge when rainfall elsewhere in the pixel is lower, and vice versa. Only by experimental testing could this be proven or otherwise, and this would require a dense network of gauges at sub-pixel level (Maidment *et al.*, in press 2012).

In the pursuit of more realistic realisations of precipitation fields, several variations of the Kriging methodology have been developed. Goovaerts (2000) explored some of these methods for incorporating secondary information, in this case elevation data in the form of a DEM, into the algorithm. The techniques were linear regression, simple Kriging (SK) with linear mean, Kriging with external drift and ordinary Kriging (OK), and it was found that the algorithms incorporating the secondary information outperformed OK (Goovaerts, 2000).

This method of Kriging with the incorporation of a secondary data set is commonly referred to as co-Kriging, with examples of the secondary data being DEM data (Goovaerts, 2000) and radar rainfall data (Azimi-Zonooz *et al.*, 1989).

The main issue with the Kriging methods commonly used in spatial interpolation of rainfall is the inability to represent the fractional coverage of rainfall, resulting in an inaccurate representation of the rainfall field: with overestimation outside the rain field and underestimation within (Barancourt *et al.*, 1992; Seo, 1998). To address this issue, both Barancourt *et al.* (1992) and Seo (1998) suggested similar methods involving the use of two Kriged random fields, 1) an indicator field showing which areas are “rainy” or “non-rainy”, and 2) a rainfall field representing the rainfall amount for areas designated as “rainy”.

The double Kriging method (DK) introduced by Barancourt *et al.* (1992) allows for separate representation of the different spatial characteristics of rainfall occurrence and rainfall amount (Maidment *et al.*, in press 2012), which is particularly useful when working with higher spatial and temporal resolutions. Maidment *et al.* (in press 2012) noted that when a rainfall field is not primarily fractional, a DK methodology is unnecessary – the example being dekadal rainfall in the wet season of Uganda where there was little zero rainfall in the data. Referring to the technique as combined Kriging (CK), Symeonakis *et al.* (2009) used DK to interpolate a relatively dense network of Global Telecommunication System (GTS) gauges and compared it against satellite estimates, finding that in most instances the DK estimates performed better but offered little advantage over the satellite estimates that were easier to obtain.

Teo (2006) used a cross-validation method, sequentially removing a single raingauge point from the Kriging method for each timestep, to assess the capabilities of both DK and OK for determining point estimates. Using numerous skill measures, the DK method outperformed OK, the latter was found to reduce the heterogeneity of intermittent rainfall fields.

The Double Kriging (DK) Method

The DK method was first described in Barancourt *et al.* (1992). For this thesis the KrigeRain algorithm (Greatrex, 2009) was used to conduct the DK on the raingauge data from the study area, and this section provides a summary of the DK method and the functionality of the KrigeRain algorithm. The description of the method in Teo (2006) should be seen for a full methodology and background.

The DK method involves the production and combination of two random fields (RF) which together produce a fractional mean areal rainfall field. The two RFs required are –

1. a binary 'indicator' rain/no-rain field of thresholded rainfall probabilities - I .
2. a 'no-zero rainfall' field showing the variability of rainfall with the zero values removed - F .

Equation 4.1

$$Z(u) = I(u).F(u)$$

Equation 4.1 shows the combination of the two RFs outlined above, where Z is the DK product of the two RFs and u is a pixel location. The remainder of this section is divided into first summarising the generation of the Indicator (I) field, and then summarising the generation of the no-zero rainfall (F) field.

Generation of I , the Indicator Field

In order to produce daily fractional mean areal rainfall field it is necessary to determine which areas are likely to be raining, and which are not. In the DK method of Barancourt *et al.* (1992) this was achieved by using a binary indicator, rain/no-rain, RF of thresholded rainfall probabilities.

Equation 4.2

$$I(u) = \begin{cases} 1 & I(u)^{OK} > I_c \\ 0 & \text{otherwise} \end{cases}$$

The production of the binary field is shown in Equation 4.2. $I(u)^{OK}$ is the probability of rainfall at pixel u , produced by OK of the binary rainfall state of the raingauges. I_c represents the probability threshold which is determined for each day so that the resulting field will produce the same proportion of raining pixels as the proportion of raingauges recording rain for that day. If the probability of rainfall for a pixel is above the threshold it is assigned a rainy status, 1, and if it is below it is assigned a non-rainy status, 0.

Generation of F , the ‘No-Zero Rainfall’ Field

With the indicator field representing the areas that are likely to be raining or not raining, it is then necessary to produce a rainfall field showing the rainfall volumes at each pixel. The resulting field needs to produce a total volume of rainfall across the field that is in line with the total volume of rainfall suggested by the raw raingauge data. The DK method described of Barancourt *et al.* (1992) used a ‘no-zero rainfall’ method to produce this field.

The ‘no-zero rainfall’ field, F , is produced by OK of the raingauge data only for raingauges that record positive rainfall, for each day, for the entire study area. The resulting rainfall field obviously shows much greater rainfall volumes than an OK produced rain field from all of the raingauge data, but when combined with the ‘indicator’ field the total volume is reduced to a more representative amount.

4.3 – Implementation of the DK Method

4.3.1 – Introduction

This section details the implementation specifics for the double Kriging (DK) method for the spatial interpolation of the daily rain field for the Senegal Basin.

4.3.2 shows the calibration using the historic raingauge data, and 4.3.3 part

demonstrates how DK daily rain field relates to the original gauge data. This section concludes in 4.3.4.

4.3.2 – Calibration

The daily raingauge data covering the Senegal Basin area, for 1986 to 1996, was spatially interpolated using the DK method detailed above. The process was performed using the KrigeRain V1.1 algorithm for the R environment (Greatrex, 2009).

Chapter 3 looked at the raw raingauge data and showed that the likelihood of rain and the rainfall amount was heterogeneous over the region, and because of this it is impossible to represent the true nature of the rain field statistics with a stationary and ergodic rain field. Goovaerts (2000) showed how secondary information, incorporated into the Kriging process, can be an effective way of producing a non-stationary, non-ergodic underlying rain field, but with the paucity of raingauges available it is unlikely that sufficient detail would be available to fully represent the heterogeneity. However, considering the above limitations, it is reasonable to compromise and treat the spatial characteristics of rainfall occurrence and amount as stationary and ergodic – represented by climatological variograms.

The ideal situation would be the generation of variograms that describe each individual storm event, but in reality it is unusual for sufficient data to be available to do this and climatological variograms are a reasonable alternative

(Grimes and Pardo-Iguzquiza, 2010). With data used in this thesis there was not enough sufficient coverage, and/or enough positive rainfall in the record to produce climatological variograms for each month, so a wet season variogram was used instead. There was insufficient positive rainfall to produce a dry season variogram.

Figures 4.1 and 4.2 show the standardised experimental variograms and the fitted climatological variograms for the wet season. In comparison to other studies, the nugget effect in the indicator variogram is relatively modest – Teo (2006) produced nuggets of 70-80% of the sill, suggesting that this showed intermittencies at a scale smaller than the gauge network could detail. The nugget effect here of 37% could suggest that such intermittencies are less prevalent for this region, but could be a result of the bin size selected.

The climatological variograms were generated after experimental variograms were produced, and the parameters adjusted to produce a suitable modelled variogram. Figures 4.3 and 4.4 shows an example of experimental variograms - demonstrating the selection of a suitable binsize. The binsize was required to be narrow enough to reflect the relationship over distance, yet not be so narrow that the relationship becomes noisy. For both the no-zero and indicator variograms a binsize of 25km was selected.

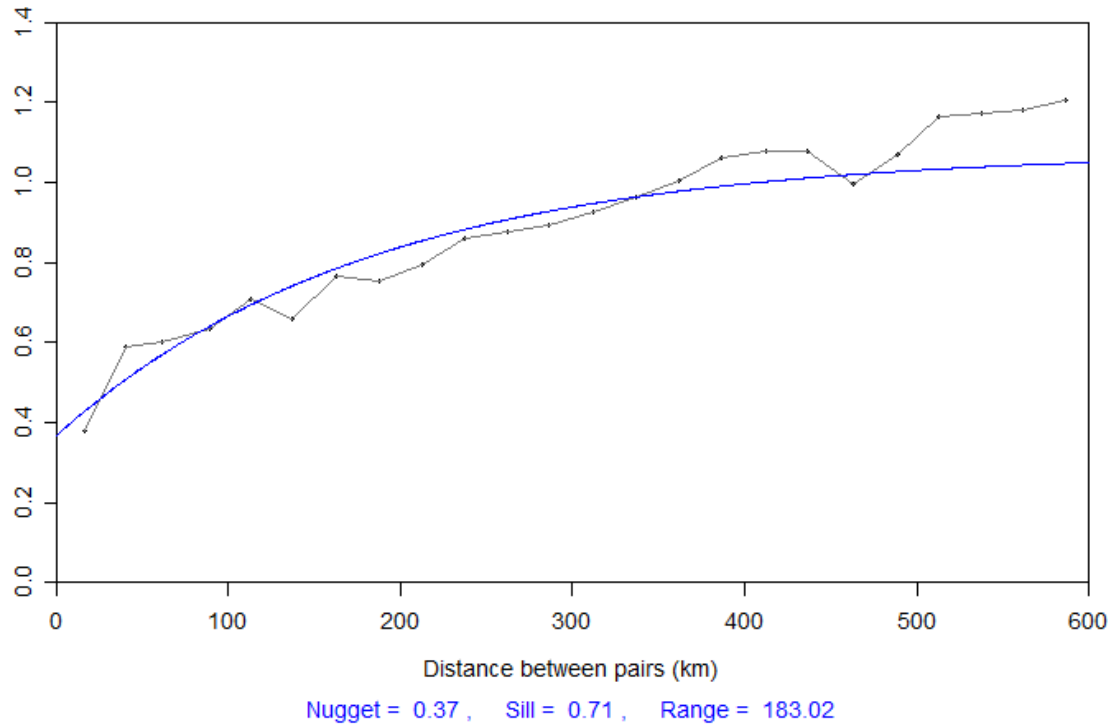


Figure 4.1 – Wet season climatological Indicator variogram for the daily Senegal Basin rainfall field. Range is defined as the distance where the semivariance is 95% of the sill.

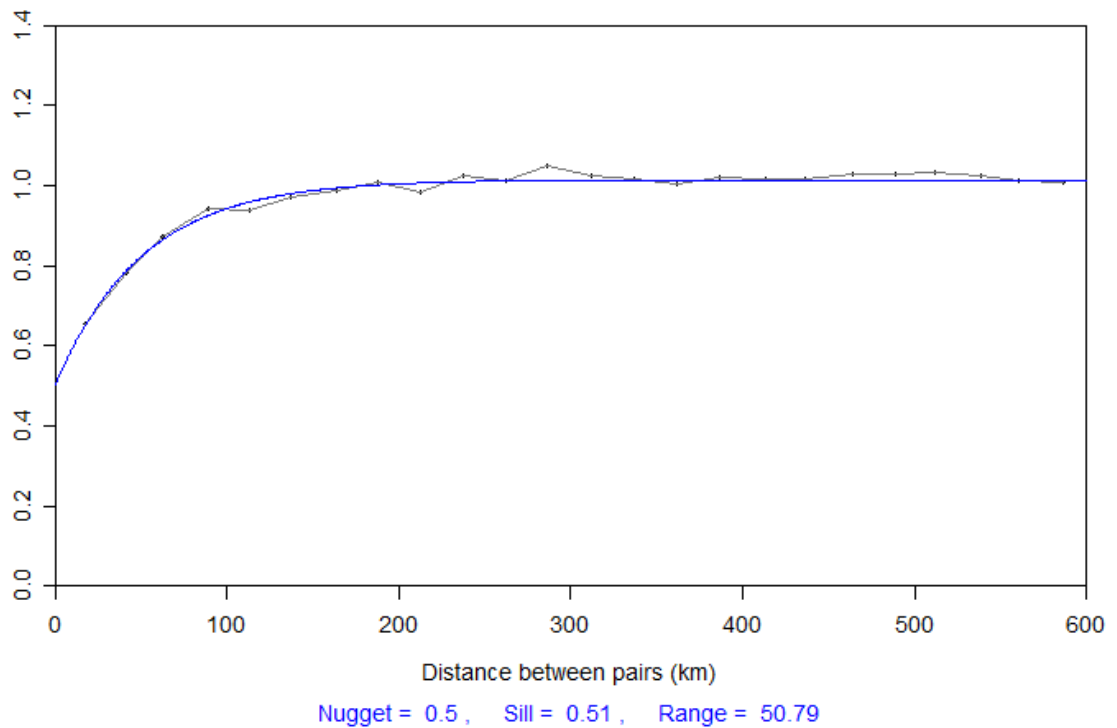


Figure 4.2 - Wet season climatological no-zero rainfall variogram for the daily Senegal Basin rainfall field. Range is defined as the distance where the semivariance is 95% of the sill.

The experimental variograms shown in Figures 4.3 and 4.4 were also used to set the maximum extent of the variograms, this being the distance where the relationship begins to degrade and becomes noisy. Figures 4.5 and 4.6 are plots showing the number of station pairs over distance, which were also used in the selection of a maximum extent distance – the maximum distance should be set before the number of pairs becomes too low. For both the no-zero and indicator variograms, this maximum extent was set at 600km. Although at that distance both fields retain a reasonable number of station pairs, it is at this distance where the variograms clearly start to degrade.

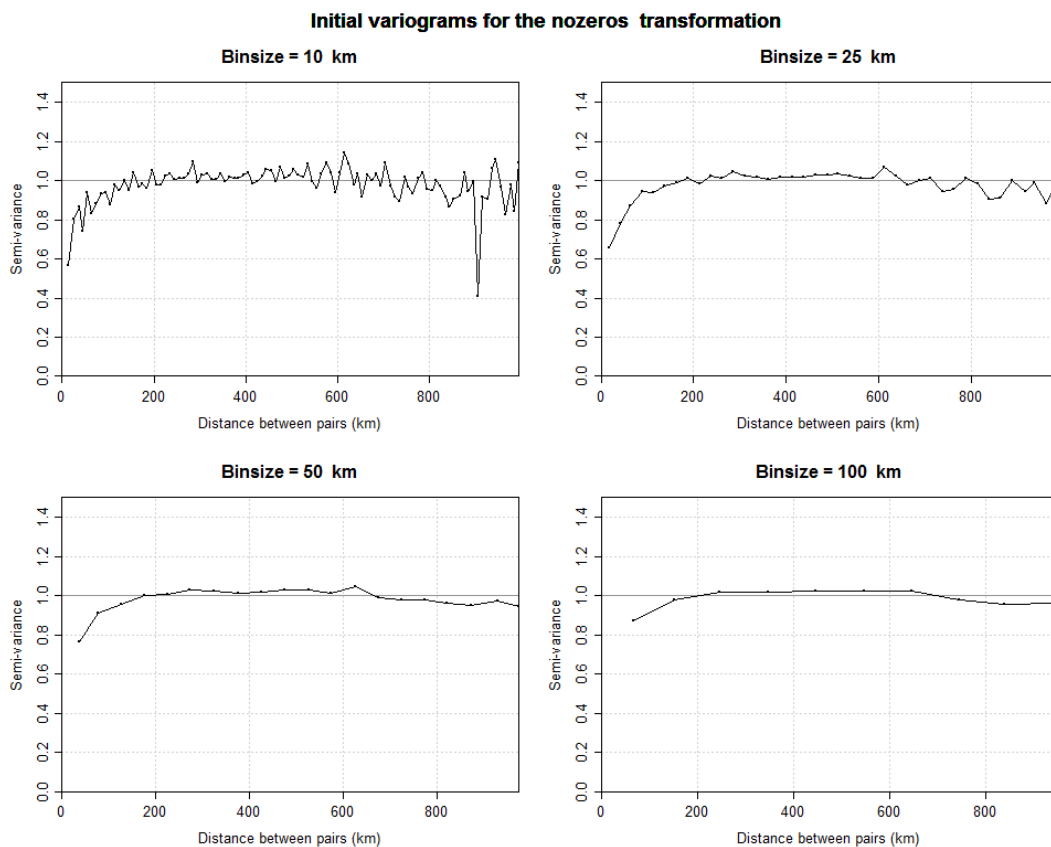


Figure 4.3 – Experimental ‘no-zero’ variograms generated by KrigeRain using different binsize settings.

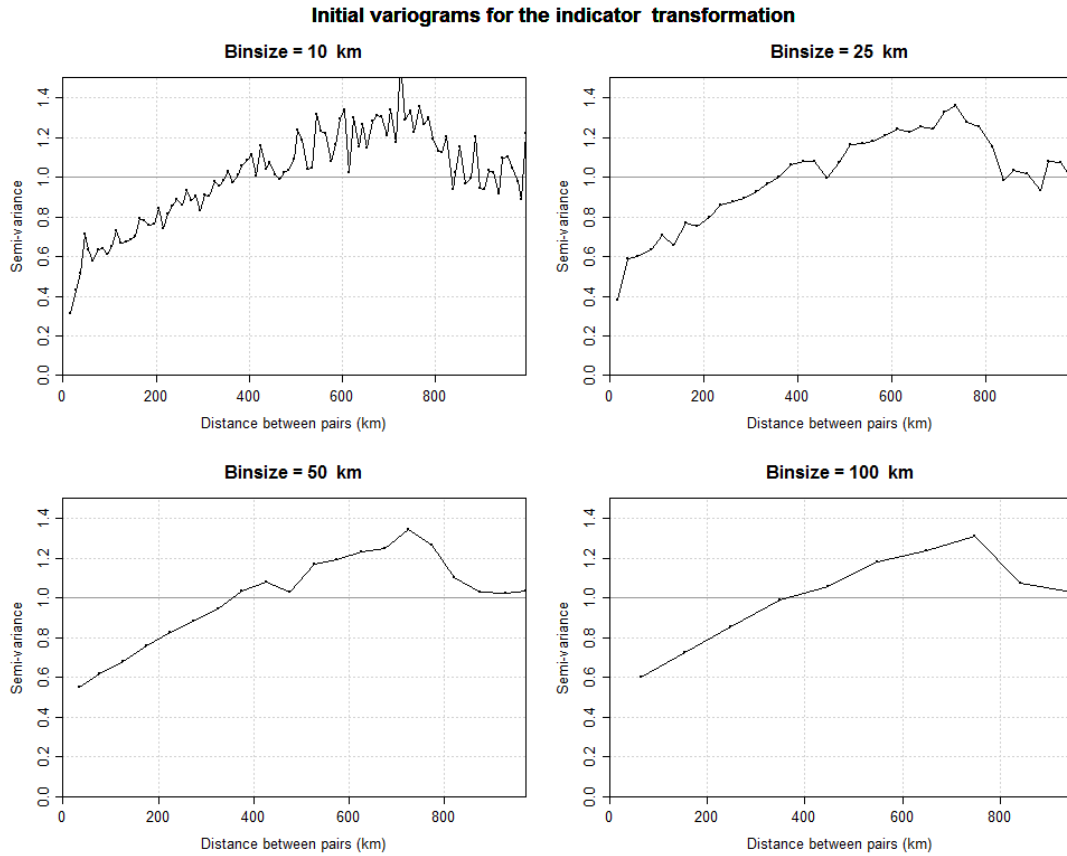


Figure 4.4 – Experimental ‘indicator’ variograms generated by KrigeRain using different binsize settings.

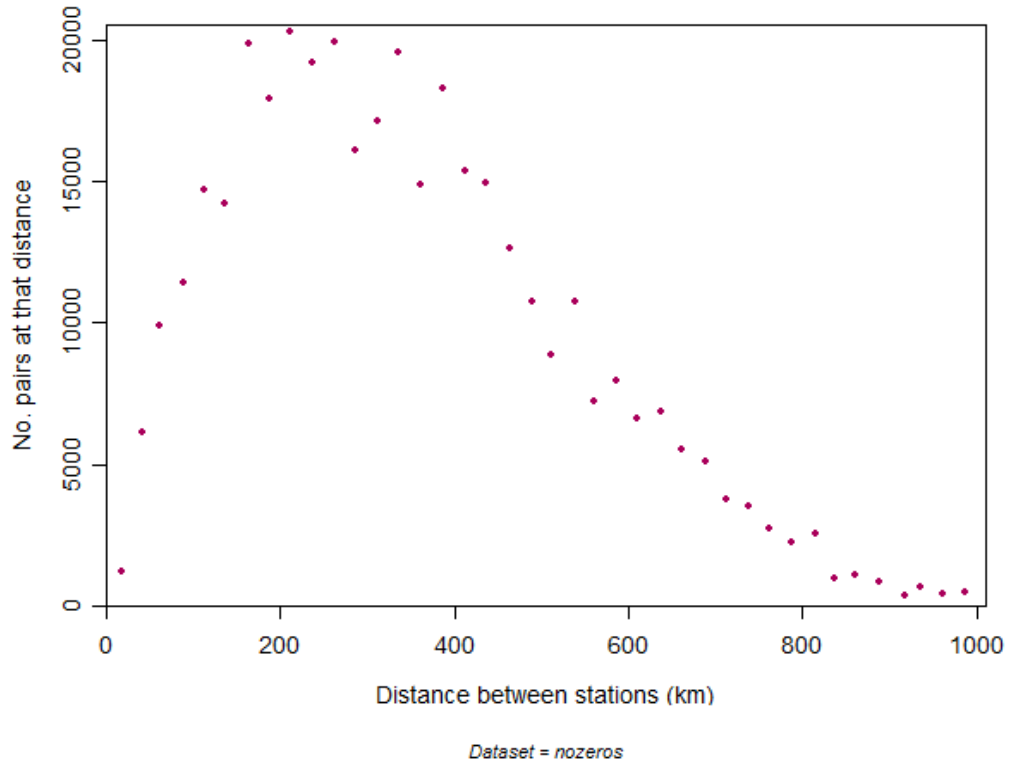


Figure 4.5 – Chart showing number of station pairs at distance for ‘no-zero’ rain field.

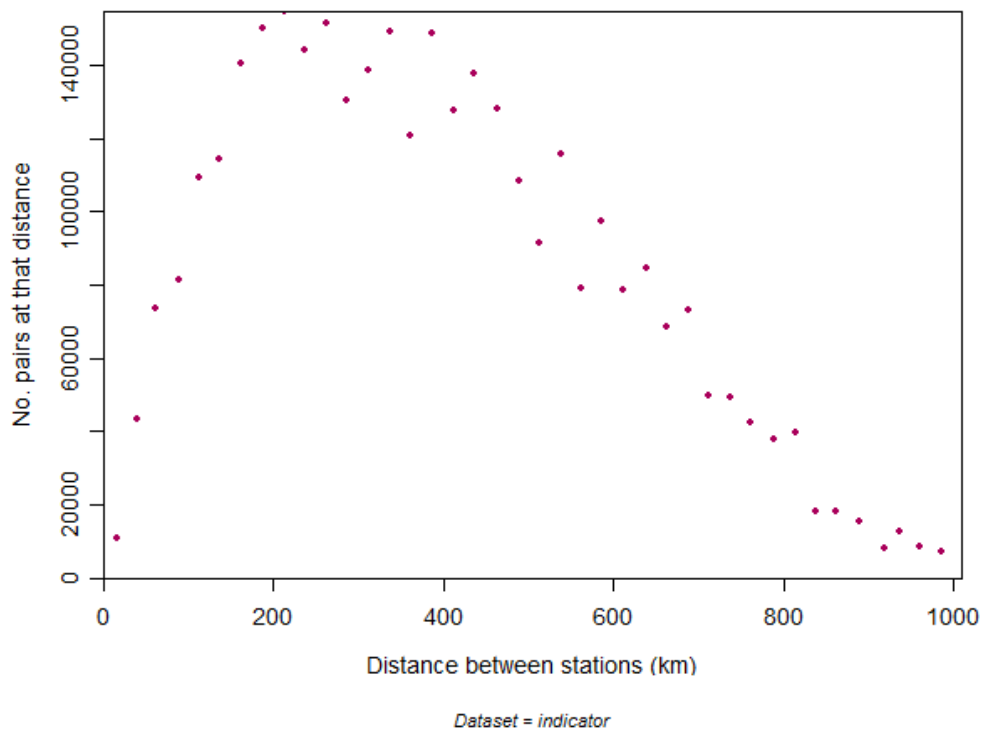


Figure 4.6 – Chart showing number of station pairs at distance for ‘indicator’ rain field.

Four different methods of variogram modelling were tested – Spherical and Exponential, as well as Double Spherical and Double Exponential (Double Spherical and Double Exponential are shown here in a development stage).

Figures 4.7 and 4.8 show the variograms fitted with each of these methods – for both the Exponential fit was selected.

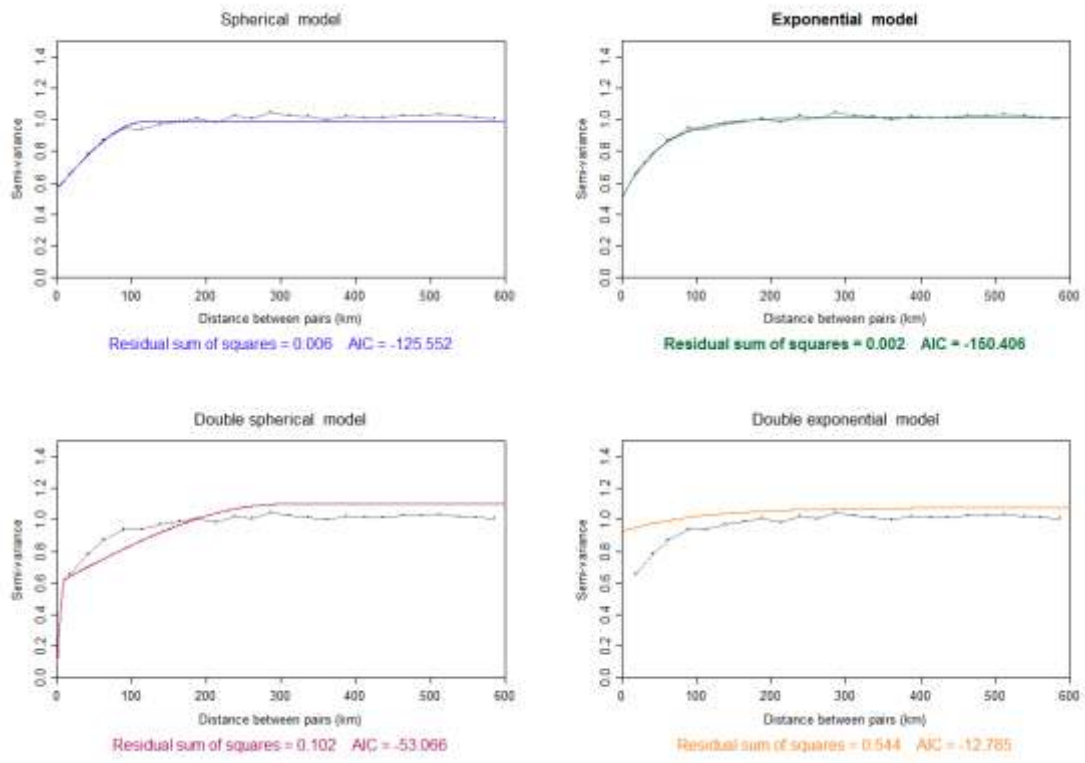


Figure 4.7 – The ‘no-zero’ rain field variogram fitted using different modelling methods.

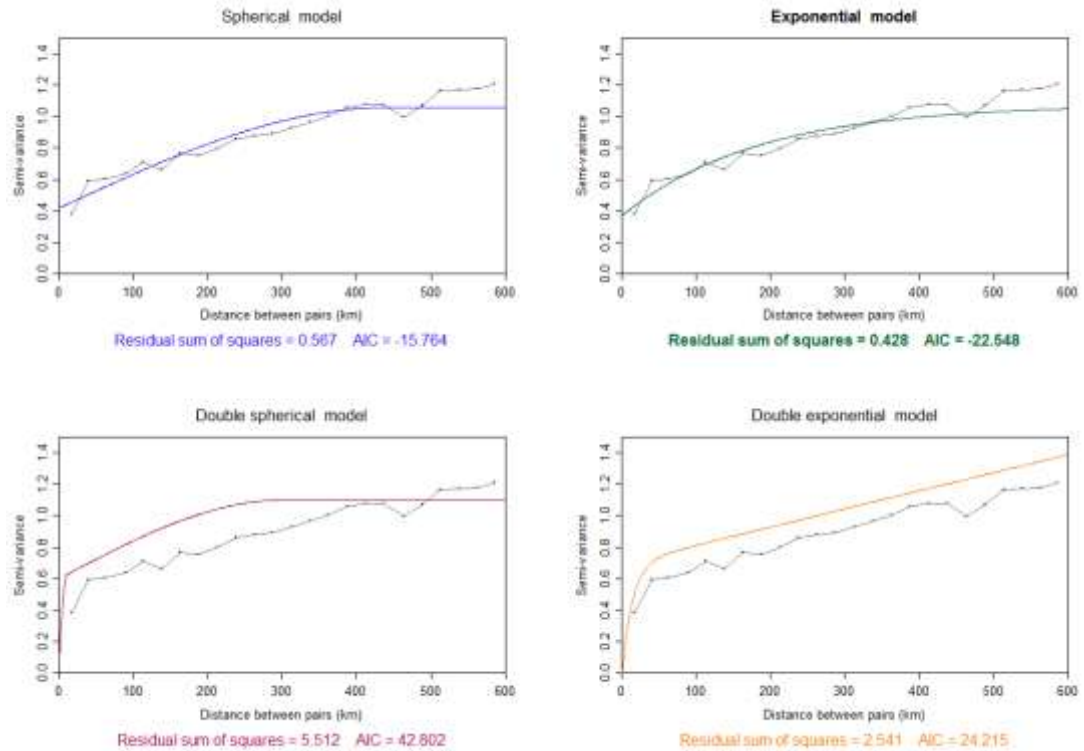


Figure 4.8 – The ‘indicator’ rain field variogram fitted using different modelling methods.

4.3.3 - Validation

In order to assess the reliability of the DK estimates it is necessary to compare the values against the point raingauge data, as well as estimates derived from OK to provide a comparison. It should be noted that the DK and OK estimates represent block average values, whilst the raingauges are point values, so a direct comparison is not possible in this instance. The validation was conducted at both gauge-pixel and catchment scales.

Comparison of Gauge, OK Rain fields and DK Rain fields at Gauge-Pixel Scale

For the comparison, all days where all raingauges recorded zero rainfall were removed from the record, as their inclusion would only provide trivial results. Similarly, days where all raingauges recorded rainfall were removed as in these cases the rain field would not be fractional and the DK method would behave identically with the OK method, although there were no days recording 100% rainfall in this dataset. R^2 was used as a measure of fit between the data sets.

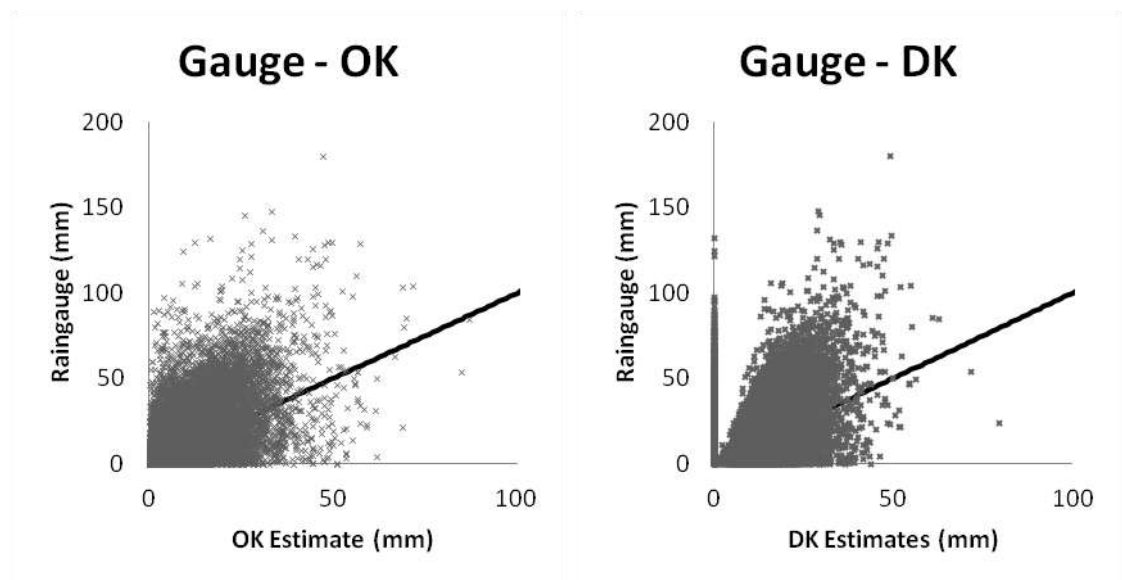


Figure 4.9 – Charts showing comparison between point raingauge and Kriging estimates for the block average of pixels containing that raingauge. The chart on the left shows comparison with OK and the chart on the right shows the comparison with DK. The solid black line indicates the 1:1 relationship.

Figure 4.9 shows the comparison between the point raingauge data and the block estimates for the pixels containing gauges, for both OK and DK. The R^2 values for both methods indicate that DK more closely resembles the raingauge rainfall, with a score of 0.52, compared to the score for OK of 0.36. DK was also

able to predict the fractional field better and was able to match correctly a pixel's rainfall status with that of the corresponding raingauge in 86.4% of cases.

Frequency Distribution - Gauge-Pixels

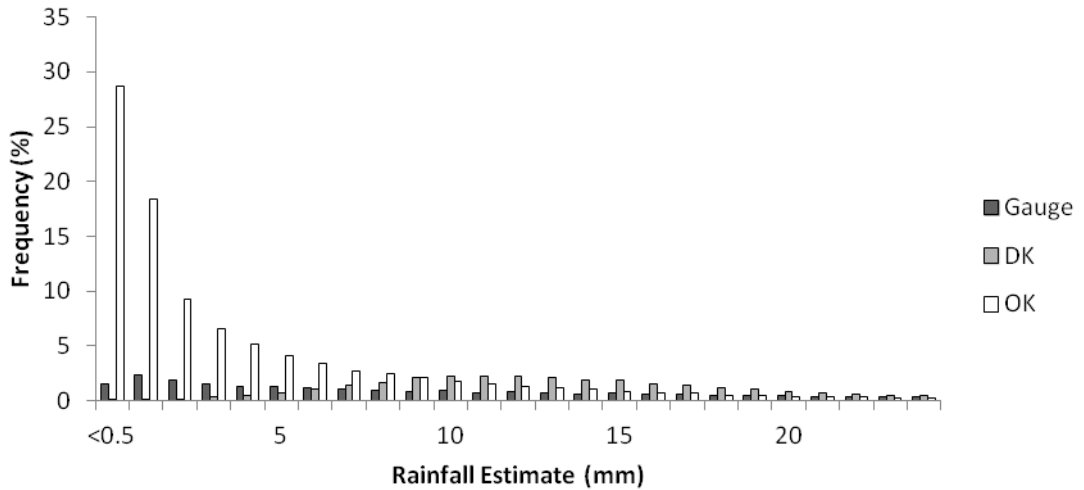


Figure 4.10 – Frequency distribution of raingauge values and block average estimates for DK and OK. Frequency includes values for zero rainfall that are not shown on the chart, these were Gauge = 72.7%, DK = 69.4% and OK = 4.1%.

The frequency distributions of rainfalls are shown in Figure 4.10, and it demonstrates a lack of comparison between the raingauges and block averaged estimates for DK and OK. DK does compare well in the frequency of rainfall with raingauges (72.7% zero rainfall for raingauges, 69.4% for DK), yet the main distribution of rainfall peaks at 12mm, much higher than the raingauge peak of 2mm. The raingauge data is also more spread, with 4.7% of the rainfall above 25mm, whilst both OK and DK predicted 1.6% of the rainfall to be above 25mm.

This is consistent with the findings of Haylock *et al.* (2008) and Maidment *et al.* (in press 2012) who noted that when using block Kriging, grid cell values will display a different distribution to point values, with the tendency of block values to converge around the mean rainfall value.

Comparison of Gauge, OK Rain fields and DK Rain fields at Catchment Scale

As previously mentioned, the point raingauge values make for a poor comparison with the block average Kriged estimates. Catchment average values for the Bakoye catchment would provide a better comparison and Table 4.1 shows this. For the Kriged estimates, the catchment average was determined by the mean of the all the pixels within the Bakoye catchment boundary – for those pixels through which the boundary intersects, the pixel was split into 100 $0.05^{\circ} \times 0.05^{\circ}$ pixels and weighted depending on the percentage of the smaller pixels within the catchment boundary. To compare the catchment average estimates of rainfall to the raingauge data, an area weighted Gauge Average estimate was produced using Thiessen Polygons, each adjusted to account for orographic effects.

Table 4.1 and Figure 4.11 compare the catchment average rainfalls from the Gauge Average and DK data at various temporal scales. It is seen in Table 4.1 that the DK estimates rainfalls that generally of greater volume than the Gauge Average, however if the possible error within each of the estimates were to be considered, the two cannot be distinguished. For example, Nespor and Sevruk (1998) suggested that wind-induced error alone can cause errors of up to 10%,

and applying such an error to the Gauge Average estimate would position the DK catchment estimate well within those bounds. Similarly, the DK method is not without error, both from cascading effects of the raingauge error and error from the interpolation method. Using 10% as a conservative estimate on the DK estimate would also put the Gauge Average estimate within those bounds of error, and when considering both together there is significant overlap.

	Gauge Average Rainfall (mm)	DK Rain (mm)
Total	7289.94	7798.91
Mean	662.72	708.99
1986	665.16	726.77
1987	562.38	595.34
1988	844.20	805.87
1989	680.03	772.00
1990	495.89	637.99
1991	672.73	683.09
1992	565.60	598.98
1993	660.21	635.16
1994	799.96	851.95
1995	685.42	763.98
1996	658.36	727.78

Table 4.1 – Table showing the total Bakoye catchment average rainfall, mean annual Bakoye catchment average rainfall and yearly wet-season totals for the Gauge Average estimate and the daily DK rain fields.

Figure 4.11 shows how the annual wet season totals vary across the period. The DK catchment average resembles the Gauge Average estimate in regards to the interannual variation of rainfall, and closely matches the totals – slightly

estimating more rainfall in most years but indistinguishable with a conservative estimate of error of 10% applied to each.

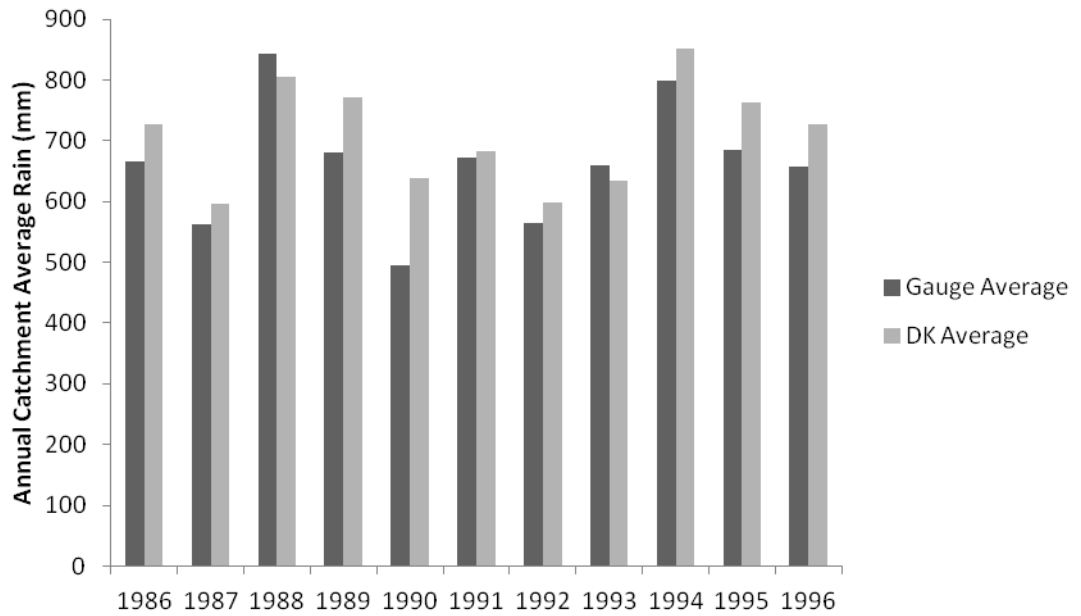


Figure 4.11 – Chart showing the annual Bakoye catchment average rainfall totals for the wet seasons of 1986-1996, for the Gauge Average estimate and the DK daily rain fields.

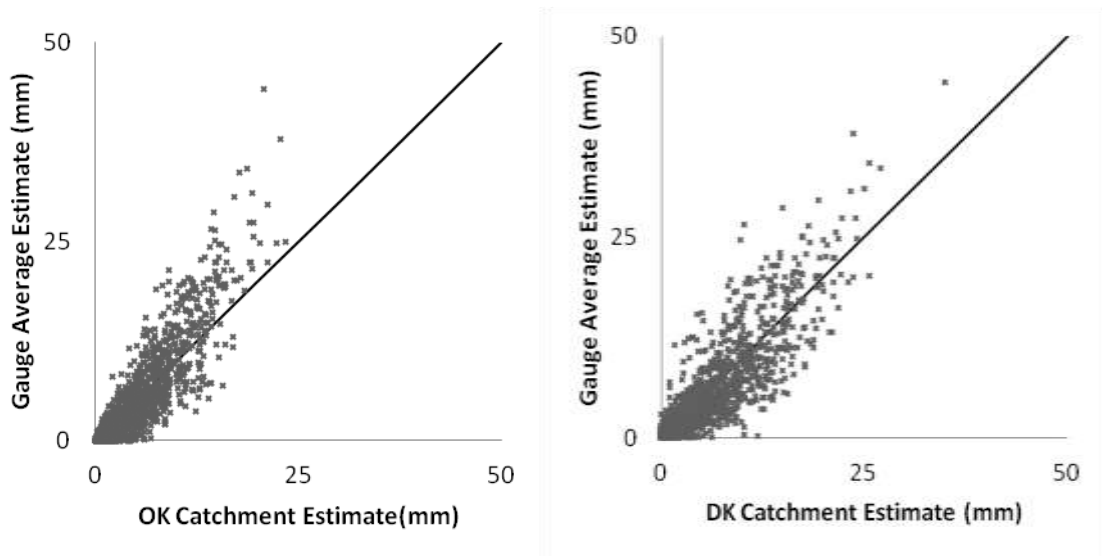


Figure 4.12 - Charts showing comparison between Bakoye catchment averages for the Gauge Average estimate and the Kriged estimates. The chart on the left shows comparison with OK and the chart on the right shows comparison with DK. The comparisons shown use all data from the wet seasons, 1986 to 1996. The solid black line indicates the 1:1 relationship.

As with the comparisons shown in Figure 4.9, the comparisons in Figure 4.12 also show that the DK method is superior, with an R^2 score of 0.83 compared to the score for OK of 0.55. Both OK and DK show significantly better comparisons with the raingauges over a catchment average than against individual pixel-point comparisons.

Figure 4.13 shows the frequency distribution of rainfall over the catchment average for the raingauge, DK and OK estimates. This shows a much stronger correlation than the frequency distribution shown in Figure 4.11, especially between the Gauge Average estimate and that for the DK catchment average. All three catchment averages peak at 2mm rainfall, but the OK produces far

more low level rainfall at the expense of zero rainfall, and rainfall of 11mm or more.

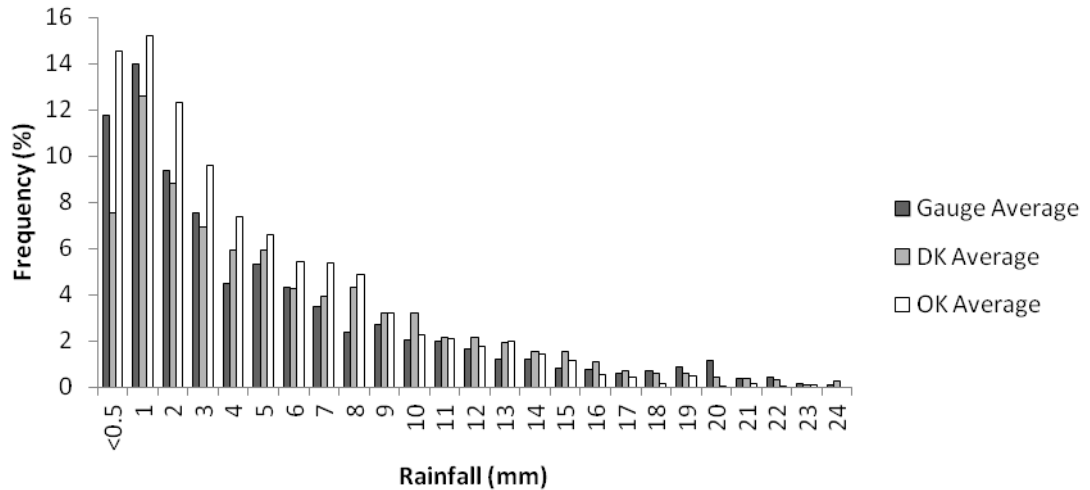


Figure 4.13 – Frequency distribution of Bakoye catchment average raingauge values and catchment average estimates of DK and OK. Zero rainfall values are included in the frequency but not shown on the chart, these were Gauge = 19.5%, DK = 19.3% and OK = 2.9%.

Influence of Spatial Resolution

The sections above have demonstrated the implementation of the DK method for the Senegal Basin for the generation of daily rain field, which are block Kriged to a spatial resolution of 0.5° and compared to point raingauge data. It is unreasonable to assume block averaged DK rainfall estimates will correlate directly with point data because of the effects of block average, as described by Maidment *et al.* (in press 2012). It was possible to produce daily rain field at a finer spatial resolution for the data available (0.05°), and the difference in the

rainfall characteristics have been used to observe the effects of spatial resolution on the block averaging of the DK rain fields.

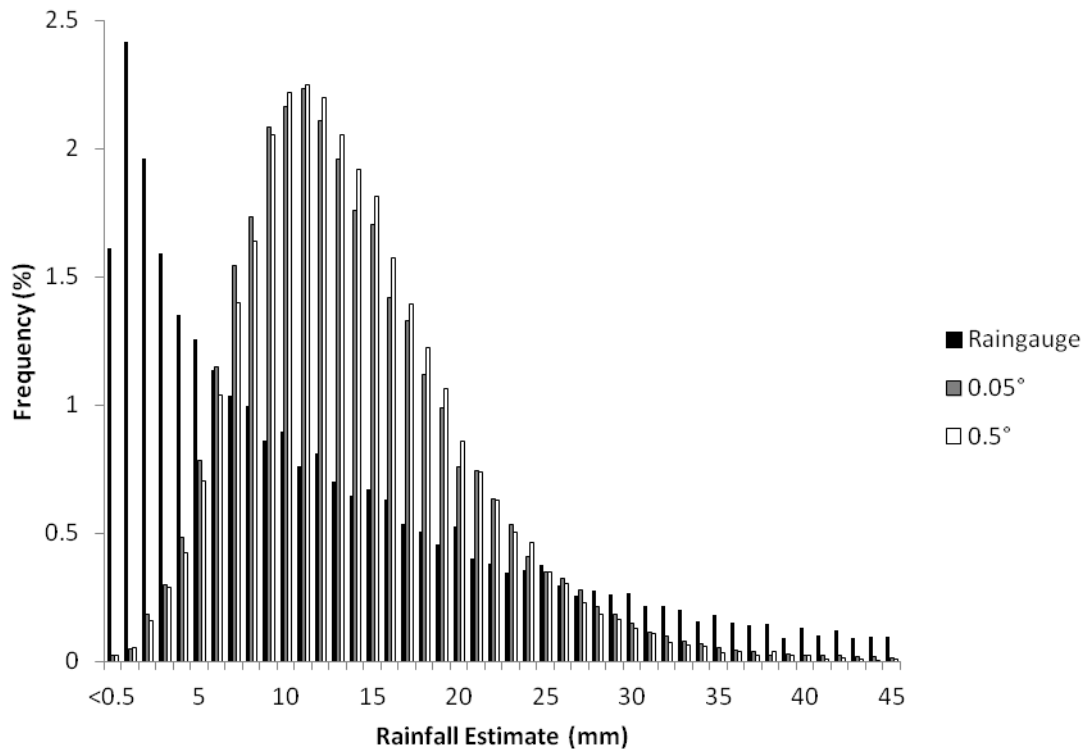


Figure 4.14 – Frequency distributions of raingauge data and block average values of DK rainfall at 0.05° and 0.5° pixel resolution. Zero rainfall is included in the frequency but not shown, these are Gauge = 72.7%, 0.05° = 69.6%, and 0.5° = 69.4%.

Figure 4.14 shows the frequency distribution of rainfall estimates for 0.05° resolution DK estimate, compared to the point value raingauge values and the 0.5° resolution estimates. It is clear that the influence of the spatial averaging by block Kriging has a more significant effect on the rainfall estimate than the difference in spatial resolution, but a slight skewness to lower rainfall values exists in the distribution when compared to the 0.5° resolution estimate and this is more in line with the raingauge values.

Table 4.2 shows the catchment average wet season rainfall estimates for the Bakoye catchment, using both the 0.5° and 0.05° pixel resolution estimates. Like the distribution of rainfall seen in Figure 4.14, there is little difference between the two estimates, especially when compared to the difference to the catchment average rainfall produced by the average of the raingauges.

	DK 0.5° Rain (mm)	DK 0.05° Rain (mm)
Total	7798.91	7905.31
Mean	708.99	718.66
1986	726.77	723.19
1987	595.34	630.04
1988	805.87	805.88
1989	772.00	776.51
1990	637.99	637.61
1991	683.09	695.48
1992	598.98	607.19
1993	635.16	656.65
1994	851.95	868.14
1995	763.98	780.77
1996	727.78	723.85

Table 4.2 – Table showing the catchment average wet season rainfall estimates for the DK rain fields, block averaged to different spatial resolutions, for the Bakoye catchment.

It has been shown in Figure 4.14 and Table 4.2 that the spatial resolution used for the block Kriging of the DK estimate has little influence over the distribution of the rainfall and the totals. Although there are slight difference these are insignificant in comparison to the difference between point estimates of rainfall – from the raingauges – and areal averages.

4.4 - Summary

The observed raingauge data has been used to obtain the mean daily rainfall for the Senegal Basin region at an aggregated Meteosat pixel resolution of $0.5^\circ \times 0.5^\circ$. A DK method was used so that not just the rainfall amount, but also a rainy/non-rainy status could be determined for each pixel. The rainfall over the Senegal Basin region is dominantly fractional, with not a single day in the record where all functional gauges reported rainfall, and the DK method showed that 86.4% of the pixel estimates for pixels containing a gauge, showed the same rainfall status of the gauge. The DK estimates compared favourably with the OK, showing far better correlation with the point raingauge values.

The method presented in this chapter, and results derived from it, are suitable for use in the calibration of TAMSAT and TAMSIM, but they could be improved. A co-Kriging technique, such as those described by Goovaerts (2000), could be employed to incorporate secondary data into the method. This data could be a DEM of the area to account for the effects of the topography described in Chapter 3, or for this catchment, it could prove beneficial to account for the large rainfall gradient across the catchment.

However, the effect of any of these improvements will be limited, just as the method described in this chapter is, by the paucity of data available for the study, especially for the Bakoye catchment area which contains just 13 raingauges for over $86,000\text{km}^2$. This lack of raingauges required the method to be applied to a much wider region in order to produce the necessary variograms – an area that displays a greater rainfall gradient than that for the catchment

area alone. Ideally the method would have been employed with a denser set of raingauges focussed around the Bakoye catchment, as this would have likely produced a better correlation between the raingauges and the DK estimates.

5

Methodology – Ensemble Representation of Satellite Rainfall Uncertainty

5.1 – Introduction

This chapter is the second of the methodology chapters and details the methods used to produce a deterministic satellite rainfall estimate (SRFE), and the methods for characterising the uncertainty within that estimate. The method used to produce a deterministic SRFE was TAMSAT1, and TAMSIM was used to characterise the uncertainty. Both methods were introduced by Teo (2006) and Teo and Grimes (2007).

5.2 – TAMSAT1

Of the available SRFE methods summarised in Chapter 2, the expanded TAMSAT method of Teo and Grimes (2007) was used to produce daily SRFE for the Senegal Basin. The method, known as TAMSAT1, was introduced in Teo (2006) and has some important advantages over the other methods making

it suitable for this area, namely its ability to be calibrated locally using historic raingauge networks, its requirement for only a single TIR satellite input and the long operational history of the method in sub-Saharan Africa. In addition, the TAMSIM algorithm for characterising the uncertainty has been previously successfully presented in Teo (2006) and Teo and Grimes (2007) – a significant advantage of using TAMSAT1.

Previous studies have shown that global SRFE that incorporate PM inputs show greater skill in estimating rainfall for Africa, over those that only use TIR and/or raingauges for more complex, mountainous terrain (Dinku *et al.*, 2007 & 2010). However, the use of PM sensors has limitations for certain types of land surface which are often mistaken for raining areas (Dinku *et al.*, 2010). In the study by Dinku *et al.* (2007) the dekadal TAMSAT estimate was found to outperform all of the more sophisticated, multi-sensor SRFE, largely attributed to its use of a regional calibration as opposed to a global calibration. The algorithms that make use of PM data have yet to be calibrated for the semi-arid regions of Africa, and such a task is complicated as it would require a large volume of ground data that is unlikely to be available (Morland *et al.*, 2001).

As TIR based SRFE generally rely upon an indirect relationship between cloud top temperature and actual rainfall, the rainfall estimations contain significant uncertainties, principally in three aspects:

1. Temporal - When it is raining
2. Spatial - Where it is raining

3. Rate - How much it is raining

The TAMSAT method, and TAMSAT1, is subject to these uncertainties and therefore there is a requirement for an accurate and appropriate method to characterise this uncertainty, in such a way that can be translated into downstream applications.

The TAMSAT1 method has been selected for the generation of a deterministic SRFE for the Senegal Basin area, at a daily time-step. Teo and Grimes (2007) introduced the TAMSAT1 method, an extension of the TAMSAT method, to produce daily rainfall estimates. This section provides a summary of the method, a comprehensive methodology can be found in Teo (2006). The method implemented here is a modification to that of Teo (2006), in that it does not include a representation of the DK error which was sacrificed to allow for a more accurate method of modelling the gamma distribution of no-zero DK rainfall at gauge-pixels plotted at D_T bins.

The TAMSAT method, as described in the previous section, uses a locally calibrated relationship between cloud top temperature and the historic raingauge record. A full description of the method can be found in Milford and Dugdale (1990). TAMSAT uses a Cold Cloud Duration (CCD) technique, where Meteosat TIR data is used to obtain cloud top temperatures at 15 minute time-steps with cloudy pixels below a specified temperature threshold assumed to be rainy – cold clouds are associated with high topped cumulonimbus clouds, synonymous with convective rainfall. The total period in a day that a pixel is

below the threshold is its CCD, or D_T . For TAMSAT the CCD represents the total period below the threshold for a given dekad and is used to calculate a dekadal estimate of rainfall, R_{10} .

Equation 5.1

$$R_{10} = \begin{cases} a_0 + a_1(D_T) & D_T > 0 \\ 0 & D_T = 0 \end{cases}$$

Equation 5.1 shows the simple linear relationship used to generate the dekadal estimate of rainfall, R_{10} , using the TAMSAT method. The values for the parameters a_0 and a_1 are calibrated by plotting CCD values against DK rainfall values for pixel's containing at least one raingauge (gauge-pixels).

The linear relationship used in Equation 5.1 has been found to be successful at dekad scale (Dinku *et al.*, 2007), but is too simplistic to represent the more spatially and temporally varied nature of daily rainfall. Of particular importance is the representation of the fractional nature of the rainfall field which is greater at smaller time-steps. In order to address these issues Teo (2006) developed the TAMSAT1 method and found that it outperformed the original TAMSAT method for estimation of daily rainfall fields for the Gambia region. Equation 5.2 shows the calculation of daily rainfall, Z at pixel location u in its simplest form, and is expanded below.

Equation 5.2

$$Z_{(u)} = p \cdot \mu$$

Equation 5.2 shows the principal of TAMSAT1, where the rainfall is the product of the probability of rainfall at D_T , p , and the mean rainfall at D_T with the zero values removed, μ . The calculation of p is shown in Equation 5.3 and the calculation of μ is shown in Equation 5.4.

Equation 5.3

$$p = \frac{1}{e^{-(b_0 + b_1 D_T)}}$$

The parameters b_0 and b_1 are found by plotting the probability of rainfall from the DK gauge-pixels against D_T , and fitting the relationship using logistic regression. The probability of rainfall at $D_T = 0$, p_0 , is excluded from the fit and the actual probability is used instead.

Equation 5.4

$$\mu = a_0 + a_1 D_T$$

In Equation 5.4, μ is the mean rainfall at D_T , derived from gamma fits of no-zero DK rainfall at gauge-pixels plotted at D_T bins, using a maximum likelihood method (n.b. – the original method in Teo (2006) used a method of moments fit). The shape and rate functions of each gamma distribution are modelled to D_T so that a linear relationship between mean rainfall and D_T is produced, when μ is equal to the product of the shape and rate functions. This linear relationship is expressed in Equation 5.4.

The combination of Equation 5.2 with the components shown in Equations 5.3 and 5.4 allows the calculation of $Z_{(u)}$ to be expanded into its complete form, as seen in Equation 5.5.

Equation 5.5

$$Z_{(u)} = \begin{cases} \frac{1}{e^{-(b_0+b_1D_T)}} (a_0 + a_1D_T) & D_T > 0 \\ p_0(a_0) & D_T = 0 \end{cases}$$

The calibration of the parameters required by Equation 5.5 is detailed in Section 5.4. The rainfall characteristics generated by the TAMSAT1 method are also used in the TAMSIM method of producing stochastic ensemble rainfall sets, as detailed in Section 5.3. As can be seen in Equation 5.5, TAMSAT1 does not produce a fractional rain field, with small amounts of rainfall simulated at $D_T = 0$. Corrections can be applied, for example Teo (2006) applied a Large Domain Zeros (LDZ) check that set the entire rain field to zero rain on days where 95% of the pixels recorded zero CCD. This produced more realistic looking rainfall estimates, but made them less optimal in regards to point errors.

5.3 – TAMSIM

The TAMSIM method was used for the characterisation of the uncertainty within the TAMSAT1 SRFE, described in the previous section. As well as having already been successfully implemented and validated for use with the TAMSAT1 method, for generation of Gambian daily rain fields (Teo, 2006, Teo and Grimes, 2007), it has some distinct advantages over other methods.

Importantly, TAMSIM retains the geostatistical properties of the raingauge derived rainfall field and allows for the generation of fractional rainfall fields. As the Senegal Basin shows a large rainfall gradient (see Chapter 3), it is important that the ensemble rain fields are able to distinguish between the areas where it is raining and the areas where it is not.

With the uncertainty within the SRFE characterised, it needs to be translated to a downstream application to measure the extent of propagation. In Teo (2006) and Teo and Grimes (2007) this was a crop yield model, and for this thesis this will be a hydrological model.

The remainder of this section presents a methodology for the TAMSIM algorithm, as introduced by Teo (2006) and Teo and Grime (2007), where a comprehensive methodology can be seen.

In its simplest form the equation governing TAMSIM is the same as Equation 4.1, the Equation used for DK from Barancourt *et al.* (1992). In this case, the two RFs, $I(u)$ and $F(u)$, are generated using sequential sequencing techniques outlined below. The TAMSIM algorithm is thus divided into two separate algorithms that calculate the two necessary RFs:

1. **Sequential Indicator Simulation (sls)** – produces a binary rain/no-rain ‘indicator’ field demarcating the areas that are rainy and those that are not.

2. **Sequential Gaussian Simulation (sGs)** – produces a rainfall field by simulating rainfall amounts for the pixels identified as rainy during sls.

This section will look at the sls and sGs stages separately before demonstrating how TAMSIM combines them.

Sequential Indicator Simulation (sls)

The first stage of the TAMSIM algorithm is the sls that produces a binary RF of rain/no-rain areas. Before running it requires a calibration of the probability of rainfall at each specified CCD bin and this is derived using Equation 5.3, in the same way as for TAMSAT1. The method also uses a simple Kriging (SK) method and this requires a variogram of the indicator residuals to be produced. More details of the TAMSIM calibrations can be found in Section 5.4.

Figure 5.1 shows a schematic taken from Teo and Grimes (2007) detailing the steps taken by sls to produce the indicator RF, for a theoretical nine cell grid.

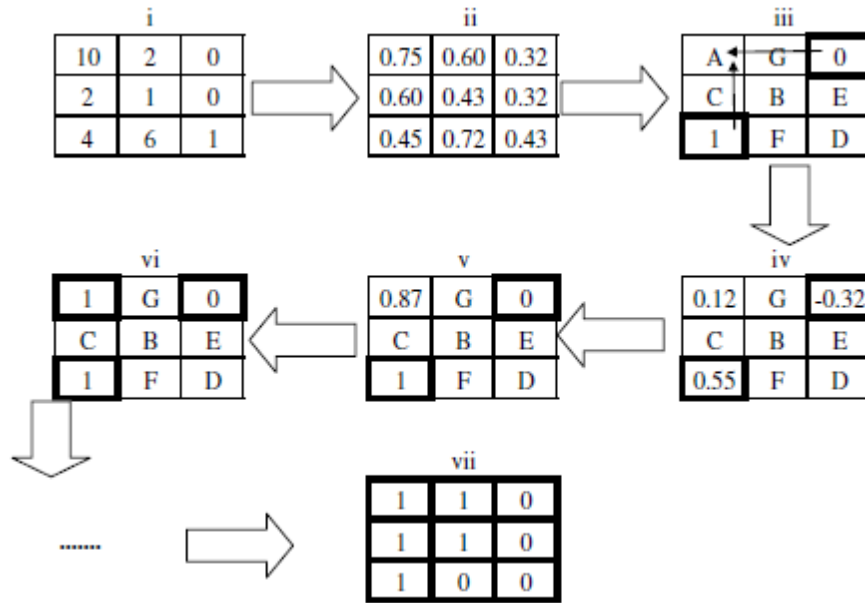


Figure 5.1 – Schematic from Teo and Grimes (2007) showing the steps required for the operation of the sIs algorithm on a theoretical nine cells system. The steps are (i) input initial CCD values for each pixel. (ii) CCD values are substituted with the probability of rain at that CCD using Equation 5.3. (iii) Independent seed pixels are selected and given a rain/no-rain status via Bernoulli trial. (iv) Residuals are calculated for each of the seed pixels by subtracting the probability of rain for that pixel from the binary rainfall status it was assigned. A random path is determined for the remaining pixels A-G. The residuals are used to produce a residual value for pixel A using simple Kriging (SK). (v) The residual value for pixel A is added to the probability of rain for the pixel for its total probability of rainfall. (vi) Pixel A is assigned a rain/no-rain status, based on the probability of rainfall at that pixel’s CCD value, and is added to the set of seed pixels. (vii) Steps iii-vi are repeated until each pixel is assigned a rainfall status.

Sequential Gaussian Simulation (sGs)

After producing the indicator RF via sIs, TAMSIM then uses this field to start the sGs stage to estimate rainfall for each pixel designated as raining. This step requires a distribution of rainfall to be modelled for each specified CCD bin, and

this was done by modelling a gamma distribution by fitting to CCD-binned no-zero DK rain data, in the same way as described for TAMSAT1. The shape and rate functions are then modelled in a way to produce a linear fit of mean rainfall. In addition, sGs requires a variogram of no-zero rainfall residuals to be produced. Further details of the calibration can be found in Section 5.4.

Figure 5.2 shows a step-by-step schematic of the sGs process, taken from Teo and Grimes (2007).

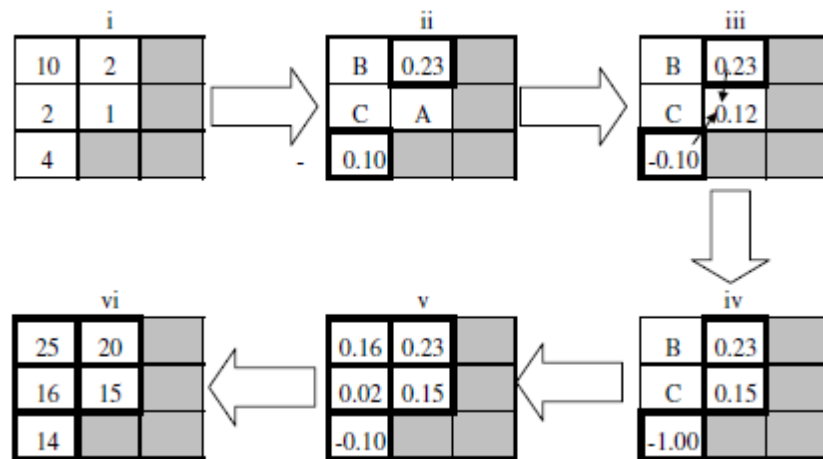


Figure 5.2 – Schematic from Teo and Grimes (2007) showing the steps taken by the sGs algorithm, for the same theoretical nine cells system shown in Figure 5.1. (i) CCD values for pixels designated as raining by sIs are inputted. (ii) Independent seed pixels are selected and allocated Gaussian residual values. A random path is assigned for the remaining pixels A-C. (iii) A Gaussian residual value is calculated for pixel A by SK of the seed pixels. (iv) A final residual value is assigned to Pixel A by sampling within the SK bounds, and is added to the set of seed pixels. (v) Steps iii and iv are repeated until all pixels are assigned a Gaussian residual value. (vi) The Gaussian residuals are back-transformed and added to the original estimate for that pixel’s CCD value, providing an estimate of rainfall for that pixel.

Combining the Field – Producing Ensembles

By combination of a single sls field and a single sGs field the TAMSIM algorithm will produce a single ensemble representation of a probable rainfall field. The algorithm produces a set of equiprobable ensemble members by combining the two fields, saving computational time by running the sGs algorithm multiple times for each sls realisation.

5.4 – Implementation of TAMSAT1 and TAMSIM

5.4.1 – Introduction

This section looks at the implementation of the TAMSAT1 algorithm, its calibration, production of a deterministic estimate of the rainfall field and the validation of that field. The TAMSIM algorithm shares much of the same calibration procedure as TAMSAT1, and the necessary extensions for TAMSIM are also detailed here.

Both the TAMSAT1 and TAMSIM rainfall fields were produced using a modified version of the Genrain (SIMU) algorithm in the Matlab environment, written by Teo (2006) and provided by Dr David Grimes, Department of Meteorology, University of Reading.

5.4.2 – Calibration

The TAMSAT1 and TAMSIM algorithms were detailed in Sections 5.2 and 5.3.

The calibration of TAMSAT1 can be split into three stages:

- Determination of the optimal temperature threshold
- Determining the probability of rainfall at CCD
- Determination of positive rainfall rate at CCD

Determining the optimal temperature threshold

A suitable temperature threshold (T) needs to be identified for determining the Cold Cloud Duration (CCD) for each pixel of the satellite image – the threshold being the temperature below which a cloud can be said to be rainy. The TAMSAT CCD data is provided at $0.05^\circ \times 0.05^\circ$ pixel resolution, but as it was not possible to complete the test at this resolution it was necessary to aggregate the data to $0.5^\circ \times 0.5^\circ$ pixels to match the pixels representing the DK rain fields. This was taken as the mean CCD of every pixel within corresponding DK pixels.

The most suitable temperature threshold was selected by directly comparing the CCD data with the indicator field from the DK data, for gauge-pixels only – those pixels which contain at least one raingauge. Table 5.1 shows a contingency table used as part of the calibration, where Z is the rainfall of a DK gauge-pixel and D_T is the CCD at the same gauge-pixel at a particular temperature threshold. The calibration was conducted for daily rainfall and

CCD, using only the wet season data. Ideally an individual calibration would be performed for each month, however due to the paucity of data available only a single calibration was conducted for the whole wet season. Similarly, because of the large area used for the study, zonal calibrations would have been useful but not possible in this circumstance.

	$D_T=0$	$D_T>0$
$Z=0$	n_{11}	n_{12}
$Z>0$	n_{21}	n_{22}

Table 5.1 – Example contingency table for the selection of a temperature threshold for TAMSAT CCD (T) (after Teo, 2006).

The selected temperature threshold is the one that best satisfies the selection criteria outlined by Milford and Dugdale (1990) and Grimes *et al.* (1999), which can be summarised as:

$$\text{Criteria 1} = \frac{n_{11} + n_{22}}{n_{12} + n_{21}} \gg 1$$

$$\text{Criteria 2} = \frac{n_{21}}{n_{12}} \approx 1$$

The TAMSAT CCD data is provided at temperature thresholds of -20°C , -30°C , -40°C , -50°C and -60°C .

Table 5.2 shows the calibration data for the Senegal Basin area for the study period, at each available temperature threshold. A ‘hit’ is when a gauge-pixel shows either both zero rainfall and zero CCD, or positive rainfall and positive

CCD. All other cases are 'misses'. The best performing temperature threshold is -60°C , where 65.35% of the gauge-pixels showed a hit. This is similar to that determined by Teo (2006) for the Gambia region, where the -60°C was selected for each month of the wet season, except for August where -50°C was used.

CCD Threshold ($^{\circ}\text{C}$)		$D_T=0$	$D_T>0$	Total	Criteria 1	Criteria 2	% correct																																																																							
-20	Z=0	34573	34261	103696	1.29	0.25	53.45																																																																							
	Z>0	8611	20851							$D_T=0$	$D_T>0$	Total				-30	Z=0	41305	27951	103696	1.53	0.40	57.58	Z>0	11080	18401			$D_T=0$	$D_T>0$	Total				-40	Z=0	46921	22801	103696	1.73	0.59	60.64	Z>0	13510	15964			$D_T=0$	$D_T>0$	Total				-50	Z=0	52783	17588	103696	1.94	0.93	63.52	Z>0	16441	13088			$D_T=0$	$D_T>0$	Total				-60	Z=0	58625	11600	103696	2.14
		$D_T=0$	$D_T>0$	Total																																																																										
-30	Z=0	41305	27951	103696	1.53	0.40	57.58																																																																							
	Z>0	11080	18401							$D_T=0$	$D_T>0$	Total				-40	Z=0	46921	22801	103696	1.73	0.59	60.64	Z>0	13510	15964			$D_T=0$	$D_T>0$	Total				-50	Z=0	52783	17588	103696	1.94	0.93	63.52	Z>0	16441	13088			$D_T=0$	$D_T>0$	Total				-60	Z=0	58625	11600	103696	2.14	1.73	65.35	Z>0	20098	9138														
		$D_T=0$	$D_T>0$	Total																																																																										
-40	Z=0	46921	22801	103696	1.73	0.59	60.64																																																																							
	Z>0	13510	15964							$D_T=0$	$D_T>0$	Total				-50	Z=0	52783	17588	103696	1.94	0.93	63.52	Z>0	16441	13088			$D_T=0$	$D_T>0$	Total				-60	Z=0	58625	11600	103696	2.14	1.73	65.35	Z>0	20098	9138																																	
		$D_T=0$	$D_T>0$	Total																																																																										
-50	Z=0	52783	17588	103696	1.94	0.93	63.52																																																																							
	Z>0	16441	13088							$D_T=0$	$D_T>0$	Total				-60	Z=0	58625	11600	103696	2.14	1.73	65.35	Z>0	20098	9138																																																				
		$D_T=0$	$D_T>0$	Total																																																																										
-60	Z=0	58625	11600	103696	2.14	1.73	65.35																																																																							
	Z>0	20098	9138																																																																											

Table 5.2 – TAMSAT temperature threshold calibration table, where z represents DK rainfall at gauge-pixels and D_T represents the CCD at gauge-pixels at specified threshold.

Determination of Probability of Rain at CCD

The calibration of probability of rain at CCD was conducted by comparing DK and CCD gauge-pixel data. The DK was converted to a binary rain/no-rain field and the CCD data was binned to nearest CCD hour (D_T). The probability of rain

at each CCD hourly bin was calculated from the DK gauge-pixel data, and modelled by fitting using logistic regression. As shown in the methodology in Section 5.3, it is necessary to estimate the empirical constants of b_0 and b_1 , when –

$$\ln\left(\frac{p}{1-p}\right) = b_0 + b_1 \times D_T$$

where p is the sample probability of rainfall at D_T .

The empirical constants b_0 and b_1 are then used to model p using the equation

–

$$p = \frac{1}{1 + e^{-(b_0 + b_1 \times D_T)}}$$

As there were too few values corresponding to $D_T > 8$, these were excluded from the fit. As the probability of rain at $D_T = 0$ is much less than at $D_T > 0$, this too was excluded from the fit, and the actual probability of rain at $D_T = 0$ was used instead. The fitted relationship between the probability of rain and CCD is shown in Figure 5.3.

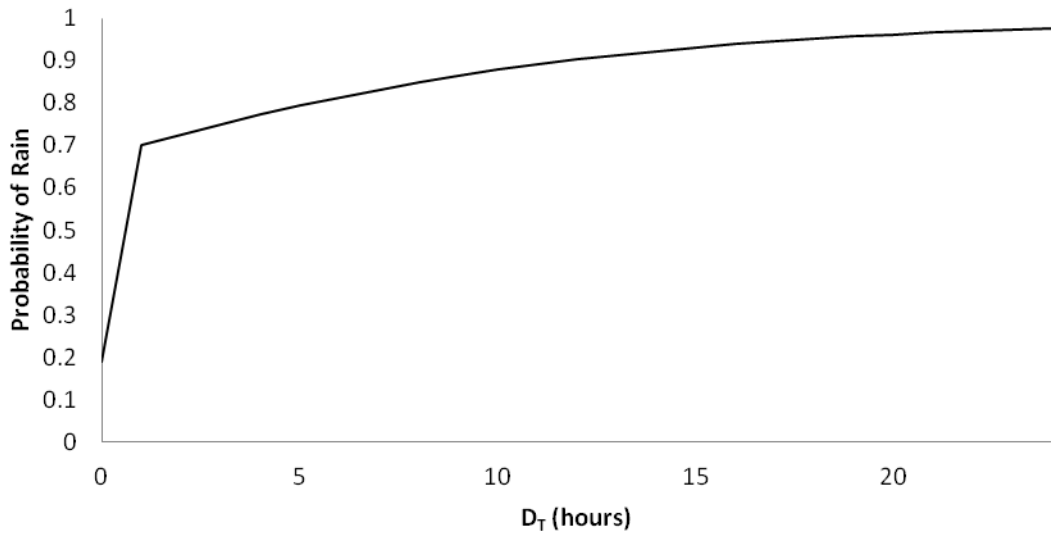


Figure 5.3 – Chart showing the modelled relationship between probability of rain and CCD at hourly bins (D_T).

Determination of Positive Rainfall Rate at CCD

To determine the rainfall rate at CCD for use in the TAMSIM algorithm the DK gauge-pixel data, with zero rainfall values removed, was compared against the CCD gauge-pixel sorted into hourly bins. A gamma distribution was fitted to the rainfall at each of these hourly bins.

Teo (2006) used a method of moments technique for fitting the gamma distributions, but for this thesis a maximum likelihood technique was used instead as it provides a better fit for the distributions. The simple representation of DK error used by Teo (2006) was not directly transferable to the maximum likelihood method used in this thesis and has not been included.

The shape and rate parameters from each of the modelled distributions were fitted to produce modelled parameter values for the TAMSIM algorithm. For values of $D_T > 7$ hours there was not enough data to produce a suitable distributions so these values were excluded from the fit, as was $D_T = 0$ where the actual parameters were used.

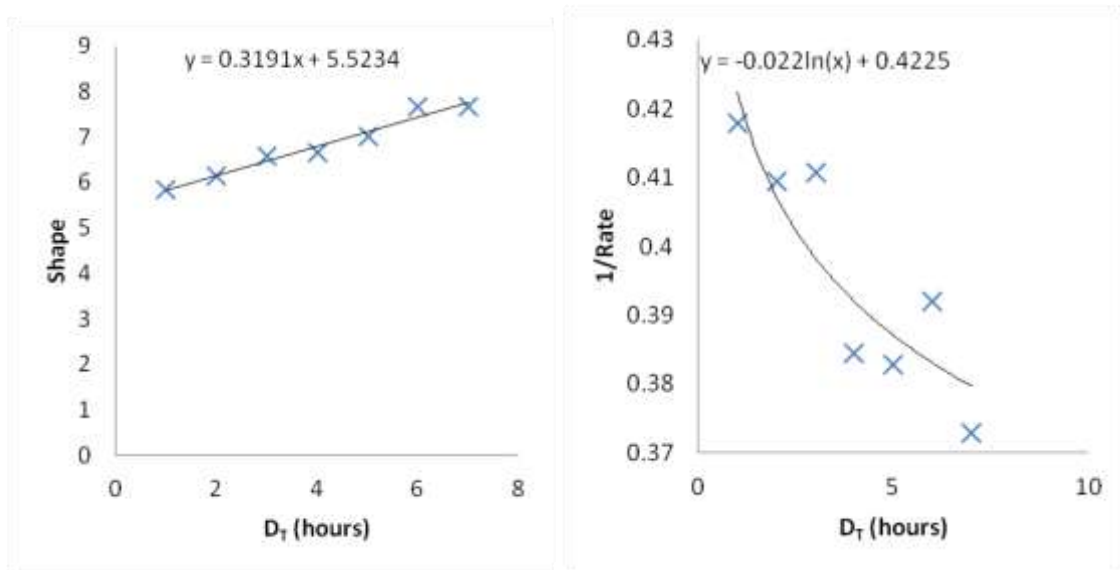


Figure 5.4 – The fitted α (shape) and β (rate) parameters for generation of gamma distributions of rainfall at D_T .

The shape parameter, α , was modelled by using a linear fit, shown in Figure 5.4. The rate function, β , was fitted using a logarithmic regression of the $1/\text{rate}$ values, also shown in Figure 5.4. By using a logarithmic regression fit it was possible to produce a linear mean for rainfall, \hat{u} , against CCD, consistent with TAMSAT, when:

$$\hat{u} = \alpha \cdot \beta$$

The relationship between modelled mean rainfall against CCD is shown in Figure 5.5.

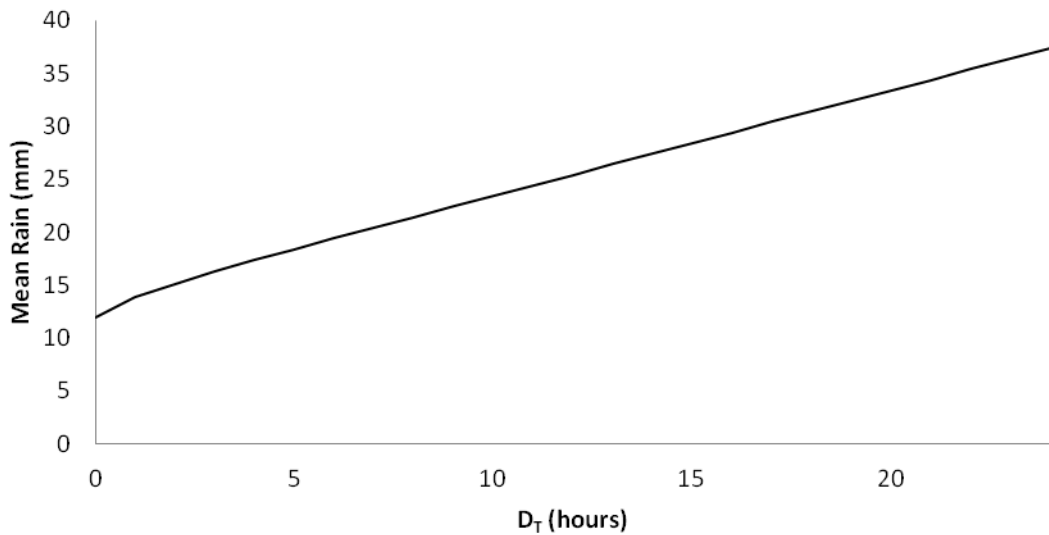


Figure 5.5 – Fitted mean rainfall at D_T . Mean rainfall at $D_T=0$ is not included in the fit and the mean is derived from the actual mean.

5.4.3 – Validation of the TAMSAT1 SRFE

A deterministic SRFE has been produced for the Senegal Basin, for the wet seasons of the study period (1986-1996), using the TAMSAT1 method. The daily rain fields produced were clipped to the Bakoye catchment to produce a catchment average TAMSAT1 estimate for use in the Pitman model. The TAMSAT1 method was validated for the Bakoye catchment by comparing the characteristics of the catchment average TAMSAT1 estimate to the catchment average DK estimates. Table 5.3 shows the totals of these catchment average rainfalls at various temporal scales.

	DK Rain (mm)	TAMSAT1 Rain (mm)
Total	7798.91	7227.58
Mean	708.99	657.05
1986	726.77	628.28
1987	595.34	641.72
1988	805.87	726.89
1989	772.00	636.52
1990	637.99	685.87
1991	683.09	649.99
1992	598.98	657.55
1993	635.16	617.84
1994	851.95	697.28
1995	763.98	676.27
1996	727.78	609.36

Figure 5.3 – Table showing the total catchment average rainfall, mean annual Bakoye catchment average rainfall and yearly wet-season totals for DK and TAMSAT1 daily rain fields.

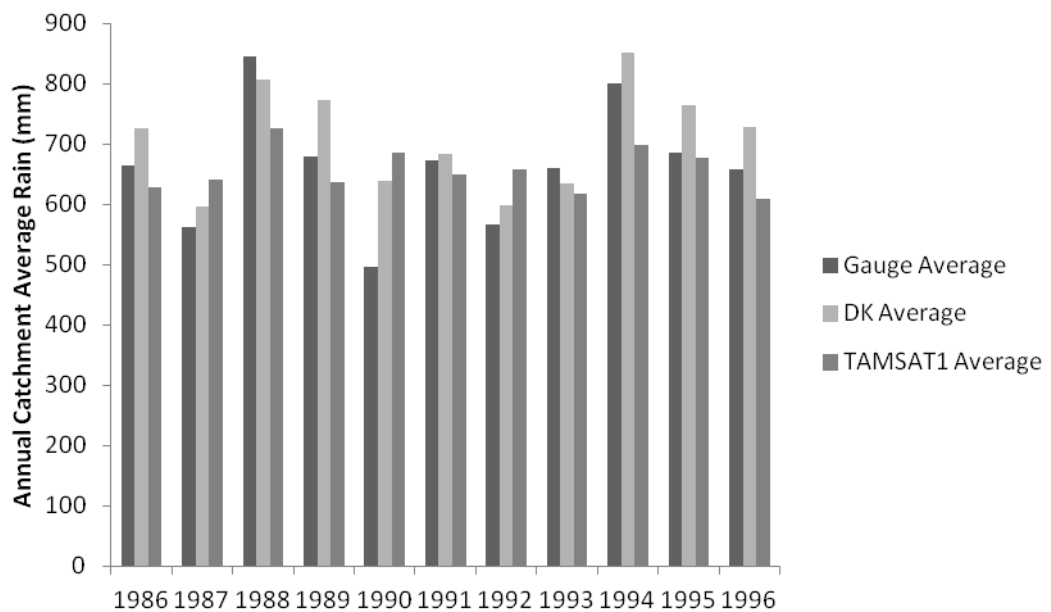


Figure 5.6 – Bar chart showing the annual Bakoye catchment average rainfall totals for the wet seasons of 1986-1996, for raingauge data, the DK and TAMSAT1 daily rain fields.

Table 5.3 and Figure 5.6 compare the catchment average rainfalls for the DK and TAMSAT1 rainfall estimates for the entire 11 year period (wet seasons only), and for each individual wet season. The TAMSAT1 catchment averages estimate a lower level of rainfall than the DK catchment averages, although even using a conservative estimate of error (due to raingauge measurement and interpolation errors) of 10% the three estimates of rainfall show significant overlap and could be said to be indistinguishable. However, the TAMSAT1 catchment averages also fail to reproduce the interannual variation evident in the DK catchment averages – this is caused by the use of a climatic calibration, which will cause smoothing of interannual variability and introduces a systematic bias for years of anomalous rainfall.

Figures 5.7 and 5.8 compare the distributions of catchment average rainfalls for the TAMSAT1 estimate and the DK estimate. TAMSAT1 does not produce a fractional rainfall field and as such does not model any zero rainfall in the record. This results in greater frequency of low level rainfall, especially 1.5-2.5mm.

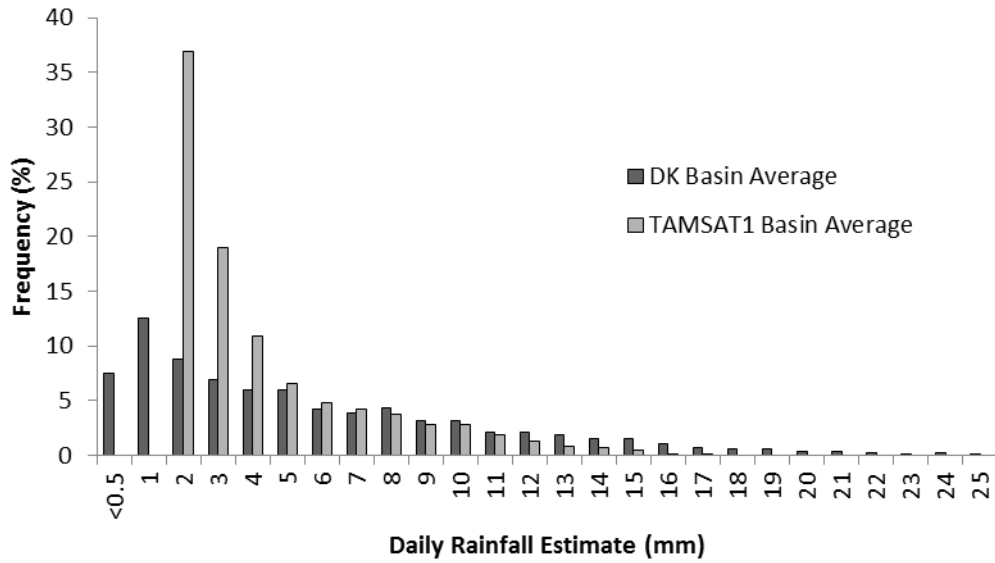


Figure 5.7 – Frequency distribution of catchment average DK and TAMSAT1 rainfall for the Bakoye catchment. Zero rainfall is excluded from the distribution (DK = 19.3%).

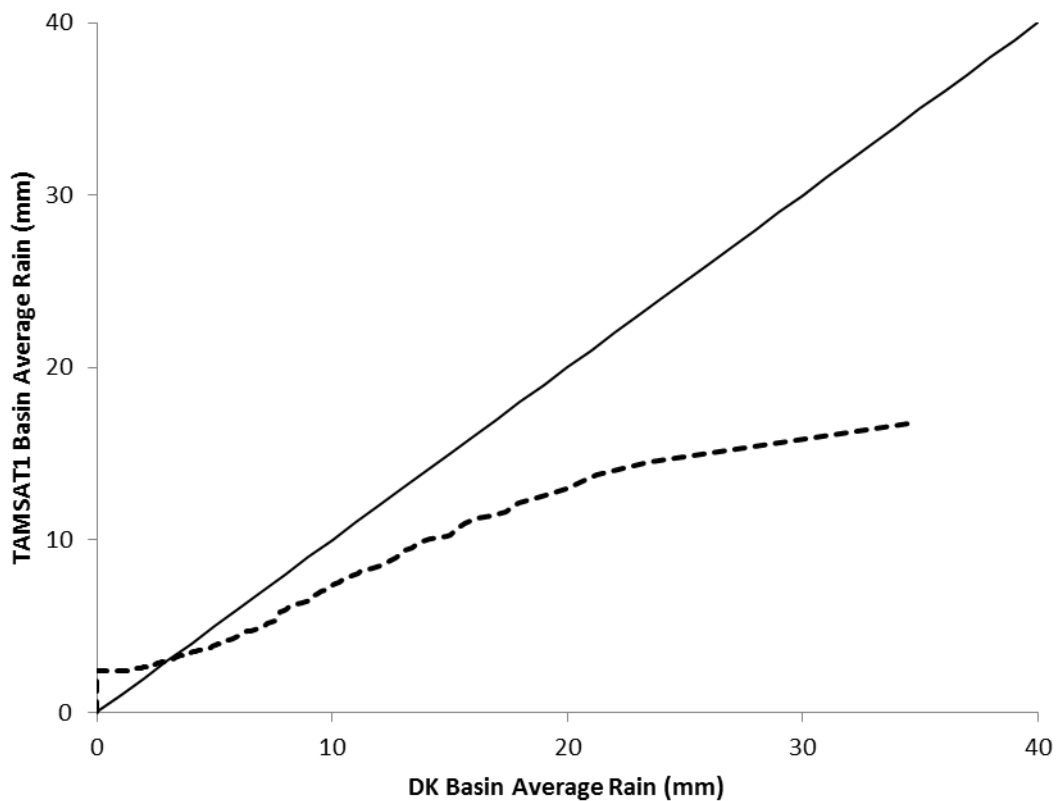


Figure 5.8 – QQ distribution plot showing quantile rainfalls for DK Bakoye catchment average rainfall and TAMSAT1 Bakoye catchment average rainfalls (dashed line) and a modelled 1:1 relationship (solid line).

5.4.4 – Implementation of TAMSIM

In addition to the calibrated relationships above, the TAMSIM algorithm requires three further steps for implementation. These are –

- Generation of indicator residuals and variogram
- Generation of no-zero rainfall residuals and variogram
- Parameters required for generation of ensembles

Generation of Indicator Residuals and Variogram

The calculation of residual values at each gauge-pixel is required for the generation of the residual variogram, the parameters of which are a key requirement for the TAMSIM algorithm. The residual for each gauge-pixel is binary rain status of the pixel (0 = no rain, 1 = rainy), minus the probability of rain at the corresponding CCD hourly bin. The residual values at each gauge-pixel are then used to generate a variogram using KrigingRain in the same way as demonstrated in Chapter 4. Figure 5.9 shows the residual indicator variogram and its parameters.

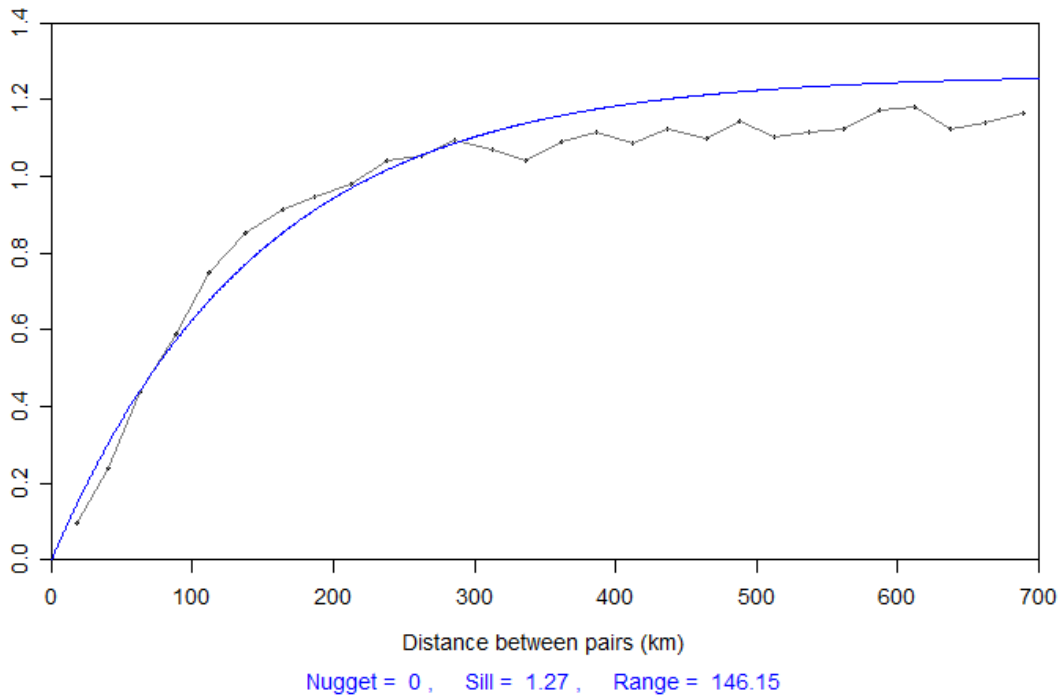


Figure 5.9 – Residual ‘indicator’ variogram and parameters for use in the TAMSIM algorithm.

Generation of No-Zero Rainfall Residuals and Variogram

To generate a no-zero residual variogram it is necessary to first calculate residuals values for no-zero rainfall at gauge-pixels. For each gauge-pixel no-zero rainfall value, the probability of that rainfall occurring on the gamma distribution of the corresponding CCD hourly bin is found, and the residual is then calculated by applying that probability to an inverse normal distribution, with a mean of zero and standard deviation of 1. As with the indicator residuals the residuals are used to generate a residual variogram using KrigeRain. The residual no-zero variogram is shown in Figure 5.10.

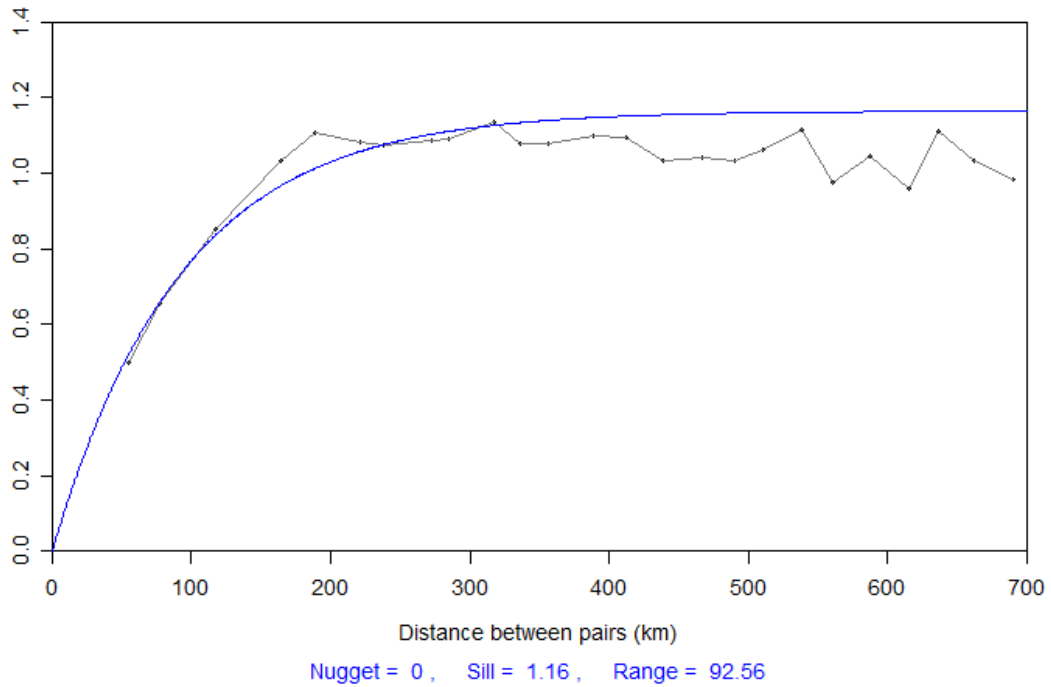


Figure 5.10 – Residual ‘no-zero’ variogram and parameters for use in the TAMSIM algorithm.

Parameters Required for Producing Ensembles.

TAMSIM produces individual ensemble members by combining an indicator field with a no-zero rain field. A description of the methodology has been given in Section 5.3. Teo (2006) showed that at least 200 ensemble members were required for the mean and variance to converge in experimentations, so 200 ensembles were produced. It is not necessary to produce unique indicator fields and no-zero fields for each individual ensemble member, as fields can be combined to produce unique realisations. For this thesis 50 indicator fields and 4 no-zero rain fields were produced, for a total of 200 unique yet equiprobable ensemble rain fields. A validation and analysis of TAMSIM can be found in Chapter 7.

5.5 - Summary

This chapter has shown the methodologies for TAMSAT1, used to produce a deterministic SRFE for the Senegal Basin. It has shown its calibration and implementation for the region, and a catchment average estimate has been calculated for the Bakoye catchment which is used as an input to drive the Pitman lumped CRR model (as demonstrated in Chapter 6). The Bakoye catchment average TAMSAT1 estimate has been validated against the DK catchment average for the Bakoye catchment, finding that it compares favourably in regards to the volumes of rainfall, but fails to fully reflect the interannual variability of rainfall – likely a result of the use of a climatic calibration.

To characterise the uncertainty within the TAMSAT1 estimates, the TAMSIM algorithm was used, and Section 5.3 provided the methodology. Section 5.4 showed how TAMSIM was calibrated and used to produce 200 unique, yet equiprobable realisations of the daily Senegal Basin rain field.

Chapter 6 is the final of the three methodology Chapters and demonstrates the methodology for the Pitman lumped CRR model, and its calibration using the Shuffled Complex Evolution (SCE-UA) method. The characteristics of the TAMSIM ensemble SRFE are assessed in Chapter 7, and the propagation of the uncertainty they reflect is detailed in Chapters 8 and 9.

6

Methodology – Hydrological Modelling

6.1 – Introduction

This chapter is the final of three methodology chapters and details the methods used for the hydrological modelling of the Bakoye catchment. The model used was the Pitman model, a lumped conceptual rainfall-runoff (CRR) model, with 11 adjustable parameter values. The calibration was carried out using an automatic optimisation algorithm, the Shuffled Complex Evolution model implemented at the University of Arizona (SCE-UA).

6.2 – The Pitman Model

The Pitman model is a lumped CRR model introduced by Pitman (1973), and has been used widely across Africa with success in applications involving water resources assessments (Middleton *et al.*, 1981, Hughes, 1995). The unmodified, monthly model has 2-buckets and 12 parameters.

Hughes *et al.* (2006) applied a modified Pitman model to the Okavango Basin in south-west Africa, modelling 24 sub-catchments using raingauge and TRMM SRFE as rainfall inputs to drive the models at a monthly timestep. Hughes *et al.* (2006) found that the calibrated Pitman models could represent catchment response to SRFE satisfactorily for periods outside the calibration period, claiming that other CRR models were unlikely to perform significantly better than the Pitman model, but no others were tested.

The Pitman model, modified to model daily rainfall instead of monthly, was used to model the catchment response of the upstream sub-catchments of the Senegal Basin to TAMSAT SRFE in Hardy *et al.* (1989) and Grimes and Diop (2003). Both studies found the Pitman model performed well with both a raingauge rainfall estimate and the TAMSAT estimate. Grimes and Diop (2003) applied the Pitman model to the Bakoye catchment itself.

The modified daily Pitman model used by Grimes and Diop (2003) has been used in this thesis. With previous studies having successfully applied the Pitman model to the region and the actual study site, it has been shown to perform well in these conditions. Additionally the previous studies can provide a suitable comparison to the model outputs produced.

Methodology

The Pitman model is a lumped CRR model, first developed by Pitman (1973), modified to run at a daily timestep. This model was used in Grimes and Diop

(2003) and was provided through personal correspondence with David Grimes (2009). The model is summarised in Figure 6.1.

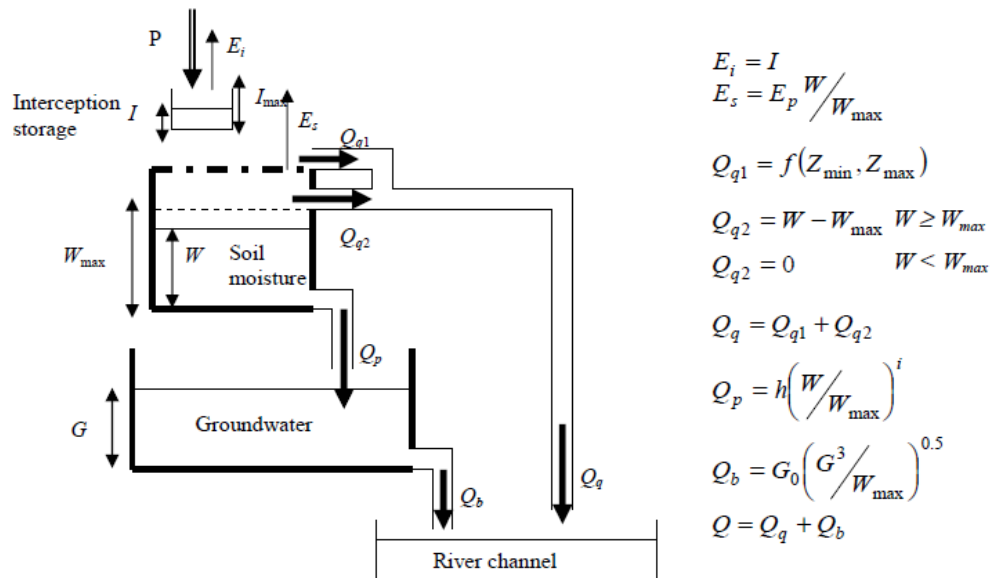


Figure 6.1 – The Pitman Model (from Grimes and Diop, 2003). (Key terms – P (Precipitation Input), I (Interception Storage, I_{max} = maximum storage), W (Soil Moisture, W_{max} = maximum storage), G (Groundwater), E_i (Evaporation from Interception Storage), E_s (Evaporation from Soil Moisture), E_p (Potential Evaporation), Z (Infiltration Rate Z_{min} and Z_{max} = minimum and maximum rates), Q_q (Quick, or surface flow rate), Q_{q1} (Quick flow of rainfall rate exceeding Z_{max}), Q_{q2} (Quick flow from saturated soil), Q_b (Baseflow rate), Q (Total discharge flow rate, sum of appropriately lagged Q_q and Q_b). i and h are empirical values.

The Pitman model shown in Figure 6.1 requires only daily rainfall and potential evaporation as an input and its operation at a daily timestep can be summarised as –

- Rainfall (P) added to the surface store (I) and allowed to evaporate (E_i)

- The remaining water infiltrated to the soil moisture (W), unless the maximum threshold (I_{max}) is exceeded, in which case the excess runs off as surface flow (Q_{q1})
- Water in W either percolates (Q_p) to the groundwater store (G), or evaporates (E_s). If the maximum threshold of the soil moisture store (W_{max}) is exceeded then the excess rainfall runs off as surface flow (Q_{q2}).
- Water stored in G flows out at a specified rate (Q_b)
- Lagged combined surface flow (Q_q) and baseflow (Q_b) are summed for the daily discharge (Q)

For the calibration of the Pitman model there are eleven variable parameters, in addition to the daily inputs and a value corresponding to the catchment area. These parameters, and an initial set of parameter values, provided by David Grimes (personal correspondence, 2009), can be seen in Table 6.1.

Although the initial parameter set provided in Table 6.1 provides a suitable starting point for calibration, it should be noted that it does not allow for the full complexity of the model to be utilised. The value provided for h , being 0, does not allow for any percolation from the soil moisture store to the groundwater stores, restricting the model to operating as a 1-bucket model. Although this may suit the catchment, the calibration will allow for the Pitman model to operate as a 2-bucket model and use its full complexity.

Parameter	Description	Value	Units
Z_{min}	Minimum infiltration rate	0	mm.day ⁻¹
Z_{max}	Maximum infiltration rate	23	mm.day ⁻¹
W_{max}	Storage threshold of Soil Moisture	460	mm
W_{min}	Storage threshold below which no percolation occurs	0	mm
I_{max}	Storage threshold of Interception Storage	1	mm
h	Empirical constant used to calculate percolation rate	0	mm.day ⁻¹
i	Empirical constant used to calculate percolation rate	2	
GL	Recession time constant for baseflow ($G0 = 1/GL$)	3	days
TL	Contant used for calculation of the surface flow	11	days
$Q_q Lag$	Lag for surface (quick) flow	1	days
$Q_b Lag$	Lag for baseflow	1	days

Table 6.1 – Table showing the variable parameters in the Pitman model to be calibrated, and an initial set of parameter values provided by David Grimes (personal correspondence, 2009).

6.3 - The Shuffled Complex Evolution method implemented at the University of Arizona (SCE-UA)

A popular method of automatic optimal calibration is the Shuffled Complex Evolution (SCE) method implemented at the University of Arizona (Duan *et al.*, 1993). Duan *et al.* (1993) details the SCE algorithm, based around four components –

1. A mix of deterministic and probabilistic approaches
2. Clustering
3. A systematic evolution of a complex of points within the parameter space, towards improvement

4. Competitive evolution

SCE is a global optimisation method in that it is able to examine the entire parameter space, identify the areas of local minima and narrow down the search before refining the final optimal parameter set (Duan *et al.*, 1993), as opposed to a local minima optimisation method that is dependent on a suitable initial set of parameters (Wang *et al.*, 2010). The method has been shown to be successful at estimating reliable optimal parameter sets for complex CRR models (Duan *et al.*, 1994), and outperforming other global optimisation techniques available at the time (Duan *et al.*, 1993).

The method is widely used and still found to perform well. Wang *et al.* (2010) found that of three global optimisation methods, SCE was the most robust although all the methods produced similar outcomes. There have been efforts to improve the technique, such as the Shuffled Complex Evolution Metropolis (SCEM) (Vrugt *et al.*, 2003) which adapted the Monte Carlo Markov Chain (MCMC) method within the model, and the Shuffled Complex with Principal Component Analysis (SP-UCI) (Chu *et al.*, 2010), however, the core principals of the original algorithm have been retained.

Another adaption of the original SCE-UA algorithm was demonstrated by Yapo *et al.* (1998) with the Multi-Objective Complex Evolution (MOCOM-UA) global optimisation method, which fits the parameters by calibrating to more than one objective function. A similar method was applied to the MIKE SHE distributed model in Madsen (2003). Although this method could potential produce a

hydrograph that better reflects the recorded discharge, it is likely to prove computationally expensive, and not provide a single measure of goodness-of-fit for use in comparisons which the SCE-UA can provide.

Methodology

As previously stated, the SCE-UA method was implemented at the University of Arizona and introduced in Duan *et al.* (1993). It is a global optimisation method that has been widely used for hydrological model calibration and shown to be robust (see above). This section provides a summary of the algorithm, a full methodology can be found in Duan *et al.* (1993).

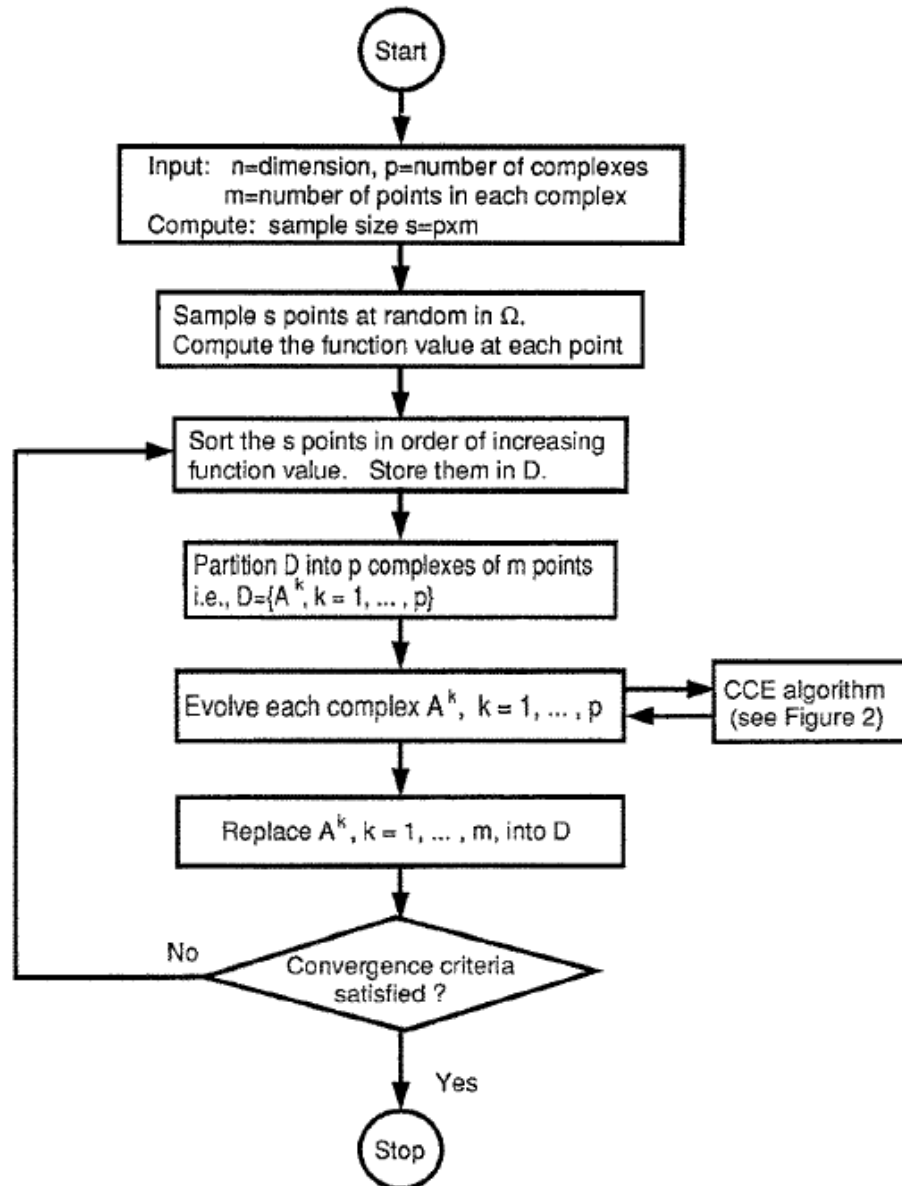


Figure 6.2 – Flow chart showing the main steps required for shuffled complex evolution (from Duan *et al.*, 1993) – The CCE algorithm can be seen in Figure 6.3.

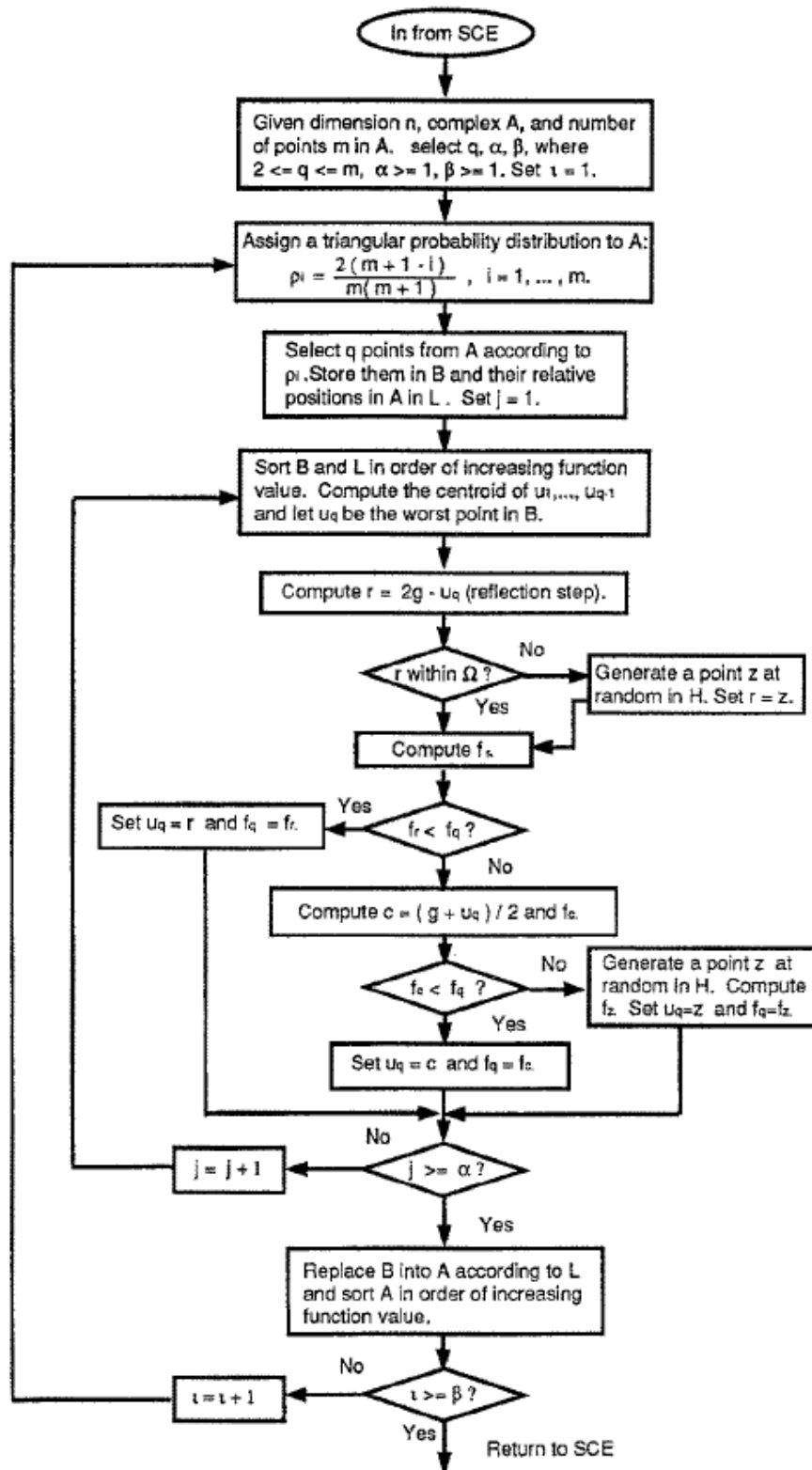


Figure 6.3 – Flow chart of the Competitive Complex Evolution (CCE) strategy, part of the SCE algorithm shown in Figure 6.2 (from Duan *et al.*, 1993).

The flow charts shown in Figures 6.2 and 6.3 describe the full method of the SCE algorithm and the incorporated Competitive Complex Evolution (CCE) strategy. The SCE process can be summarised as:

1. Set up the algorithm – decide number of complexes to use and number of points in each complex
2. The algorithm generates a sample within the reasonable space
3. The points sampled are ranked depending on model performance and stored in an array
4. The space is partitioned into complexes of equal points
5. Each complex is evolved according to the CCE strategy detailed below, and shown in Figure 6.3
6. The complexes are shuffled according to model performance
7. Check whether the model performance has reached the convergence criteria. If not, the algorithm returns to step 3.

The CCE strategy can be summarised as:

1. Initialise the algorithm – decide on number of iterations to run
2. Weights are assigned to each point via a triangular probability distribution
3. Randomly select 'parent' points according to the distribution in Step 2, and store in an array
4. 'Offspring' points are generated from the parent points by attempting improve the model performance, keeping those offspring points that show improvement

5. The parent points are replaced by the offspring points and rank in order of performance
6. Repeat the iterations of Steps 2-4 by the specified number
7. Return to SCE algorithm

6.4 – Calibration of the Pitman Model using SCE-UA

The previous sections have shown the methodologies used for the hydrological modelling of the Bakoye catchment, detailing the Pitman CRR model and the SCE-UA algorithm that was used to calibrate the 11 variable parameters.

A sensitivity analysis could have been run on the Pitman model before calibration to determine those parameters that have the most influence on the calibration, which would help reduce the computational time of the SCE-UA algorithm, however, there was no prior knowledge of the physical properties of the parameters and the Bakoye catchment and it was sensible to allow all parameters to be included in the optimisation, with appropriately wide parameter spaces.

The SCE-UA algorithm used was the SCEoptim package in the R environment, written by Andrews (2012), and provided under open license.

As far as possible the default parameters within the SCEoptim algorithm were used, however, it was necessary to adjust them in order to ensure that the

algorithm converged upon the optimal parameter set, or as close to within sensible limits, without excessive computational expense.

The calibration was tested using an input composed of the mean values of the raingauges associated with the Bakoye catchment, as detailed in Chapter 3.

The algorithm performed within the bounds of the minimum and maximum set for each parameter - the use of wider bounds resulting in processing times over ten times longer, with little benefit.

In order for the algorithm to consistently converge upon the optimal parameter set the numbers of complexes required was increased from 5 to 50 – it should be noted that increasing the number of complexes is the main source of computational expense and a balance needs to be struck between computational time and the robustness of the final calibration (Madsen, 2003).

By using 50 complexes the impact of the initial parameter values bore little relevance on the final result. By increasing the convergence threshold from $1e-5$ to $1e-2$, the computation time was significantly decreased without significant loss of final error value.

The objective function used was the RMSE of daily recorded discharge and the daily modelled discharge. The equation for the RMSE is shown in Equation 6.1, where z_i is the recorded discharge, and z_i^* is the modelled discharge, for a given timestep:

Equation 6.1

$$RMSE = \sqrt{\frac{\sum_{i=1}^N (z_i - z_i^*)^2}{N}}$$

The SCE-UA was found to significantly improve the performance of the Pitman model in comparison with the default parameters shown in Table 6.1, and this can be seen in hydrographs, using a calibration for all eleven years when driven by the Gauge Average rainfall estimate (an area weighted estimate produced using a Thiessen Polygon method, and adjusted for orographic effects) . An example of the hydrograph from the 1988 wet season is shown in Figure 6.4.

The hydrograph in Figure 6.4 show the effect of calibrating the variable parameters in the Pitman model, using the SCE-UA algorithm. It is clear that the modelling of discharges using SCE-UA calibrated parameters significantly increases the fit of the hydrograph, both visually and quantitatively. The RMSE values for both modelled outputs for the 11 year period are $80.92\text{m}^3.\text{s}^{-1}$ for the calibrated model, and $157.61\text{m}^3.\text{s}^{-1}$ for the model using the default parameters.

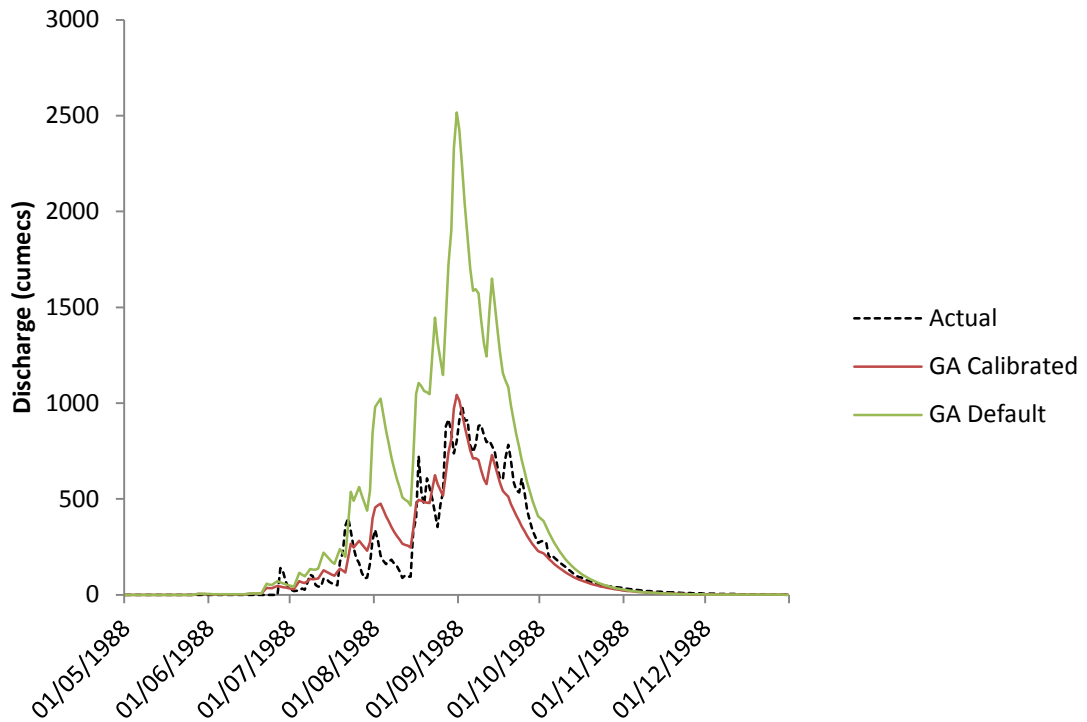


Figure 6.4 – Hydrograph showing the actual and modelled discharge from the Pitman model for the Bakoye catchment, for 1988. The dashed line shows the recorded discharge, the solid red line is the modelled discharge, driven and calibrated by the Gauge Average estimate of rainfall for the period 1986-1996, and the solid green line is the modelled discharge, driven by the Gauge Average estimate and using the default parameters.

To allow interannual comparison, and also comparison with studies on other catchments, the RMSE error will be converted into a percentage of the mean daily discharge of the observed period. In this case, the errors are 123% of mean daily discharge for the calibrated model, and 239% of mean daily discharge when using the default parameters.

6.5 - Summary

This chapter has demonstrated the Pitman lumped CRR model and the SCE-UA method that has been used to optimised the parameter values. A starting set of default parameters have been used and the SCE-UA was used to alter the values of the parameters, minimising the RMSE for daily discharges. The final error is expressed as a percentage of the mean daily discharge for the calibration period to allow more direct comparison between periods under different conditions.

7

Validation of the Ensemble Representation of the Daily Senegal Basin Rain Field

7.1 – Introduction

The TAMSAT1 method and the TAMSIM algorithm were described in Chapter 5, detailing their calibration and implementation. As shown, the TAMSAT1 and TAMSIM algorithms have been calibrated against a historic raingauge network covering the Senegal Basin for the period between 1986-1996, using the wet season data only. Finally, an ensemble realisation of the Senegal daily rain field, consisting of 200 unique yet equiprobable members, has been produced and the Bakoye catchment averages calculated.

This chapter will address two of the key questions posed in Chapter 1 of this thesis. It will firstly investigate the capability of the TAMSIM algorithm to reproduce the daily Senegal rainfall field by comparing it to the underlying DK rainfall field – both at gauge-pixel and catchment average scales. Secondly, the main forms of uncertainty will be observed, including the extent of error, spatial biases and temporal biases.

7.2 – Daily Senegal Basin Rain Field

The daily wet season (June-October) rainfall fields for the Senegal Basin have been generated using TAMSIM for the period between 1986 and 1996. Specific details concerning the implementation have been highlighted in Chapter 5. The ensemble rain fields produced by TAMSIM should, individually and combined, reproduce the statistical characteristics of the DK rain field at both gauge-pixel and catchment scale.

The performance of the ensemble rainfall fields can be assessed by comparison with the underlying DK rainfall field at gauge-pixel scale (pixels that contain at least one raingauge), both as a collective and at individual gauge-pixels.

Rainfall Characteristics at Gauge-Pixel Scale

In order to assess the TAMSIM it is necessary to first determine that the rainfall fields for the ensembles retain the statistical properties of the DK obtained gauge-pixel rainfall fields.

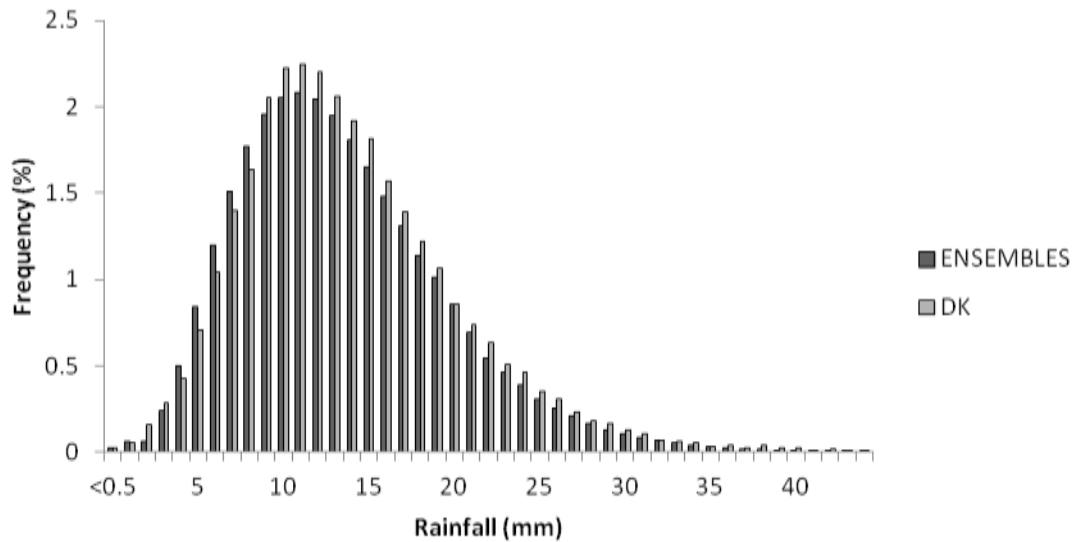


Figure 7.1 – Frequency distribution chart showing the distributions of all the ensemble rainfall and the DK rainfall, at gauge-pixels. Zero rainfall is included in the frequency, but not shown (Ensembles = 70.8%, DK = 69.4%)

Figure 7.1 shows the frequency distribution of rainfall for all of the ensemble rainfall fields and the distribution of rainfall for the DK obtained rainfall field, for gauge-pixels. Both distributions show a very similar frequency of zero rainfall (70.8% for TAMSIM, 69.4% for DK), and similar distribution of rainfall, both showing most rainfall in the 12mm bin. It is beyond the bounds of this thesis to provide a full, comprehensive analysis of all the sources of error in the DK estimate, such as raingauge measurement and interpolation errors, but a conservative estimate can be taken at 10% of the rainfall volume. At this magnitude there would be significant overlaps between the distributions of the DK rainfall estimates and the ensemble estimates. This suggests that over 200 ensembles, the TAMSIM model is adequately reproducing the statistical properties of the DK obtained rainfall field.

To assess whether individual ensemble members were also displaying the same statistical properties, five ensemble members were chosen randomly to compare with the DK obtained rainfall fields. Figure 7.2 shows the frequency distribution of the five ensemble rainfall fields, in comparison with the DK obtained field. It shows a similar pattern to the distribution of all the TAMSIM rainfall shown in Figure 7.1, suggesting that each individual ensemble member is consistent with the statistical properties of the DK obtained rainfall.

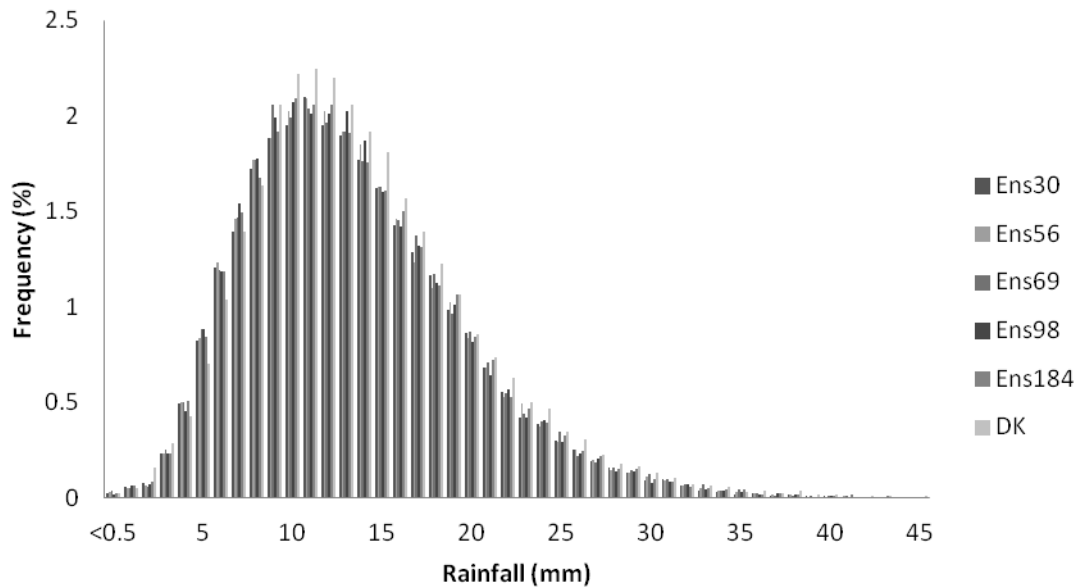


Figure 7.2 – Frequency distributions of five randomly chosen ensemble rainfall fields and DK obtained rainfall field, at gauge-pixels. Zero rainfall was included in the distribution but now shown (Ens30 = 71.5%, Ens56 = 71.1%, Ens69 = 70.8%, Ens98 = 71.0%, Ens184 = 71.0% and DK = 69.4%).

The distribution of the rainfall estimates were also compared using Quantile-Quantile (QQ) plots. These plots are shown in Figure 7.3. Each of the ensembles displays a similar pattern, with the TAMSIM generated rainfall showing lower rainfall values than DK when comparing quantiles throughout the

plot. However, there is a close match between 10 and 25mm rainfall but a poor match at the low and high end of the plots.

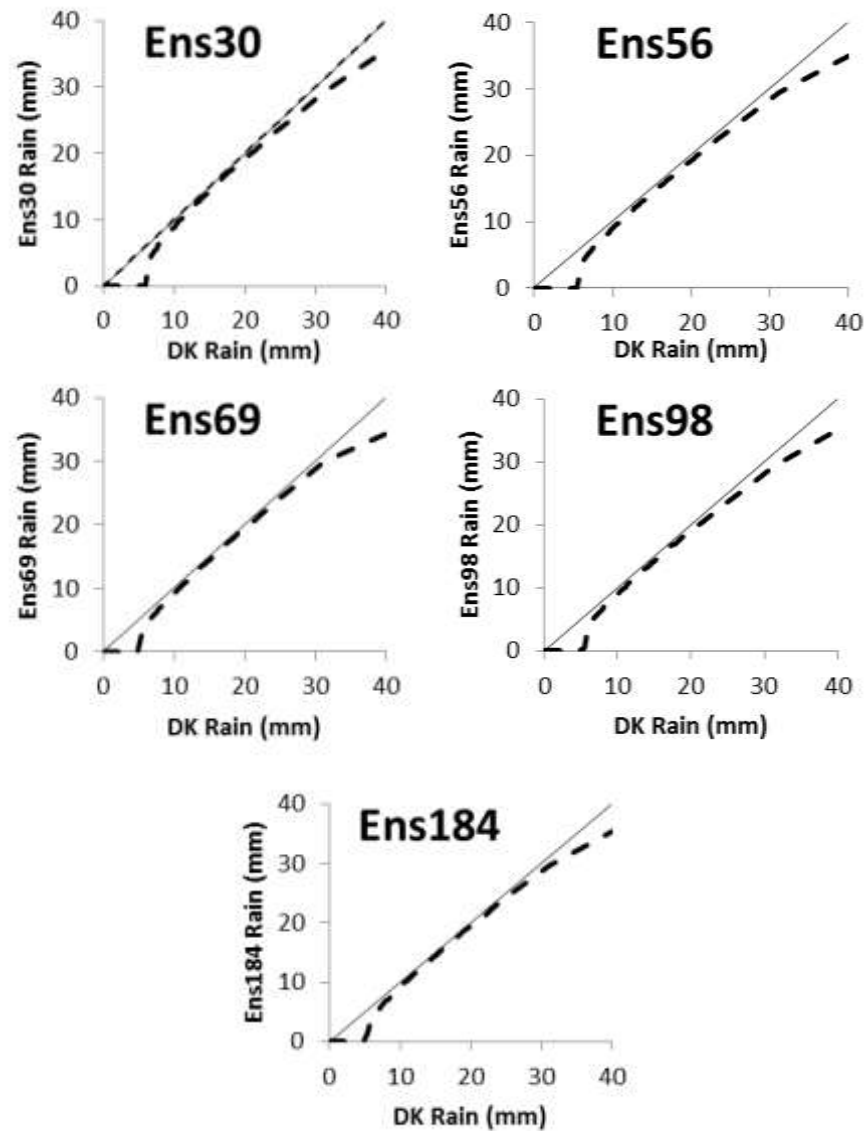


Figure 7.3 – QQ distribution plots showing DK and sample ensemble rainfall at gauge-pixels.

Rainfall Characteristics at Catchment Average Scale

For use as an input driving the Pitman lumped CRR model, daily averages of rainfall needed to be calculated from each ensemble member for the Bakoye

Chapter 7 – Validation of the Ensemble Representation of the Daily Senegal Basin Rain Field catchment, as described in Chapter 5. The catchment average rainfall estimate can be assessed by comparison with a catchment average determined from the underlying DK rainfall field, and its skill can be compared with the deterministic TAMSAT1 estimate, for all the ensembles together, individual ensemble members, and a mean of all the ensemble estimates.

Figures 7.4 and 7.5 show the frequency distributions of rainfall at Bakoye catchment scale, for TAMSIM, the five randomly selected ensemble members and DK obtained rainfall. Interestingly, when averaged over the Bakoye catchment scale, the proportion of zero rainfall is much lower for TAMSIM generated rainfall fields (3.6%), than for DK obtained rainfall (19.3%). This is caused by the amount of uncertainty for rainfall at $CCD=0$ in the TAMSIM calibration – there is a 19% probability of rainfall at $CCD=0$, so even when the whole Bakoye catchment shows $CCD=0$, it is likely that TAMSIM will estimate rainfall somewhere within the catchment.

Frequency Distribution - Bakoye Catchment

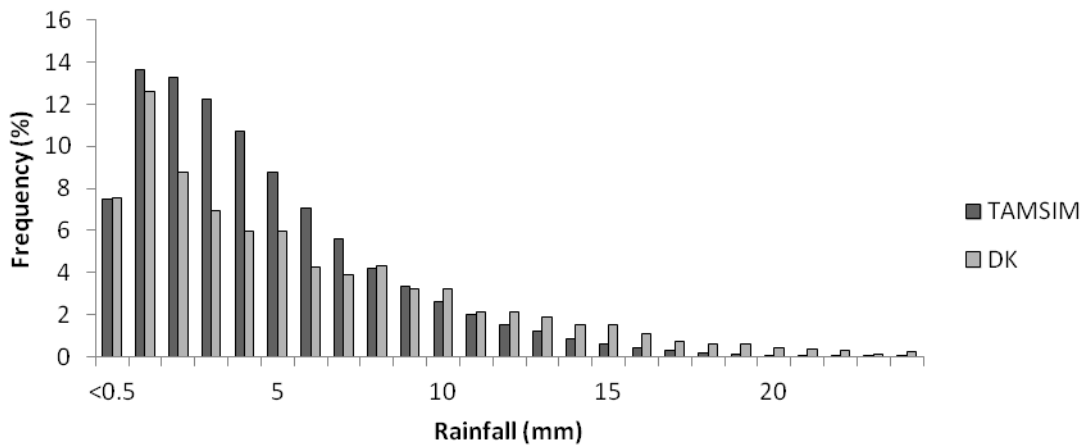


Figure 7.4 – Frequency distribution showing the distributions of all the ensemble rainfall fields and the DK obtained rainfall field, at the Bakoye catchment scale. Zero rainfall is included in the distribution but not shown (Ensembles = 3.6%, DK = 19.3%).

Frequency Distribution - Ensemble and DK Bakoye Catchment

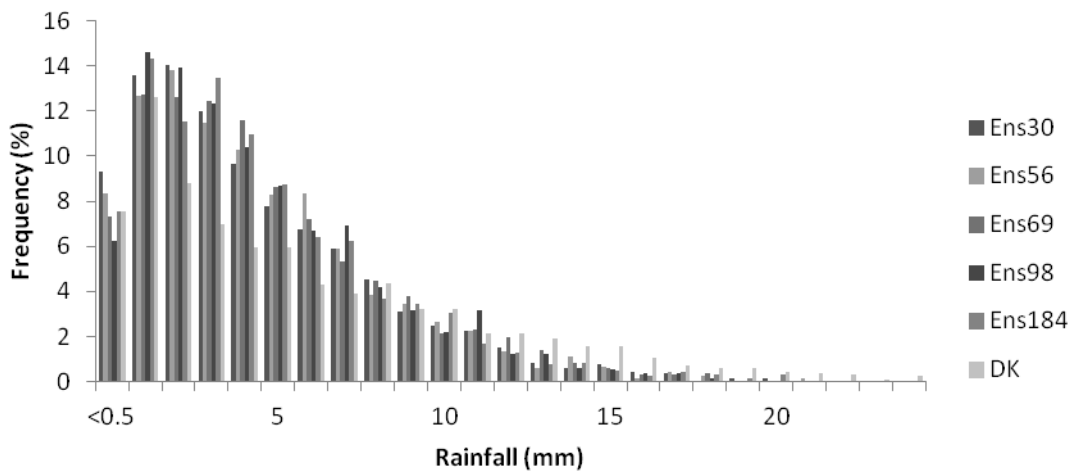


Figure 7.5 – Frequency distribution of five randomly chosen ensemble rainfall fields and DK obtained rainfall fields at Bakoye catchment scale. Zero rainfall is included in the distribution but not shown (Ens30 = 3.7%, Ens56 = 4.0%, Ens69 = 3.5%, Ens98 = 3.0%, Ens184 = 4.0%, DK = 19.3%).

The QQ plot in Figure 7.6 shows the DK and combined TAMSIM quantile rainfalls at catchment scale. The TAMSIM rain fields are producing more low level rainfall than the DK rain fields at catchment scale, and less high level rainfall. However, the mean rainfall appears to occur at the same quantile for both rain fields.

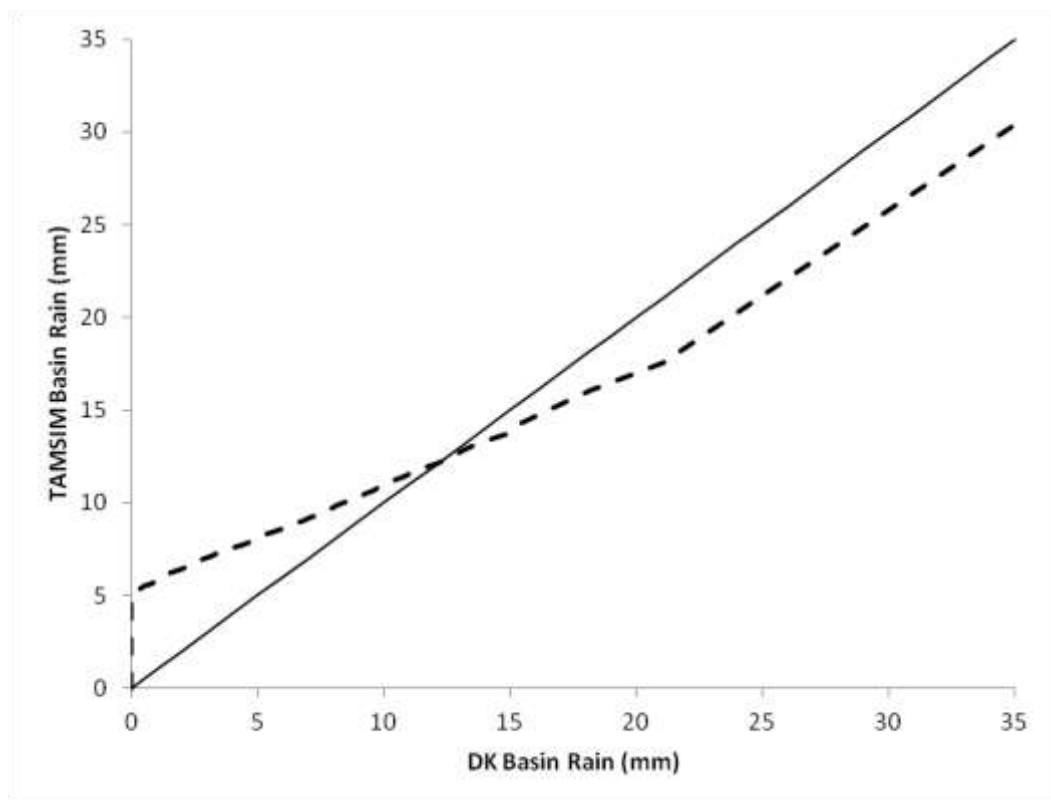


Figure 7.6 – QQ distribution plot showing the quantile rainfalls for DK Bakoye catchment average rainfall and combined TAMSIM Bakoye catchment average rainfall.

The TAMSIM data shows a close match with TAMSAT1 at the Bakoye catchment scale for rainfall between 2.5mm and 15mm, but the relationship breaks down for rainfall >15mm (Figure 7.7).

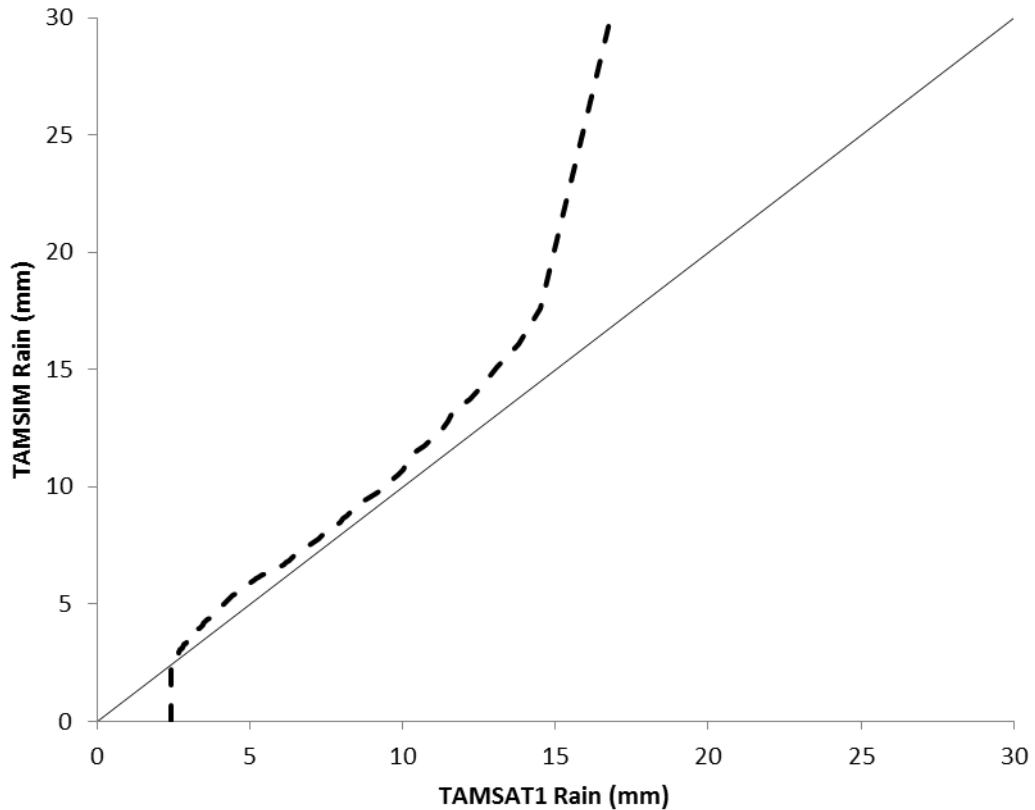


Figure 7.7 – QQ distribution plot showing the quantile rainfall for TAMSAT1 Bakoye catchment average rainfall and TAMSIM Bakoye catchment average rainfall.

The ability of the TAMSIM algorithm to estimate rainfall at the catchment scale can be compared to that of the deterministic TAMSAT1 estimate by using measurements of relative skill, in comparison with the estimate produced by the underlying DK daily rain field. Three skills scores were used for the quantitative assessment, Root-Mean-Squared-Error (RMSE), the coefficient of determination (R^2), and Bias (BIAS), as defined below:

Equation 7.1

$$RMSE = \sqrt{\frac{\sum_{i=1}^N (z_i - z_i^*)^2}{N}}$$

Equation 7.2

$$R^2 = \frac{\sum_{i=1}^N (z_i^* - \bar{z})^2}{\sum_{i=1}^N (z_i - \bar{z})^2}$$

Equation 7.3

$$BIAS = \frac{\sum_{i=1}^N (z_i - z_i^*)}{N}$$

where N is the number of daily rainfall estimates in the dataset, z_i is the DK daily catchment rainfall estimate, z_i^* is the SRFE daily catchment rainfall estimate (either TAMSAT1, or TAMSIM) and \bar{z} is the mean of the DK daily catchment rainfall estimates.

The skill scores were applied to the TAMSAT1 estimate, the collective of TAMSIM ensemble estimates (SIMAll) and the mean of the ensemble estimates (SIMMean), for the period between 1986 and 1996, and for each individual year between. The results can be seen in Table 7.1.

Period	Method	RMSE	R ²	BIAS
All	TAMSAT1	3.94	0.31	0.34
	SIMAll	4.59	0.51	0.41
	SIMMean	3.94	0.31	0.41
1986	TAMSAT1	3.89	0.36	0.64
	SIMAll	4.57	0.56	0.68
	SIMMean	3.94	0.35	0.68
1987	TAMSAT1	3.60	0.38	-0.30
	SIMAll	4.31	0.64	-0.25
	SIMMean	3.62	0.37	-0.25
1988	TAMSAT1	4.39	0.34	0.52
	SIMAll	5.04	0.52	0.61
	SIMMean	4.40	0.34	0.61
1989	TAMSAT1	4.45	0.33	0.89
	SIMAll	4.97	0.49	0.92
	SIMMean	4.41	0.33	0.92
1990	TAMSAT1	2.91	0.38	-0.31
	SIMAll	3.78	0.64	-0.25
	SIMMean	2.91	0.37	-0.25
1991	TAMSAT1	3.85	0.28	0.22
	SIMAll	4.48	0.49	0.30
	SIMMean	3.81	0.28	0.30
1992	TAMSAT1	3.71	0.31	-0.38
	SIMAll	4.33	0.54	-0.27
	SIMMean	3.66	0.30	-0.27
1993	TAMSAT1	3.64	0.28	0.11
	SIMAll	4.29	0.51	0.16
	SIMMean	3.63	0.27	0.16
1994	TAMSAT1	4.59	0.35	1.01
	SIMAll	5.19	0.57	1.06
	SIMMean	4.60	0.35	1.06
1995	TAMSAT1	3.90	0.31	0.57
	SIMAll	4.61	0.49	0.66
	SIMMean	3.94	0.31	0.66
1996	TAMSAT1	4.14	0.23	0.77
	SIMAll	4.75	0.39	0.85
	SIMMean	4.16	0.24	0.85

Table 7.1 – Table showing comparison skill scores for Bakoye catchment rainfall estimates from TAMSAT1, all of the TAMSIM ensembles (SIMAll), and the mean of the TAMSIM ensembles (SIMMean), the whole 11 year study period, and for individual years (wet season data only).

The skill scores shown in Table 7.1 portray a mixed picture. In terms of R^2 , the TAMSIM ensembles outperform the TAMSAT1 estimate, but TAMSAT1 shows a better fit in terms of RMSE and less bias, for the whole 11 year period.

Generally, and as would be expected, the mean of the TAMSIM ensembles shows similar error scores to TAMSAT1, and the same bias as the whole TAMSIM ensemble estimates. In regards to bias, overall the SRFE slightly

underestimates in comparison with the DK estimate, but overestimates in 1987, 1990 and 1992 – each anomalously dry years.

Reliability of Ensemble Estimates

The reliability of ensemble estimates can be assessed using the forecast reliability method detailed by Toth *et al.* (2003). The reliability plots use a threshold on the ensemble data, and bins the data for each day into percentage of ensemble members above the threshold. For each bin the percentage of days that show recorded data above the threshold is calculate and plotted against the binned ensemble data. A reliable ensemble set will show a 1:1 relationship on the plot, for example if 40% of ensembles estimate rainfall above 5mm, than there should be a 40% chance of rainfall occurring above 5mm on that day.

Figure 7.8 shows reliability plots for the catchment average TAMSIM SRFE, compared to the DK catchment average rainfall estimate, for three threshold levels – low rainfall (25th percentile from the DK rain), mean rainfall and high level rainfall (75th percentile). The TAMSIM ensembles show good reliability at mean and high level rainfall, but poor reliability at the low level rainfall threshold – this is most likely due to the known problem that SRFE have with estimating trace levels of rainfall.

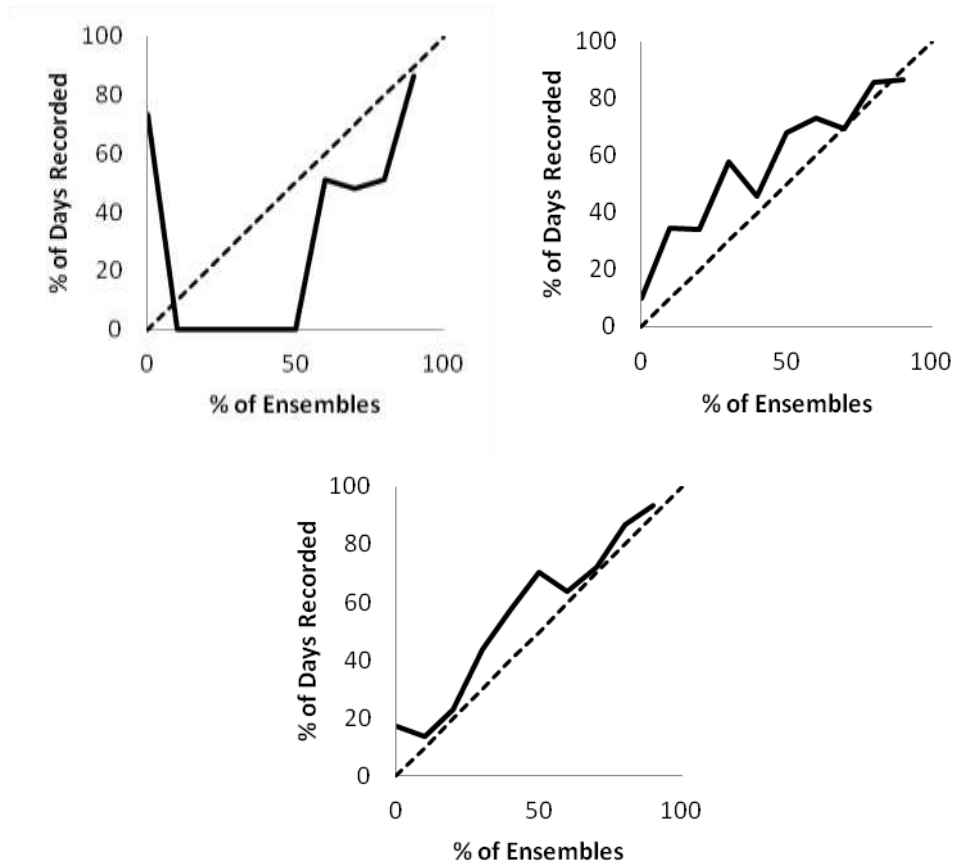


Figure 7.8 – Forecast reliability plots showing the catchment average TAMSIM SRFEs compared to the DK catchment average rainfall estimate. The top-left chart shows values >0.4mm (the 25th percentile of the DK rainfall), top-right shows values >7.4mm (the 75th percentile of the DK rainfall) and the bottom chart shows values >4.6mm (the mean daily DK rainfall). The dashed lines show the 1:1 relationship.

Variogram Replication

It has been shown that both the ensembles as a whole and each individual ensemble retain similar statistical properties to the DK rain field, at pixel and catchment scales. However, one area of concern is that TAMSIM does not reproduce the geostatistics in regards to the modelled climatological variograms. Figures 7.9 and 7.10 show the indicator and no-zero rainfall variograms generated by the gauge-pixel data from Ensemble 30.

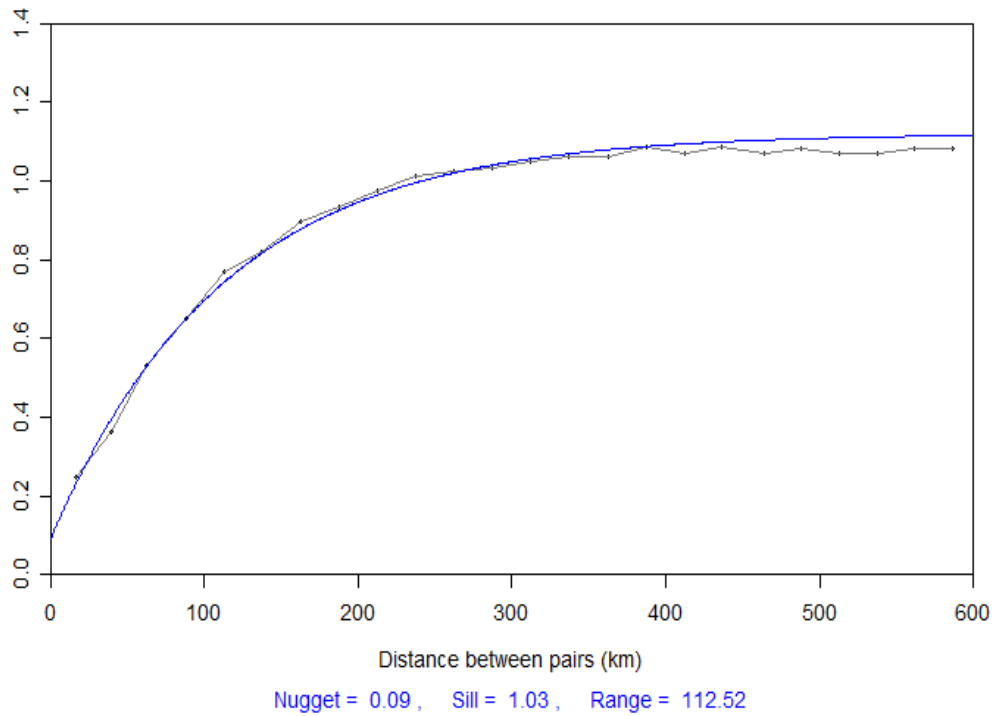


Figure 7.9 – Modelled wet-season climatological ‘indicator’ variogram generated from Ens30 gauge-pixel data.

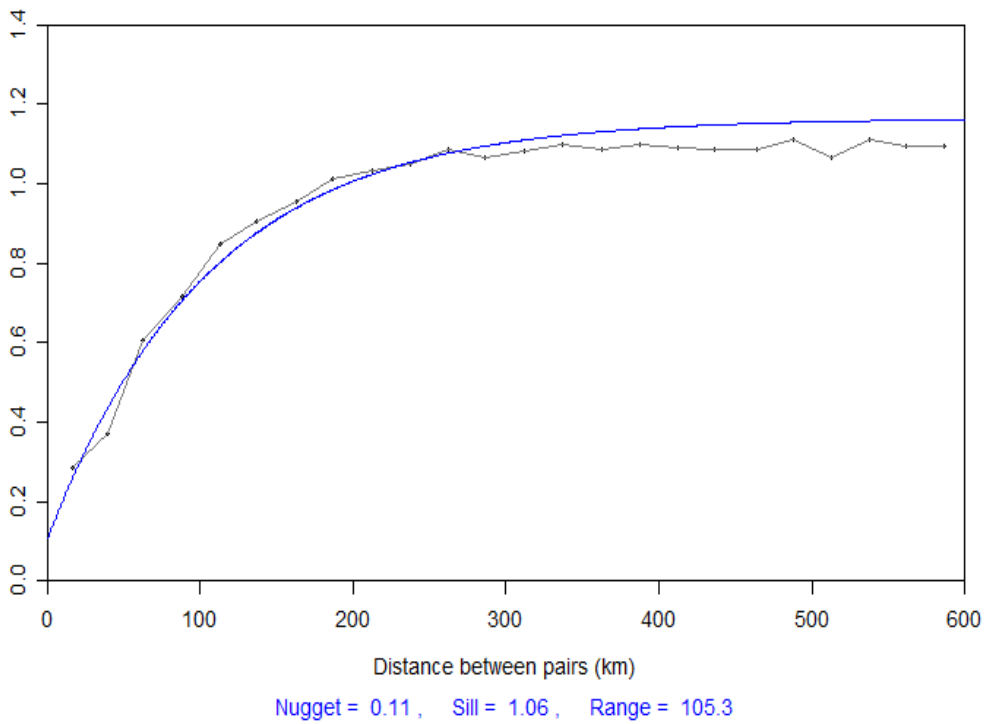


Figure 7.10 – Modelled wet-season climatological ‘no-zero’ variogram generated from Ens30 gauge-pixel data.

The two modelled variograms shown in Figures 7.9 and 7.10 show little resemblance to the modelled variograms shown for the DK in Chapter 4, derived directly from the raingauge data. Table 7.2 and 7.3 compare the parameters between the modelled variograms for the DK rain fields, the residual variograms used for TAMSIM, and the variograms generated from each of the sample ensemble members.

	Nugget	Sill	Range (km)
From Gauges	0.37	0.71	183.02
Residual	0.00	1.27	146.15
Ens30	0.09	1.03	112.52
Ens56	0.09	1.02	113.30
Ens69	0.07	1.04	110.57
Ens98	0.10	1.03	117.27
Ens184	0.10	1.02	112.92

Table 7.2 – Table showing the modelled ‘indicator’ variogram parameters for variograms from the gauges, the residual variogram, and variograms generated from the sample ensemble members.

	Nugget	Sill	Range (km)
From Gauges	0.50	0.51	50.79
Residual	0.00	1.16	92.56
Ens30	0.11	1.06	105.30
Ens56	0.04	1.12	100.60
Ens69	0.05	1.11	101.64
Ens98	0.07	1.11	106.71
Ens184	0.09	1.09	109.80

Table 7.3 – Table showing the modelled ‘no-zero’ variogram parameters for variograms from the gauges, the residual variograms, and variograms generated from the sample ensemble members.

From Tables 7.2 and 7.3 it can be seen that the variogram parameters for each of the sample ensemble members are relatively consistent. Both the indicator and the no-zero variograms for the Ensemble members also show a low nugget, much lower than the gauge derived variograms. The Ensemble variograms also show greater similarity to the residual variogram, especially in the case of the no-zero transforms, and this is not unexpected as the residual variogram is used directly in the generation of the variograms. However, it is of concern that each individual ensemble rain field does not reproduce a variogram more reflective of the geostatistics shown by the raingauges – this is most likely a result of TAMSIM being unable to reproduce the rainfall gradient across the region using a single calibration.

7.3 – Influence of Uncertainty on the Estimates

The sections above have demonstrated the ability of the TAMSIM algorithm to reproduce the rainfall characteristics of the daily Senegal rainfall field, at both gauge-pixel and catchment average scale. It has been previously stated that the types of uncertainty with a SRFE are likely to emerge from errors in estimating where it is raining, when it is raining, and the rainfall rate. These can be observed in the ensemble estimates as spatial biases and temporal biases, in addition to error.

Spatial Bias

The spatial biases within the TAMSIM ensemble estimates can be seen by observing the rainfall distributions at gauge-pixel scale for individual raingauges. In order to show this, five raingauges were randomly selected from the whole record and the TAMSIM pixel rainfall for each gauge compared to the DK obtained pixel average for that gauge – the frequency distributions shown in Figure 7.11 to 7.15, with the raingauges ordered from most northerly to most southerly.

Aero-Lao

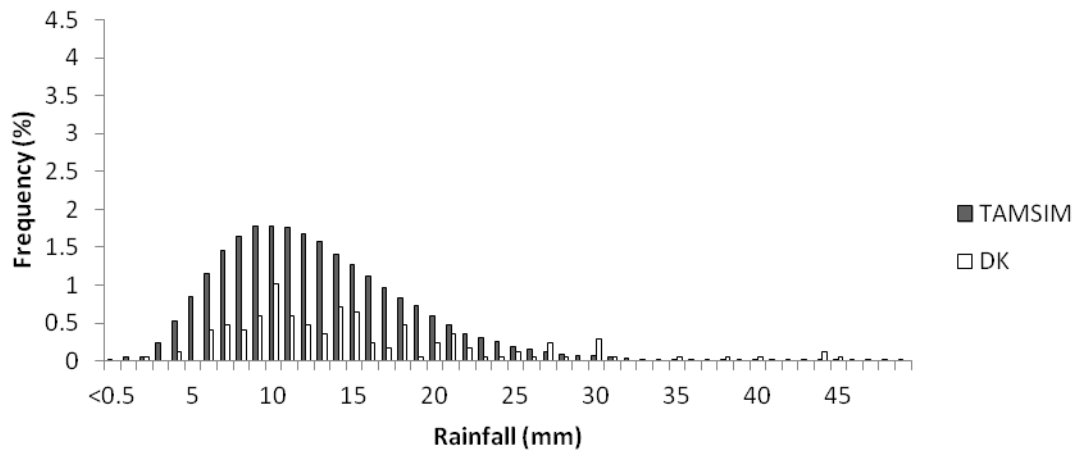


Figure 7.11 – Frequency distribution of TAMSIM rainfall fields and DK obtained rainfall for the Aero-Lao gauge-pixel. Zero rainfall is included in the distribution but not shown (TAMSIM = 76.2%, DK = 91.1%).

Renerou

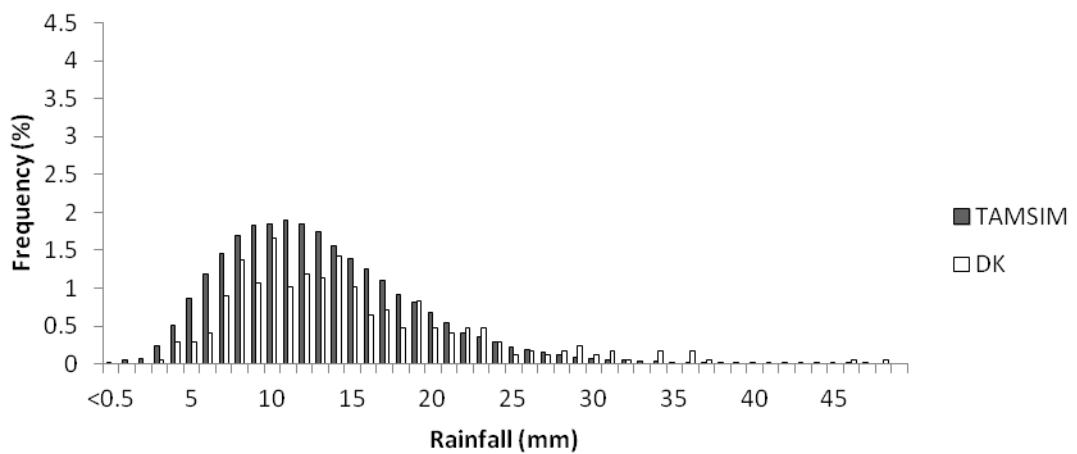


Figure 7.12 – Frequency distribution of TAMSIM rainfall fields and DK obtained rainfall for the Renerou gauge-pixel. Zero rainfall is included in the distribution but not shown (TAMSIM = 74.3%, DK = 81.6%).

Thiel

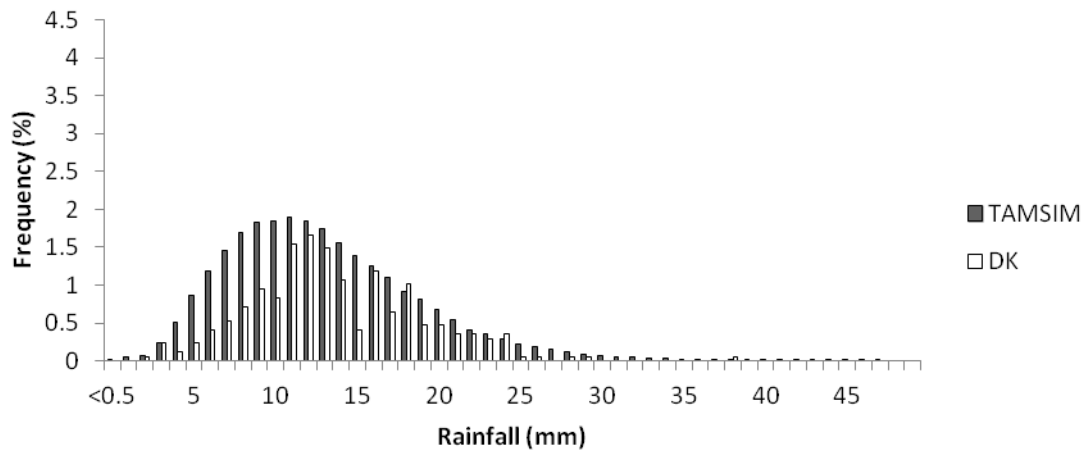


Figure 7.13 – Frequency distribution of TAMSIM rainfall fields and DK obtained rainfall for the Thiel gauge-pixel. Zero rainfall is included in the distribution but not shown (TAMSIM = 74.3%, DK = 84.3%).

Guene-Gore

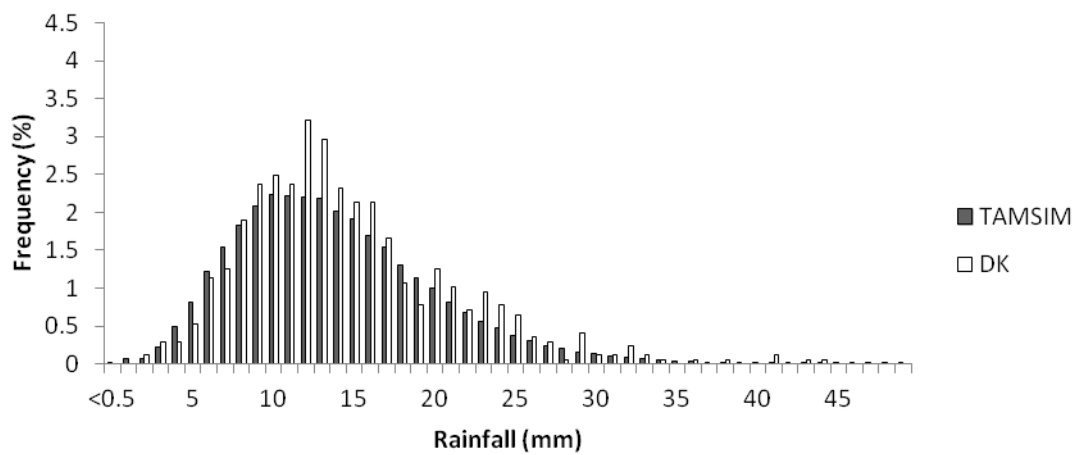


Figure 7.14 – Frequency distribution of TAMSIM rainfall fields and DK obtained rainfall for the Guene-Gore gauge-pixel. Zero rainfall is included in the distribution but not shown (TAMSIM = 67.7%, DK = 63.4%).

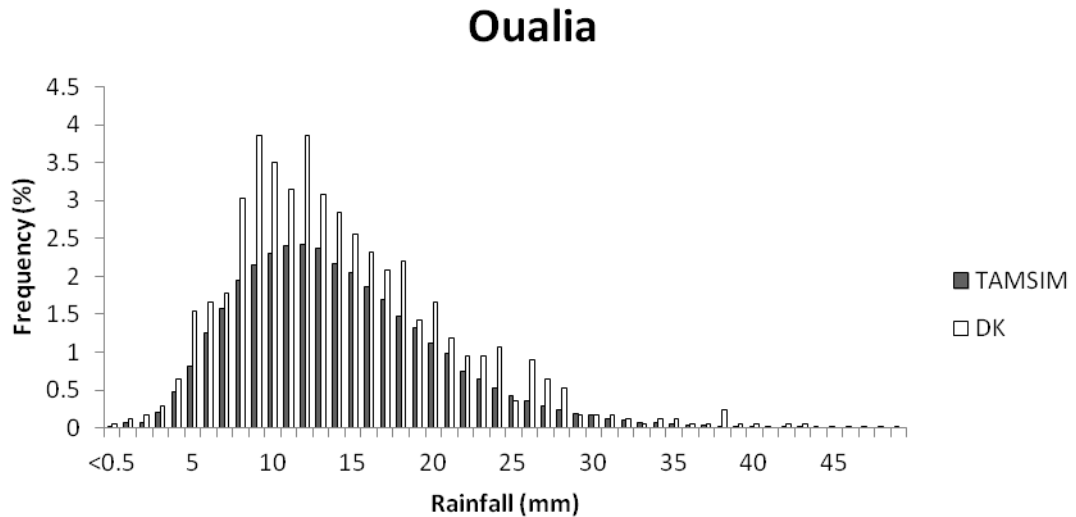


Figure 7.15 – Frequency distribution of TAMSIM rainfall fields and DK obtained rainfall for the Oualia gauge-pixel. Zero rainfall is included in the distribution but not shown (TAMSIM = 65.1%, DK = 50.0%).

It can be seen from Figures 7.11 to 7.15 that the TAMSIM rainfall fields do not recreate the rainfall statistics at individual gauge-pixel level. However, this manifests itself differently for each gauge, for example at the Aero-Lao gauge-pixel (in the drier, northern part of the Senegal Basin), TAMSIM overestimates the distribution of rainfall with the DK rainfall estimate showing a greater proportion of zero rainfall (TAMSIM = 76.2%, DK = 91.1%). In contrast, for the Oualia gauge-pixel (in the wetter, southern part of the Senegal Basin), TAMSIM underestimates the rainfall distribution, with the DK estimate showing less zero rainfall (TAMSIM = 65.1%, DK = 50.0%). This same north to south variation can be observed by comparing the QQ plots for the sample gauge-pixels (Figure 7.16).

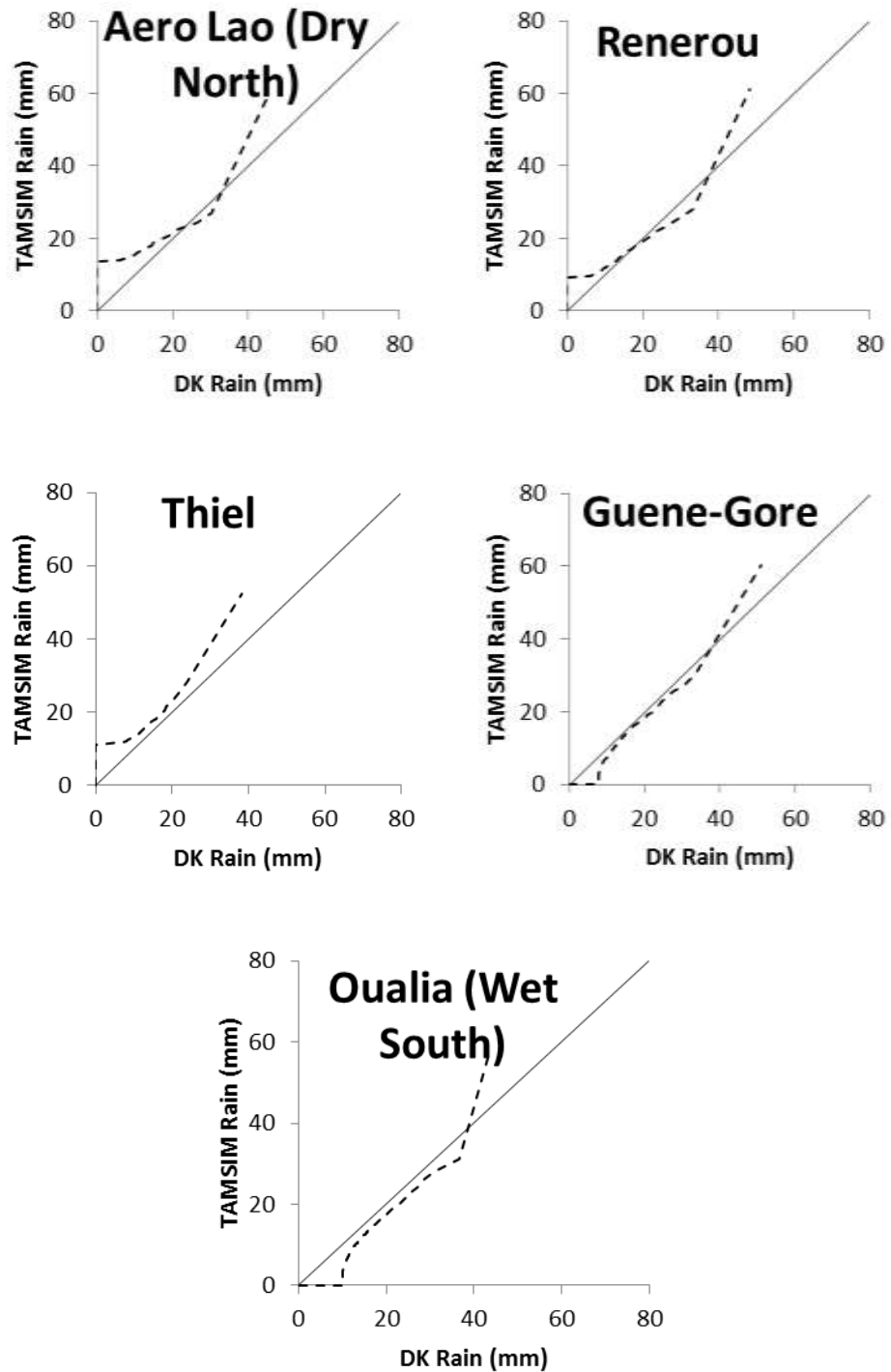


Figure 7.16 – QQ distribution plots showing quantile rainfall at sample gauge-pixels for DK rain fields and combined TAMSIM rain fields.

The QQ plots in Figure 7.16 show that out of the sample gauge-pixels, the Guene-Gore pixel shows the best match between the TAMSIM quantile rainfalls

Chapter 7 – Validation of the Ensemble Representation of the Daily Senegal Basin Rain Field and the DK quantile rainfalls. This matches the distributions of rainfall shown in Figure 7.11 to 7.15.

The reliability of the ensembles can also be observed at gauge-pixel scale, using the TAMSIM ensemble and DK data from pixels containing the selected raingauge stations used previously. The reliability plots for these are shown in Figures 7.17 to 7.21, ordered from most northerly to most southerly. Along with each reliability plot is a bar chart showing the number of samples in each bin, the low number of samples for the 40, 50, 90 and 100% bins generally contain very few samples and this causes a lot of the noise in the charts.

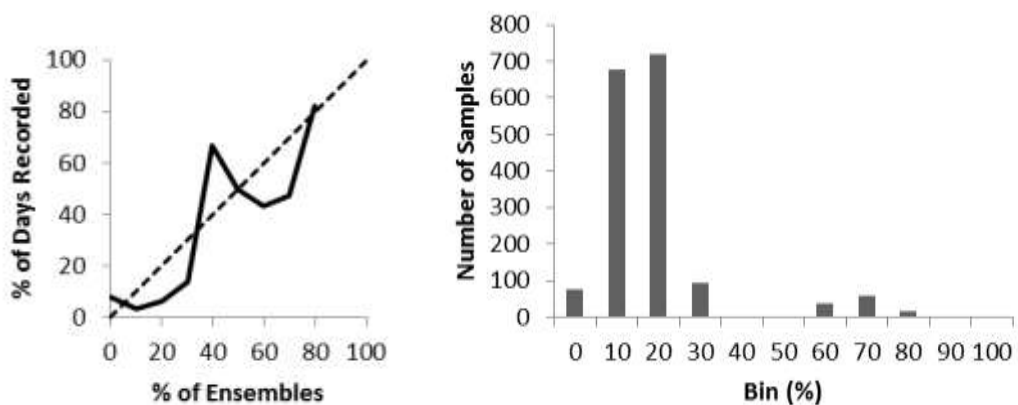


Figure 7.17 – Forecast reliability plots showing the TAMSIM SRFE compared to the DK catchment average rainfall estimate for the pixel containing the Aero-Lao raingauge station. The chart shows values >1.4mm (the mean daily DK rainfall). The dashed lines show the 1:1 relationship. The bar chart on the right shows the number of samples in each bin.

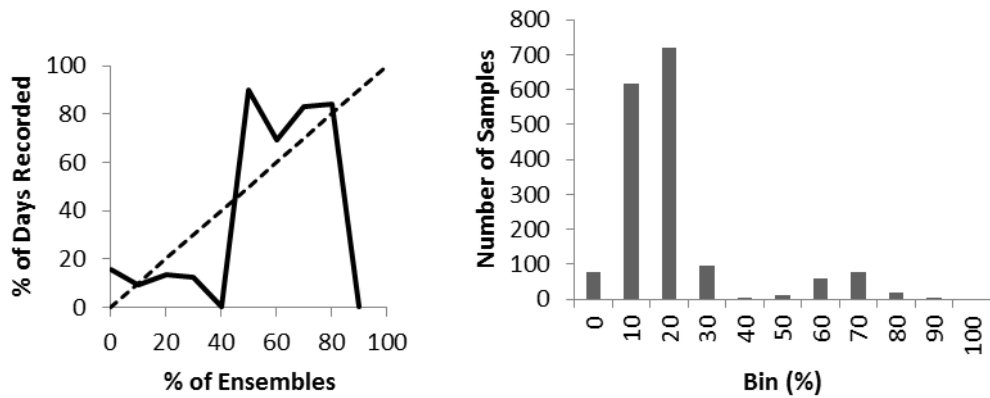


Figure 7.18 – Forecast reliability plots showing the TAMSIM SRFE compared to the DK catchment average rainfall estimate for the pixel containing the Renerou raingauge station. The chart shows values $>2.7\text{mm}$ (the mean daily DK rainfall). The dashed lines show the 1:1 relationship. The bar chart on the right shows the number of samples in each bin.

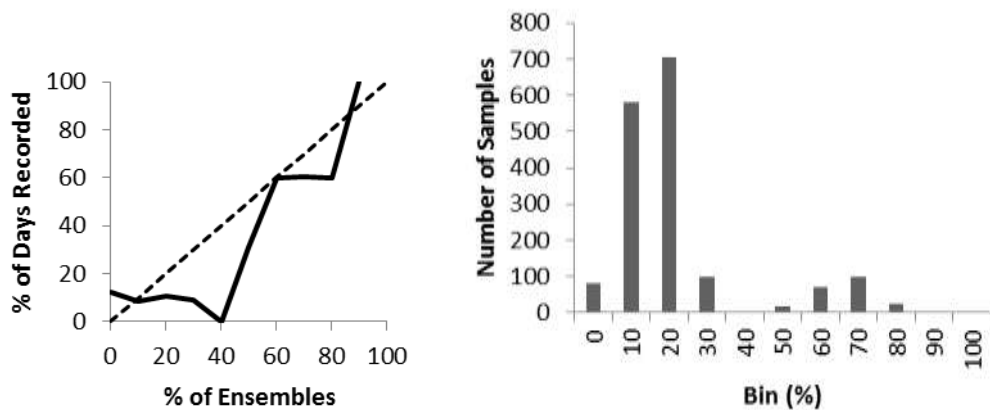


Figure 7.19 – Forecast reliability plots showing the TAMSIM SRFE compared to the DK catchment average rainfall estimate for the pixel containing the Thiel raingauge station. The chart shows values $>2.2\text{mm}$ (the mean daily DK rainfall). The dashed lines show the 1:1 relationship. The bar chart on the right shows the number of samples in each bin.

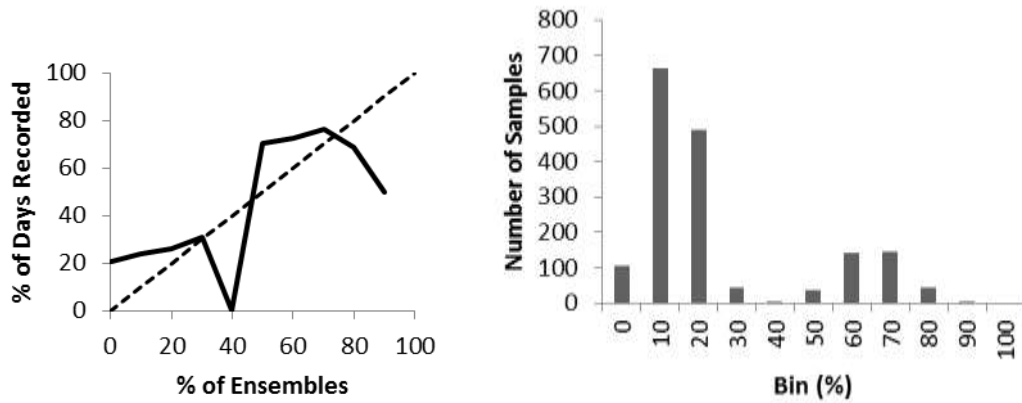


Figure 7.20 – Forecast reliability plots showing the TAMSIM SRFE compared to the DK catchment average rainfall estimate for the pixel containing the Guene-Gore raingauge station. The chart shows values >5.3mm (the mean daily DK rainfall). The dashed lines show the 1:1 relationship. The bar chart on the right shows the number of samples in each bin.

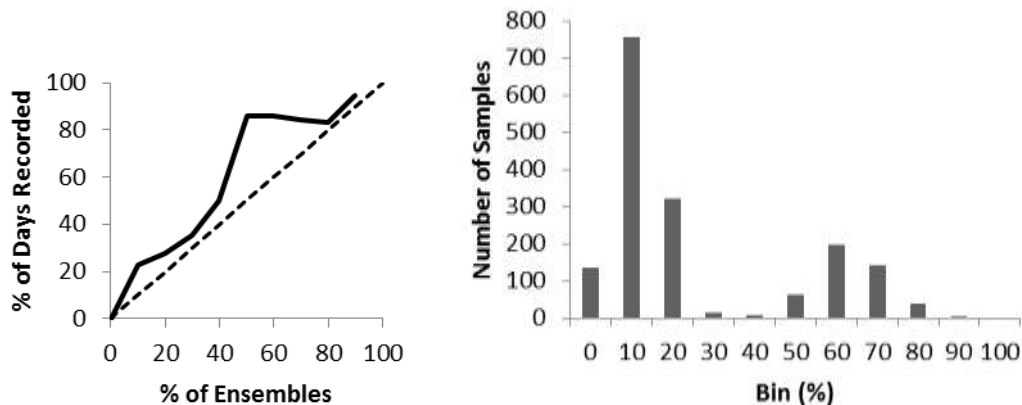


Figure 7.21 – Forecast reliability plots showing the TAMSIM SRFE compared to the DK catchment average rainfall estimate for the pixel containing the Oualia raingauge station. The chart shows values >7.1mm (the mean daily DK rainfall). The dashed lines show the 1:1 relationship. The bar chart on the right shows the number of samples in each bin.

The reliability plots of Figures 7.17 to 7.21 demonstrate how the heterogeneity of the Senegal Basin area influences the reliability of the TAMSIM ensembles, clearly showing that the relationship between CCD and rainfall is non-stationary

Chapter 7 – Validation of the Ensemble Representation of the Daily Senegal Basin Rain Field across the regions and TAMSIM is unable to capture this. The pixels further to the north of the region overestimated the occurrence of rainfall in the ensembles, which was clear for the pixels containing the Aero-Lao and Thiel raingauges, but for the pixel containing the Oualia raingauge the probability of rainfall in the ensembles was underestimated – consistent with the pattern seen in the distributions of rainfall previously observed.

A likely cause of this is the TAMSIM being less able to reproduce the rainfall gradient that transects the Senegal Basin. With only a single calibration of TAMSIM to represent the entire catchment, it is unlikely that the TAMSIM model is able to reproduce the different rainfall characteristics across the catchment, and would not be an appropriate approach if more data was available. This is demonstrated by those pixels within the drier regions overestimating rainfall amount and occurrence and vice versa.

Temporal Bias

To compare the TAMSIM data with the DK data at catchment scale, daily catchment average rainfalls were calculated for each ensemble member. Table 7.3 shows the totals for the catchment average rainfalls at various temporal scales.

Table 7.4 and Figure 7.22 compare the total Bakoye catchment average rainfalls for the daily DK rain fields and the mean daily TAMSIM rain fields, at various temporal scales, and it is clear that the TAMSIM ensemble estimates of

rainfall are not able to reflect fully the interannual variations of rainfall in the same way as the DK estimate.

	DK Rain (mm)	TAMSIM Mean Rain (mm)
Total	7798.91	7116.43
Mean	708.99	646.95
1986	726.77	623.46
1987	595.34	633.14
1988	805.87	712.89
1989	772.00	630.76
1990	637.99	675.50
1991	683.09	637.74
1992	598.98	640.83
1993	635.16	610.81
1994	851.95	690.01
1995	763.98	663.51
1996	727.78	597.77

Table 7.4 – Table showing the total catchment average rainfall, mean annual catchment average rainfall and yearly wet-season totals for DK and TAMSIM mean daily rain fields.

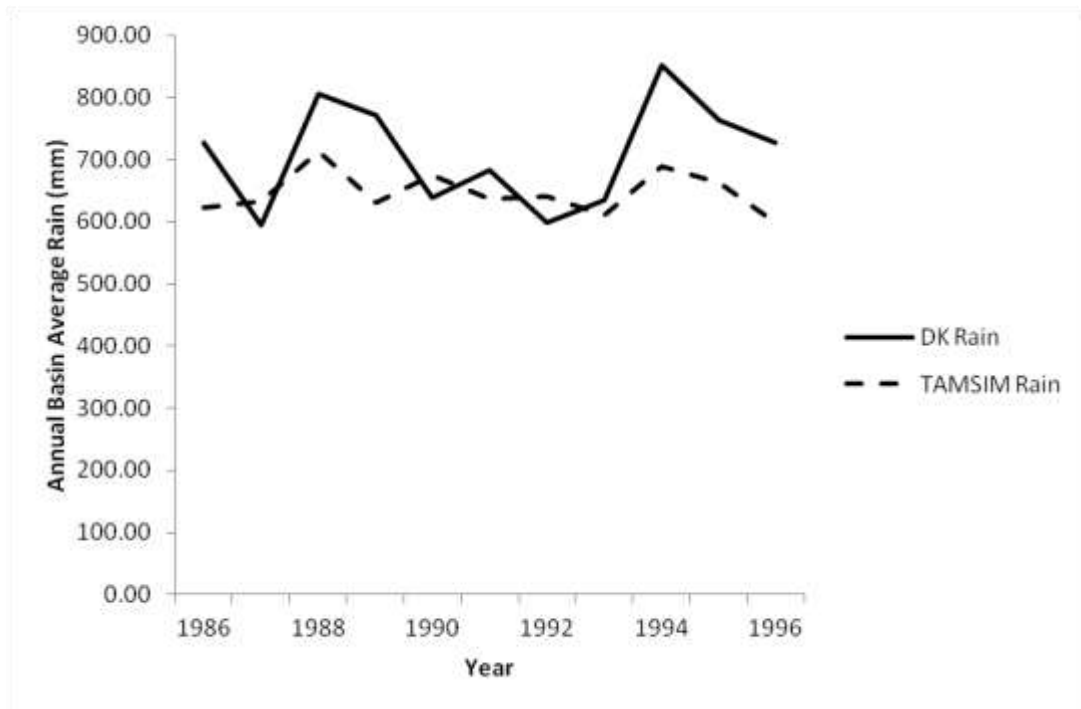


Figure 7.22 – Chart showing the annual Bakoye catchment average rainfall totals for the wet seasons of 1986-1996, for the DK daily rain fields and the mean TAMSIM daily rain fields.

If it is assumed that the bias calculated for the TAMSIM ensemble estimates for the whole 11 year study period is a result of spatial bias, it is possible to adjust the bias for each wet season to remove the influence of the spatial bias – leaving the systematic bias during years of anomalous rainfall. Figure 7.23 shows the bias anomalies for each wet season in the record and it is clear that it shows a similar pattern to the rainfall anomalies seen in the raingauge data, as shown in Figure 3.17.

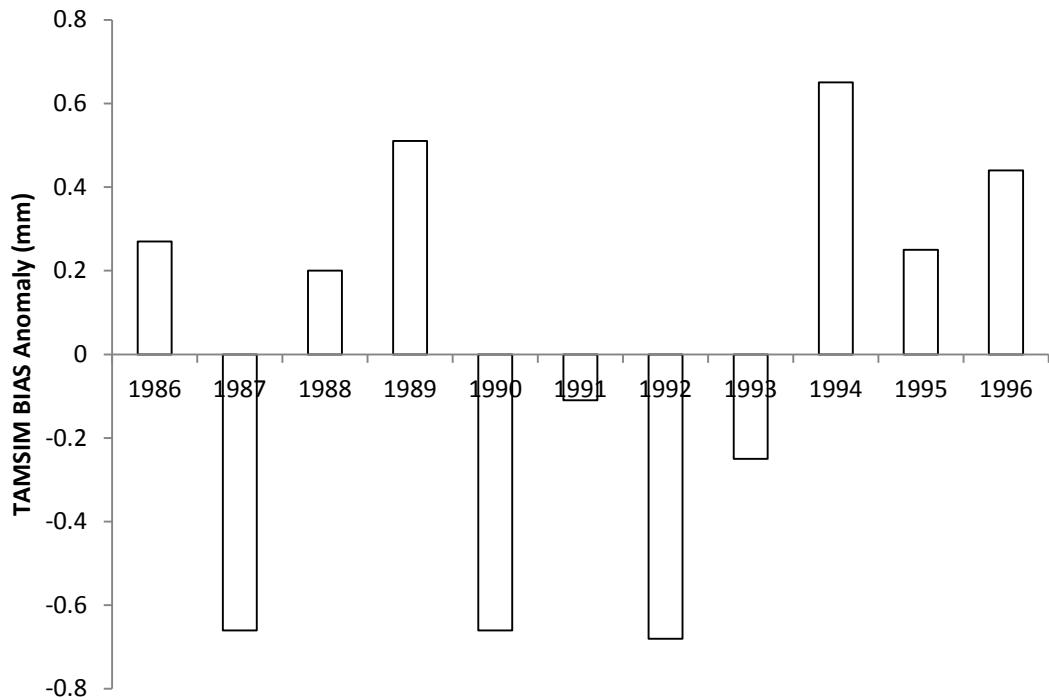


Figure 7.23 – Chart showing the bias anomalies for each wet season, as deviated from the BIAS calculated for the whole 11 year study period, for the TAMSIM ensemble catchment average rainfall estimates.

7.4 – Conclusions

The Senegal Basin daily rainfall fields, produced by the TAMSIM algorithm have been analysed at various spatial and temporal scales, including at gauge-pixels and catchment scales. The ensemble estimates of rainfall have been assessed as a collective, from a sample individual ensemble members, and as a mean of all the members. At catchment scale, the algorithm’s performance has been directly compared to a deterministic estimate of rainfall produced by the TAMSAT1 method.

Overall, the algorithm has performed well in estimating the daily rainfall field, for both the collective of the ensembles and for each individual ensemble member. The distribution of rainfall values closely matches that estimated by the DK rain field at both gauge-pixel and catchment scale. These relationships are replicated when looking at individual ensemble members.

Of particular note from the results is the systematic biases that exist within the SRFE, when compared to the DK gauges based rainfall estimation. Teo (2006) noted that TAMSAT1 and TAMSIM both showed biases for years with anomalous rainfall, and this is also evident with the data for the Senegal Basin. In all there are four types of bias that can be said to exist in the data:

1. Overall bias – both TAMSAT1 and TAMSIM are shown to estimate lower volumes of rainfall than the underlying DK rain field, but are indistinguishable within the bounds of conservative error estimates.
2. Bias due to local variations in rainfall – there are biases in the catchment rainfall estimates for the Bakoye catchment due to local variations in rainfall, in respect to the overall Senegal Basin from which the calibration is derived.
3. Bias due to intraseason variations – it is clear that the relationship between CCD and rainfall is not stationary over the wet season and these variations will result in biased estimates for periods where the relationship has altered.

4. Bias due to interannual variations – the majority of the years in the study period do not demonstrate rainfall close to the mean for the period, and for these years there exists systematic bias in the estimates. The SRFE overestimates rainfall for dry years and vice versa.

The bias resulting from sources 2 and 3 are particularly marked in this thesis due to the paucity of raingauge data available. With a denser network it would have been possible to focus the calibration of the SRFE on data collected in and around the Bakoye catchment. With a denser network it would have been possible to use finer temporal resolutions for calibrations, such as the monthly calibrations adopted by Teo (2006) and Teo and Grimes (2007). Greatrex (2012) demonstrated how regional calibrations could be adopted into the method, subdividing the region into fairly homogenous zones and calibrating separately for each but still producing a single rainfall field. The addition of more extensive ground data in the manner above would reduce the biases, possibly significantly so, but not remove it completely – thus it is important to understand how the bias in the SRFE propagates to downstream applications.

The systematic bias caused by interannual variations of rainfall deviating from the mean over the calibration period may be reduced somewhat with additional ground data, but as it was evident in the study by Teo (2006) it is likely to be significant even for areas with a dense network. To reduce this it is likely that an additional data set would be required, such as sea surface temperature (SST) would need to be incorporated into the study – this is discussed in Chapter 10.

For production of daily catchment estimates of rainfall - which will be used to drive the Pitman lumped CRR model - the TAMSIM estimates performed favourably compared to the TAMSAT1 showing a better fit in regards to the R^2 score.

Chapter 8 demonstrates how the catchment averages of the TAMSIM ensemble SRFE can be used to show the propagation of the uncertainty through the Pitman lumped CRR model, and showing how a fully spatio-temporally distributed stochastic ensemble approach is superior to a simpler perturbation method for this application.

8

The Influence of SRFE Input Uncertainty on Hydrological Model Output

8.1 – Introduction

Chapter 7 demonstrated how significant uncertainties exist within the TAMSAT1 satellite rainfall estimate (SRFE) of the daily rain fields for the Senegal Basin. These uncertainties have been characterised and represented by an ensemble of 200 unique yet equiprobable rainfall estimates using the TAMSIM algorithm, from which catchment averages were calculated for use as an input in a lumped conceptual rainfall-runoff (CRR) model. The lumped CRR model used was the Pitman model calibrated using the Shuffled Complex Evolution (SCE-UA) method - details of both can be seen in Chapter 6.

The use of ensemble representations of uncertainty allows for a simple way of representing the uncertainty in the input, as each can be used as an individual estimate of the rainfall and applied in turn as a rainfall input in the model. The

distribution of the ensemble of modelled outputs, in this case discharges, can be said to show the bounds of uncertainty of the output with regard to the input uncertainty. However, the influence of uncertainty within the hydrological model itself, in particular in the form of model structure and parameter uncertainty, and the way that the SRFE uncertainty interacts with them, cannot be ignored. To this end, before the influence of the uncertainty within a SRFE can be measured propagating through the Pitman model a suitable set of parameter values must be established for use with ensemble inputs.

The EnsAll parameterisation is introduced as a new method for calibrating a deterministic hydrological model for use with ensemble rainfall inputs. The method incorporates each ensemble member in turn - looping the recorded discharge data and resetting the initial conditions at the end of each 11 year period. This method of parameterisation was shown to outperform all the alternative methods, with little overall bias, and showed similar levels of performance when compared to outputs from calibrations against each individual ensemble input.

This chapter addresses three of the key research questions outlined in Chapter 1. Section 8.2 details the performance of the Pitman model driven by the TAMSIM ensemble rainfall estimates when calibrated by different rainfall estimates, showing that a calibration method that incorporates each of the TAMSIM ensemble estimates (EnsAll) is the most favourable option. Section 8.3 describes in detail the performance of the Pitman model using the EnsAll parameterisation, detailing the envelope hydrographs representing the

propagation of the uncertainty as shown by the TAMSIM ensemble SRFE, demonstrating that biases within the SRFE are directly passed on resulting in biases in the discharge output. Section 8.4 will demonstrate how the TAMSIM ensemble SRFE are superior in representing the full range of input uncertainty when compared to a simpler perturbation approach. Finally, Section 8.5 concludes the chapter.

8.2 – Ensemble Parameterisation of the Pitman Model

The Pitman lumped CRR model is a deterministic model, which is designed to operate when driven by a single rainfall input, and models a single discharge output for each timestep. For calibration using the SCE-UA algorithm a deterministic estimate of rainfall is required to drive the Pitman model, whilst the parameter values are adjusted to match the deterministic output against the recorded discharge data. The TAMSIM approach to characterising SRFE uncertainty produces a group of ensemble rainfall inputs that each resemble a deterministic input that can be used to drive the Pitman model, and although a parameter set can be produced for each individual ensemble this is not appropriate for operational purposes, especially if ensemble inputs are to be used to forecast discharges. There is a requirement to determine a single parameter set that can be said to be optimal for the data, and transferable between the ensembles and temporal periods.

The Pitman model was calibrated against several available deterministic estimates of rainfall using SCE-UA, and each calibrated parameter set is

referred to as a parameterisation henceforth when used with the TAMSIM ensemble estimates:

- **EnsStart** – Calibration of the Pitman model provided by David Grimes (personal correspondence, 2009). This parameter set was also used as the initial parameter set in the SCE-UA calibrations.
- **EnsGA** – Calibration against the Gauge Average estimate (an area weighted estimate using a Thiessen Polygons method with an adjustment for orographic effects).
- **EnsDK** – Calibration against the catchment average of the DK rainfall.
- **EnsTAM1** – Calibration against the TAMSAT1 estimate.

In addition to the deterministic estimates the Pitman model was calibrated using rainfall inputs using the Bakoye catchment average TAMSIM ensemble estimates:

- **EnsMean** – Calibration against the daily mean of the 200 TAMSIM ensemble estimates.
- **EnsAll** – Calibration against each of the 200 TAMSIM ensemble members in turn, effectively a 2,200 year record with the recorded discharge looped and the stores reset to 0 at the end of each 11 year period.

The relative performance of each parameterisation when driven by the TAMSIM ensemble estimates can be seen in Figure 8.1. It is evident that the EnsAll

calibration displays the best performance, with a mean RMSE of 133.91% of the mean daily recorded discharge. Both the EnsMean and EnsTAM1 parameterisation show poor transferability when driven by different TAMSIM ensemble estimates, which is most likely a result of overparameterisation.

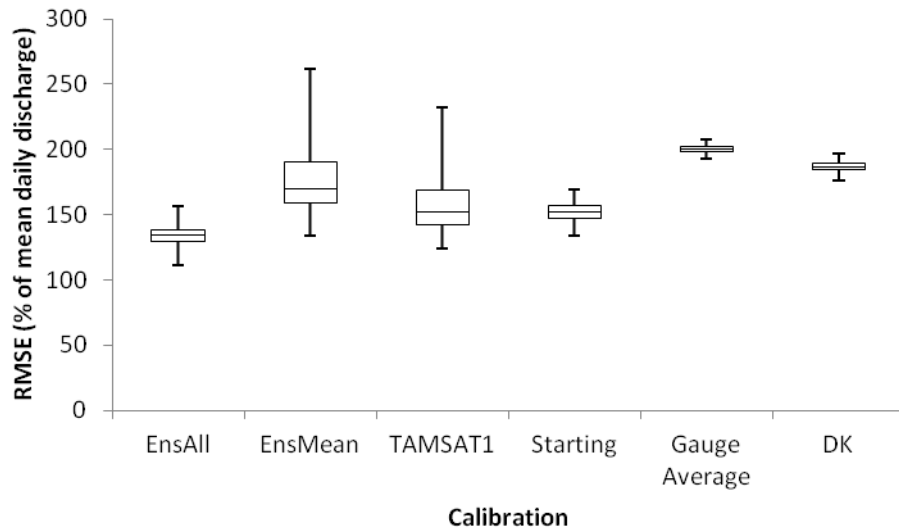


Figure 8.1 – Chart showing the relative performances for different parameterisations of the Pitman model, when driven by the TAMSIM ensemble estimates for the Bakoye catchment, 1986-1996.

The influence of the parameterisation of the modelling of discharge can be seen in Figure 8.2, which compares the EnsAll and EnsMean outputs for the 1992 wet season.

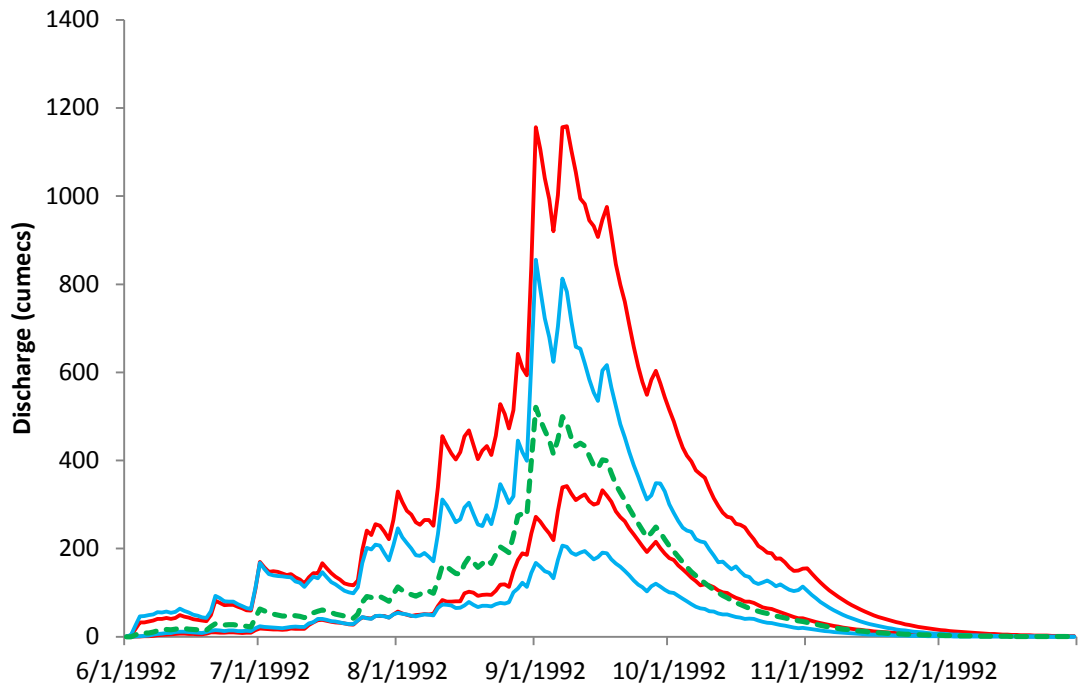


Figure 8.2 – Envelope hydrographs showing the modelled discharges for the 1992 wet season, from both the EnsMean (red) and the EnsAll (blue) parameterisation. The TAMSAT1 deterministic discharge is shown by the dashed green line. The envelopes show the 95% confidence bounds from the modelled discharges.

From Figure 8.2 it is clear that the EnsMean modelled discharges do not show a good representation of the propagation of the SRFE uncertainty as it propagates through the Pitman model, as the parameter uncertainty within the Pitman model is high and interacting with the input uncertainty to produce a wide envelope of modelled discharges. For the late wet season the EnsMean discharges become entirely uncoupled from the TAMSAT1 deterministic estimate. A similar pattern is seen for each year of the record.

To assess the performance of each parameterisation when the Pitman model is driven by the TAMSIM ensemble estimates, the Pitman model was calibrated using each ensemble individually. The collected output from the 200

parameterisations is referred to as **EnsInd** and is used as a proxy for the optimal model. Table 8.1 shows performance statistics for each of the parameterisation methods derived from the SRFE.

	Calibration Regime	RMSE (%)	R ²	BIAS (%)
1986-1996	EnsTAM1	114.42	1.10	24.34
	EnsInd	85.65	0.57	3.83
	EnsMean	116.68	1.63	-163.61
	EnsAll	89.08	0.52	0.80

Table 8.1 – Table showing performance statistics for the parameterisations derived from the SRFE, comparing them to the EnsInd output. The table shows values for wet season data only. RMSE and BIAS shown as percentages of the mean daily discharge for the period.

The values in Table 8.1 show that the Pitman model performs best when calibrated to each individual ensemble, as in EnsInd, although the performance of the EnsAll model is similar. EnsAll actually shows a less biased output than the EnsInd output over the 11 years of the study period. EnsTAM1 and EnsMean both perform very poorly and display high biases.

8.3 – The Propagation of Input Uncertainty through the Pitman Model

The previous section analysed the available parameterisations that can be used for the Pitman model when driven by the TAMSIM ensemble estimates, showing that calibrations against deterministic estimates based on the SRFE are not suitable for this purpose. The EnsAll parameterisation incorporates each

individual ensemble member in a single record and provides a robust calibration of the Pitman model, which outperforms each of the alternative methods. EnsAll was also shown to be comparable to the optimal proxy, EnsInd.

With the EnsAll parameterisation shown to be the optimal method available it can be used to model the envelope hydrographs for each year of the record, displaying the 95% confidence discharge envelope of the modelled discharges between the 2.5th percentile and the 97.5th percentile for each day. These are shown in Figures 8.3 to 8.13.

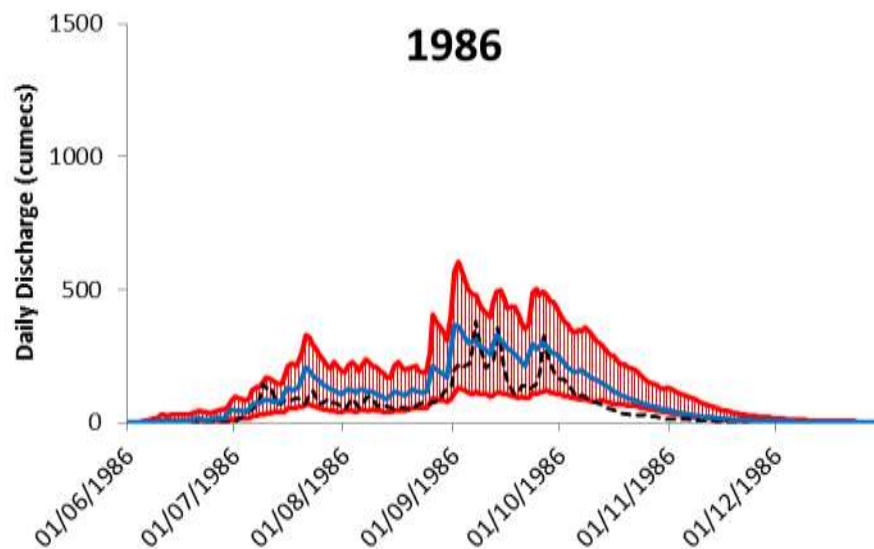


Figure 8.3 – Hydrograph showing the 95% confidence discharge envelope (in red) for 1986 for the Bakoye Catchment, driven by the TAMSIM ensemble SRFE using the EnsAll parameterisation. The solid blue line shows the deterministic TAMSAT1 discharge, and the dashed line shows the recorded discharge. (Note – 1986 represents the first year of the modelling and is therefore subject to the ‘charging period’)

Figure 8.3 shows the 95% confidence discharge envelope for the 1986 wet season for the period 1986-1996. Due to the nature of the dry season in the region there appears to be little influence of a charging period in the

hydrograph, and the TAMSAT1 estimate (blue line) closely follows the recorded discharge (dashed black line). Between July and October the discharge envelope roughly lies equally above and below the TAMSAT1 estimate, but TAMSAT1 becomes decoupled after October dropping to the lower end of the envelope. From the raingauges 1986 displayed rainfall close to the mean for the period, 592.95mm and 607.83mm respectively. The discharge from the TAMSAT1 and TAMSIM estimates show little bias.

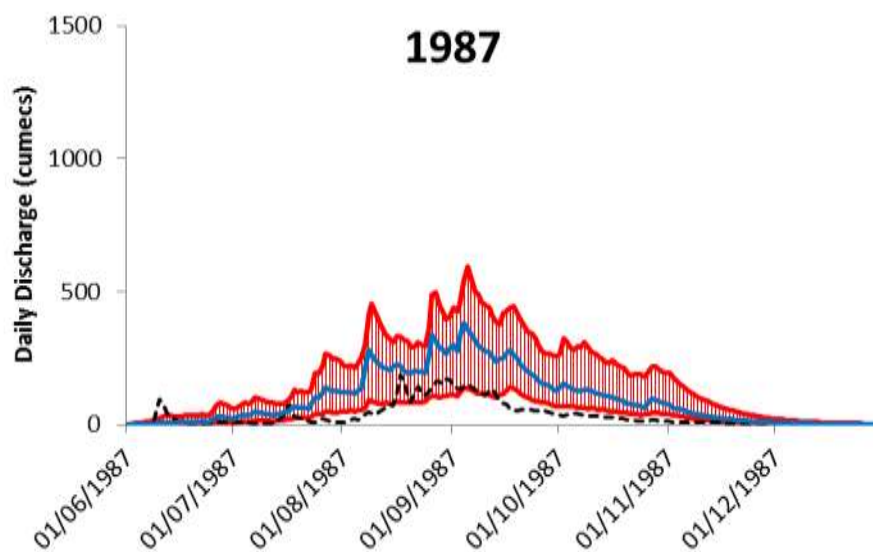


Figure 8.4 – Hydrograph showing the 95% confidence discharge envelope (in red) for 1987 for the Bakoye Catchment, driven by the TAMSIM ensemble SRFE using the EnsAll parameterisation. The solid blue line shows the deterministic TAMSAT1 discharge, and the dashed line shows the recorded discharge.

The raingauges in 1987 showed rainfall below the mean for the period for the Senegal Basin region. For the gauges associated with the Bakoye catchment this was particularly significant, with rainfall 150mm below the mean for the year, being the driest year in the record. The hydrograph shows significant bias, the Pitman model overestimating the discharge throughout the wet season. The

bias is such that most of the recorded discharge is below the bounds of the modelled uncertainty.

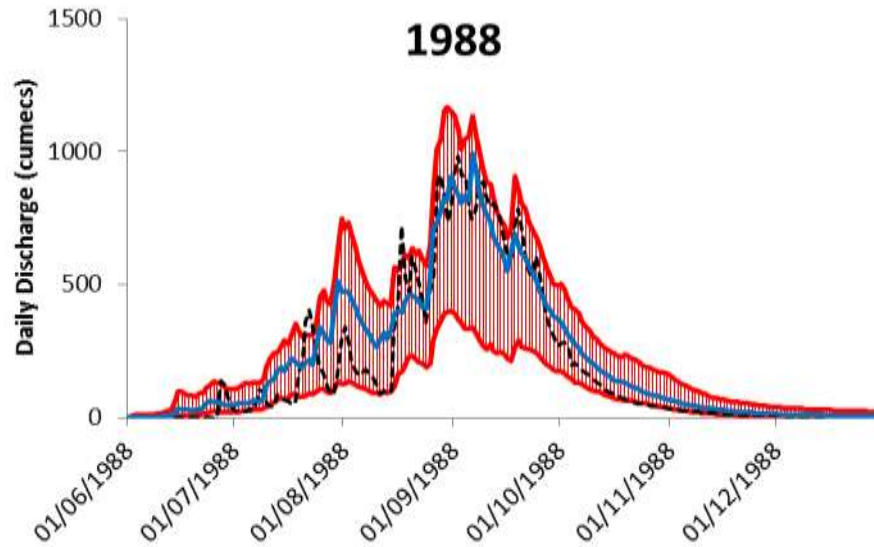


Figure 8.5 – Hydrograph showing the 95% confidence discharge envelope (in red) for 1988 for the Bakoye Catchment, driven by the TAMSIM ensemble SRFE using the EnsAll parameterisation. The solid blue line shows the deterministic TAMSAT1 discharge, and the dashed line shows the recorded discharge.

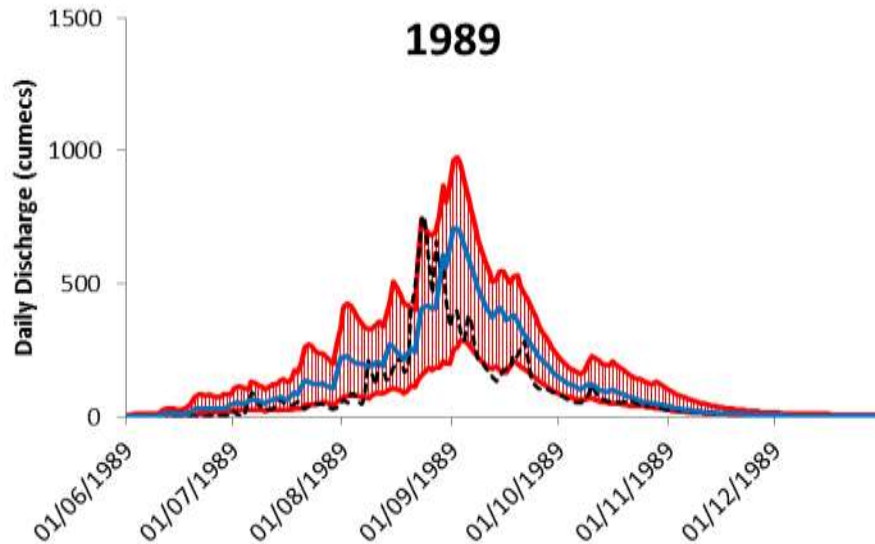


Figure 8.6 – Hydrograph showing the 95% confidence discharge envelope (in red) for 1989 for the Bakoye Catchment, driven by the TAMSIM ensemble SRFE using the EnsAll parameterisation. The solid blue line shows the deterministic TAMSAT1 discharge, and the dashed line shows the recorded discharge.

Both 1988 and 1989, shown in Figures 8.5 and 8.6, displayed above average rainfall to similar degrees. This was more significant in the Bakoye catchment gauges. The deterministic and ensemble modelled discharges show little bias, with 1988 being a particularly close match with the recorded discharge, yet the timing of the peak discharge in the 1989 wet season is late.

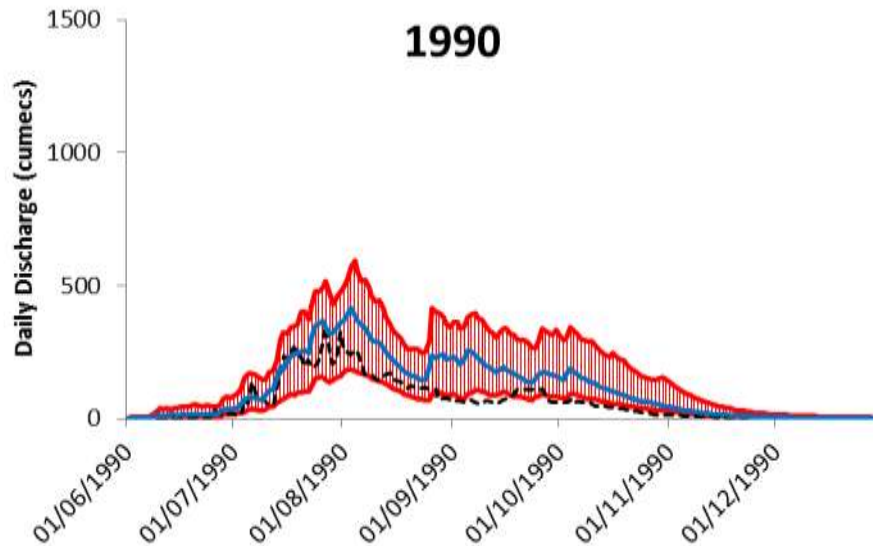


Figure 8.7 – Hydrograph showing the 95% confidence discharge envelope (in red) for 1990 for the Bakoye Catchment, driven by the TAMSIM ensemble SRFE using the EnsAll parameterisation. The solid blue line shows the deterministic TAMSAT1 discharge, and the dashed line shows the recorded discharge.

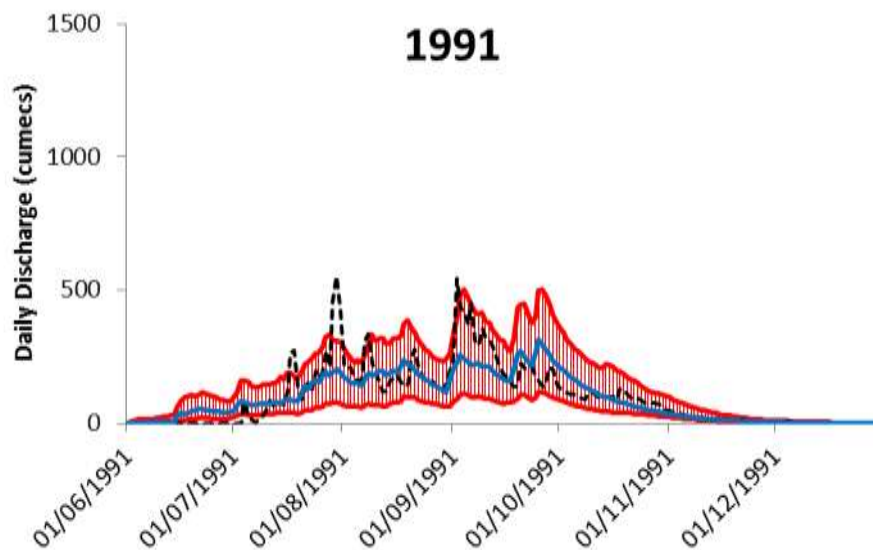


Figure 8.8 – Hydrograph showing the 95% confidence discharge envelope (in red) for 1991 for the Bakoye Catchment, driven by the TAMSIM ensemble SRFE using the EnsAll parameterisation. The solid blue line shows the deterministic TAMSAT1 discharge, and the dashed line shows the recorded discharge.

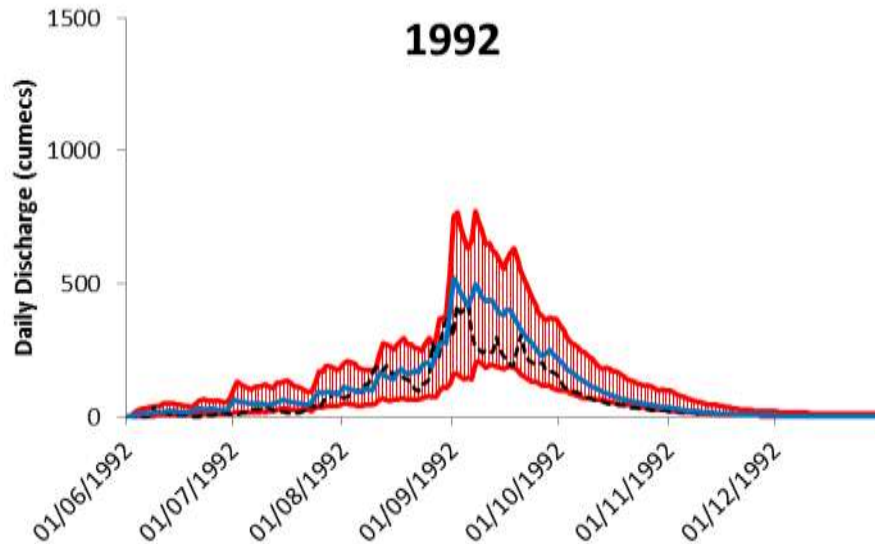


Figure 8.9 – Hydrograph showing the 95% confidence discharge envelope (in red) for 1992 for the Bakoye Catchment, driven by the TAMSIM ensemble SRFE using the EnsAll parameterisation. The solid blue line shows the deterministic TAMSAT1 discharge, and the dashed line shows the recorded discharge.

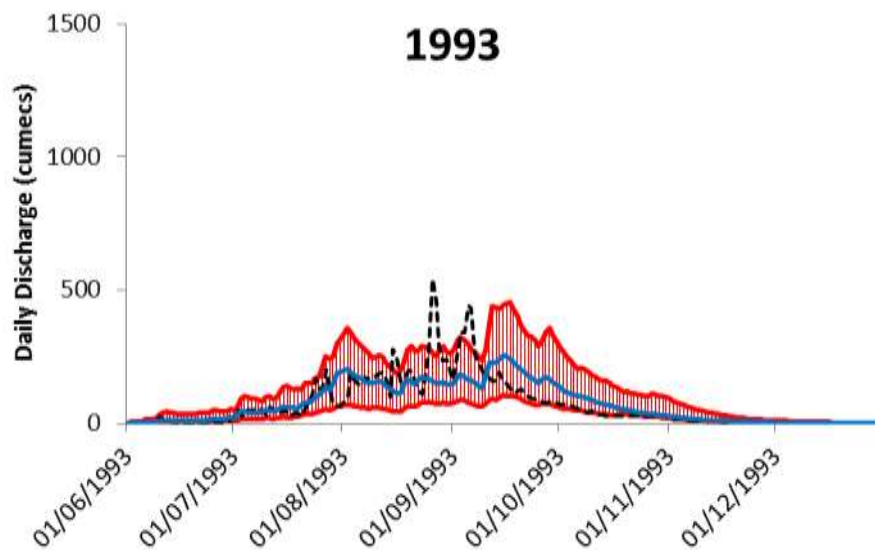


Figure 8.10 – Hydrograph showing the 95% confidence discharge envelope (in red) for 1993 for the Bakoye Catchment, driven by the TAMSIM ensemble SRFE using the EnsAll parameterisation. The solid blue line shows the deterministic TAMSAT1 discharge, and the dashed line shows the recorded discharge.

Figure 8.7 to 8.10 show the hydrographs for the period 1990 to 1993, a period that displayed consistently below average rainfall for both the whole Senegal Basin area and the Bakoye catchment. There is some bias evident in 1990, with an overestimation of the discharge by the models, but a close match with the recorded discharge for the rest of the years in this dry period.

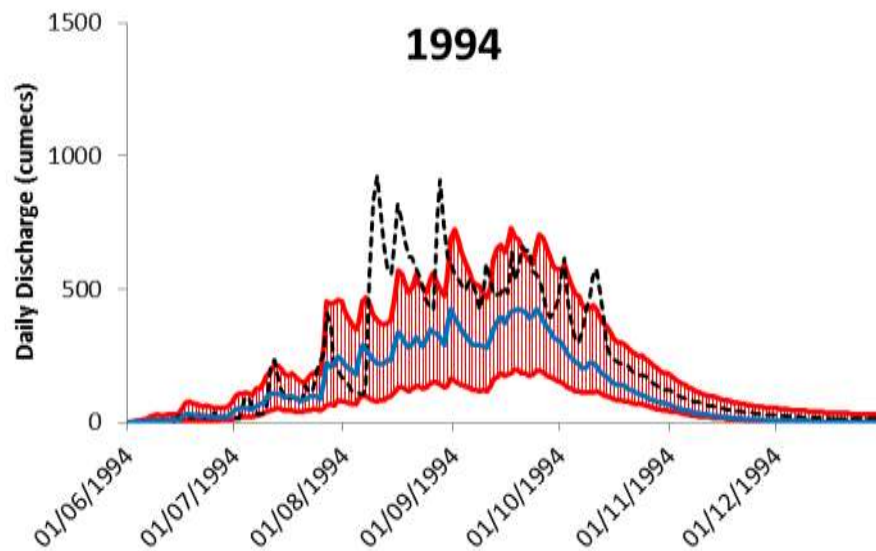


Figure 8.11 – Hydrograph showing the 95% confidence discharge envelope (in red) for 1994 for the Bakoye Catchment, driven by the TAMSIM ensemble SRFE using the EnsAll parameterisation. The solid blue line shows the deterministic TAMSAT1 discharge, and the dashed line shows the recorded discharge.

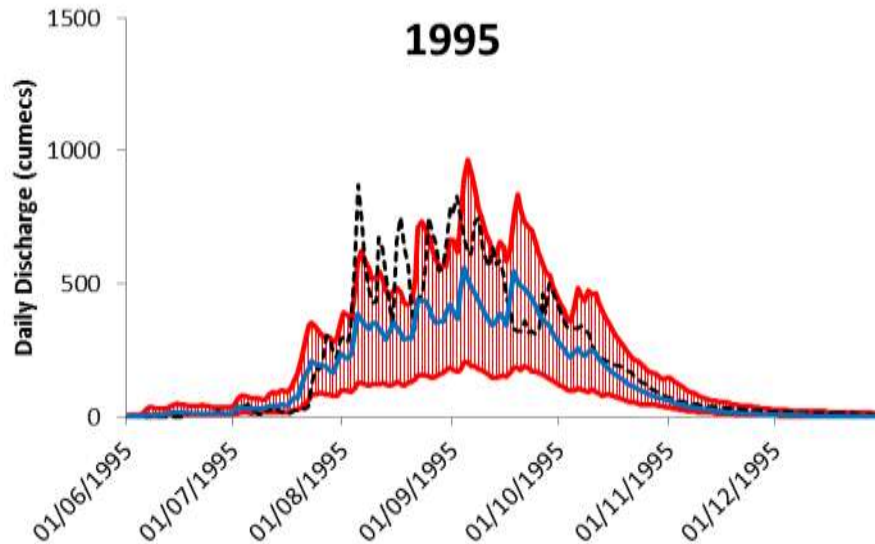


Figure 8.12 – Hydrograph showing the 95% confidence discharge envelope (in red) for 1995 for the Bakoye Catchment, driven by the TAMSIM ensemble SRFE using the EnsAll parameterisation. The solid blue line shows the deterministic TAMSAT1 discharge, and the dashed line shows the recorded discharge.

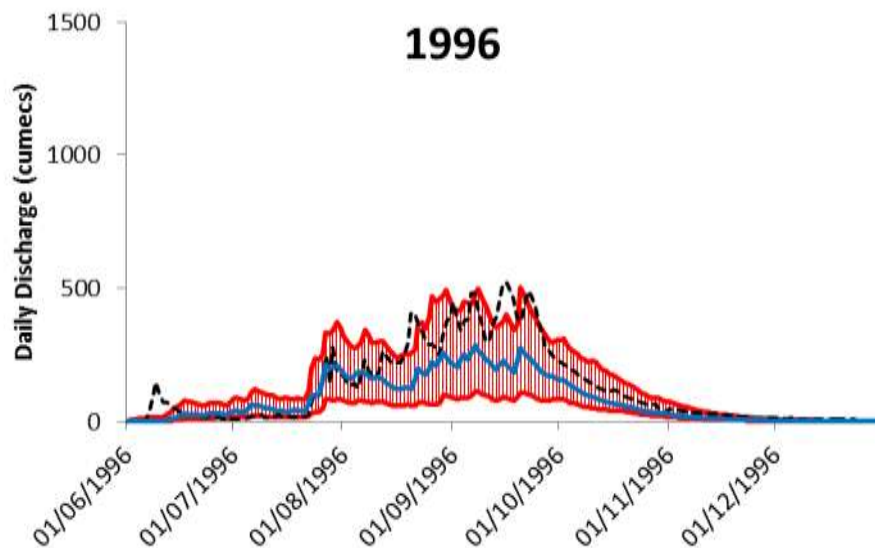


Figure 8.13 – Hydrograph showing the 95% confidence discharge envelope (in red) for 1996 for the Bakoye Catchment, driven by the TAMSIM ensemble SRFE using the EnsAll parameterisation. The solid blue line shows the deterministic TAMSAT1 discharge, and the dashed line shows the recorded discharge.

The final three years of the period all displayed above average rainfall for the gauges in the Senegal Basin area, yet 1996 is slightly below average over the Bakoye catchment. Each of the years, 1994-1996, showed bias in the discharge modelling, each underestimating the recorded discharge with significant periods where the recorded discharges lay above the modelled uncertainty bounds.

Performance Measures for the TAMSIM driven Pitman Model

The hydrographs show how the TAMSAT1 SRFE for the Senegal Basin area, in particular the Bakoye catchment average, can be a poor representation of the reality when modelled through the Pitman model. Even when representing the range of uncertainties, there are significant periods where the daily recorded discharge lies outside of the 95% confidence envelopes. For the entire 11 year period this accounts for 57.0% of days, and 40.1% of days when just accounting for the wet season. The occurrences occur mainly in years where the mean rainfall is either significantly greater or less than the mean for the whole. For example, 1987 was an exceptionally dry year and on 71.2% of the days the recorded discharge was outside the envelope for the wet season. Although this thesis does not provide for a full accounting of the error present in the process, there should be a consideration of influence of observation error in the discharge measurements when analysing the hydrographs in Figures 8.3 to 8.13. Di Baldassarre and Montanari (2009) found that discharge observations could contain errors up to 25%, and by applying an estimate of observation of up to 25% the number of days where the observed discharges falls outside of

the modelled envelope could be reduced to 50.1% in total and to 28.3% for wet season only.

There is a relationship between the number of days where the recorded discharge lies outside the envelope and the mean daily discharge, as shown in Figure 8.14, with wet seasons with a lower mean daily discharge showing less overlap between recorded discharge and the envelope – this is most likely due to the large bias in the SRFE (and therefore the Pitman model output) for anomalously dry years, overestimating in such years.

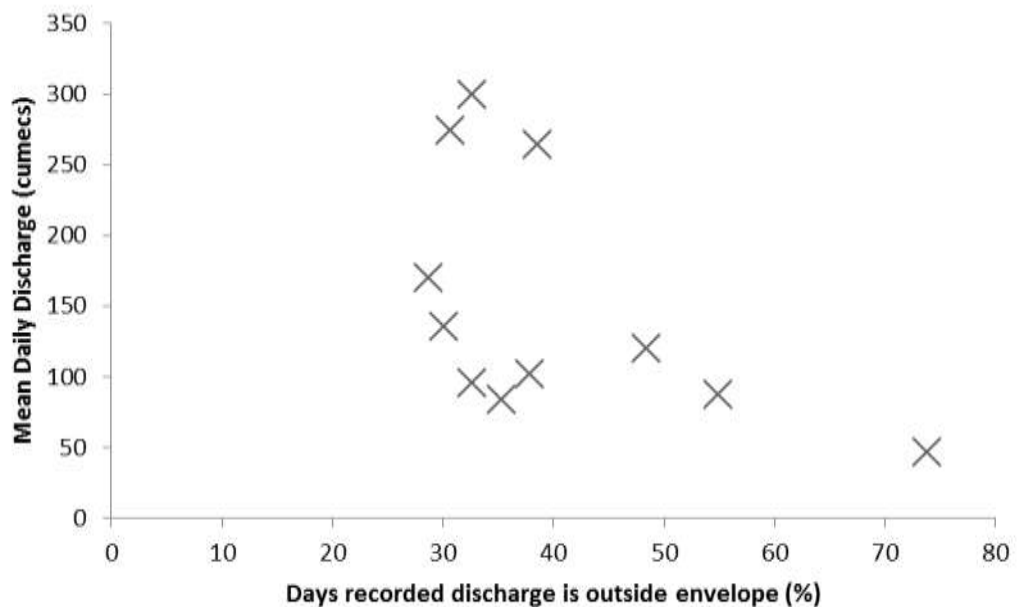


Figure 8.14 – Plot showing the mean daily discharge for each of the wet seasons between 1986 and 1996, and the percentage of days where the recorded discharge is either greater or lower than the modelled 95% confidence envelope of Pitman model modelled discharges, for the Bakoye catchment.

Figures 8.15 and 8.16 show the distributions of daily modelled discharges from the TAMSIM ensemble driven Pitman model, compared to the distribution of the daily recorded discharge from the Oualia gauging station, for wet season data only. The modelled discharge distributions shows no zero discharge during the wet seasons, which is consistent with the lack of zero rainfall within the TAMSIM estimates compared to the DK rainfall estimate. For positive discharge the modelled discharges produce more lower level discharge >0 to 100cumecs, but less higher discharges, especially >500cumecs.

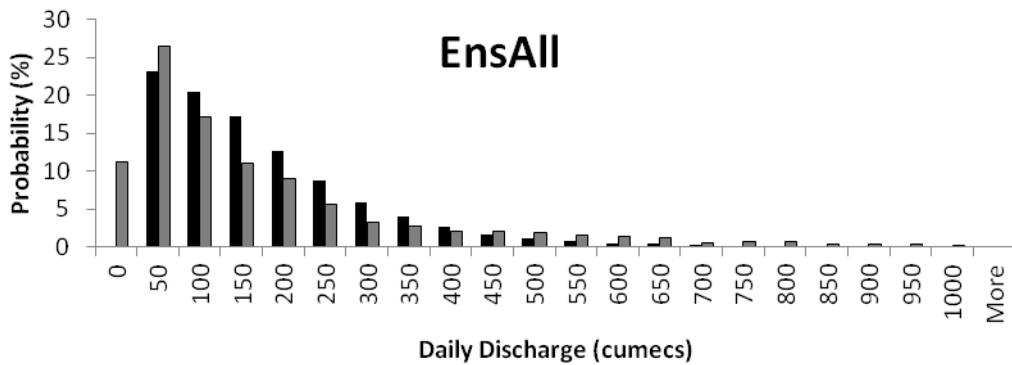


Figure 8.15 – Probability distributions of daily wet season discharges for the Bakoye catchment for the period 1986-1996 for the Pitman models driven by the TAMSIM ensemble estimates. The distribution of the recorded discharge is shown in grey and the modelled discharges in black.

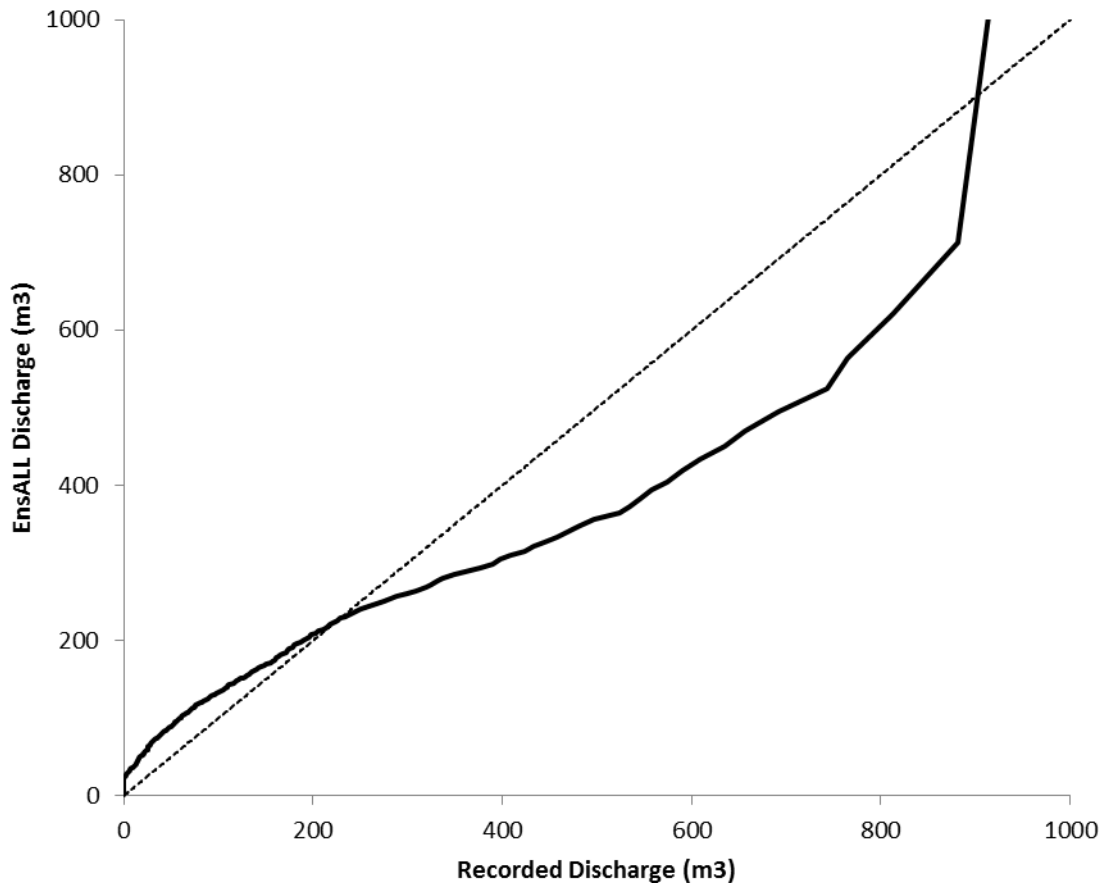


Figure 8.16 – QQ distribution plot showing the distribution of modelled wet season discharges from the EnsAll parameterised Pitman model against the recorded discharge, when driven by the TAMSIM ensemble estimates for the Bakoye catchment, 1986-1996.

The ability of TAMSIM to produce ensemble rainfall estimates that were consistent with the rainfall characteristics was assessed in Chapter 7 using a forecast reliability method. The same method can be used to check the ensemble discharge outputs, and this can be seen in Figure 8.17. Although the ensembles show little reliability when thresholded at a low discharge level (the 25th percentile of recorded discharge), they show a high level of reliability when thresholded at mean recorded discharge, and especially so at the 75th percentile level. This is a similar pattern to that observed with the rainfall estimates and shows that TAMSIM is a very reliable method for recreating

rainfall characteristics for rainfall above trace level, and that this is passed on through the Pitman model with some evidence that the reliability has been strengthened further.

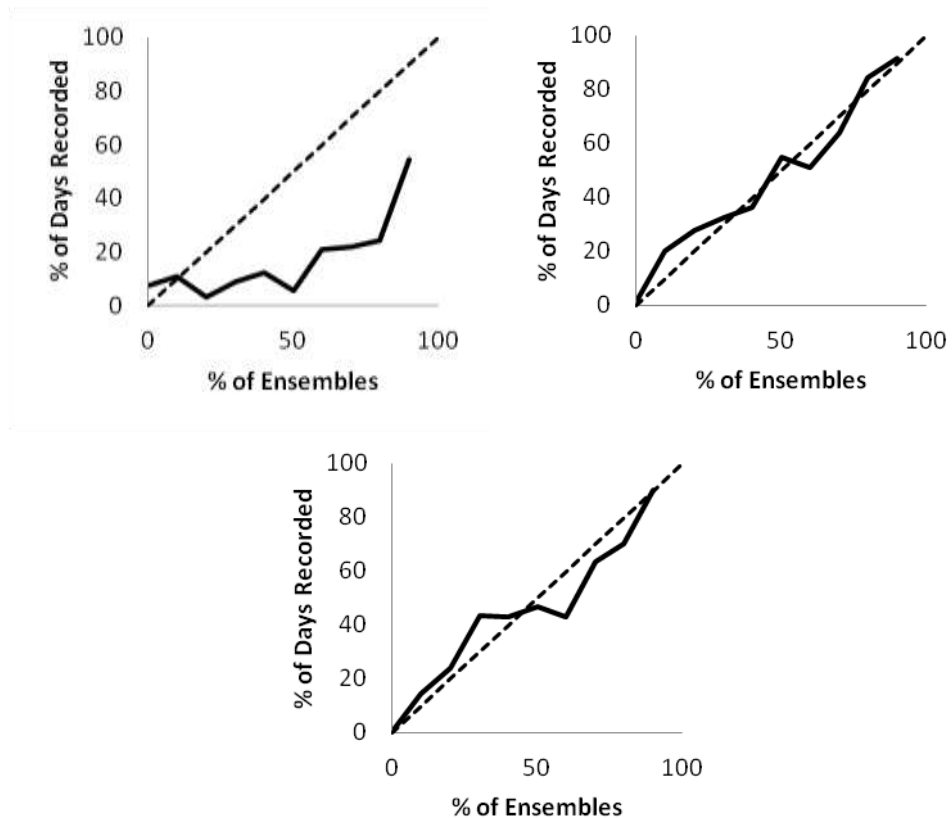


Figure 8.17 – Forecast reliability plots for daily wet season discharges for the Bakoye Catchment for the period 1986-1996 for the Pitman model driven by the TAMSIM ensemble estimates. The plot on the top-left shows values >23cumecs (the 25th percentile of the recorded discharge), the top-right shows values >202cumecs (the 75th percentile of the recorded discharge), and the bottom plot shows values >153cumecs (the mean daily discharge of the recorded discharge). The dashed lines show the 1:1 relationship.

The final way to observe the performance of the TAMSIM ensemble estimate driven Pitman model is to calculate performance statistics, for the entire 11 year

study period, and also for each individual wet season. The statistics can be seen in Table 8.2.

	RMSE (%)	R ²	BIAS (%)
1986-1996	89.08	0.52	0.80
1986	102.13	1.97	-52.73
1987	250.12	7.47	-177.86
1988	68.15	0.51	10.63
1989	105.58	1.14	-37.50
1990	108.17	2.26	-68.30
1991	73.65	0.61	2.44
1992	81.80	1.56	-32.09
1993	94.84	0.65	-9.80
1994	73.99	0.54	41.27
1995	70.20	0.53	32.43
1996	68.59	0.53	31.23

Table 8.2 – Performance statistics for the TAMSIM ensemble estimate driven Pitman model for the whole 11 year study period, and for each individual wet season. RMSE and BIAS are presented as a percentage of the mean daily discharge for each period.

The Influence of SRFE Bias on the Pitman Model

Chapter 7 demonstrated that TAMSIM was able to characterise the rainfall characteristics for the daily Senegal rainfall field for the 11 year study period, but it was also shown that the rainfall field displayed significant spatial and temporal biases. The Pitman model has been used to model the hydrology in the Bakoye catchment, an area that itself is affected by significant heterogeneity in rainfall gradient. At its outlet the TAMSIM ensembles were shown to underestimate the rainfall volumes compared to the underlying DK rain field, and that this was a pattern seen in areas in the southern area of the Senegal Basin, and the relationship changes with rainfall overestimated in the drier

north. The catchment average estimates for the TAMSIM ensemble rainfall inputs were shown to be biased against the DK field, slightly underestimating the rainfall in comparison – this can be attributed to the spatial biases in the estimates. More significantly, the TAMSIM ensembles showed significant interannual biases, with the method struggling to account for the large variations of rainfall displayed by the catchment.

The EnsAll parameterisation of the Pitman model showed the least bias when compared to the recorded discharge, with a BIAS of 0.8% of the mean daily discharge. This suggests that the spatial bias in the TAMSIM SRFE is not transferred to the Pitman model output as it pervades the entire rainfall input and the SCE-UA calibration is able to compensate. The inability of TAMSIM to estimate the interannual variations fully, however, has been observed propagating through the model. Figures 8.18 to 8.20 show the relationship between the TAMSIM estimate bias, the EnsAll model bias and the error in the EnsAll model.

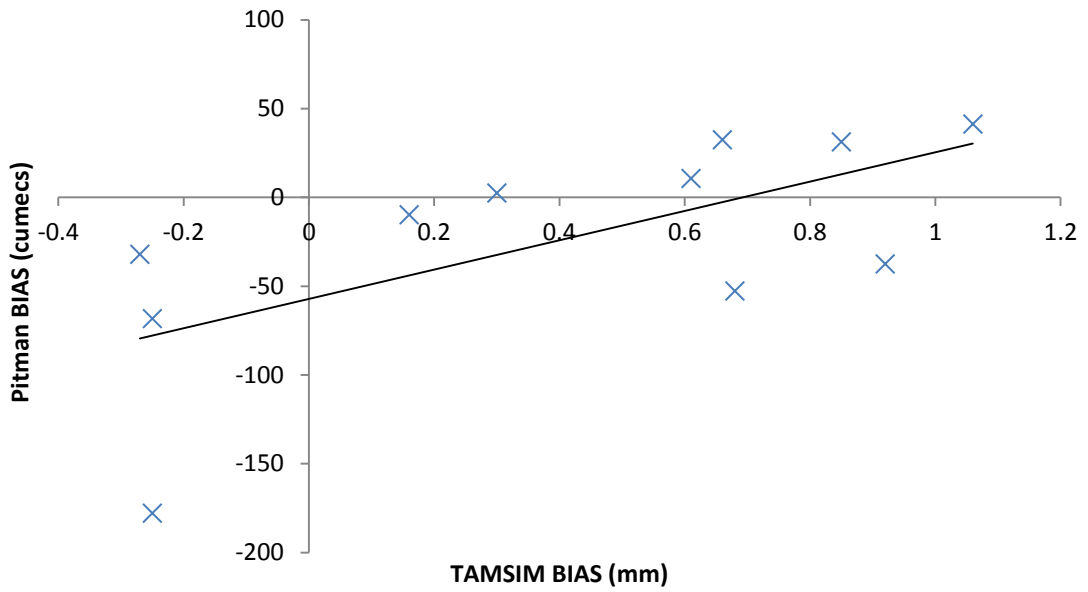


Figure 8.18 – Chart showing the relationship between the BIAS within the TAMSIM rainfall estimates and the resulting BIAS from the EnsAll parameterised Pitman model – the BIAS score is from all ensemble members.

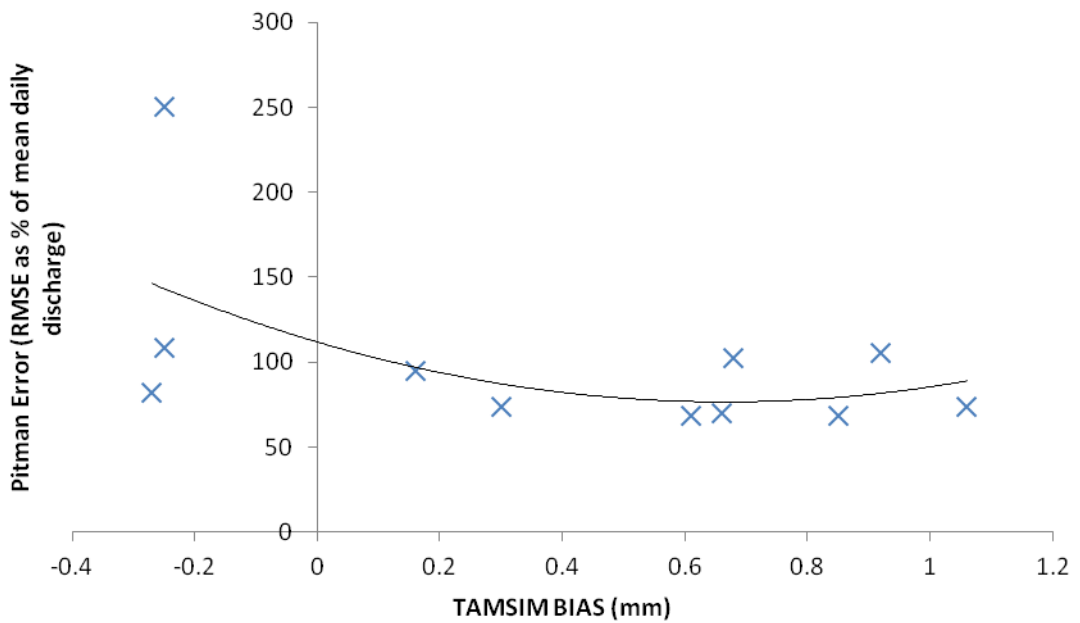


Figure 8.19 – Chart showing the relationship between the BIAS within the TAMSIM rainfall estimates and the mean RMSE from the EnsAll parameterised Pitman model – the BIAS score is from all ensemble members.

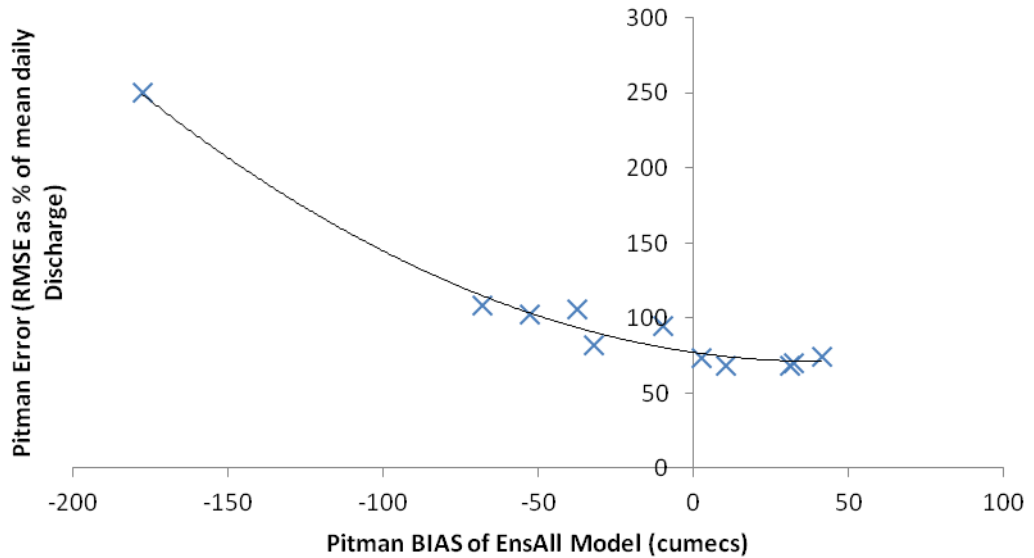


Figure 8.20 – Chart showing the relationship between the BIAS within the EnsAll parameterised Pitman model and the mean RMSE from the same model – the BIAS score is from all ensemble members.

It is clear from the charts shown in Figures 8.18 to 8.20 that the propagation of the bias is not direct. Although the propagation of the bias does appear to be roughly linear between TAMSIM and the EnsAll, it is not straightforward - an unbiased TAMSIM rainfall estimate can be expected to result in a discharge output with a BIAS of around -60cumeecs. An unbiased discharge output is likely to be produced by a TAMSIM estimate with a BIAS of 0.7mm. The best performing models are driven by rainfall estimates showing a BIAS of 0.7mm.

The TAMSIM SRFE were shown in Chapter 7 to have a mean BIAS of 0.41mm over the 11 year period, as overall TAMSIM underestimates rainfall in relation to the DK rain field. This is overall BIAS influences the calibration of the Pitman model, as it is calibrated against the biased estimate which explains why the unbiased Pitman model exists when driven by a positively biased TAMSIM

estimate. This compensation for the overall underestimation of the rainfall by TAMSIM results in an overestimation of the discharge even when the rainfall estimate is lower than the DK estimate – for years when the TAMSIM overestimates the rainfall, this bias is magnified by the Pitman model.

The charts shown in Figures 8.18 to 8.20 appear to be skewed by the data from the 1987 wet season that displayed particularly poor correlation with the recorded discharge. It is tempting to remove this year from the analysis but there is no reason to assume that the data for that year is incorrect – it is likely that it is limitations in the model processes that are the cause and it represents an issue likely to be faced by such methods when applied to contemporary data. In actuality, similar patterns remain visible even without the representation of the 1987 data. It is not clear why the modelling of the 1987 wet season was so poor, however the Bakoye average rainfall from the raingauges in 1987 showed a far greater deviation from the mean for the period than for the whole catchment, and it is possible that this has been lost since the DK stage of the process.

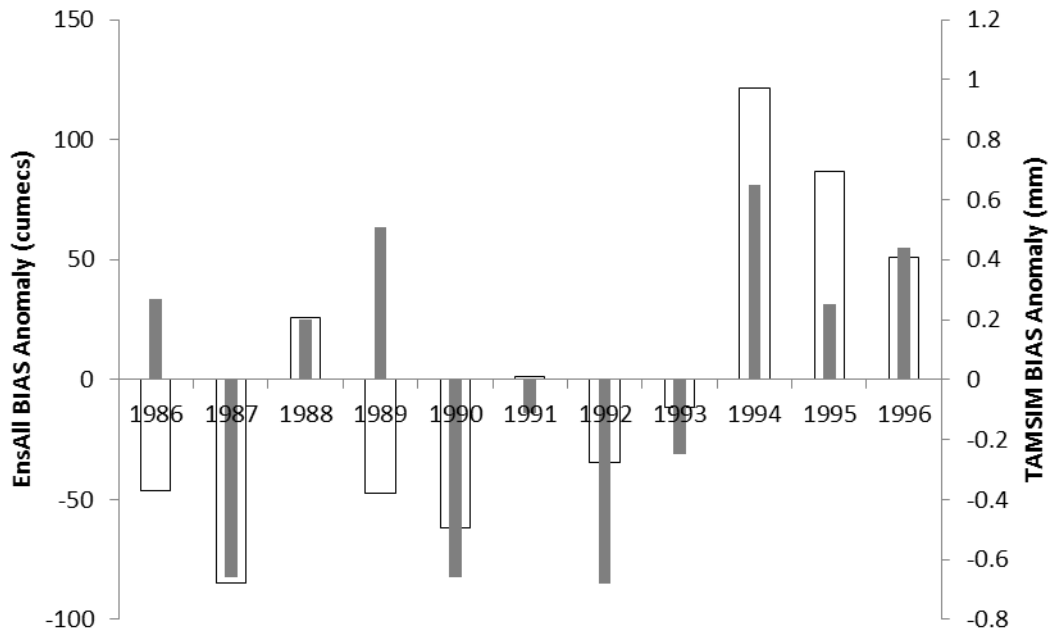


Figure 8.21 – Chart showing the yearly BIAS anomaly for the modelled discharges for the Pitman model, driven by TAMSIM ensemble estimates for the Bakoye catchment, 1986-1996 (in white), and the BIAS anomaly for the TAMSIM rainfall estimates (in grey).

Figure 8.21 shows the BIAS anomaly for each wet season and it affirms the biases that were observed from the envelope hydrographs of Figure 8.3 to 8.13. It also shows that there is a good comparison between the interannual biases in the TAMSIM rainfall estimates and the biases in the Pitman modelled discharges, suggested a direct propagation. However, 1986 and 1989 show biases in opposite directions.

8.4 – Comparison with a Perturbation Method

The potential benefits of a method of representing rainfall uncertainty such as TAMSIM over a simpler perturbation method were discussed in Chapter 2, Section 2.2. Although the common perturbation methods vary in complexity and

direct relationship with the rainfall statistics, they generally only vary the amount of rainfall in each timestep and do not account for occurrences when the rainfall estimation fails to predict rainfall, or predicts rainfall when there was none. The TAMSIM method is able to do this, as has been demonstrated in the section above.

To demonstrate how a perturbation method will characterise rainfall uncertainty differently from a full spatio-temporal distribution approach, the TAMSAT1 daily rainfall values were randomly perturbed to produce a set of 200 ensemble representations of rainfall. Although different ranges of values were tested, a perturbation of up to 50% of the daily rainfall value produced an uncertainty range of a similar magnitude to TAMSIM.

The hydrographs shown in Figures 8.22 to 8.31 compare the 95% confidence discharge envelopes using the EnsAll parameterisation, when driven by the TAMSIM ensemble SRFE inputs, and an ensemble input based on perturbing the TAMSAT1 estimate by a randomly selected value from a uniform distribution equal to 50% of the rainfall estimate (plus and minus).

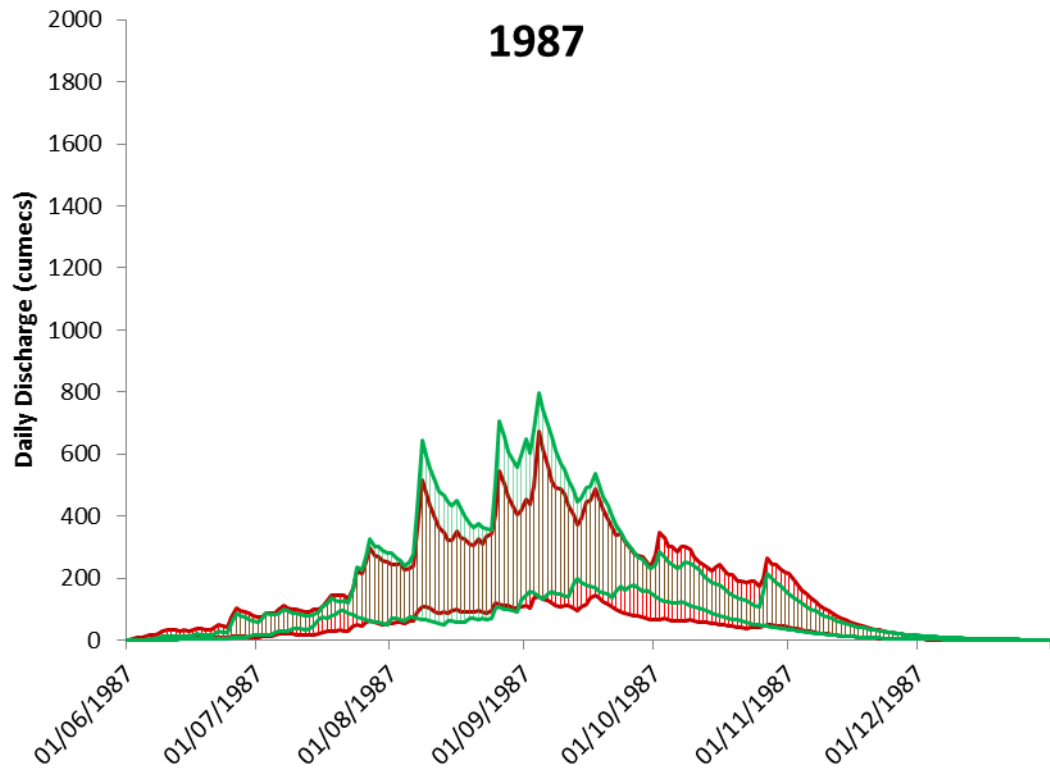


Figure 8.22 – Hydrograph showing the 95% confidence discharge envelopes modelled by the Pitman model for the Bakoye catchment in 1987, driven by TAMSIM ensemble SRFE (shown in red) and an ensemble of up to 50% perturbed TAMSAT1 estimates (shown in green).

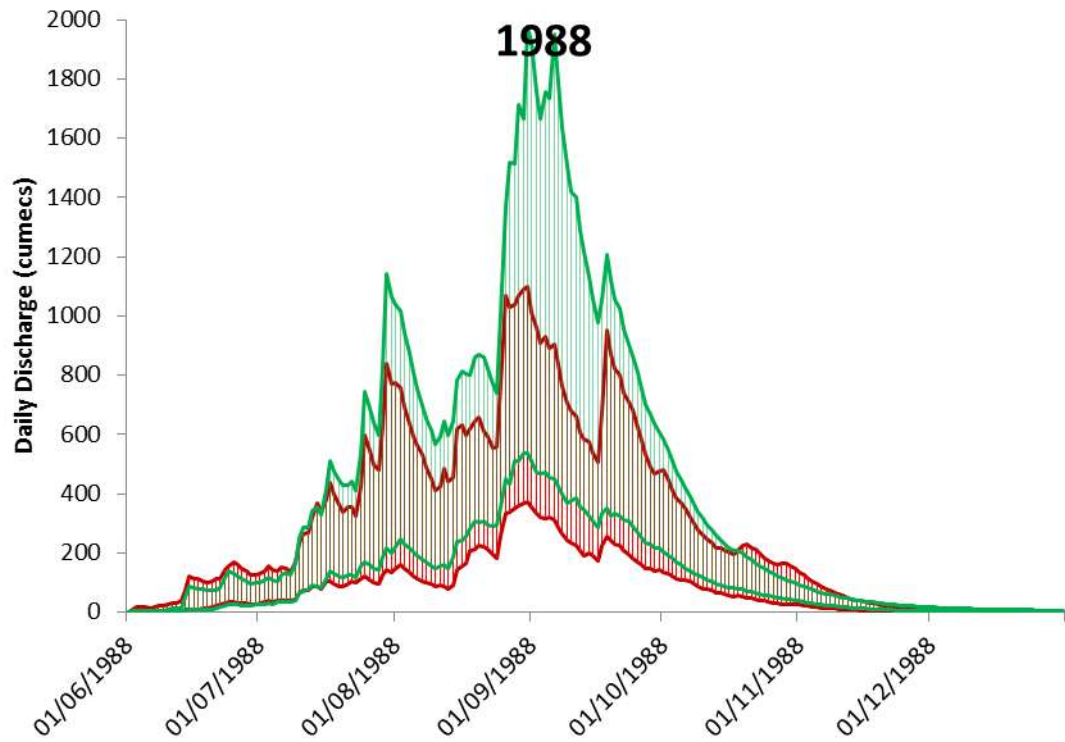


Figure 8.23 – Hydrograph showing the 95% confidence discharge envelopes modelled by the Pitman model for the Bakoye catchment in 1988, driven by TAMSIM ensemble SRFE (shown in red) and an ensemble of up to 50% perturbed TAMSAT1 estimates (shown in green).

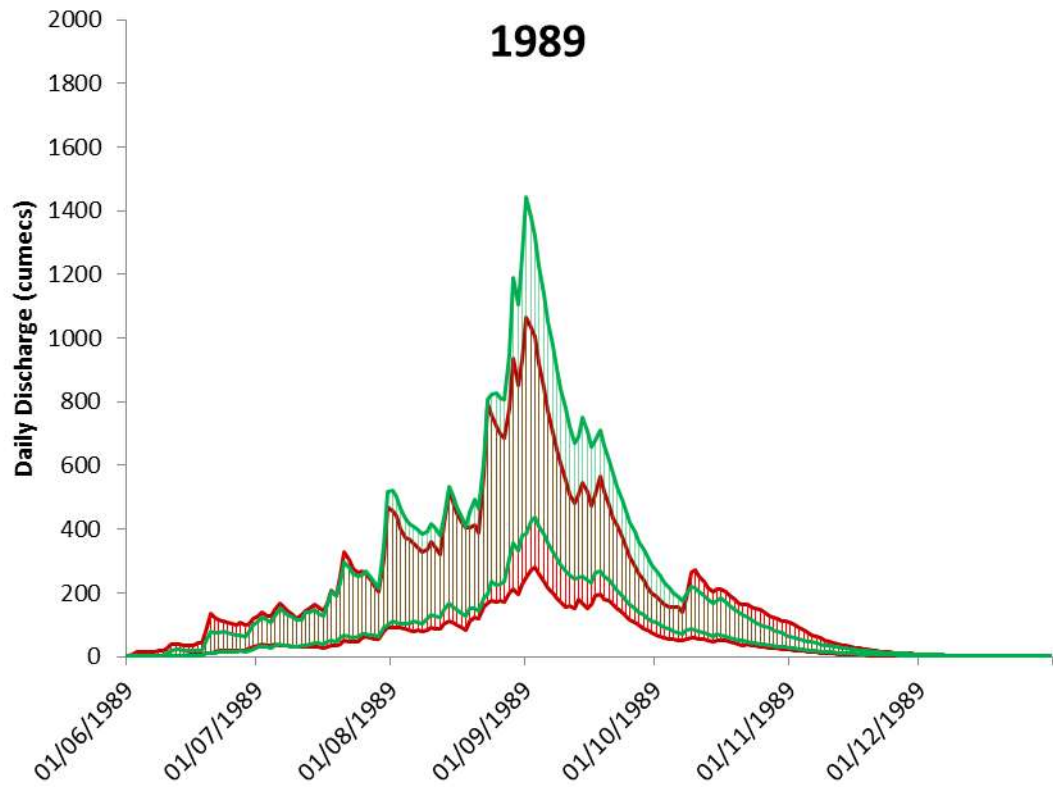


Figure 8.24 – Hydrograph showing the 95% confidence discharge envelopes modelled by the Pitman model for the Bakoye catchment in 1989, driven by TAMSIM ensemble SRFE (shown in red) and an ensemble of up to 50% perturbed TAMSAT1 estimates (shown in green).

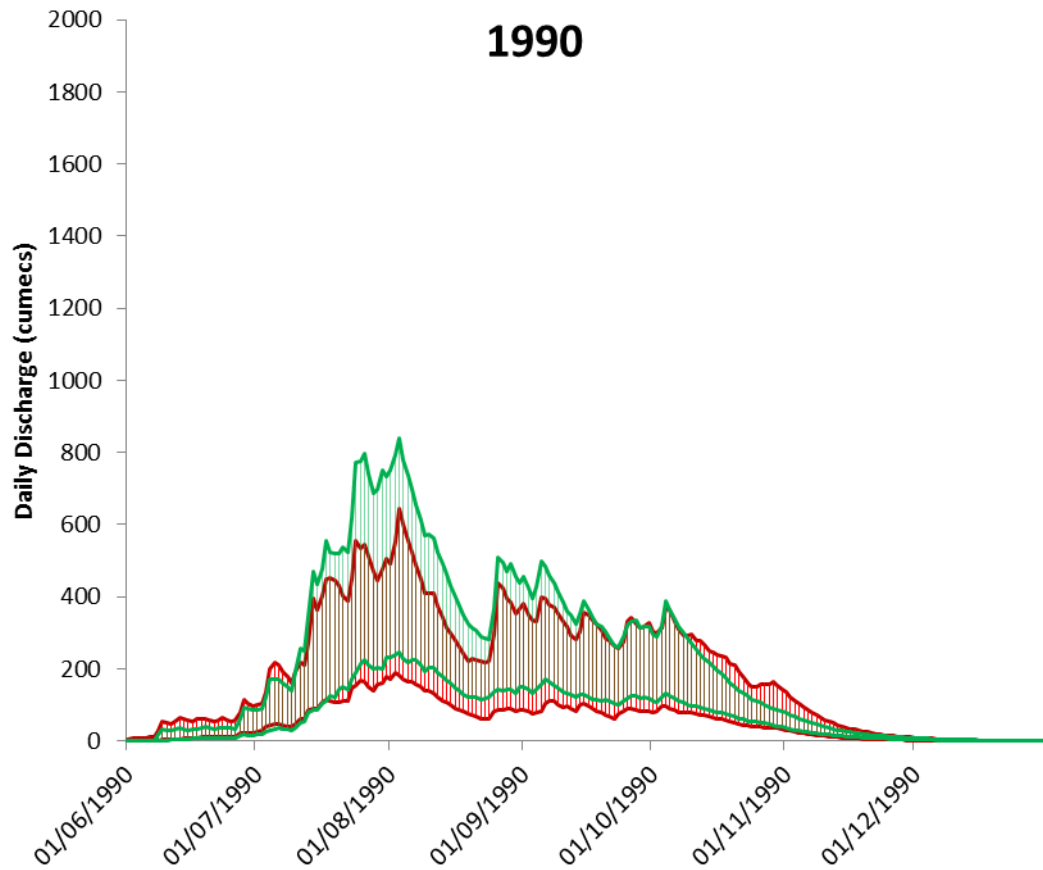


Figure 8.25 – Hydrograph showing the 95% confidence discharge envelopes modelled by the Pitman model for the Bakoye catchment in 1990, driven by TAMSIM ensemble SRFE (shown in red) and an ensemble of up to 50% perturbed TAMSAT1 estimates (shown in green).

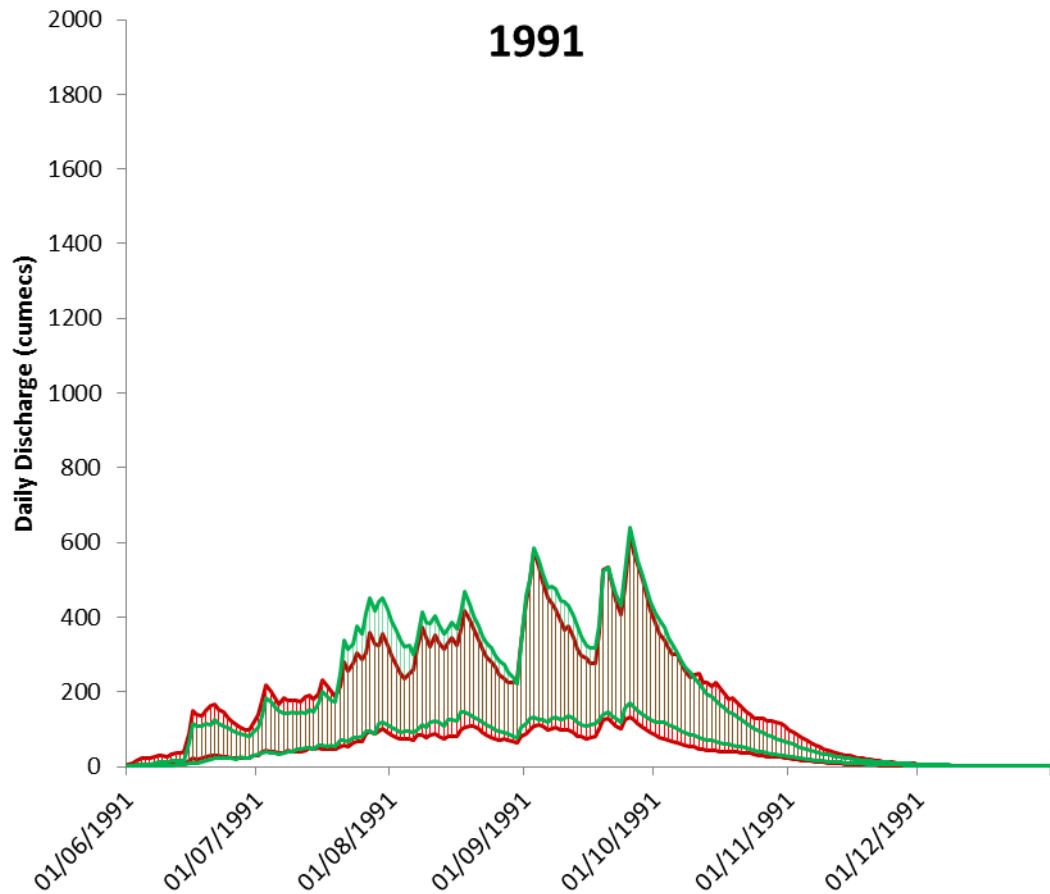


Figure 8.26 – Hydrograph showing the 95% confidence discharge envelopes modelled by the Pitman model for the Bakoye catchment in 1991, driven by TAMSIM ensemble SRFE (shown in red) and an ensemble of up to 50% perturbed TAMSAT1 estimates (shown in green).

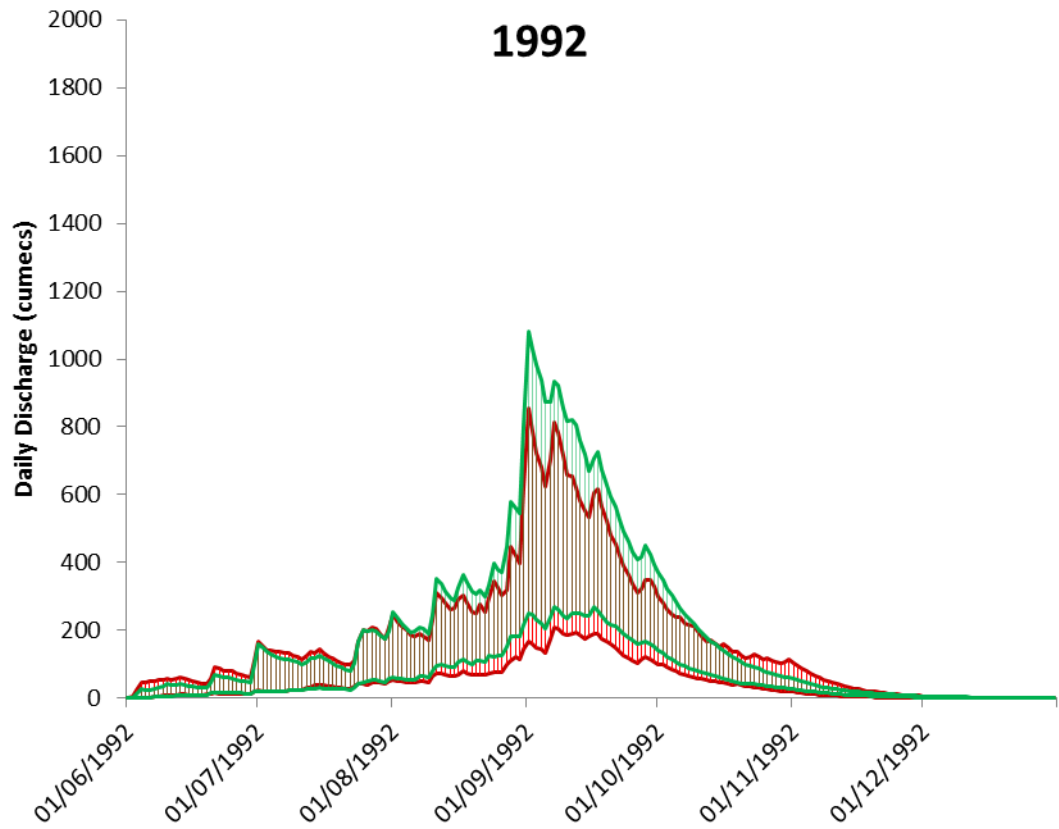


Figure 8.27 – Hydrograph showing the 95% confidence discharge envelopes modelled by the Pitman model for the Bakoye catchment in 1992, driven by TAMSIM ensemble SRFE (shown in red) and an ensemble of up to 50% perturbed TAMSAT1 estimates (shown in green).

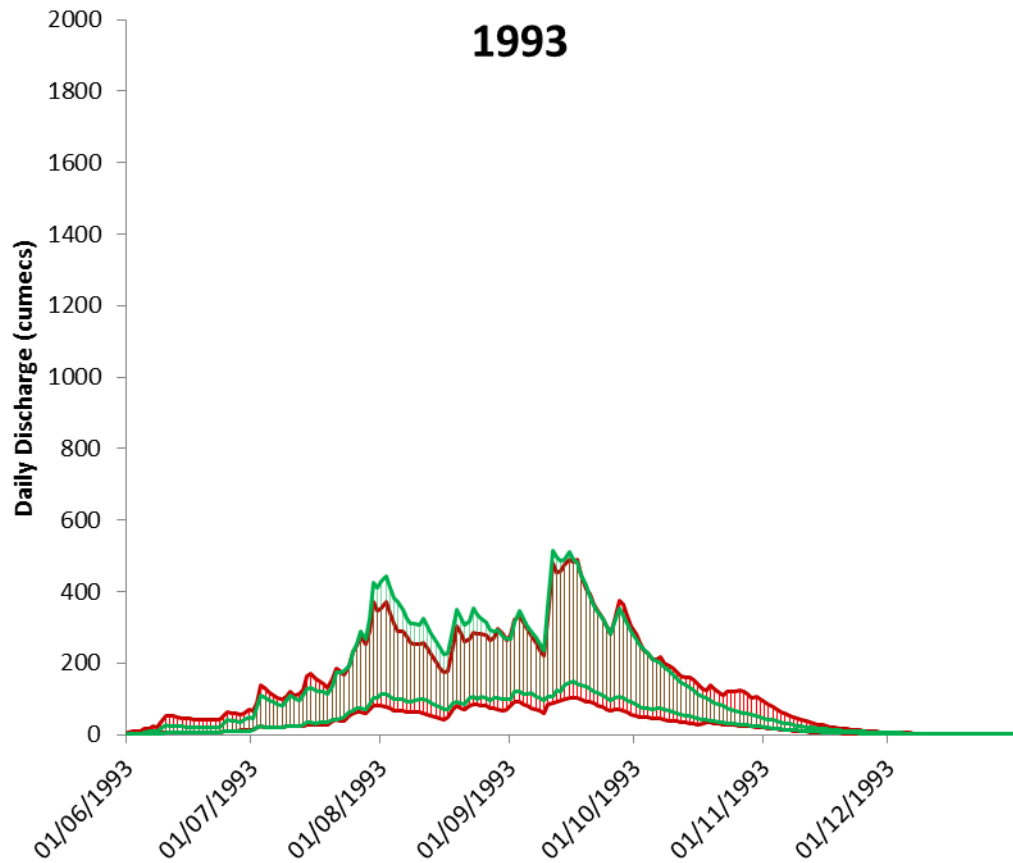


Figure 8.28 – Hydrograph showing the 95% confidence discharge envelopes modelled by the Pitman model for the Bakoye catchment in 1993, driven by TAMSIM ensemble SRFE (shown in red) and an ensemble of up to 50% perturbed TAMSAT1 estimates (shown in green).

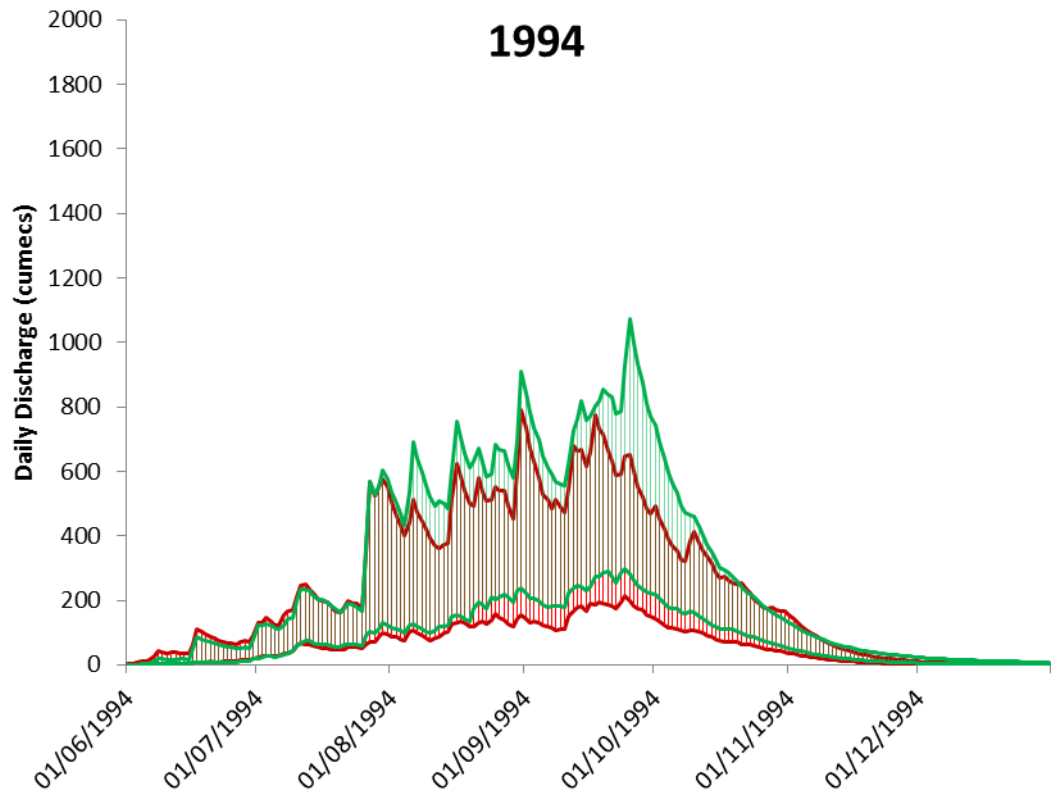


Figure 8.29 – Hydrograph showing the 95% confidence discharge envelopes modelled by the Pitman model for the Bakoye catchment in 1994, driven by TAMSIM ensemble SRFE (shown in red) and an ensemble of up to 50% perturbed TAMSAT1 estimates (shown in green).

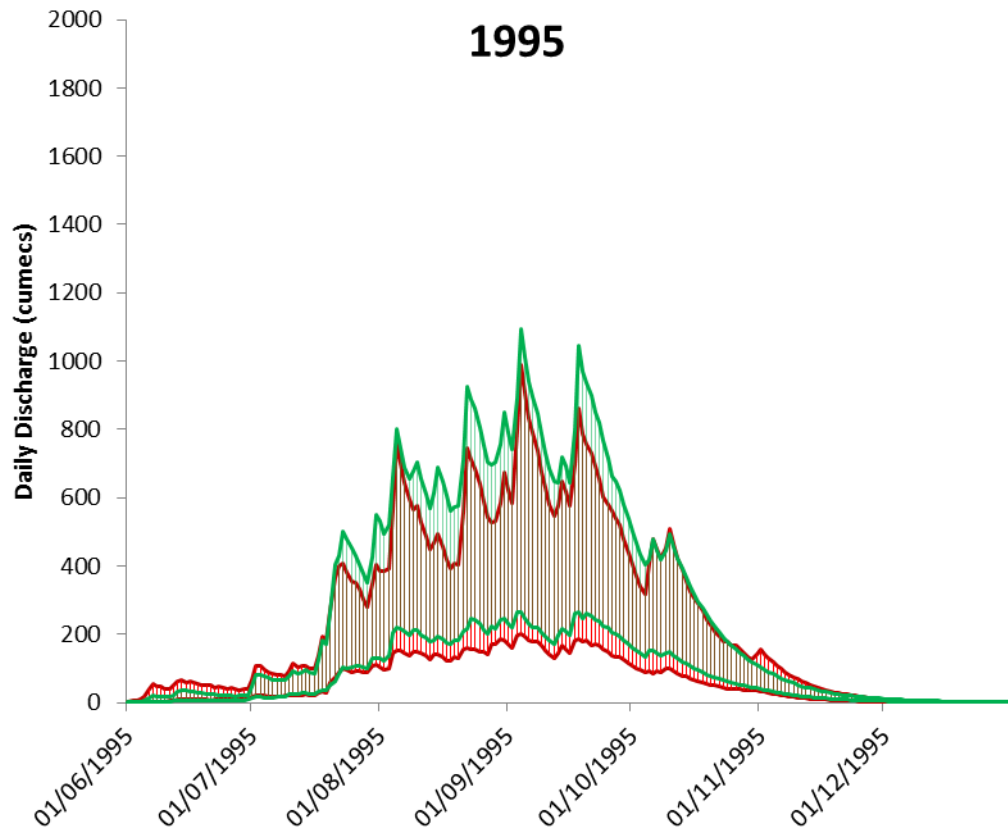


Figure 8.30 – Hydrograph showing the 95% confidence discharge envelopes modelled by the Pitman model for the Bakoye catchment in 1995, driven by TAMSIM ensemble SRFE (shown in red) and an ensemble of up to 50% perturbed TAMSAT1 estimates (shown in green).

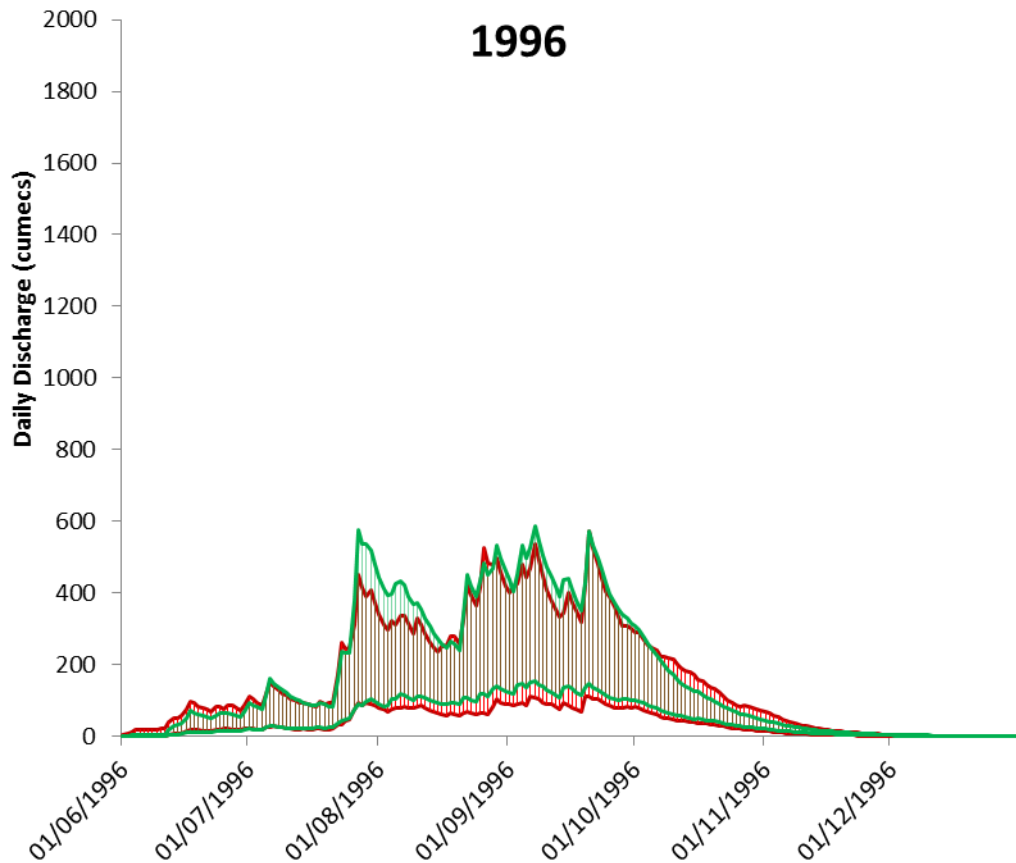


Figure 8.31 – Hydrograph showing the 95% confidence discharge envelopes modelled by the Pitman model for the Bakoye catchment in 1996, driven by TAMSIM ensemble SRFE (shown in red) and an ensemble of up to 50% perturbed TAMSAT1 estimates (shown in green).

Although the perturbation method adopted for this test was a non-sophisticated method and was not based on any measured statistics of uncertainty, the hydrographs in Figures 8.22 to 8.31 do demonstrate the predicted principle that a perturbation method is not fully characterising the uncertainty within the TAMSAT1 rainfall estimate.

By comparing the two envelopes in each hydrograph, TAMSIM shows that the uncertainty bounds within the TAMSAT1 SRFE are not symmetrical. This is an

assumption of the 50% perturbation method, which displays an envelope that often exceeds the maximum values predicted by TAMSIM, yet does not predict the lowest flows, especially for the months of August and September.

Section 8.2 demonstrated how TAMSIM was able to account for the temporal non-stationarity of the relationship between CCD and rainfall, which was particularly evident in the 95% confidence discharge envelopes after October of each year. The perturbation method is dependent on the TAMSAT1 deterministic estimate, so makes the assumption that as the rainfall rate decreases, so does the uncertainty – which is propagated into the discharge output uncertainty. This is not the reality, as it has been seen that estimates become relatively more uncertain and unreliable for lower discharges. TAMSIM produces ensemble estimates that are independent of the TAMSAT1 deterministic estimate, and for the period after October for each year the uncertainty envelopes are wider, and from Figures 8.3 to 8.13 there were even some signs that the envelope and the deterministic estimate were becoming decoupled.

8.5 – Conclusions

The Pitman model was calibrated using several estimates of rainfall and each parameterisation was tested for use with the TAMSIM ensemble estimates. The EnsTAM1 and EnsMean parameterisations showed particularly poor transferability with use with ensemble inputs, but a calibration that incorporated each ensemble member in turn, EnsAll, showed the best performance of all the

parameterisations, with little bias evident over the entire 11 year period when driven by the TAMSIM estimates. The EnsAll parameterisation was used to model the ensemble discharge output from the Pitman model, and the output used to produce the 95% confidence discharge envelopes for each year of the record.

The influence of the input uncertainty on the Pitman model can be seen to be great, with wide 95% confidence discharge envelopes visible in the hydrographs of Figures 8.3 to 8.13, and 40.3% of days in the wet season seeing the recorded discharge falling outside of these uncertainty bounds, and even with consideration of up to 25% of observation error in the discharge data this was only reduced to 28.8% - although the impact of this error propagating into model parameter has not been considered and could be significant. This is not unexpected as the data available for the calibration of TAMSAT1 was extremely limited, and therefore the SRFE produced contained wide uncertainties, for all three forms – spatial, temporal and rate. The cause of the mismatch between the 95% confidence discharge envelopes and the recorded discharge is likely to be bias resulting from anomalous years of rainfall, which, as a result of the large interannual variations of rainfall in the regions, is almost every year. From Figure 3.17 it can be seen that for the Bakoye catchment only three of the 11 years in the study displayed rainfall near the mean value for the period.

The bias within the TAMSIM SRFE is propagated directly to the Pitman model, although due to interactions with the automatic calibration approach, the EnsAll parameterised Pitman model favoured SRFE that display a positive bias. This

further erodes the performance of the Pitman model for years that display less rainfall than the mean for the period.

The results for 1987 also show that local variations of the rainfall, relative the catchment as a whole, have been lost. In 1987 the raingauges associated with the Bakoye catchment showed that the area displayed lower rainfall than the entire Senegal Basin, and this has been lost by assumptions of heterogeneity inherent in the process – resulting in the poor representation of the 1987 wet season discharges.

The TAMSIM algorithm has been shown to produce a more complete portrayal of the uncertainty than a basic perturbation method. As TAMSIM is able to account for all forms of uncertainty within the TAMSAT1 SRFE rather than just an adjustment of the rate of rainfall, it is able to fully account for the uncertainty caused by the non-stationary nature of the calibration, importantly in a way that was independent to the TAMSAT1 SRFE itself. This becomes most evident for the late wet season period from October each year, where the envelope produced by the perturbation method narrows significantly when compared to the TAMSIM modelled envelope. In addition the TAMSIM envelope shows signs of independence from the TAMSAT1 deterministic estimate, which the perturbation method does not as its envelope is symmetrical around TAMSAT1, and the magnitude of uncertainty is dependent on the rain rate.

It is anticipated that when the presented methodology is repeated for a catchment with greater data resources, where monthly climatic calibrations can

be calculated for TAMSAT1 and TAMSIM, the influence of the above effect will become less visible. The non-stationarity of the calibration will logically be less within a single month than over a highly variable 5 month wet season, however, it is still a cause of uncertainty and had this test been performed on such a catchment then this benefit of TAMSIM may have been missed.

It is suggested that when accounting for the influence of SRFE input uncertainty on downstream models that the use of perturbation methods are inadequate, and this has been demonstrated in this chapter. Only a fully spatially and temporally distributed method, that uses a full conditional distribution in respects to the input data, and not the deterministic estimate itself, to account for input uncertainty is appropriate. This thesis has only investigated the influence of the TAMSIM ensemble SRFE on a lumped CRR model, and there remains a pressing research need for an investigation into the influence of full SRFE uncertainty characterisation on distributed models – this is likely to be more complex than for a lumped model structure.

The EnsAll method of parameterisation has been introduced in this chapter and was shown to outperform all the alternative methods for calibrating the Pitman model for use with ensemble inputs. However, the method still requires validation against an independent dataset – this can be done using the 1997-2005 discharge data from the Oualia gauging station, using TAMSIM SRFE produced for the period using the 1986-1996 calibrations. This would be the next logical step for expanding this research.

9

The Influence of Ensemble Rainfall Input on the Calibration of the Pitman Model

9.1 – Introduction

The previous chapter demonstrated how the uncertainty associated with the TAMSAT1 SRFE propagated through the Pitman lumped CRR model, using ensemble input and output datasets, and plotting 95% discharge confidence envelopes, using the EnsAll parameterisation which was shown to be the optimal calibration for use with the TAMSIM ensemble estimates. This chapter further investigates the influence of the uncertainty on the calibration of the Pitman model, with a particular focus on the model behaviour and the relationship between model performance, behaviour and the parameters selected.

Section 9.2 observes the model behaviour under different calibrations and different rainfall inputs. Section 9.3 takes a closer look at the EnsInd parameter sets, observing the relationships between the parameter values selected and the model behaviour and performance. Section 9.4 concludes the chapter.

9.2 – Pitman Model Behaviours

This section looks at the various calibrations of the Pitman model, observing their relative performance, and how the different inputs impact on the performance and behaviour of the model. It will compare the performance of the Pitman model using the four deterministic rainfall records, calibrated for the 1986-1996 study period.

	RMSE as % of mean daily discharge			
	Gauge Average	DK	TAMSAT1	EnsMean
1987-1996	128.03	108.32	112.49	106.79

Table 9.1 – Table showing the 11 year calibration for the four rainfall inputs for the period 1987-1996.

The RMSE as % of mean daily discharges are shown in Table 9.1 for the period of 1987 to 1996. The recorded and modelled discharges for 1986 were included as part of the calibration but excluded from calculation of the errors, as the modelled discharges from 1986 will be influenced by the initial conditions of the Pitman model – although this was observed to be negligible in Chapter 8. The best performing Pitman model was driven and calibrated using the daily mean of the TAMSIM ensemble members, the EnsMean input, but the performance of the DK driven and calibrated Pitman model showed comparable performance. The TAMSAT1 driven and calibrated Pitman model outperformed the Gauge Average driven and calibrated Pitman model, suggested that the additional

information provided by the satellite data improves the hydrological modelling of the Bakoye catchment.

Annual	RMSE as % of mean daily discharge			
	Gauge Average	DK	TAMSAT1	EnsMean
1987	84.21	152.71	344.67	368.23
1988	92.98	67.34	61.85	61.28
1989	62.83	223.30	153.09	171.68
1990	186.44	87.11	149.13	162.29
1991	82.95	72.40	86.87	90.41
1992	87.61	75.96	100.68	120.27
1993	207.43	103.02	118.02	122.18
1994	112.29	102.10	94.98	87.95
1995	111.96	80.16	80.51	72.76
1996	83.76	72.59	89.51	80.64
Mean	111.06	103.67	127.93	133.77

Table 9.2 – Table showing the RMSE as % of mean daily discharge for each rainfall record, separated into annual sections.

	RMSE as % of mean daily discharge			
	Gauge			
Wet Season	Average	DK	TAMSAT1	EnsMean
1987	55.49	101.42	227.50	242.89
1988	61.80	44.30	40.58	40.29
1989	41.31	148.08	101.4862	113.82
1990	123.63	57.37	97.93	106.54
1991	58.76	48.48	58.26	60.64
1992	72.57	50.50	67.07	80.14
1993	136.79	67.93	77.78	80.49
1994	76.46	69.52	64.48	59.71
1995	75.54	54.08	54.39	49.13
1996	56.47	48.92	60.28	54.29
Mean	73.95	69.06	84.98	88.79

Table 9.3 – Table showing RMSE as % of mean daily discharge for each rainfall record, separated into wet season sections.

Tables 9.2 and 9.3 show the error for each input when the discharge records are split into annual and wet season sections. The DK rainfall input shows the best performance at wet season scale, as well as annually. TAMSAT1 and EnsMean show comparable performance at both scales but are out-performed by Gauge Average estimate. The SRFE driven models, although showing superior skill over the entire period, actually show inferior performance compared to the Gauge Average estimate driven models when considered at annual, or wet season periods. It is likely this is because of the systematic biases in the SRFE caused by anomalous years of rainfall, meaning the SRFE perform well compared to a long term mean but do not have sufficient flexibility to account for shorter term variations.

Model Behaviour and Performance

Table 9.4 shows the proportion of modelled discharge originating from ground water from the Pitman model when calibrated and driven using different deterministic estimates, for 1986-1996.

	Proportion of Modelled Discharge originating from Ground Water			
	(%)			
	Gauge Average	DK	TAMSAT1	EnsMean
1986-1996	0.00	0.00	2.54	0.81

Table 9.4 – Proportions of modelled discharge originating from ground water as modelled by the Pitman model, calibrated for different rainfall inputs for the period 1986-1996.

For the period 1986-1996, when calibrated against deterministic estimates of rainfall, the Pitman model does not model a significant proportion of ground water flows, essentially operating as a single-bucket model (Table 9.4).

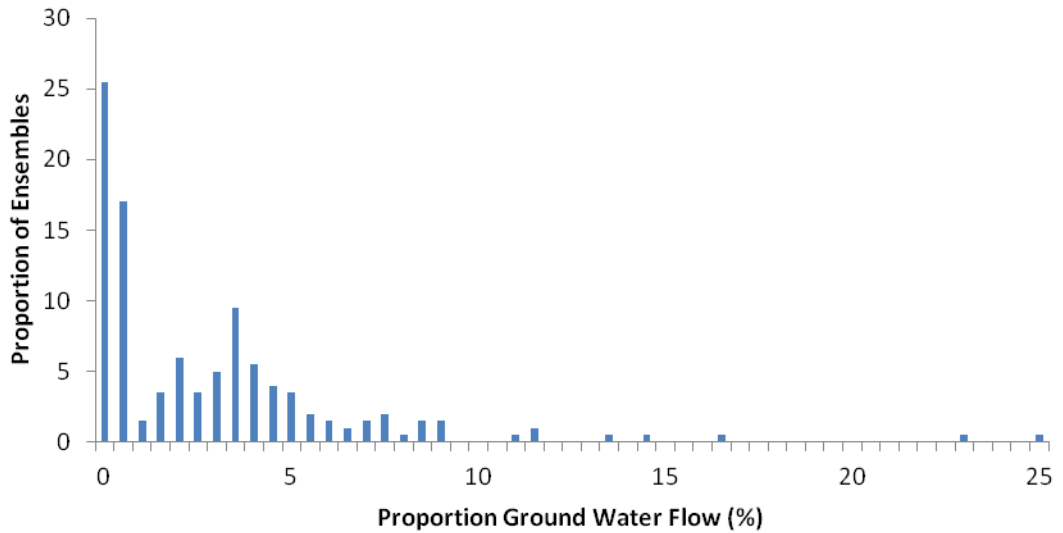


Figure 9.1 – Chart showing the proportion of Enslnd outputs against the proportion of modelled discharge originating from ground water displayed by each model.

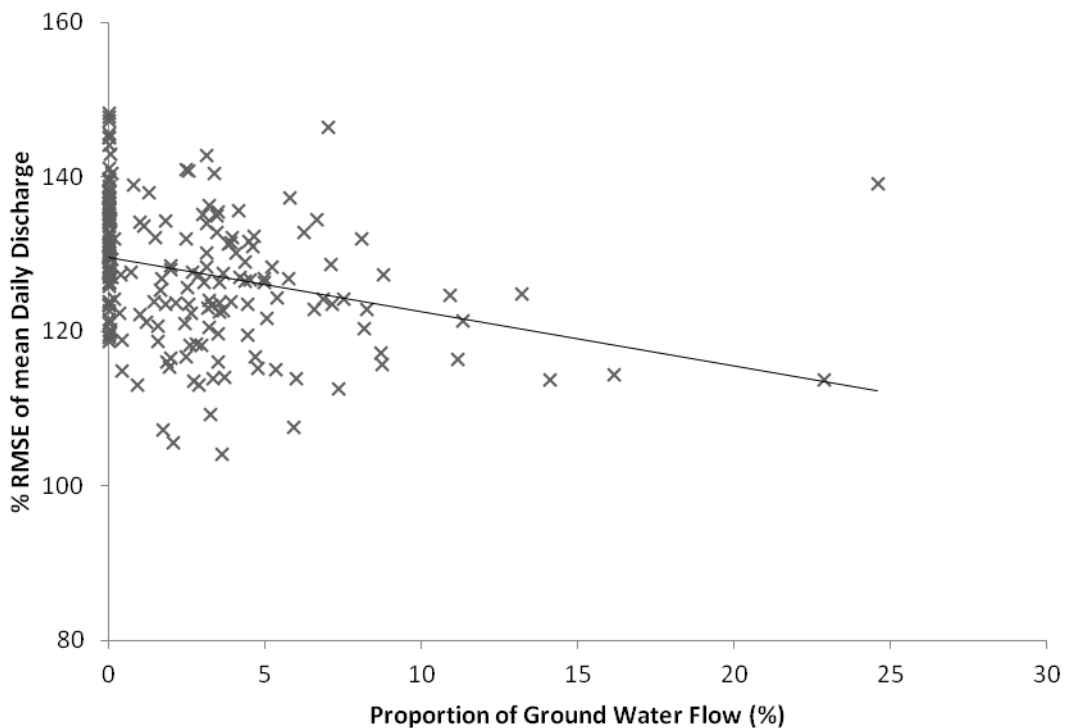


Figure 9.2 - Relationship between model performance as represented by RMSE as percentage of mean daily actual discharge, and model behaviour as represented by proportion of modelled discharge originating from ground water, for the Enslnd parameterisations.

Figure 9.1 shows the spread of model behaviours displayed by the EnsInd Pitman models, and Figure 9.2 shows the relationship between the model behaviour and model performance for the EnsInd Pitman models. Although a significant proportion of the models show zero ground water flow, or ground water flows as <0.5% of the overall discharge, there is a distribution amongst the remaining models, peaking at around 3.5% of the overall discharge.

There is a suggested relationship between model behaviour and performance, as shown in Figure 9.2, where models that allow for some ground water flow tend to display a better performance than those that allow for none, and that when expressed as a simple linear relationship model performance increases as the proportion of ground water increases.

When observing the model behaviour for the ensemble driven Pitman models under different calibration regimes, it is clear that ground water flows again only play a marginal role in determining the final modelled discharge. The EnsTAM1 outputs show a mean of 1.7% ground water flows from the TAMSIM ensemble estimates, and the EnsAll outputs result in <0.005% ground water flows for each ensemble. The EnsMean outputs, which were the most erratic and worst performing, showed ground water flows up to 5%, but over 75% were <2.5%.

9.3 – Variability of Parameter Values for an Ensemble Driven Pitman Model

This section investigates closely the individual parameter values for each calibration and how these relate to the model behaviour and performance, highlighting those parameters that are the most influential. The values for each adjustable parameter, as described in Chapter 6, are observed in turn, showing the distribution of calibrated values within the available parameter space.

The operation of the Pitman lumped CRR model has been described in Chapter 6, detailing each of the adjustable parameters and their purpose within the model. For convenience the basic functionality of each parameter will be described here also.

Z_{\min}

The Z_{\min} parameter is the minimum infiltration rate from the interception store to the soil moisture store.

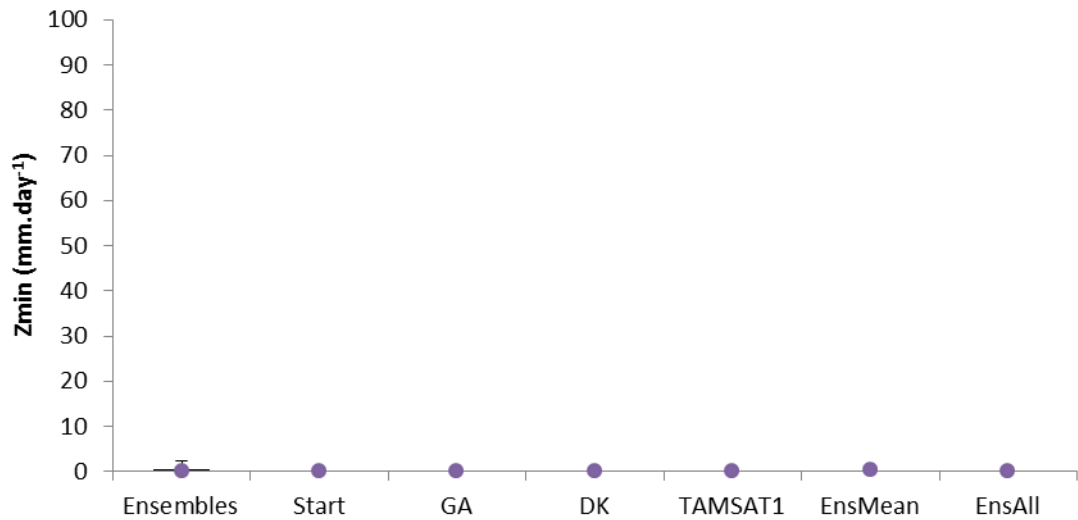


Figure 9.3 – Plot showing the box-whisker distribution of Z_{min} parameter values chosen by automatic calibration of the TAMSIM ensemble members within the available parameter space, for the Pitman lumped CRR model of the Bakoye Catchment between 1986 and 1996. The dot marks the mean value from the ensembles. Values selected by automatic calibration against the deterministic rainfall estimates are shown for comparison.

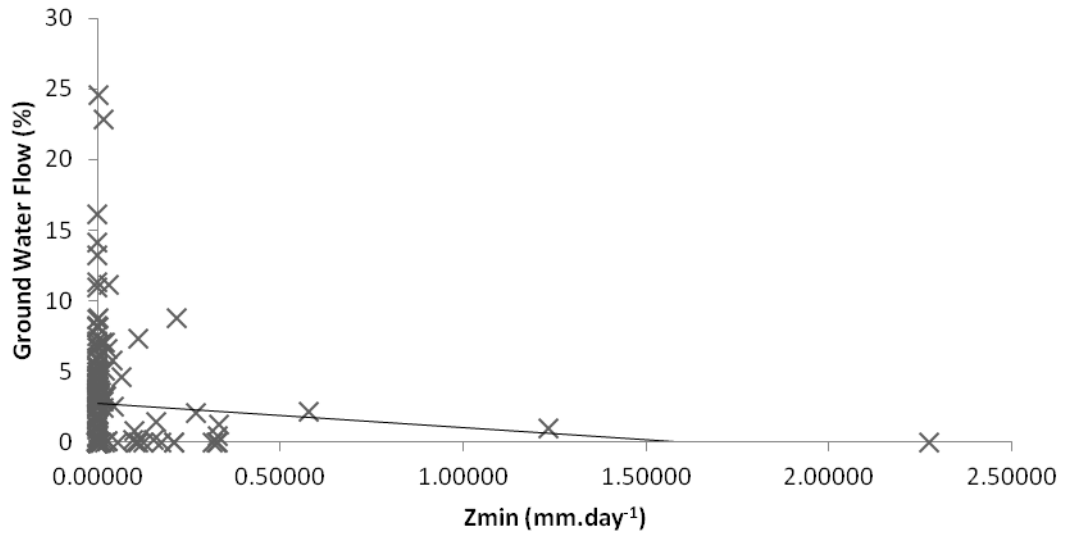


Figure 9.4 – Plot showing the relationship between the Z_{min} parameter values and the proportion of modelled discharge from ground water, for the Pitman lumped CRR model of the Bakoye Catchment for the period between 1986 and 1996, calibrated to individual TAMSIM ensemble members.

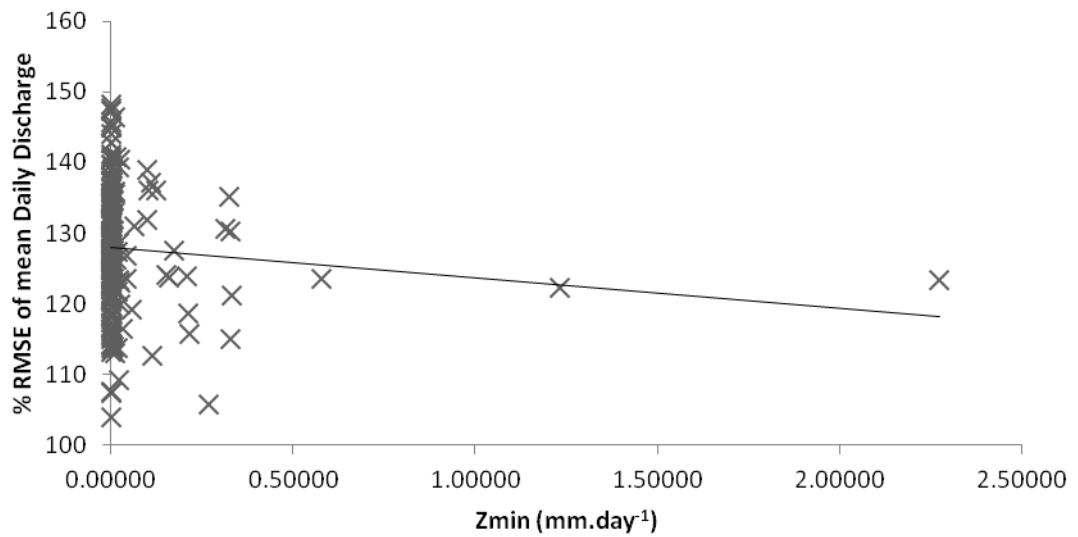


Figure 9.5 – Plot showing the relationship between the Z_{min} parameter values and model performance, for the Pitman lumped CRR model of the Bakoye Catchment for the period between 1986 and 1996, calibrated to individual TAMSIM ensemble members.

The variation of the Z_{\min} parameter between the EnsInd calibrations is minimal, with most values $<0.1\text{mm}\cdot\text{day}^{-1}$, which is also evident for the other calibrated values. The variation of Z_{\min} values does not appear to influence the proportion of modelled discharge from ground water, and does not appear to influence the model performance. As the values do not vary greatly, this suggests that Z_{\min} is an important parameter determining model performance.

Z_{\max}

The Z_{\max} parameter controls the maximum rate of infiltration from the interception store to the soil moisture store.

The Z_{\max} parameter varies between 10 and $30\text{mm}\cdot\text{day}^{-1}$ within the EnsInd outputs, and these values are similar to the other calibrated values. There appears to be a relationship between higher values of Z_{\max} and a greater proportion of modelled discharge originating from ground water, as seen in Figure 9.7 – this is likely because the soil moisture store is being filled quicker and more water is available to pass to the ground water store.

Figure 9.8 shows that the variation of the Z_{\max} parameter value does not appear to influence model performance, and the cluster of calibrations between 23 and $25\text{mm}\cdot\text{day}^{-1}$ suggest that Z_{\max} is influential to model performance.

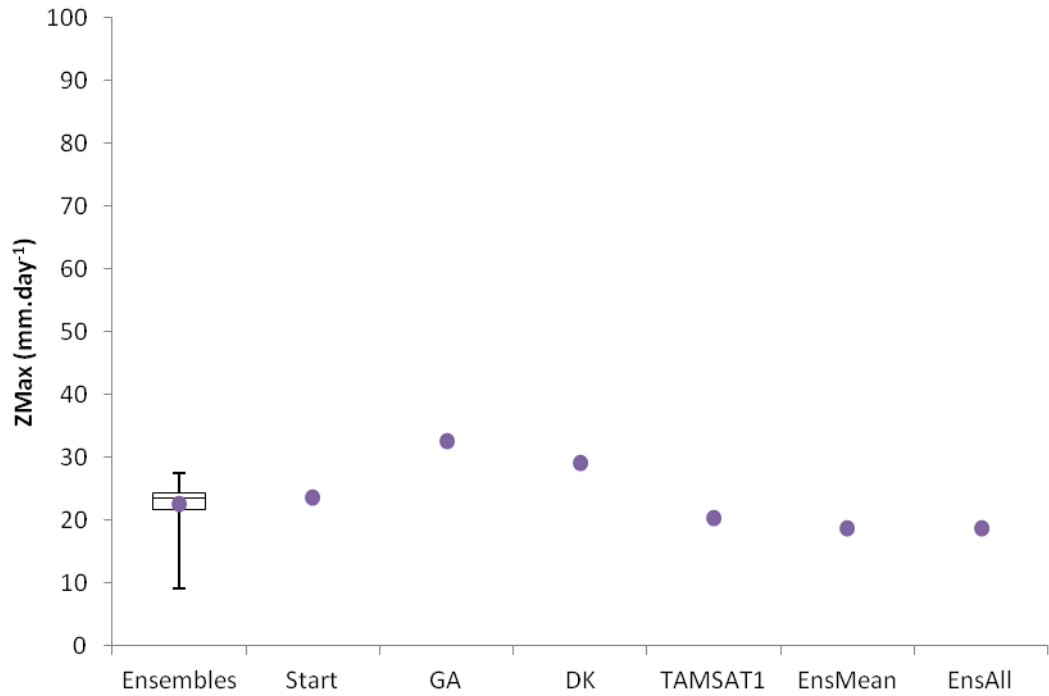


Figure 9.6 – Plot showing the box-whisker distribution of Z_{max} parameter values chosen by automatic calibration of the TAMSIM ensemble members within the available parameter space, for the Pitman lumped CRR model of the Bakoye Catchment between 1986 and 1996. The dot marks the mean value from the ensembles. Values selected by automatic calibration against the deterministic rainfall estimates are shown for comparison.

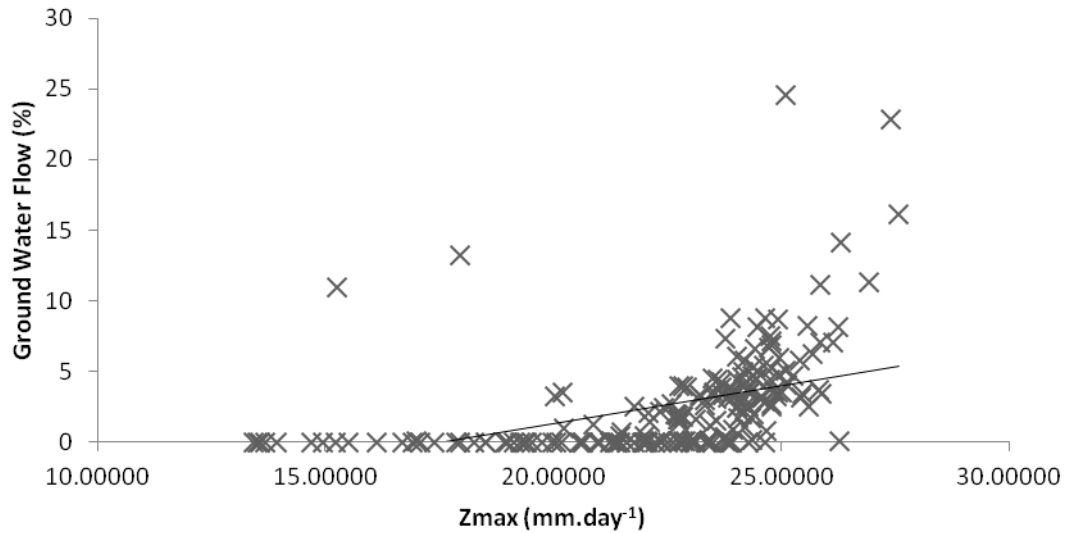


Figure 9.7 – Plot showing the relationship between the Z_{max} parameter values and the proportion of modelled discharge from ground water, for the Pitman lumped CRR model of the Bakoye Catchment for the period between 1986 and 1996, calibrated to individual TAMSIM ensemble members.

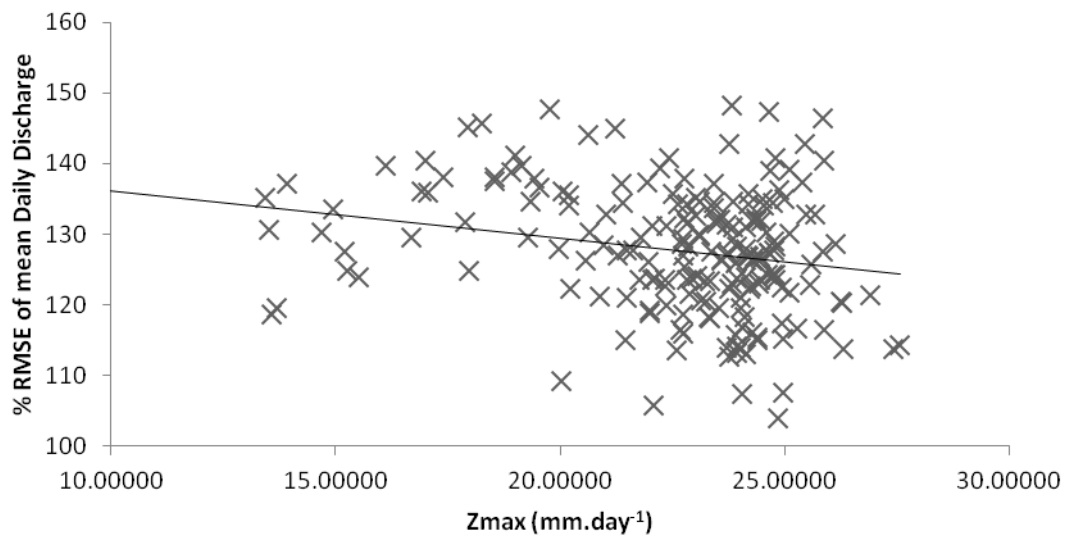


Figure 9.8 – Plot showing the relationship between the Z_{max} parameter values and model performance, for the Pitman lumped CRR model of the Bakoye Catchment for the period between 1986 and 1996, calibrated to individual TAMSIM ensemble members.

W_{max}

The W_{max} parameter controls the maximum storage capacity of the soil moisture store.

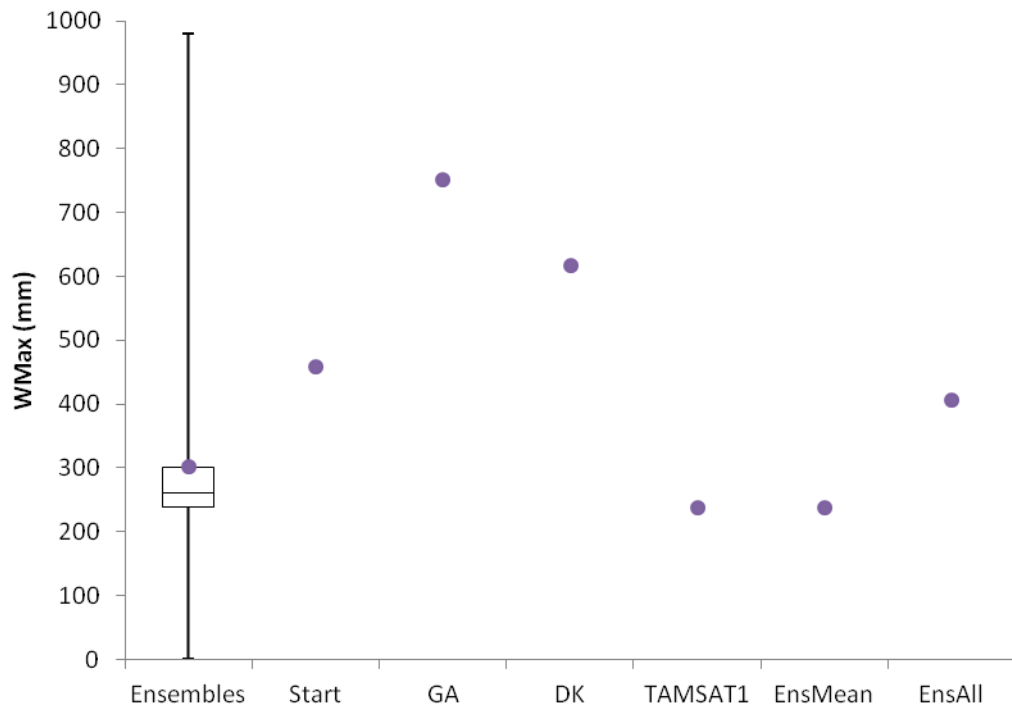


Figure 9.9 – Plot showing the box-whisker distribution of W_{max} parameter values chosen by automatic calibration of the TAMSIM ensemble members within the available parameter space, for the Pitman lumped CRR model of the Bakoye Catchment between 1986 and 1996. The dot marks the mean value from the ensembles. Values selected by automatic calibration against the deterministic rainfall estimates are shown for comparison.

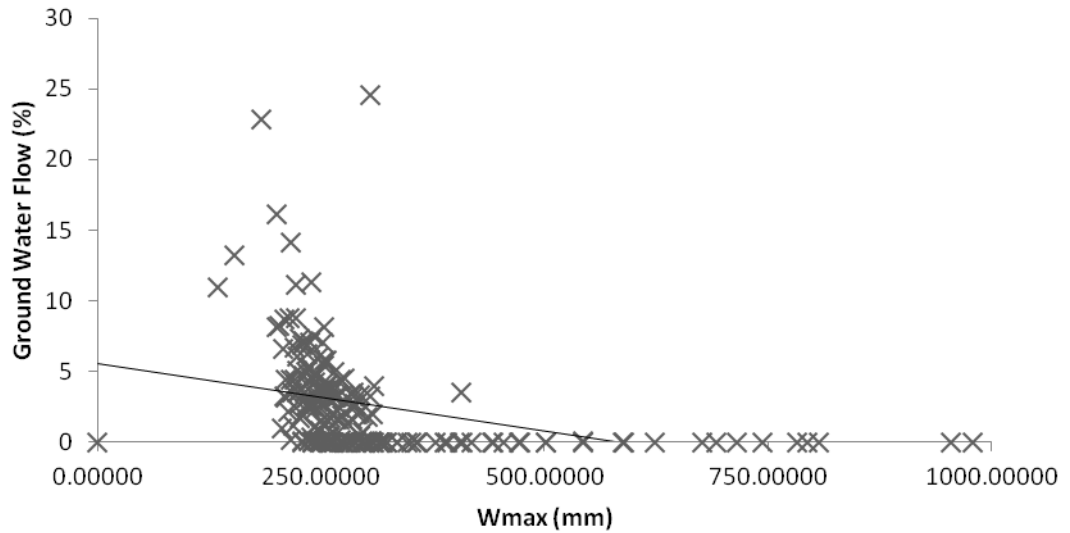


Figure 9.10 – Plot showing the relationship between the W_{max} parameter values and the proportion of modelled discharge from ground water, for the Pitman lumped CRR model of the Bakoye Catchment for the period between 1986 and 1996, calibrated to individual TAMSIM ensemble members.

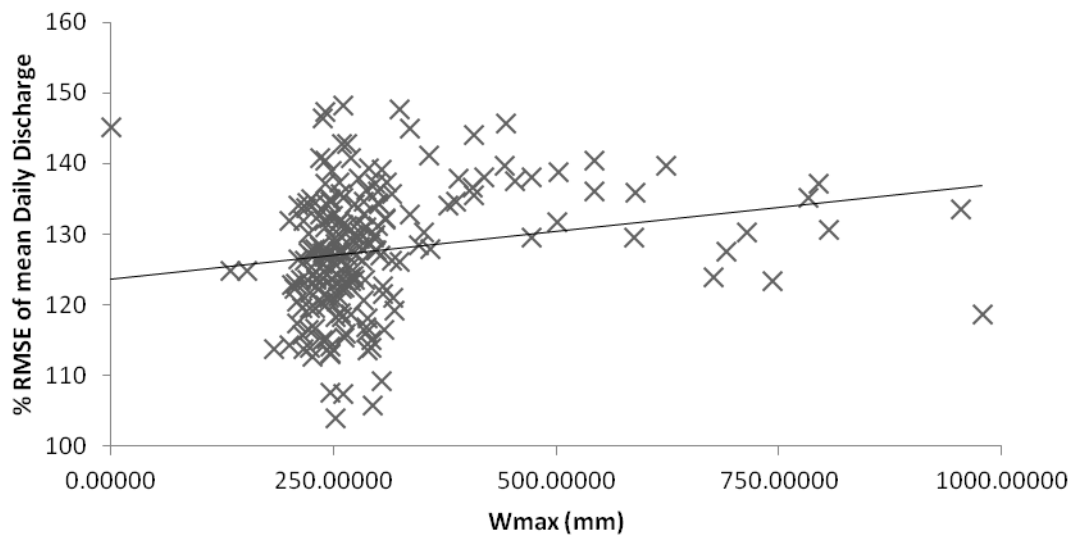


Figure 9.11 – Plot showing the relationship between the W_{max} parameter values and model performance, for the Pitman lumped CRR model of the Bakoye Catchment for the period between 1986 and 1996, calibrated to individual TAMSIM ensemble members.

The W_{\max} parameter shows some variation throughout the whole of the available parameter space, but a significant cluster of values between 200 and 300mm. Figure 9.10 shows that there is little relationship between the value of W_{\max} and the proportion of ground water in the modelled discharge. Figure 9.11 shows that there is variation in model performance within the cluster of values and that when the calibration has selected values beyond that, the model performance ability decreases. The clustering of values implies that W_{\max} is influential on the model performance.

W_{\min}

The W_{\min} parameter values controls the threshold that below which no water can percolate from the soil moisture store to the ground water store, and as such it would be reasonable to assume that the greater the W_{\min} value, the less ground water will contribute to the final modelled discharge.

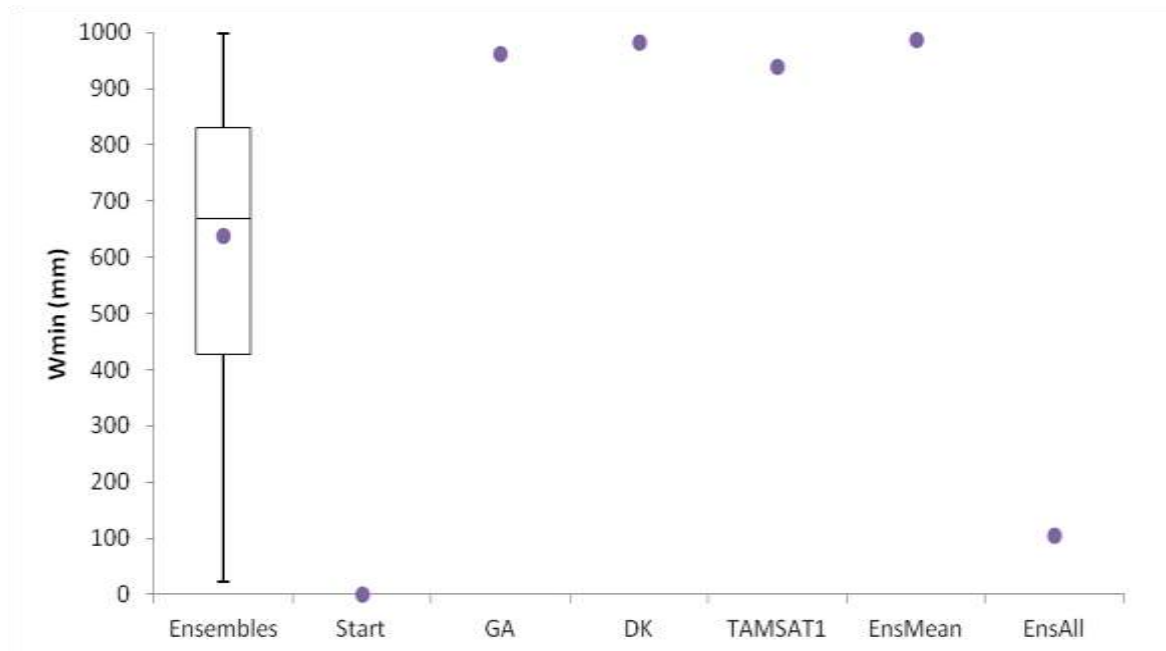


Figure 9.12 – Plot showing the box-whisker distribution of W_{\min} parameter values chosen by automatic calibration of the TAMSIM ensemble members within the available parameter space, for the Pitman lumped CRR model of the Bakoye Catchment between 1986 and 1996. The dot marks the mean value from the ensembles. Values selected by automatic calibration against the deterministic rainfall estimates are shown for comparison.

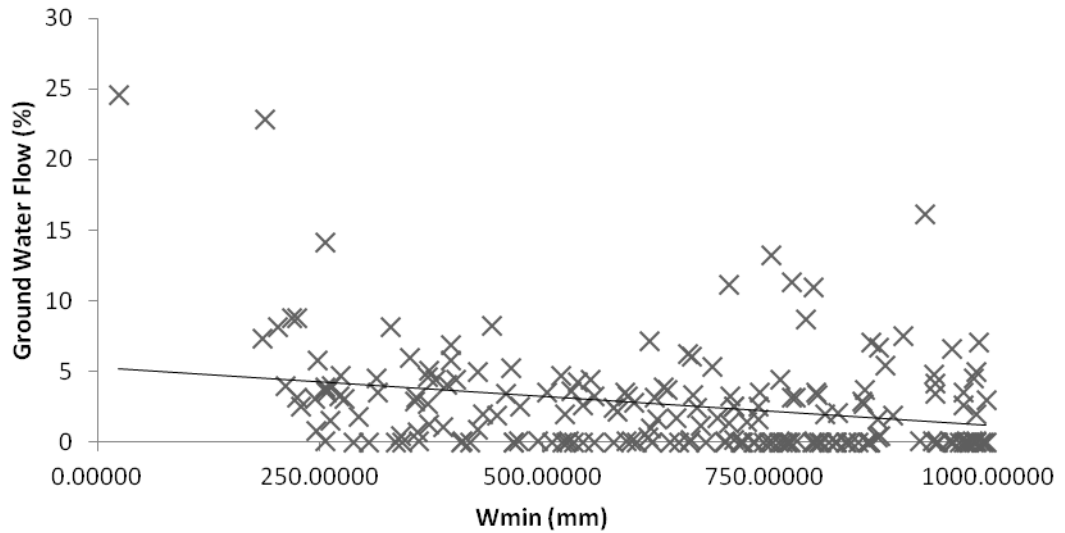


Figure 9.13 – Plot showing the relationship between the W_{min} parameter values and the proportion of modelled discharge from ground water, for the Pitman lumped CRR model of the Bakoye Catchment for the period between 1986 and 1996, calibrated to individual TAMSIM ensemble members.

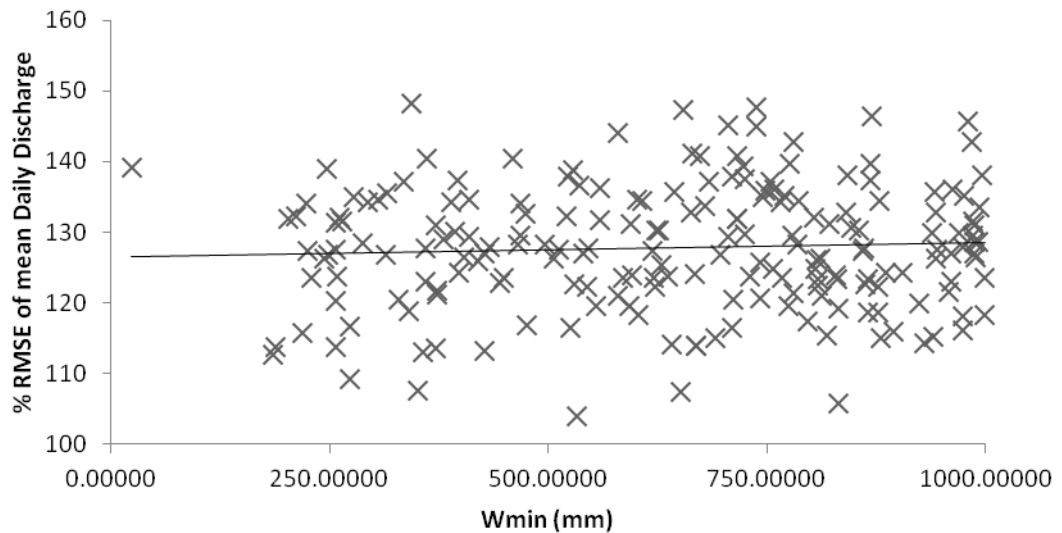


Figure 9.14 – Plot showing the relationship between the W_{min} parameter values and model performance, for the Pitman lumped CRR model of the Bakoye Catchment for the period between 1986 and 1996, calibrated to individual TAMSIM ensemble members.

There is a considerable amount of variation between the ensembles in regards to the calibrated W_{\min} values, with the majority of values between 400 and 800mm (Figure 9.12). The mean value from the ensembles is over 600mm, above the cluster of W_{\max} values, meaning the threshold for percolation is beyond the maximum capacity of the store therefore restricting the model's ability to model ground water.

Figure 9.13 shows that the expected relationship between the proportion of ground water flows and the value of W_{\min} does exist but is not very strong, likely because of the restrictions above. The variation of W_{\min} values does not have a relationship with model performance and as there is no significant clustering of values it is likely that the value of W_{\min} is not influential on the final modelled discharge.

I_{\max}

The I_{\max} parameter is the maximum capacity of the interception store and therefore restricts the potential evapotranspiration from the model.

The I_{\max} value shows almost no variation between the Enslnd calibrations and the values from other calibrations, with the model preferring to minimise the value as small as possible – the majority of values are <0.1mm (Figure 9.15). This restricts the amount of rainfall immediately lost by evapotranspiration.

The lack of variation means that there is little relationship between the varying values and model behaviour and performance, but does suggest that I_{\max} is influential to the model performance.

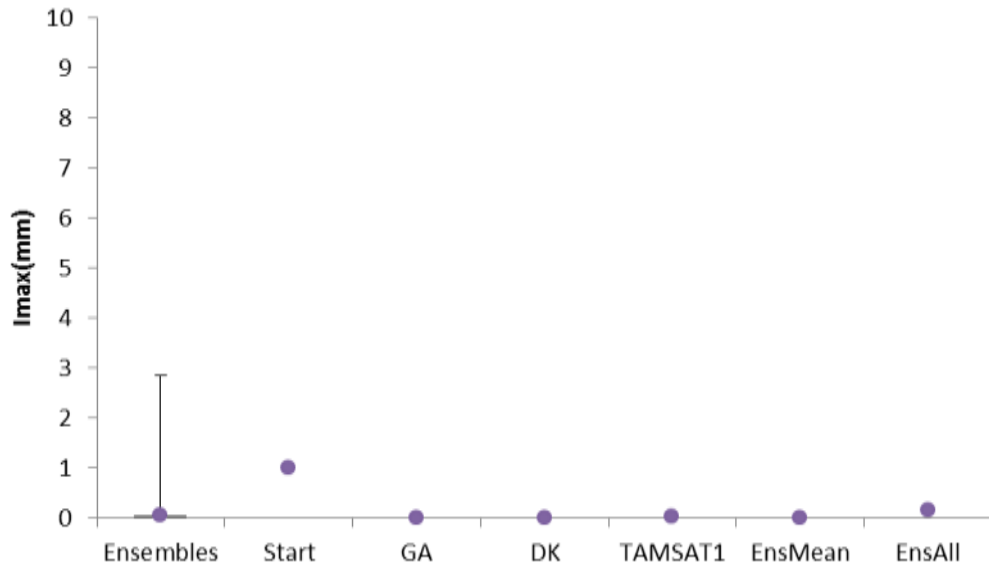
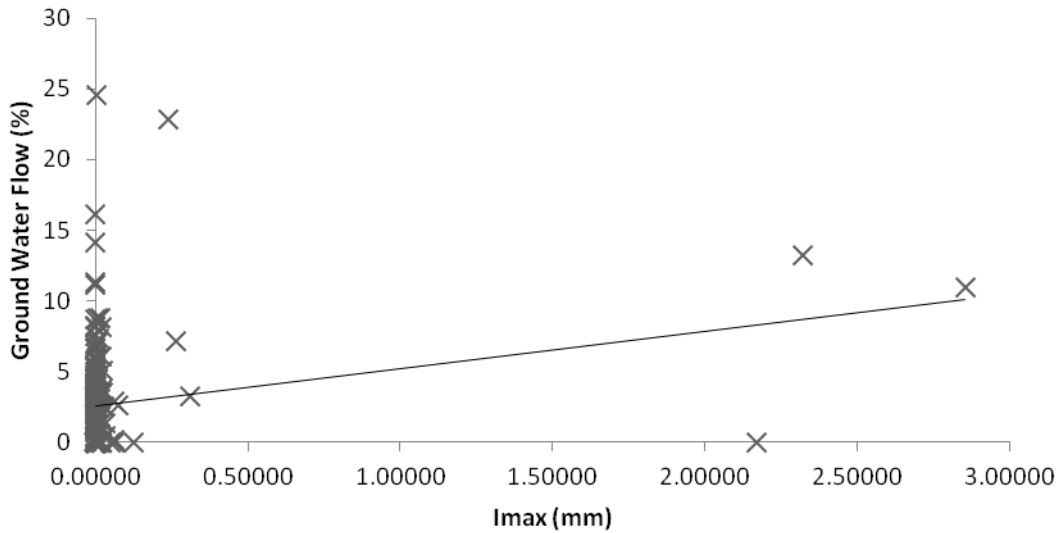


Figure 9.15 – Plot showing the box-whisker distribution of I_{\max} parameter values chosen by automatic calibration of the TAMSIM ensemble members within the available parameter space, for the Pitman lumped CRR model of the Bakoye Catchment between 1986 and 1996. The dot marks the mean value from the ensembles. Values selected by automatic calibration against the deterministic rainfall estimates are shown for comparison.



h

The h parameter is a constant that is used to calculate the percolation rate between the soil moisture store and the groundwater store. It is reasonable to assume that the greater the value of h , the greater the proportion of ground water flows, but this is restricted by values of other parameters (such as W_{min}).

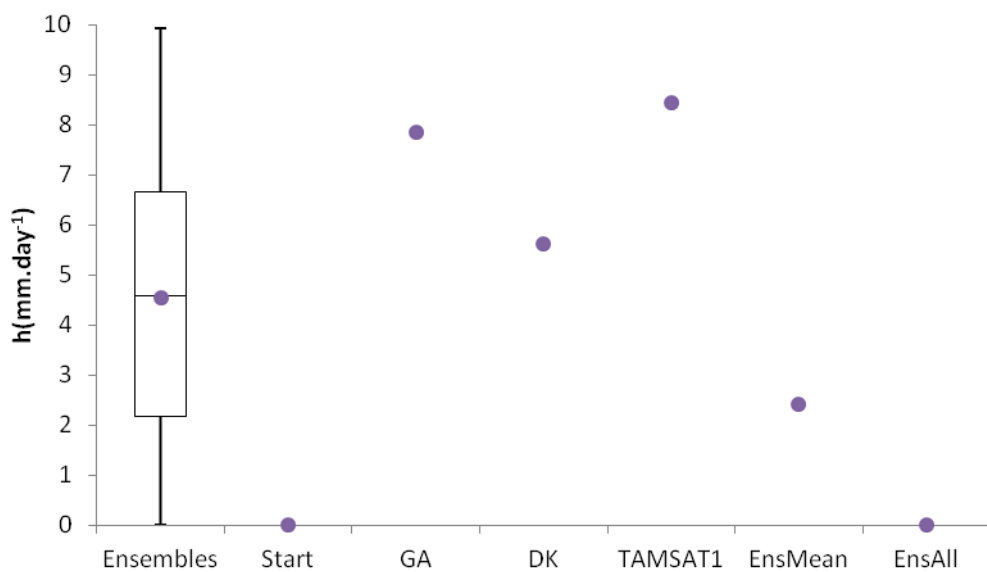


Figure 9.18 – Plot showing the box-whisker distribution of h parameter values chosen by automatic calibration of the TAMSIM ensemble members within the available parameter space, for the Pitman lumped CRR model of the Bakoye Catchment between 1986 and 1996. The dot marks the mean value from the ensembles. Values selected by automatic calibration against the deterministic rainfall estimates are shown for comparison.

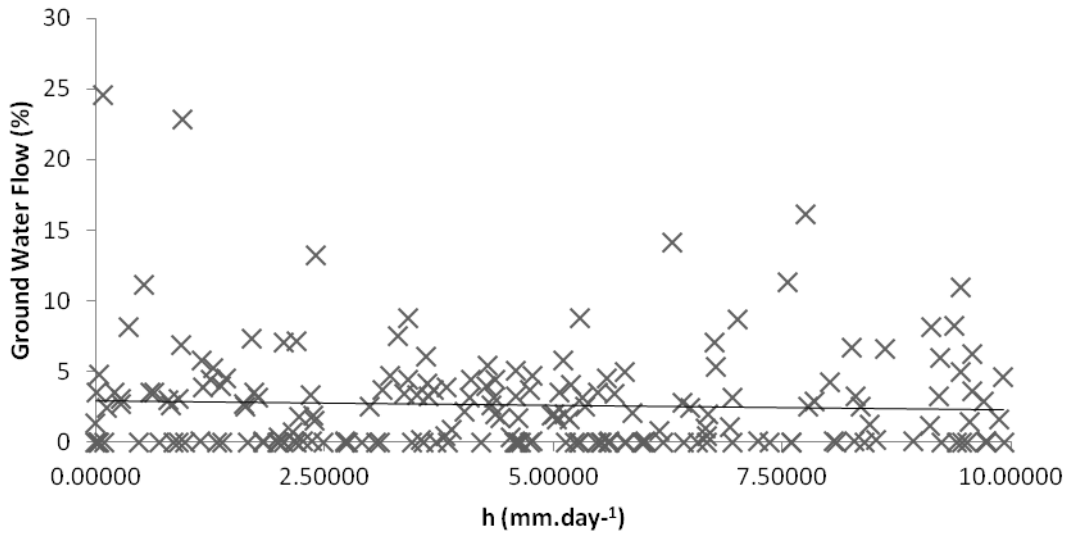


Figure 9.19 – Plot showing the relationship between the h parameter values and the proportion of modelled discharge from ground water, for the Pitman lumped CRR model of the Bakoye Catchment for the period between 1986 and 1996, calibrated to individual TAMSIM ensemble members.

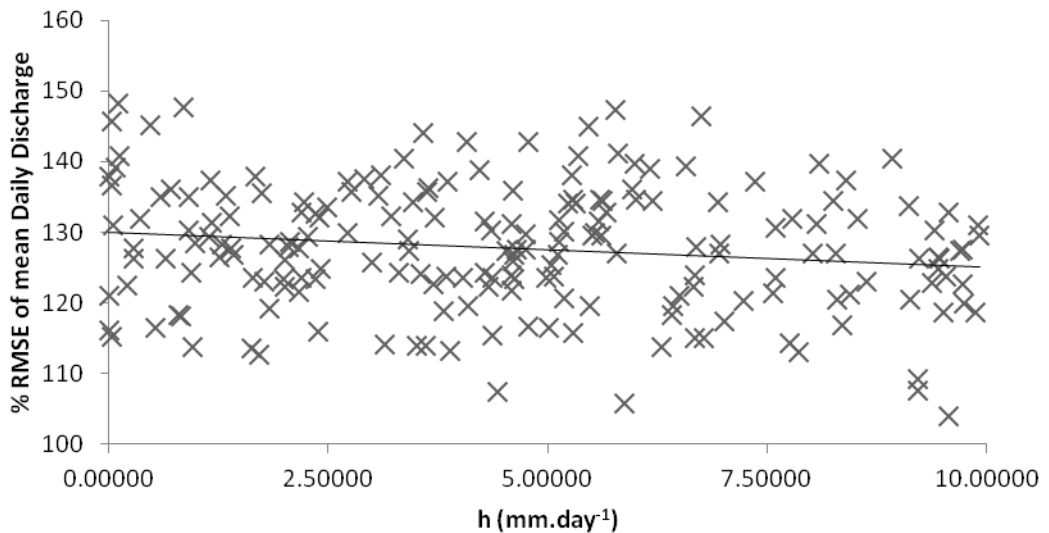


Figure 9.20 – Plot showing the relationship between the h parameter values and model performance, for the Pitman lumped CRR model of the Bakoye Catchment for the period between 1986 and 1996, calibrated to individual TAMSIM ensemble members.

The values for h are reasonably equally distributed throughout the parameter space available for the Enslnd calibrations, with a mean close to $5\text{mm}\cdot\text{day}^{-1}$, in the centre of the space (Figure 9.18). Surprisingly there is very little correlation between the value of h and the proportion of the modelled discharge originating from ground water (Figure 9.19), and a slight improvement of model performance as h increases can be seen in Figure 9.20, although with no significant clustering of values h is not influential on model performance, but this is likely because of the high values of W_{\min} observed.

i

The i parameter value is used in conjunction with the h value to calculate the percolation rate between the soil moisture store and the ground water store, and therefore should be similarly related to model behaviour and performance.

As expected, i displays a similar pattern to h in regards to spread of values and relationship between the values and model behaviour and performance, as seen in Figures 9.21 to 9.23. The influence of i is restricted by the high W_{\min} values that inhibit the periods where percolation can occur.

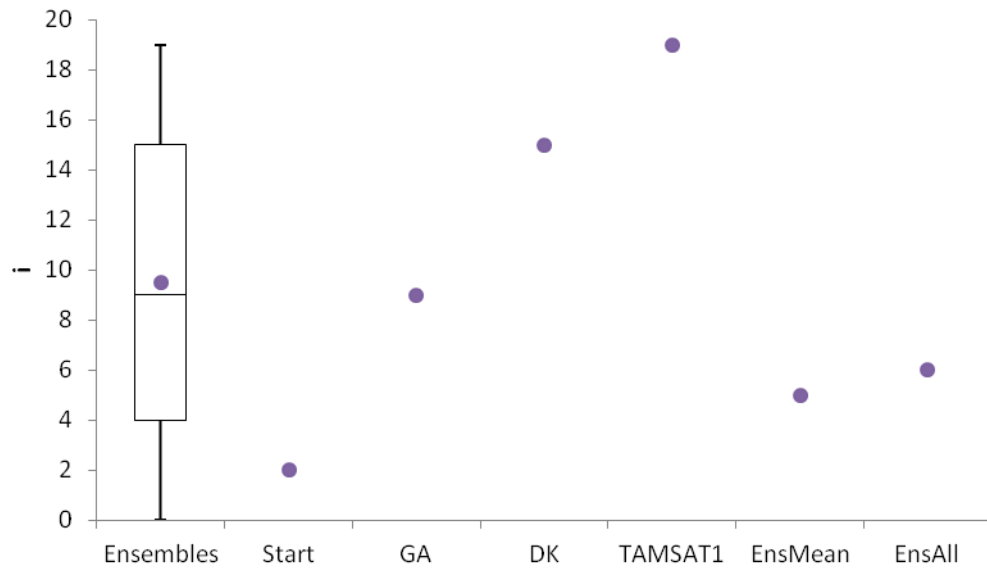


Figure 9.21 – Plot showing the box-whisker distribution of i parameter values chosen by automatic calibration of the TAMSIM ensemble members within the available parameter space, for the Pitman lumped CRR model of the Bakoye Catchment between 1986 and 1996. The dot marks the mean value from the ensembles. Values selected by automatic calibration against the deterministic rainfall estimates are shown for comparison.

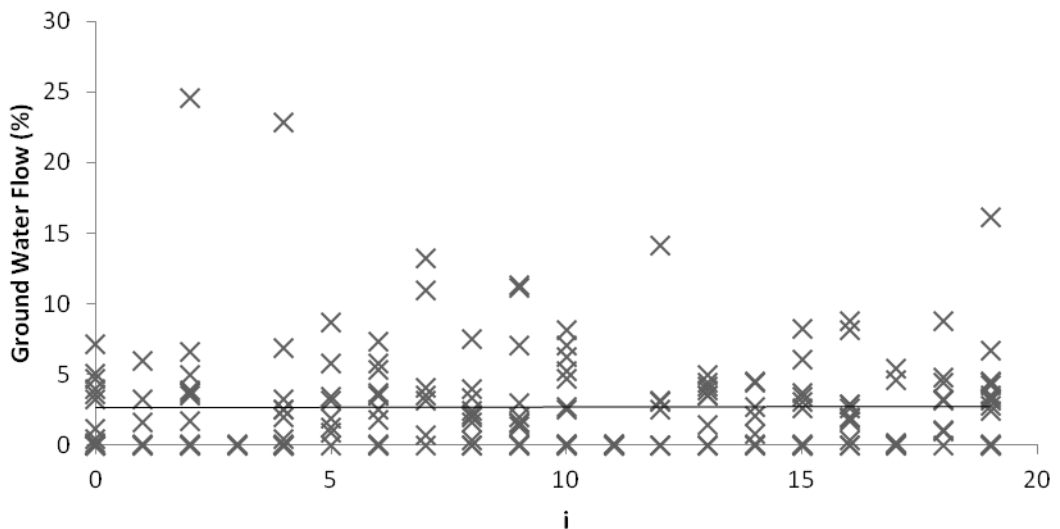


Figure 9.22 – Plot showing the relationship between the i parameter values and the proportion of modelled discharge from ground water, for the Pitman lumped CRR model of the Bakoye Catchment for the period between 1986 and 1996, calibrated to individual TAMSIM ensemble members.

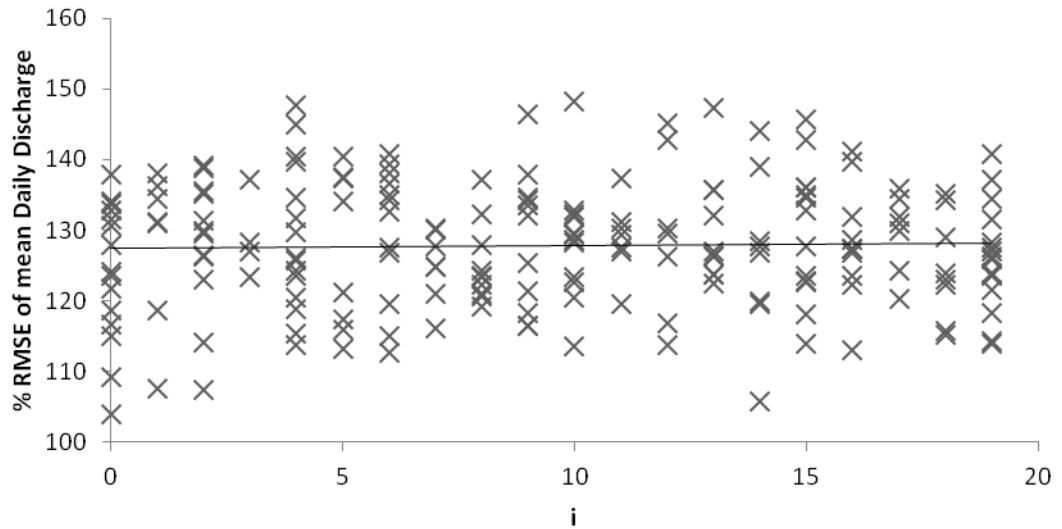


Figure 9.23 – Plot showing the relationship between the i parameter values and model performance, for the Pitman lumped CRR model of the Bakoye Catchment for the period between 1986 and 1996, calibrated to individual TAMSIM ensemble members.

GL

The GL parameter is a recession time constant for baseflow (ground water flow), and would be expected to display a similar pattern to that displayed by h and i as its influence is curtailed by the limitations to percolation imposed by W_{\min} .

Indeed, it is evident from Figures 9.25 to 9.26 that the EnsInd calibrated values of GL are equally distributed throughout the available parameter space, and that the variations show little impact on either model behaviour or performance.

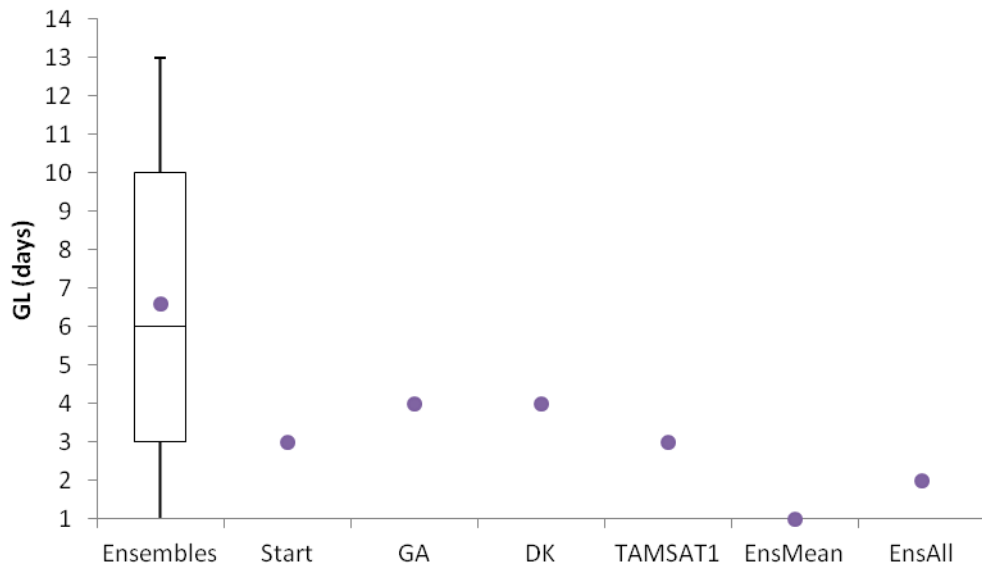


Figure 9.24 – Plot showing the box-whisker distribution of GL parameter values chosen by automatic calibration of the TAMSIM ensemble members within the available parameter space, for the Pitman lumped CRR model of the Bakoye Catchment between 1986 and 1996. The dot marks the mean value from the ensembles. Values selected by automatic calibration against the deterministic rainfall estimates are shown for comparison.

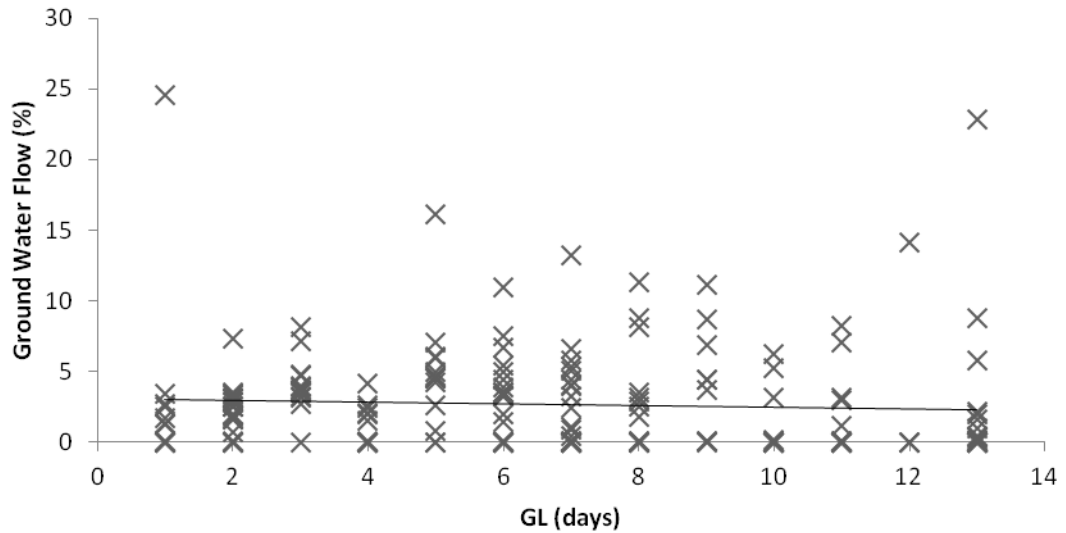


Figure 9.25 – Plot showing the relationship between the GL parameter values and the proportion of modelled discharge from ground water, for the Pitman lumped CRR model of the Bakoye Catchment for the period between 1986 and 1996, calibrated to individual TAMSIM ensemble members.

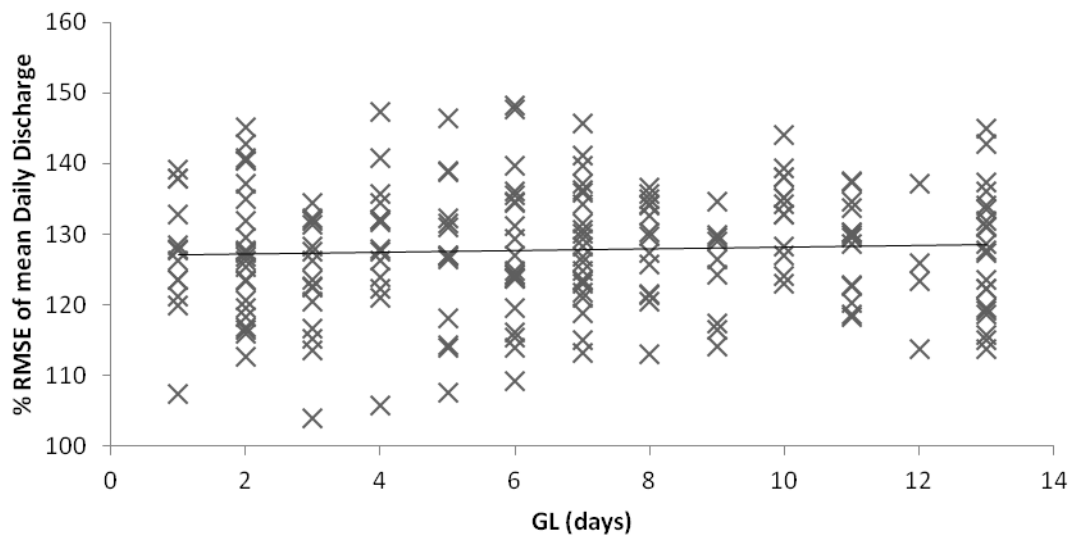


Figure 9.26 – Plot showing the relationship between the GL parameter values and model performance, for the Pitman lumped CRR model of the Bakoye Catchment for the period between 1986 and 1996, calibrated to individual TAMSIM ensemble members.

TL

The TL parameter is a constant used in the calculation of the quick flow (surface flow).

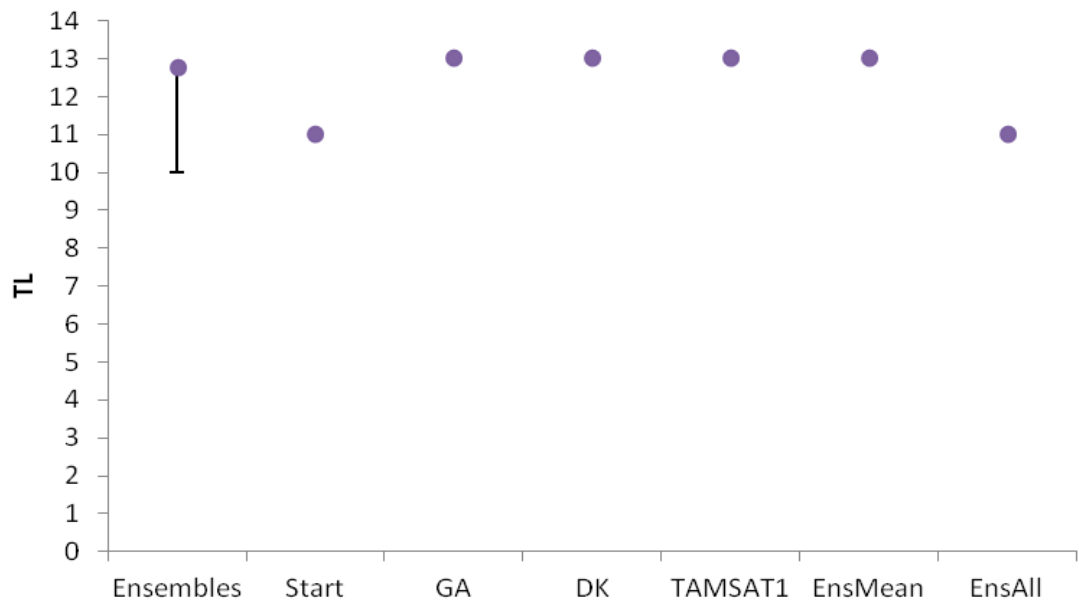


Figure 9.27 – Plot showing the box-whisker distribution of TL parameter values chosen by automatic calibration of the TAMSIM ensemble members within the available parameter space, for the Pitman lumped CRR model of the Bakoye Catchment between 1986 and 1996. The dot marks the mean value from the ensembles. Values selected by automatic calibration against the deterministic rainfall estimates are shown for comparison.

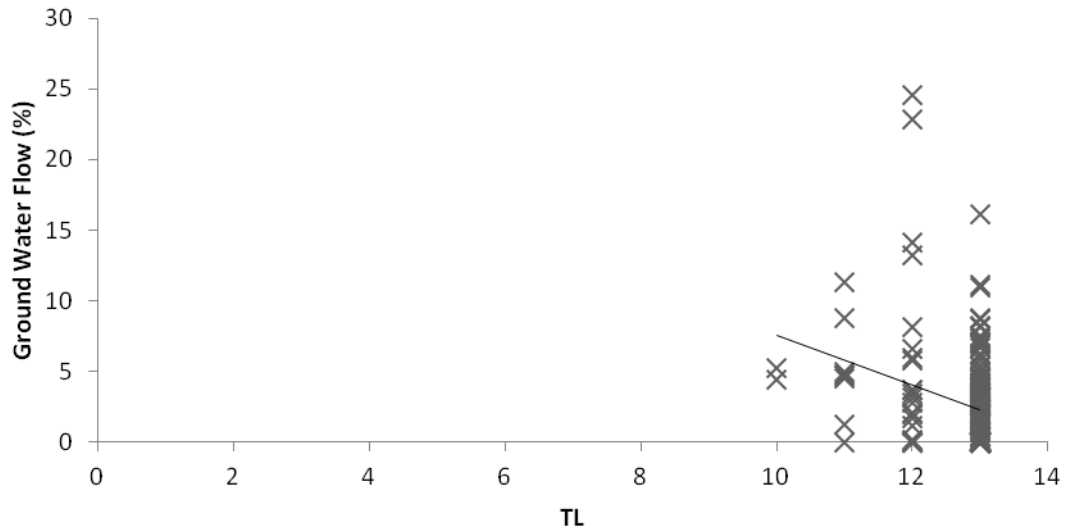


Figure 9.28 – Plot showing the relationship between the TL parameter values and the proportion of modelled discharge from ground water, for the Pitman lumped CRR model of the Bakoye Catchment for the period between 1986 and 1996, calibrated to individual TAMSIM ensemble members.

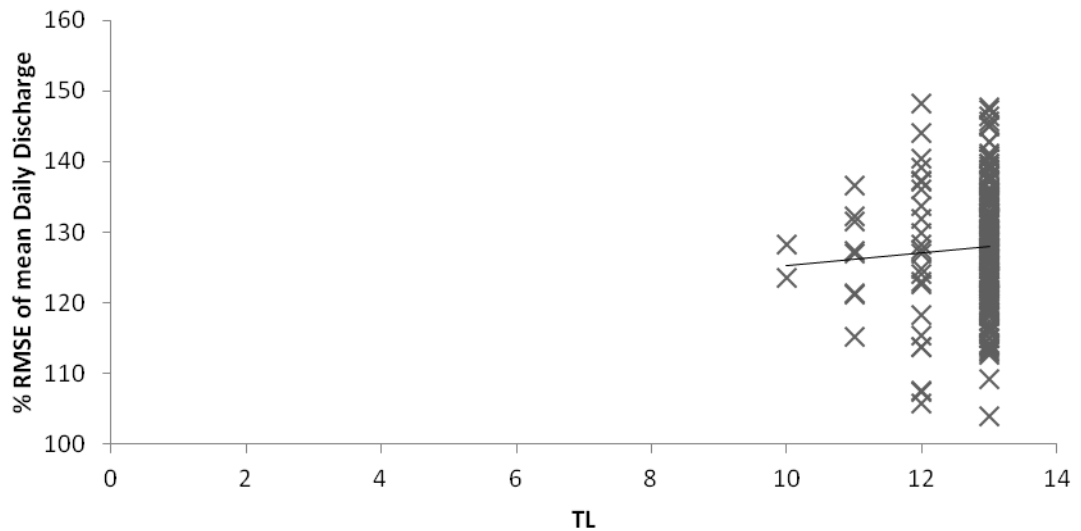


Figure 9.29 – Plot showing the relationship between the TL parameter values and model performance, for the Pitman lumped CRR model of the Bakoye Catchment for the period between 1986 and 1996, calibrated to individual TAMSIM ensemble members.

The small variation of TL values from the EnsInd calibrations, similar to the values from the other calibrations, suggests that the TL value is influential to the model performance (Figure 9.27). The lack of variation results in little relationship between the variation of values of TL and model behaviour and performance (Figure 9.28 and 9.29).

Q_q Lag

The Q_q Lag parameter is a simple lag of the quick flow (surface flow) by timesteps, in this case days.

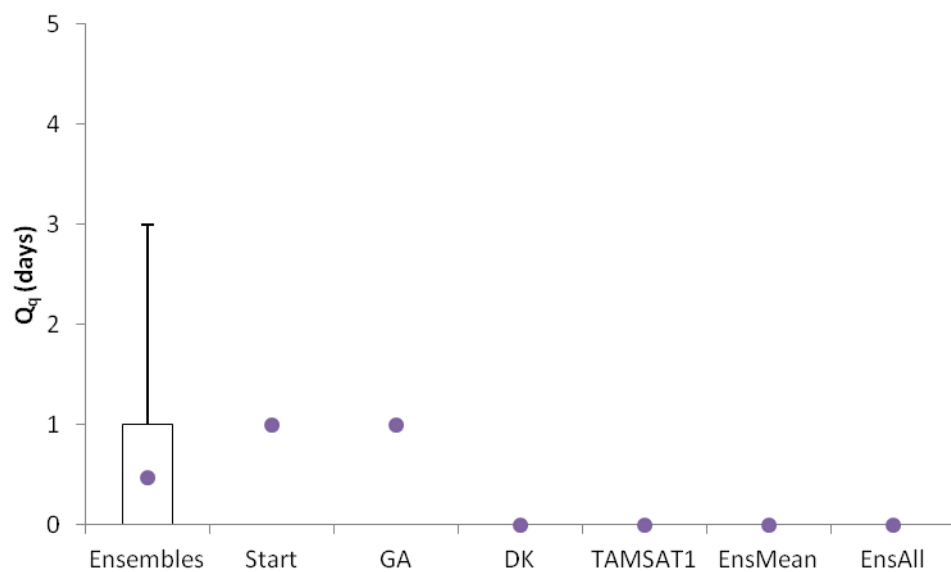


Figure 9.30 – Plot showing the box-whisker distribution of Q_q Lag parameter values chosen by automatic calibration of the TAMSIM ensemble members within the available parameter space, for the Pitman lumped CRR model of the Bakoye Catchment between 1986 and 1996. The dot marks the mean value from the ensembles. Values selected by automatic calibration against the deterministic rainfall estimates are shown for comparison.

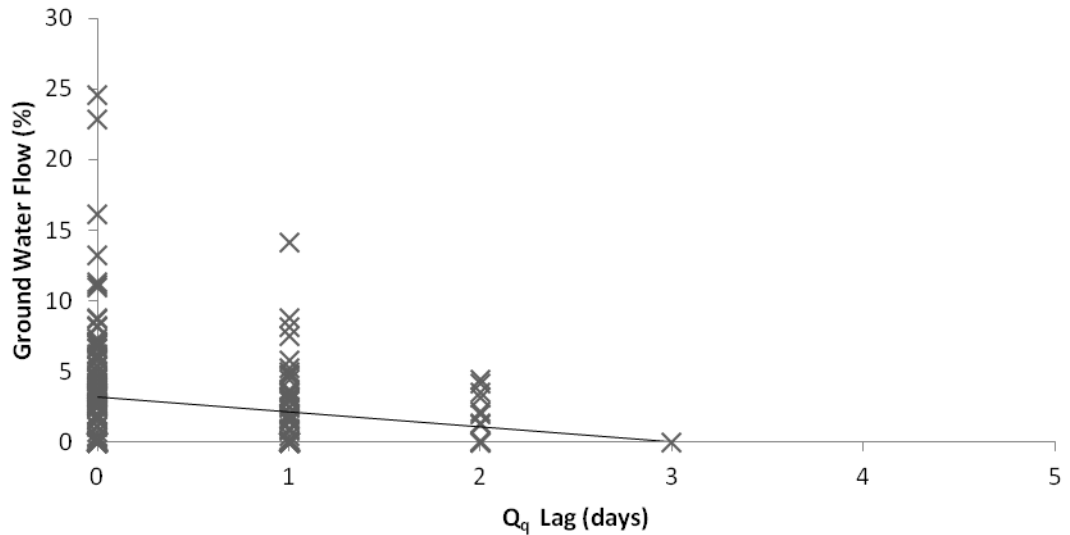


Figure 9.31 – Plot showing the relationship between the Q_q Lag parameter values and the proportion of modelled discharge from ground water, for the Pitman lumped CRR model of the Bakoye Catchment for the period between 1986 and 1996, calibrated to individual TAMSIM ensemble members.

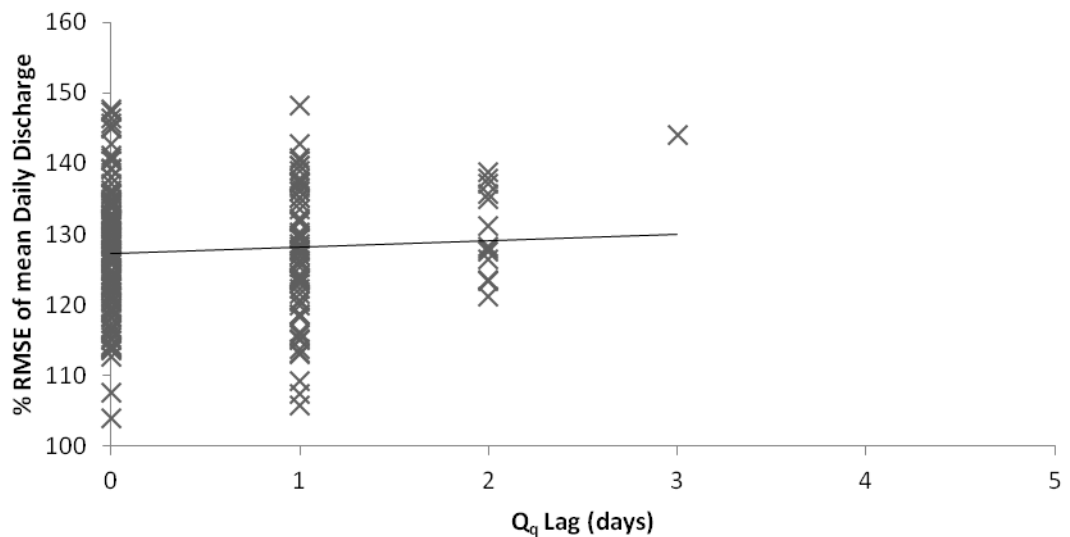


Figure 9.32 – Plot showing the relationship between the Q_q Lag parameter values and model performance, for the Pitman lumped CRR model of the Bakoye Catchment for the period between 1986 and 1996, calibrated to individual TAMSIM ensemble members.

The majority of the Enslnd calibrations showed a Q_q Lag of 1 day (Figure 9.30), but there is some variation up to 2 days. Figure 9.31 shows that the higher Q_q Lag displays lower proportions of ground water flows, suggesting that the model is attempting to compensate, probably at the end of the wet season. Figure 9.32 also suggests that there is a slight degradation in model performance as the values increase.

Q_b Lag

The Q_b Lag parameter is a simple timestep (days) lag on the base flow (ground water flow). Any influence of this parameter on model performance is dictated largely by values of W_{min} , h and i , which control the amount of rainfall reaching the ground water store. As seen above, the W_{min} values have constricted percolation to the ground water store, so the influence of Q_b Lag is likely to be slight.

There is little to be seen in Figure 9.33 to 9.35 as regards to the possible contribution of the Q_b Lag on the performance of the Pitman lumped CRR because of the restrictions from the high values of W_{min} .

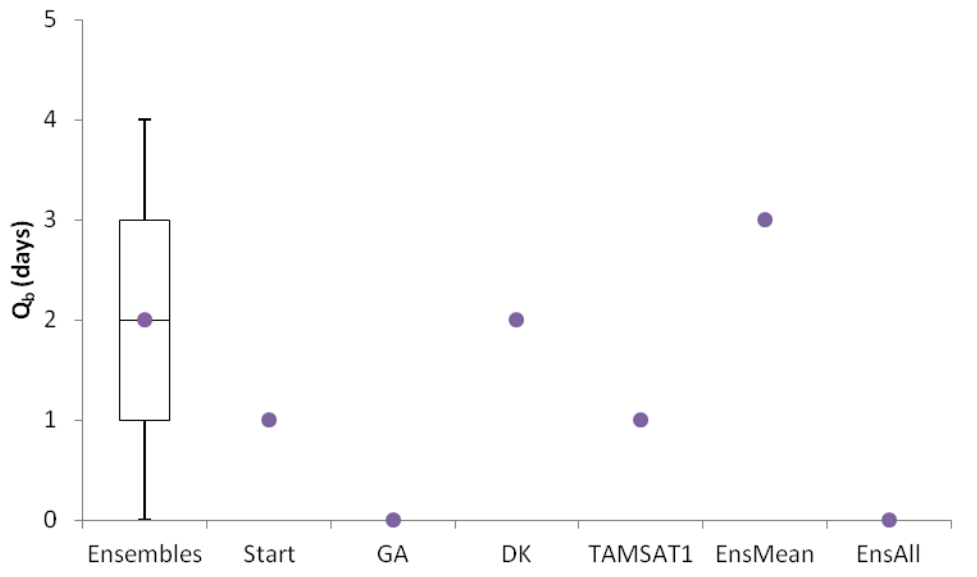


Figure 9.33 – Plot showing the box-whisker distribution of Q_b Lag parameter values chosen by automatic calibration of the TAMSIM ensemble members within the available parameter space, for the Pitman lumped CRR model of the Bakoye Catchment between 1986 and 1996. The dot marks the mean value from the ensembles. Values selected by automatic calibration against the deterministic rainfall estimates are shown for comparison.

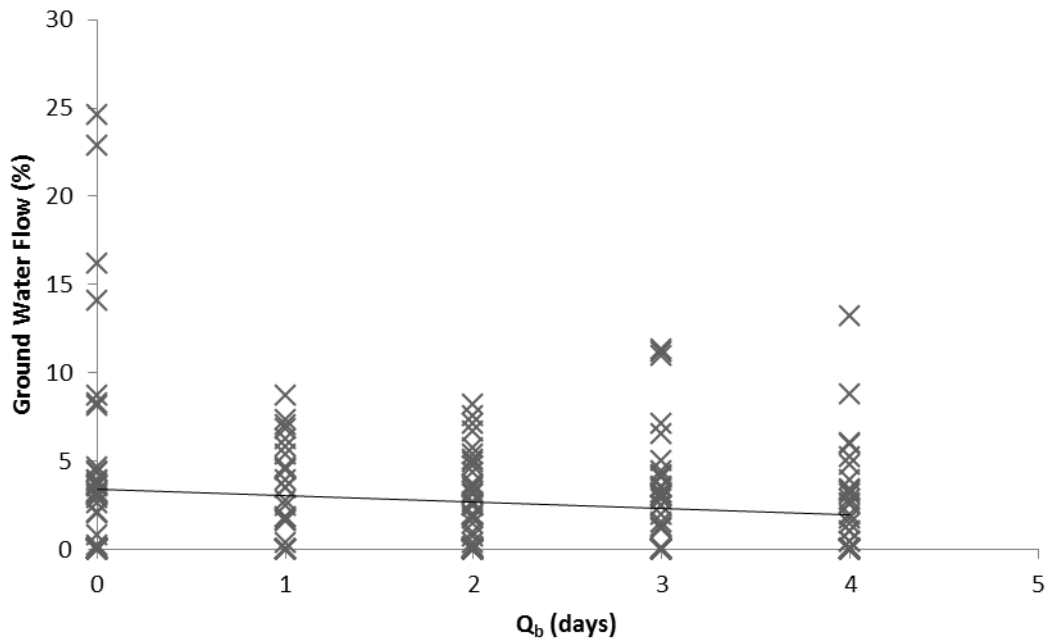


Figure 9.34 – Plot showing the relationship between the Q_b Lag parameter values and the proportion of modelled discharge from ground water, for the Pitman lumped CRR model of the Bakoye Catchment for the period between 1986 and 1996, calibrated to individual TAMSIM ensemble members.

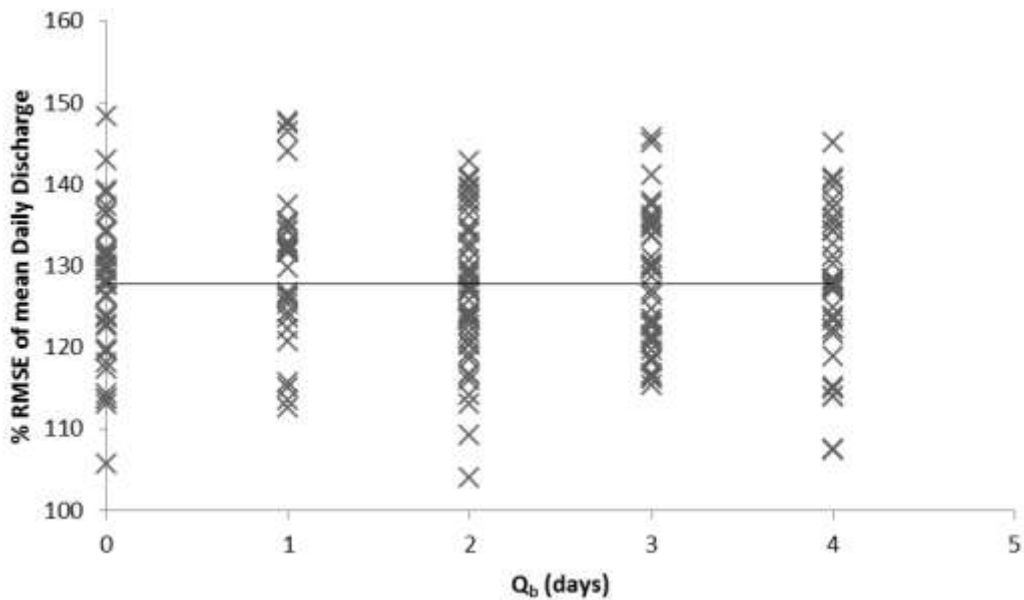


Figure 9.35 – Plot showing the relationship between the Q_b Lag parameter values and model performance, for the Pitman lumped CRR model of the Bakoye Catchment for the period between 1986 and 1996, calibrated to individual TAMSIM ensemble members.

9.4 – Conclusions

This chapter has investigated the influence of SRFE uncertainty on the calibration, performance and behaviour of a hydrological model. The TAMSIM algorithm has been used to produce 200 ensemble realisations of the daily Senegal Basin rain field, each unique yet equiprobable within the bounds of uncertainty when using the TAMSAT1 method for producing a SRFE. For each ensemble member a rainfall input was produced and used to calibrate a Pitman lumped CRR model of the Bakoye catchment for the period 1986 to 1996.

Using the proportion of modelled discharge originating from ground water as a proxy for model behaviour, the majority of the Pitman calibrations resulted in only a minor fraction of the total discharge as having originated from groundwater flows. Of the deterministic Pitman models, the TAMSAT1 driven and calibrated Pitman model showed the greatest proportion of ground water flows but this was still only 2.52% of the total discharge.

For the EnsInd calibrations of the Pitman model to each of the 200 TAMSIM ensemble inputs, the calibrations were also biased towards model behaviours of very little or no ground water flows. The highest proportion of ground water in modelled discharge was 25%, but the vast majority of the models showed <5% and most 0%. Despite this, there is evidence that a greater proportion of ground water modelled by the Pitman model does produce a better model performance (Figure 9.2).

The relationship between model behaviour and model performance observed in the EnsInd calibrations is contradictory, with the calibrations overwhelmingly favouring a set of parameters that produce minimal or no ground water flows, yet those that do show a greater proportion of ground water flows have a tendency towards superior performance. Observation of the relationship between model behaviour and parameter values suggests that the proportion of ground water is largely dependent on the W_{\min} parameter, which controls the minimum threshold of water stored in W , the soil moisture bucket, before percolation can begin between the soil moisture store and the ground water store. The calibration of W_{\min} is not dependent on the parameter selected for W_{\max} , and both have the same parameter space available - in numerous cases the W_{\min} threshold was greater than the W_{\max} maximum storage for the bucket, resulting in the inability of water to transfer into the ground water store. This can be seen as a flaw in the Pitman model and the calibration method selected, yet the parameter spaces were wide and the calibration method was sufficiently open for it to select parameter values that allowed for percolation and it favoured not doing so. This could be tested fully by replacing the numerical calibration of W_{\min} with a proportion of the W_{\max} value instead, and observing whether the SCE-UA algorithm still opts for a restricted calibration – initial tests have shown no improvement in model performance.

In terms of the impact of uncertainty within the SRFE on the calibration of the Pitman model, this appears to be quite limited. The calibration of the parameters that had the most influence on the model performance are reasonably consistent throughout the EnsInd calibrations. This would indicate

that the majority of the spread of discharges seen in the hydrograph envelopes of Chapter 8 has originated from variations in the input and not because of variations between the hydrological models.

The model behaviours do suggest an element of equifinality that the SCE-UA cannot reflect. The SCE-UA algorithm has been seen to be consistent in selecting optimal sets of parameters, especially for those parameters that have been shown to be influential for the performance of the model, but some variability in the parameters show greater proportions of ground water flows with increased model performance. This suggests that there are parameter sets which allow greater proportions of ground water flow, with comparable performance, that could be used for the Pitman model. A possible solution to this would be to perform recalibration of the Enslnd models using a modified Pitman, where the W_{\min} value is a proportion of W_{\max} , rather than a set value in the parameter space – although initial tests have shown no improvement in model performance, there may be differences in model behaviour.

10

Discussion

10.1 – Key Results

The main aim of this thesis was to demonstrate how a fully spatio-temporally distributed stochastic ensemble method could be used to characterise uncertainty within a satellite rainfall estimate, and how the ensembles produced could be used to drive and calibrate a deterministic hydrological model using traditional hydrological methods. The thesis used the Senegal Basin as its study area and daily rainfall estimates were produced using the TAMSAT1 method, calibrated using a sparse raingauge network. The uncertainty within the deterministic TAMSAT1 estimate was characterised using the TAMSIM method, and 200 unique yet equiprobable rainfall estimates for the 1986-1996 study period were produced.

It would be prudent here to highlight the benefits of using satellite data to estimate rainfall for use as a driver for hydrological modelling. This thesis has not used the full spatial distribution afforded by the method, which could be achieved with the use of a distributed, or semi-distributed hydrological model, however, the additional information provided by the SRFE can be seen to improve the hydrological modelling of the Bakoye catchment when compared to

an estimate from the raingauges. Table 9.1 shown in the previous chapter showed the relative skill of each Pitman model, driven and calibrated by the same input, showing that both the model using the TAMSAT1 estimate and the mean of the TAMSIM ensembles displayed superior performance over the Gauge Average estimate driven model. There was little evidence from observed hydrographs that the use of the SRFE allowed for better prediction of peak discharge timings, although Figure 10.1 shows an example which demonstrates the potential of SRFE to improve discharge estimation.

The use of SRFE also provide additional information for areas or periods where no gauge data is available. The use of historic raingauge data for the calibration of the TAMSAT1, TAMSIM, and Pitman model methods allows for the production of rainfall and discharge estimates for time periods outside this calibration period, even if no ground recorded rainfall data is available.

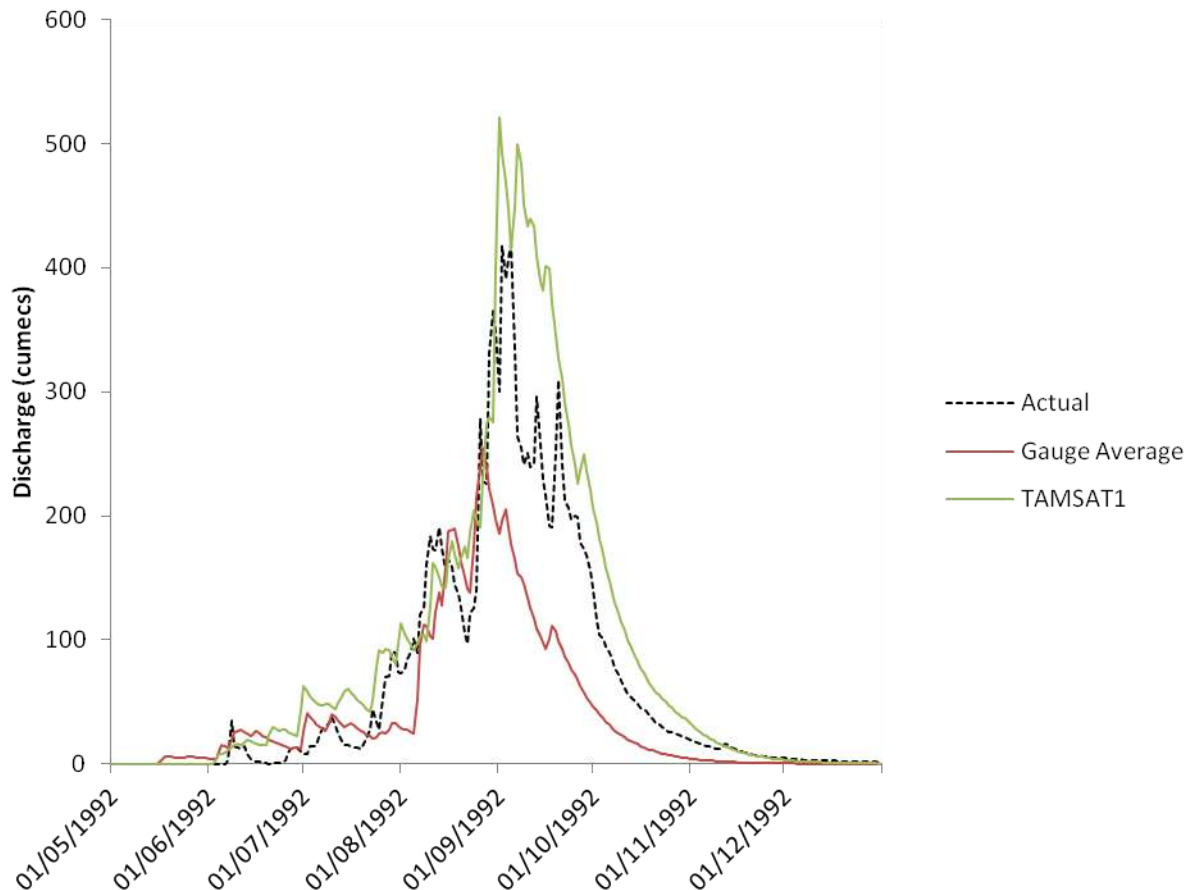


Figure 10.1 – Hydrograph showing the 1992 wet season for the Bakoye catchment. The recorded discharge is shown by the dashed line. The modelled output from the Pitman model calibrated and driven by the Gauge Average estimate for the period 1986-1996 is shown by the solid red line. The modelled output from the Pitman model calibrated and driven by the TAMSAT1 estimate is shown by the solid green line.

The ground-based rainfall retrieval data was extremely limited, comprising of 81 raingauges, and for the Bakoye catchment that was modelled, the raingauge density was 1 gauge per 7,000km². In addition, the Senegal Basin area displayed significant heterogeneity in climate, topography, geology and other physical factors. This seriously hampered the strength of the calibration of the spatial interpolation of the raingauge data, the TAMSAT1 method and the

TAMSIM algorithm, resulting in a wet season climatic calibration having to be adopted for each when a monthly calibration would have been preferred.

Teo (2006) found that because TAMSAT1 relied upon a climatic calibration based on historic raingauge data it displayed significant bias in years of anomalous rainfall – underestimating in years of heavy rainfall and overestimating in drier years. This was also found to be the case for the Senegal Basin, which was particularly marked due to the high degree of interannual variation of rainfall for the region and within the study period. The same was true for TAMSIM.

The TAMSIM ensembles were shown to be able to reproduce the spatial and temporal distributions of rainfall, as well as the fractional nature of the rainfall as displayed by the DK rain fields. However, the TAMSIM ensemble rain fields were not able to reflect the significant rainfall gradient across the Senegal Basin region, showing overestimation of rainfall in the drier north, and underestimation in the wetter south. The full analysis of the performance of the TAMSIM algorithm to reproduce the underlying DK rain field is shown in Chapter 7.

It was found that the Pitman model calibrated using the TAMSAT1 input was not transferable for use with the TAMSIM ensemble inputs, neither was a calibration against the daily mean of the TAMSIM ensembles. A calibration of the Pitman model was performed using an input that incorporated all of the ensemble members, essentially a 2,200 year record of rainfall and discharge data. This proved to be computationally expensive but did produce a calibration for the

Pitman model, that when driven by the ensemble members showed good transferable performance and little overall bias.

The output from the TAMSIM ensemble driven Pitman model was used to model the propagation of the input uncertainty through the Pitman model, and 95% confidence discharge envelopes were produced for each wet season in the study period, showing the bounds of the uncertainty. The bounds showed that the TAMSIM algorithm could not reflect the full uncertainty in the TAMSAT1 calibration, with the interannual variations in rainfall resulting in considerable biases, with 40.3% of days in the wet seasons 1987-1996 showing the recorded rainfall outside of the uncertainty bounds modelled.

However, TAMSIM displayed skill in representing uncertainty due to the non-stationary nature of the calibration of TAMSAT1 over the wet season, with the bounds better representing the recorded discharges for each year after the 1st October, displaying independence from the deterministic estimate.

Despite the evident bias associated with interannual variations of rainfall, the fully spatio-temporally distributed method of TAMSIM was shown to be superior to the more established perturbation method. TAMSIM has the significant advantage of modelling uncertainty independent of the deterministic estimate, which the simple perturbation method could not, resulting in the reflection of uncertainty bounds that were not symmetrical and occasionally decoupled altogether as in the case above (Chapter 8).

Finally, it was shown that the influence of the input uncertainty on the calibration of the Pitman model was minimal. The review in Chapter 9 showed the relationship between parameter values and model behaviour and performance when the Pitman model was calibrated against the individual ensemble members. For those parameters that were shown to be influential to the performance there was little variation across the calibrations, indicating that an optimal set of parameters, or a small distribution of parameter values, was appropriate for use with all the ensemble members.

Model behaviour across the calibrations was fairly consistent with the majority of the calibrated models preferring to limit the amount of discharge that originated from ground water. It is not clear whether this was an issue with the model structure, related to the way the W_{\min} value is determined in an automatic calibration method, but the SCE-UA had sufficient freedom to model higher proportions of groundwater if this improved performance. However, there was significant variation in the performances to point to equifinality in the method, with some models showing improved performance with greater proportions of groundwater.

10.2 – Issues and Recommendations

The results from this thesis, as summarised above, demonstrate the ability of the TAMSIM algorithm to fully characterise the uncertainty within a TAMSAT1 SRFE in a way that can be applied to a hydrological model to show the propagation of that uncertainty. It has also demonstrated the principle that the

full spatial and temporal characterisation of the uncertainty, within the bounds of the underlying DK rain field, is superior to a simpler perturbation method.

Systematic Bias and Interannual Variations in Rainfall

The major issue that emerges from this thesis is the same as that observed by Teo (2006), with significant bias evident in the TAMSAT1 estimate for anomalous years of rainfall. This is particularly important for the Bakoye catchment where it could be said that out of the 11 years in the study period, only 3 years displayed rainfall close to the mean for the period (see Figure 3.17). The bias can be seen in the hydrographs of Figures 8.3 to 8.13, where the 95% confidence discharge envelopes overestimate discharge for the drier years of 1987 and 1990, and underestimated discharge for 1994, 1995 and 1996.

The impact of the bias in TAMSAT1 on the Pitman model is greater than Teo (2006) found it to have on the GLAM crop yield model, indicating that hydrological models are more sensitive to these variations – the GLAM model was not so affected by overestimations of rainfall. Of particular concern is how even with the full characterisation of the input uncertainty, the TAMSIM ensemble SRFE were still influenced by the bias, and the 95% confidence discharge envelopes did not contain the recorded discharge for 40.3% of the days in the wet season – this leads to the conclusion that because of the bias caused by the significant interannual variations in rainfall the TAMSIM algorithm

is not able to capture fully the true bounds of uncertainty within the TAMSAT1 estimate.

The manner in which the bias within the SRFE propagates through the Pitman model was interesting and not straightforward. Although the transfer of the bias was seen to be linear in nature, models that produced less biased modelled discharges were actually driven by positively biased rainfall estimates – and these were also the best performing models. This is a result of the SCE-UA compensating for the spatial bias in the Bakoye catchment estimates, and also due to the commonly known issue where automatic calibrations, which minimises a single objective function, tend to be biased in favour of peak flows. One way to reduce this would be to use a multi-objective approach (Yapo *et al.*, 1998, Madsen, 2003, Shaffii and Smedt, 2009) – if the additional computational expense was considered acceptable.

The results suggest that in the current form, the use of a TAMSAT1 driven Pitman model with a single calibration are limited in their applications for discharge forecasting in the Senegal Basin area, and that the TAMSIM algorithm is insufficient in accounting for all of the uncertainty, in respect to bias. In order to change this situation some element of bias correction needs to be introduced to the process.

Teo (2006) made suggestions for how the systematic bias in the TAMSAT1 estimate could be reduced:

- Incorporate real-time raingauge data if available (Grimes *et al.*, 1999).
- Incorporate real-time recalibration of the TIR rainfall retrieval relationship using PM data (Todd *et al.*, 1999, 2001).
- Incorporate NWP model fields into the process (Grimes *et al.*, 2003).

It is unlikely that a sufficiently dense raingauge network which reports timely, accurately and predictably will be in place for the incorporation of real-time raingauge data into the process, either to perform recalibration or merging into the estimate – although the ambitious aims of the TAHMO project, if fulfilled, could change this situation (Hut and van der Giesen, 2010, TAHMO, 2012).

As discussed in Chapter 2, the use of PM in the region is limited due to issues of rainfall retrieval over arid and semi-arid land surfaces (Morland *et al.*, 2001). The principle of using PM data to calibrate other SRFE methods was shown in Adler *et al.* (2000), which described how the TRMM product could be used as a “flying rain gauge”. If PM rainfall retrieval could be adequately calibrated for arid and semi-arid land surfaces then the incorporation of this data could be significant, especially in light of the planned GPM project (Hossain and Anagnostou, 2004, NASA, 2013).

Grimes and Diop (2003) and Grimes *et al.* (2003) showed how NWP model fields could be incorporated into SRFE to improve them. For the Senegal Basin the use of Sea Surface Temperatures (SST) could be particularly useful as an indicator for seasonal rainfall prediction, due to the evidence of a relationship between Atlantic Ocean SST and drought as detailed in Giannini *et al.* (2008)

and Conway (2009). The use of predictors such as EAW (Grimes and Diop, 2003), and SST could provide a useful method for reducing the bias in the estimates.

Another solution relevant to using ensembles of hydrological predictions is to apply a post-processing technique to adjust for bias, as detailed in Andel *et al.* (2013), as part of HEPEX. These post-processing techniques are used to adjust the ensemble outputs from hydrological models, in order to correct for the sorts of biases observed in this thesis and to improve the skill of the forecasts. Such an approach could be applied to the modelled discharges to correct for the bias, rather than to the SRFE input.

If the method described by this thesis were to be used for operational purposes for at near real-time estimations of discharge, then the use of an adjustable calibration of the hydrological model could be used as observational data became available. Moradkhani *et al.* (2005) demonstrated how an ensemble Kalman filter algorithm could be used to assimilate the observation data into a hydrological model to improve its calibration.

Choi and Beven (2007) used ‘seasonal’ calibrations of the TOPMODEL hydrological model, and clustered the calibrations into groups – each representing different hydrological conditions, acknowledging that the behaviour of the system may vary as the conditions change. A similar approach could be applied by splitting the data into monthly periods and applying the best performing parameter set to each antecedent month, and predicting discharge

using all parameter sets (adopting the one that best fits at the end of the month) – this would allow the hydrological model to respond to bias in the SRFE and adjust for it.

This poses another solution to the poor modelling of the interannual variation of rainfall, one which – much like the equifinality thesis of Beven (2006) – is a matter of philosophy. Much has been published on the nature of hydrological models, and the effects of the spatial and temporal averaging involved in their operation. For example, O’Connell and Todini (1996) suggested that the field of hydrological modelling could be better described as an art rather than a science due to the lack of understanding into the effects of heterogeneity and how it is best managed. Although the field has significantly moved on since, Stisen *et al.* (2008), suggested that the lack of understanding of physical processes involved in catchments is so great, even models regarded as ‘physical’ are actual conceptual in nature.

The model used in this thesis, the Pitman model, is a conceptual model. There was no knowledge of the physical processes in the catchment, and although the calibrations shown in Chapter 9 produced reasonably consistent model behaviours, it was not possible to show whether those model behaviours are reflective of the reality – it is most likely not and any relation is probably a result of coincidence. In this regard the model is conceptual to the extent that the stores and transfers within it reflect real world processes in name only, and would be best thought of as a ‘black-box’ model where the internal operations are merely a means to an end: the final output.

In light of this, and with regards to the emerging field of satellite rainfall applications for surface hydrology (Gebremichael and Hossain, 2010), it is necessary for a researcher/operator to assess what is the most important aspect of their modelling work – accurate rainfall estimation for input into a hydrological model or accurate discharge estimation as an output from the hydrological model. It may not be apparent that the two are exclusive, it seems plausible that accurate rainfall estimation is more likely to produce accurate discharge estimation.

If it was to be taken that the most important element of the satellite rainfall applications for surface hydrology field was the accurate modelling of output from the surface hydrology model, it can be assumed therefore that when used in a conceptual hydrological model the rainfall input itself can be thought of as conceptual. This is not an unreasonable assumption considering the poor understanding between the physical relationship between cloud top temperature and rainfall, and the average over space and time. Ultimately, this thesis could be said to have been a study of the relationship between CCD and discharge. Indeed, initial tests in this area show that whilst not achieving the same levels of performance as the rainfall estimate, a crude method of producing a mean of the CCD for the Bakoye catchment (multiplied by a factor of 5 to replicate values in the order of rainfall volumes), and using this to drive a calibrated the Pitman model in the same method as described in Chapter 6, a skill score of 131.0% RMSE of mean daily discharge can be achieved. The TAMSAT1 driven and calibrated model achieved a score of 112.5%, and Figure 10.2 compares

the hydrographs produced by both methods for the 1989 wet season showing close comparison – in fact the crude CCD estimate outperformed the TAMSAT1 estimate in 5 of the 11 wet seasons, and produced a better mean score for wet seasons (84.59% compared to 84.98% for TAMSAT1), suggesting it is better able to reproduce interannual variations of rainfall. It is a possibility that with some careful consideration into appropriate hydrological model structure a reasonable estimate of discharge could be modelled directly from the CCD data, although care must be taken that this model structure does not merely replicate similar processes to SRFE algorithms.

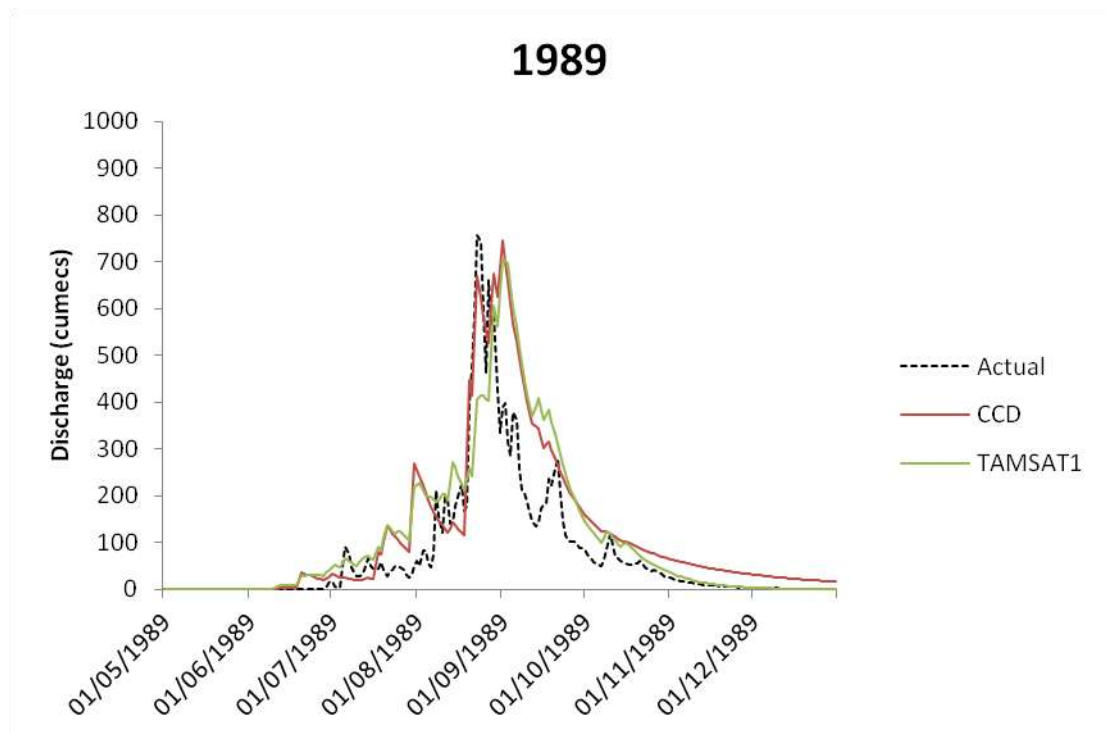


Figure 10.2 – Hydrograph showing the 1989 wet season modelled for the Bakoye catchment. The dashed line shows the recorded discharge. The solid red line shows the modelled output from a Pitman model driven and calibrated by a catchment mean of CCD multiplied by a factor of five for the period 1986-1996. The solid green line shows the modelled discharge from the modelled discharge from a Pitman model driven and calibrated by the TAMSAT1 estimate for the period 1986-1996.

In practical terms, although it is still desirable to strive for accurate, unbiased SRFE, if a researcher was to accept that the input was conceptual, the bias caused by interannual variations could be managed by using a set of calibrations that cover the range of variations, selecting the most appropriate for the conditions of each particular season. Such a method requires an acceptance of equifinality in the modelling of the system, and would operate in a similar manner to the GLUE methodology (Beven, 2006).

Performance of the Pitman model

Several authors, including Blackie and Eales (1985) and Michaud and Sorooshian (1994a) have suggested that distributed models perform better than spatially lumped models, such as the one used in this thesis. Blackie and Eales (1985) claimed that due to assumptions made about homogeneity, the use of lumped models should be limited to small catchments only. The Bakoye catchment studied here is a large catchment and displays large heterogeneity in many factors across its extent, however, the Pitman model and the SCE-UA algorithm proved worthy for their use in this application, which when driven by TAMSAT1 in the Bakoye catchment resulted in an error of 112.49% of the mean daily discharge, for the period 1986-1996. This sounds high, but with the paucity of the data available it is unlikely that major improvements could be achieved. For comparison, the MIKE SHE model used by Stisen *et al.* (2008) for the same catchment, in the period 1998-2001, produced an error of 97% - this was using a more sophisticated, distributed hydrological model and a TAMSAT SRFE,

based on a similarly sparse raingauge network. Although the model used in Stisen *et al.* (2008) clearly shows a better performance than the Pitman used in this thesis, the MIKE SHE was used to model a smaller 4 year period, which did not display the same degree of interannual variation as the 1986-1996 period – in particular without any years of below mean discharge. It is likely that much of the improved performance seen in the model of Stisen *et al.* (2008) is due to the reduced impact of the systematic bias in the SRFE as the rainfall record used showed less anomalous years.

However, as TAMSAT1 and TAMSIM have produced daily rainfall fields that are fully distributed, it is only logical that the next step in this research would be to apply the same TAMSIM ensemble set to the MIKE SHE distributed model for the Bakoye catchment, for the period 1986-1996. The focus of this should be to investigate the impacts of the spatial variations of the rainfall modelled by the individual ensemble estimates, but also the influence of the TAMSAT1 bias on the MIKE SHE for a period that demonstrates greater variations in rainfall.

It is likely that a single model structure may not be appropriate for transferable uses between catchments. For example, the Pitman model and the MIKE SHE model structures have both been shown to operate adequately for the Bakoye catchment, but neither may be the optimal structure for representing the catchment. Mwakalila *et al.* (2001) demonstrated how the data available for a semi-arid catchment could be used not only to drive and calibrate a hydrological model, but also to determine the most suitable structure for the model using a Data-Based Mechanistic Modelling (DBM) approach. Such a method is

transferable between catchments by being flexible enough to alter model structures to suit each catchment, and the data available.

Further Sources of Uncertainty

A weakness of the method presented in this thesis over the original study of TAMSIM in Teo (2006) and Teo and Grimes (2007) is that there is no accounting for the uncertainty as part of the DK method. This was sacrificed in order to improve the method used to fit the gamma distributions at each CCD bin – for completeness however, a method for incorporating the DK error into the uncertainty characterisation should be reinstated. Pardo-Iguzquiza *et al.* (2006) detailed a method for calculating the error in a DK method, and the KrigeRain algorithm (Greatrex, 2009) produces error fields for each timestep.

Di Baldassarre and Montanari (2009) demonstrated a method for incorporating an analysis of uncertainty originating from the discharge observation data, and for a full analysis of uncertainty within the entire process a similar method could be incorporated.

Communicating the Uncertainty

This thesis has demonstrated how ensemble discharge estimates can be used to produce 95% confidence discharge envelopes, showing the bounds of uncertainty within the TAMSIM ensemble SRFE when used to calibrate and drive a Pitman lumped CRR model. Although this is a method of demonstrating

the scope of uncertainty in a clear and visible way, it is insufficient for communicating the relationship between uncertainty and the implications for drought or flood forecasting.

Webster and Jian (2011) described how uncertainty could be communicated using the idea of risk, where:

$$\text{risk} = (\text{probability of an event}) \times (\text{cost})$$

Using the equation provided by Webster and Jian (2011) it is possible to incorporate the 95% confidence discharge envelopes as a measure of the probability of an event – in this example, a flood. If it assumed that flooding will occur beyond a pre-determined discharge threshold, and higher thresholds represent larger, higher cost, floods, the severity of risk can be communicated to decision makers.

Using the output from the EnsAll for the 1988 wet season, the following thresholds were established.

- Discharge > 500cumecs = minor flooding
- Discharge > 750cumecs = average flooding
- Discharge > 100cumecs = major flooding

Each threshold would be weighted and multiplied by the proportion of ensemble outputs estimating discharges above the specified threshold, so that the risk is

scored between 0 and 100 (with a score of 100 when all ensembles estimate major flooding). Figure 10.2 shows the risk as it alters over the 1988 wet season.



Figure 10.2 – Chart showing an example of the communication of flooding risk as a combination of cost and probability of event, as described by Webster and Jian (2011), using the EnsAll ensemble output for the Bakoye catchment in the 1988 wet season.

The chart shown in Figure 10.2 shows how the TAMSIM driven Pitman ensemble outputs can be used to communicate risk, with the proportions of ensembles used to calculate the probability of an event and weighting it against the relative cost of that event. This would allow decision makers to set risk thresholds for action, and as Webster and Jian (2011) suggest, implement programmes that act to reduce the cost of the event and bring the risk down below the threshold – it is unlikely that it would be possible to reduce the probability of the event.

The above example is simplistic in its nature and does not represent any physical costs of flood risk associated with the Bakoye catchment, but does act as an example of the principle of the use of ensemble SRFE in the determination of risk and their potential usefulness for driving EWS. Future research in this area would be best focussed on developing a more comprehensive characterisation of uncertainty, incorporating the additional sources detailed previously, for an area with a more extensive historic raingauge network. The study should build a risk model based on the model outputs, such as that described above, and be validated against past flood events with known costs.

11

Conclusions

The previous chapter has discussed the major findings of this thesis and the major issues that have been encountered, before making suggestions of directions in which future research could be focussed. This chapter summarises the main conclusions from the thesis.

The TAMSIM method was shown to be able to reproduce the characteristics of the daily Senegal rainfall field at both gauge-pixel and catchment average scale – much in the same way as was demonstrated by Teo (2006) and Teo and Grimes (2007). Significantly, the reliability plots of Figure 7.8 demonstrated that TAMSIM produced rainfall estimates that were reliable against the DK rainfall field, for rainfall above trace rainfall levels.

Whilst unbiased as a whole, the TAMSIM SRFE showed significant spatial and temporal biases. Spatially, the single calibration of the algorithm was shown to be unable to reproduce the rainfall gradient that pervades the Senegal Basin, and the rain fields overestimated the rainfall for gauge-pixels in the drier north of the region, and underestimated in the wetter south. For the catchment average for the Bakoye catchment this resulted in an underestimation of the rainfall input compared to the DK estimate, for the whole 11 years of the study period.

Probably more significantly, the temporal biases caused by interannual variations in rainfall were large, with TAMSIM unable to model the wide variations in rainfall between years – the result was large biases for anomalous years of rainfall which for the study period was most of the years.

Several parameterisations were tested on the TAMSIM ensemble estimate driven Pitman model, demonstrating that the choice of input influences the modelled discharge. This is because the SRFE uncertainties interact with the hydrological model uncertainties, and the latter need to be mitigated for. A new parameterisation (EnsAll) which incorporated each of the individual TAMSIM ensemble estimates in an effective 2,200 year record, provided the optimal parameterisation for use with the ensembles, with the modelled discharge showing little overall bias over the study period.

The 95% confidence hydrograph envelopes shown in Figures 8.3 to 8.13 showed the spread of error in the TAMSIM rainfall inputs, propagating into the output of the EnsAll parameterised Pitman model. Significant periods of the record for the 11 year study period showed the recorded discharge outside of the envelope – this is due to the temporal systematic bias in the TAMSIM rainfall inputs during years of anomalous rainfall.

The spatial bias is consistent throughout the record and as such its impact on the modelled discharges is minimal as the SCE-UA calibration compensates for the slight underestimation of rainfall. However, the biases caused by the interannual variations of the rainfall total cannot be compensated against and

propagate directly to the modelling of discharge by the Pitman model. In addition, because of the compensation for the spatial bias the EnsAll parameterised Pitman model performs better for some biased inputs than an unbiased estimate.

Chapter 8 demonstrated how the TAMSIM method of characterising uncertainty in a SRFE – a fully spatio-temporally distributed stochastic ensemble approach – is better able to model the influence of input uncertainty on the Pitman model than a simpler perturbation method. This was highlighted in the envelope hydrographs of Figures 8.22 to 8.31. In particular TAMSIM is able to show the non-symmetrical error distribution and represent the intraseason temporal biases. The effects of the latter point can be reduced by using a calibration of TAMSIM at a finer temporal scale, such as monthly, and it is unlikely this effect would be noticeable using such a calibration – this thesis has highlighted that the calibrated relationship between CCD and rainfall is non-stationary over time and TAMSIM is able to reflect this but a perturbation method is not.

Finally, Chapter 9 showed that the relationship between hydrological model calibration and behaviour, when driven by ensemble inputs, is a complex one. The majority of the calibrations favoured a model behaviour displaying a smaller proportion of final discharge originating from groundwater flows, in favour of surface flows – this was despite observations of the relationship between model behaviour and performance suggesting otherwise. This is a significant hint towards equifinality within the Pitman model, where a change of structure and calibration will produce a different behaviour in the model but similar

performance. Overall the calibrations against each individual TAMSIM ensemble member were seen to be similar, especially for those parameters that were observed to be more significant to the performance of the Pitman model.

B

Bibliography

Abulohom, M. S., Shah, S. M. S., and Ghumman, A. R., 2001. Development of a rainfall-runoff model, its calibration and validation. *Water Resources Management*, **15**, 149-163

Adler, R. F., Huffman G. J., Bolvin, D. T., Curtis, S., and Nelkin, E. J., 2000. Tropical rainfall distributions determined using TRMM combined with other satellite and gauge information. *Journal of Applied Meteorology*, **39**, 2007-2023

Ajami, N. K., Gupta, H., Wagener, T., and Sorooshian, S., 2004. Calibration of a semi-distributed hydrologic model for streamflow estimation along a river system. *Journal of Hydrology*, **298**, 112-135

Ali, A., Lebel, T., and Amani, A., 2003. Invariance in the spatial structure of Sahelian rain fields at climatological scales. *Journal of Hydrometeorology*, **4**, 996-1011

Ali, A., Amani, A., Diedhiou, A., and Lebel, T., 2005. Rainfall estimation in the Sahel. Part II: Evaluation of rain gauge networks in the CILSS countries and objective intercomparison of rainfall products. *Journal of Applied Meteorology*, **44**, 1707-1722

Allen, R. G., Pereira, L. S., Raes, D., and Smith, M. 1998. *Crop evapotranspiration - Guidelines for computing crop water requirements. FAO Irrigation and drainage paper 56*. Food and Agricultural Organisation of the United Nations. Available: <http://www.fao.org/docrep/X0490E/X0490E00.htm> [accessed 24 March 2013]

Anagnostou, E. N., Maggioni, V., Nikolopoulos, E. I., Meskele, T., Hossain, F., and Papadopoulos, A., 2010. Benchmarking High-Resolution Global Satellite Rainfall Products to Radar and Rain-Gauge Rainfall Estimates. *IEEE Transactions on Geoscience and Remote Sensing*, **48(4)**, 1667-1683

Andel, S. J. van., Weerts, A., Schaake, J., and Bogner, K., 2013. Post-processing hydrological ensemble predictions intercomparison experiment. *Hydrological Processes*, **27**, 158-161

Andersen, J., Dybkjaer, G., Jensen, K. H., Refsgaard, J. C., and Rasmussen, K., 2002. Use of remotely sensed precipitation and leaf area index in a distributed hydrological model. *Journal of Hydrology*, **264**, 34-50

Andersen, J., Refsgaard, J. C., and Jensen, H. J., 2001. Distributed hydrological modelling of the Senegal river basin-model construction and validation. *Journal of Hydrology*, **247**, 200-214

Andersson, L., Wilk, J., Todd, M. C., Hughes, D. A., Earle, A., Kniveton, D., Layberry, R., and Savenije, H. H. G., 2006. Impact of climate change and development scenarios on flow patterns in the Okavango River. *Journal of Hydrology*, **331**, 43-57

Andrews, F., 2012. *Shuffled Complex Evolution (SCE) Optimisation*. Available: <http://hydromad.catchment.org/man/SCEoptim.html> [Accessed 24 March 2013]

Arkin, P. A., and Meisner, B. N., 1987. The relationship between large-scale convective rainfall and cold cloud cover over the western hemisphere during 1982-84. *Monthly Weather Review*, **115**, 51-74

Azimi-Zonooz, A., Krejewski, W. F., Bowles, D. S., and Seo, D. J., 1989. Spatial rainfall estimation by linear and non-linear co-kriging of radar and raingage data. *Stochastic Hydrology and Hydraulics*, **3**, 51-67

Balme, M., Vischel, T., Lebel, T., Peugeot, C., and Galle, S., 2006. Assessing the water balance in the Sahel: Impact of small scale rainfall variability on runoff Part 1: Rainfall variability analysis. *Journal of Hydrology*, **331**, 336-348

Baret, F., and Guyot, G., 1991. Potentials and Limits in Vegetation Indices for LAI and APAR Assessment. *Remote Sensing of the Environment*, **35**, 161-173

Batchelor, C. H., 1984. The accuracy of Evapotranspiration Estimated with the FAO Modified Penman Equation. *Irrigation Science*, **5**, 223-233

Barancourt, C., Creutin, J. D., and Rivoirard, J., 1992. A method for delineating and estimating rainfall fields. *Water Resources Research*, **4**, 1133-1144

Bell, T. L., Abdullah, A., Martin, R. L. And North, G. R., 1990. Sampling errors for satellite-derived tropical rainfall – Monte-Carlo study using a space-time stochastic-model. *Journal of Geophysical Research – Atmosphere*, **95**, 2195-2205

Bellerby, T., 2012. *Ensemble conditional precipitation simulation from spatiotemporally heterogeneous multiplatform satellite data sets*. European Geosciences Union, Vienna,

27th April 2012, 09:45. Abstract Available:

<http://adsabs.harvard.edu/abs/2012EGUGA..14.9730B> [Accessed 25 March 2013]

Bellerby, T. J., and Sun, J., 2005. Probabilistic and ensemble representations of the uncertainty in an IR/Microwave satellite precipitation product. *Journal of Hydrometeorology*. **6**, 1032-1044

Bellerby, T. J., Todd, M., Kniveton, D., and Kidd, C., 2000. Rainfall estimation from a combination of TRMM precipitation radar and GOES multispectral satellite imagery through the use of an artificial neural network. *Journal of Applied Meteorology*, **39**, 2115-2128

Berry, L., 1975. *The Sahel: Climate and Soils in the Sahel: Ecological approaches to land use. MAB Technical Notes No. 1*. UNESCO.

Beven, K., 1989. Changing ideas in hydrology – The case of physically-based models. *Journal of Hydrology*, **105**, 157-172

Beven, K., 2006. A manifesto for the equifinality thesis. *Journal of Hydrology*, **320**, 18-36

Beven, K., 2008. *Environmental Modelling: An Uncertain Future?* London: Routledge

Beven, K., and Binley, A., 1992. The future of distributed models: Model calibration and uncertainty prediction. *Hydrological Processes*. **6**, 279-298

Beven, K., and Feyen, J., 2002. The Future of Distributed Modelling: Special Issue. *Hydrological Processes*. **16**, 169-172

Beven, K. J., and Kirkby, M. J., 1979. A physically based, variable contributing area model of basin hydrology. *Hydrological Science Bulletin*, **24(1)**, 43-69

Blackie, J. R., and Eales, C. W. O., 1985. Lumped Catchment Models. In, Anderson, M. G., and Burt, T. P., ed. *Hydrological Forecasting*. Chichester, UK; John Wiley and Sons. pp.311-346

Boyle, D. P., Gupta, H. V., Sorooshian, S, Koren, V., Zhang, Z., and Smith, M., 2001. Towards improved streamflow forecasts: Value of semidistributed modeling. *Water Resources Research*, **37(11)**, 2749-2759

Braman, L. M., van Aalst, M. K., Mason, S., Ait-Chellouche, Y., and Tall, A., 2012. Climate forecasts in disaster management: Red Cross flood operations in West Africa, 2008. *Disasters*, **37(1)**, 144-164

Butts, M. B., Payne, J. T., Kristensen, M., and Madsen, H., 2004. An evaluation of the impact of model structure on hydrological modelling uncertainty for streamflow simulation. *Journal of Hydrology*, **298**, 242-266

Campling, P., Gobin, A., and Feyen, J., 2001. Temporal and spatial rainfall analysis across a humid tropical catchment. *Hydrological Processes*, **15**, 359-375

Chiew, F., and McMahon, T., 1994. Application of the daily rainfall-runoff model MODHYDROLOG to 28 Australian catchments. *Journal of Hydrology*, **153**, 383-416

Choi, H. T., and Beven, K., 2007. Multi-period and multi-criteria model conditioning to reduce prediction uncertainty in an application of TOPMODEL within the GLUE framework. *Journal of Hydrology*, **332**, 316-336

Chu, W., Gao, X., and Sorooshian, S., 2010. Improving the shuffled complex evolution scheme for optimization of complex nonlinear hydrological systems: Application to the calibration of the Sacramento soil-moisture accounting model. *Water Resources Research*, **46**, W09530, doi:10.1029/2010WR009224

Clark, M. P., and Slater, A. G., 2006. Probabilistic Quantitative Precipitation Estimation in Complex Terrain. *Journal of Hydrometeorology*. **7**, 3-22

Collins (2012). *Collins English Dictionary*. Glasgow, UK: HarperCollins

Commission for Africa, 2005. *Our common interest. Report of the Commission for Africa*. Available: <http://www.commissionforafrica.info/2005-report> [Accessed 24 March 2013]

Commission for Africa, cited 2010. *Still our common interest. Report for the Commission for Africa*. Available: <http://www.commissionforafrica.info/2010-report> [accessed 24 March 2013]

Consultative Group of International Agricultural Research – Consortium for Spatial Information (GIAR-CSI), 2009. *Global Aridity Index (Global-Aridity) and Global Potential Evapo-Transpiration Index (Global-PET): Methodology and Geospatial Dataset Description*. Available: http://csi.cgiar.org/aridity/Global_Aridity_PET_Methodolgy.asp [accessed 24 March 2013]

Conway, G., 2009. *The Science of Climate Change in Africa: Impacts and Adaptation*. Grantham Institute for Climate Change Discussion Paper. Imperial College London. Available:

https://workspace.imperial.ac.uk/climatechange/public/pdfs/discussion_papers/Grantham_Institute_-_The_science_of_climate_change_in_Africa.pdf [Accessed 24 March 2013]

Courault, D., Seguin, B., and Olioso, A., 2005. Review on estimation of evapotranspiration from remote sensing data: From empirical to numerical modelling approaches. *Irrigation and Drainage Systems*, **19**, 223-249

Courty, N., and Cuzol, A., 2010. Conditional stochastic simulation for character animation. *Computer Animation and Virtual Worlds*, **21**, 443-452

Di Baldassarre, G., Montanari, 2009. Uncertainty in river discharge observations: a quantitative analysis. *Hydrology and Earth System Sciences*, **13**, 913-921

Dinku, T., Ceccato, P., Grover-Kopec, E., Lemma, M., Connor, S. J., and Ropelewski, C. F., 2007. Validation of satellite rainfall products over East Africa's complex topography. *International Journal of Remote Sensing*, **28(7)**, 1503-1526

Dinku, T., Connor, S. J., and Ceccato, P., 2010. Comparisons of CMORPH and TRMM-3B42 over mountainous regions of Africa and South America. In: Gebremichael, M., and Hossain, F., eds. *Satellite Rainfall Applications for Surface Hydrology*. Springer. pp.193-204

Diop, M., and Grimes, D. I. F., 2003. Satellite-based rainfall estimation for river flow forecasting in Africa. II: African Easterly Waves, convection and rainfall. *Hydrological Sciences Journal*, **48(4)**, 585-599

Di Piazza, A., and Di Piazza, M. C., 2009. A Kriging-Based Partial Shading Analysis in a Large Photovoltaic Field for Energy Forecast. *International Conference on Renewable Energies and Power, 2009*. Available: http://www.icrepq.com/ICREPQ'09/abstracts/475_di_piazza_abstract.pdf [Accessed 24 March 2013]

Dirks, K. N., Hay, J. E., Stow, C. D., and Harris, D., 1998. High-resolution studies of rainfall on Norfolk Island Part II: Interpolation of rainfall data. *Journal of Hydrology*, **208**, 187-193

Duan, Q. Y., Gupta, V. K., and Sorooshian, 1993. Shuffled Complex Evolution Approach for Effective and Efficient Global Minimization. *Journal of Optimisation Theory and Applications*, **76**, 501-521

Duan, Q., Sorooshian, S, and Gupta, V. J., 1994. Optimal use of the SCE-UA global optimization method for calibrating watershed models. *Journal of Hydrology*, **158**, 265-284

Duchon, C. E., Renkevans, T. M., and Crosson, W. L., 1995. Estimation of Daily Area-Average Rainfall during the CaPE Experiment in Central Florida. *Journal of Applied Meteorology*, **34**, 2704-2714

Dugdale, G., Hardy, S., and Milford, J. R., 1991. V: Daily catchment rainfall estimated from METEOSAT. *Hydrological Processes*, **5(3)**, 261-270

FAO, cited 2009. *AQUASTAT Climate Characteristics*. Food and Agricultural Organisation of the United Nations. Available: <http://www.fao.org/nr/water/aquastat/quickWMS/climcropwebx.htm> [accessed 24 March 2013]

Freer, J., Beven, K., and Ambrose, B., 1996. Bayesian estimation of uncertainty in runoff prediction and the value of data: an application of the GLUE approach. *Water Resources Research*. **32**, 2161-2173

Gan, T. Y., Dlamini, E. M., and Biftu, G. F., 1997. Effects of model complexity and structure, data quality, and objective functions on hydrological modeling. *Journal of Hydrology*, **192**, 81-103

Gebremichael, M., and Hosain, F., eds. 2010. *Satellite Rainfall Applications for Surface Hydrology*. Springer.

Germann, U., Berenguer, M., Sempere-Torres, D., and Zappa, M., 2007. REAL – Ensemble radar precipitation estimation for hydrology in a mountainous region. *Quarterly Journal of the Royal Meteorological Society*. **1**, 1-22

Giannini, A., Biasutti, M., and Verstraete, M. M., 2008. A climate model-based review of drought in the Sahel: Desertification, the re-greening and climate change. *Global and Planetary Change*, **64**, 119-128

Goovaerts, P., 2000. Geostatistical approaches for incorporating elevation into the spatial interpolation of rainfall. *Journal of Hydrology*, **228**, 113-129

Gourley, J. J., and Vieux, B. E., 2006. A method for identifying sources of model uncertainty in rainfall-runoff simulations. *Journal of Hydrology*, **327**, 68-80

Grayson, R., and Blöschl, G., eds. 2001. *Spatial Patterns in Catchment Hydrology: Observations and Modelling*. Cambridge: Cambridge University Press

Grayson, R. B., Blöschl, G., Western, A. W., and McMahon, T. A., 2002. Advances in the use of observed spatial patterns of hydrological response. *Advances in Water Resources*, **25**, 1313-1334

Greatrex, H., 2009. *KrigeRain v1.2: Geostatistical analysis of precipitation data*. University of Reading, UK

Greatrex, H., 2012. *The application of seasonal rainfall forecasts and satellite rainfall estimates to seasonal crop yield forecasting for Africa*. Ph.D. diss., University of Reading

Grimes, D. I. F., and Diop, M., 2003. Satellite-based rainfall estimation for river flow forecasting in Africa. I: Rainfall estimates and hydrological forecasts. *Hydrological Science Journal*, **48**, 567-584

Grimes, D. I. F., Pardo-Iguzquiza, E., and Bonifacio, R., 1999. Optimal areal rainfall estimation using raingauges and satellite data. *Journal of Hydrology*, **222**, 93-108

Grimes, D. I. F., and Pardo-Iguzquiza, E., 2010. Geostatistical Analysis of Rainfall. *Geographical Analysis*, **42**, 136-160

Grover-Kopec, E., Kawano, M., Klaver, R. W., Blumenthal, B., Ceccato, P., and Connor, S. J., 2005. An online operational rainfall-monitoring resource for epidemic malaria early warning systems in Africa. *Malaria Journal*, **4(6)**, doi:10.1186/1475-2875-4-6

Hardy, S., Dugdale, G., Milford, J. R., and Sutcliffe, J. V., 1989. The use of satellite derived rainfall estimates as inputs to flow prediction in the River Senegal. *New Directions for Surface Water Modeling*, **181**, 23-30

Haylock, M. R., Hofstra, N., Klein Tank, A. M. G., Klok, E. J., Jones, P. D., and New, M., 2008. A European daily high-resolution gridded data set of surface temperature and precipitation for 1950-2006. *Journal of Geophysical Research*, **113**, D20119

Hein, L., de Ridder, N., Hiernaux, P., Leemans, R., de Wit, A., and Schaepman, M., 2011. Desertification in the Sahel: Towards better accounting for ecosystem dynamics in the interpretation of remote sensing images. *Journal of Arid Environments*, **75**, 1164-1172

Hillier, D., and Dempsey, B., 2012. *A Dangerous Delay: The cost of late response to early warnings in the 2011 drought in the horn of Africa*. Oxfam and Save the Children. Available: <http://www.oxfam.org/en/policy/dangerous-delay> [accessed 24 March 2013]

Hofstra, N., Haylock, M., New, M., and Jones, P. D., 2009. Testing E-OBS European high-resolution gridded data set of daily precipitation and surface temperature. *Journal of Geophysical Research*, **114**, D21101

Hong, Y., Hsu, K-L., Sarooshian, S., and Gao, X., 2004. Precipitation Estimation from Remotely Sensed Imagery Using an Artificial Neural Network Cloud Classification System. *Journal of Applied Meteorology*, **43**, 1834-1852

Hong, Y., Hsu, K-L, Moradkhani, H., and Sorooshian, S., 2006. Uncertainty quantification of satellite precipitation estimation and Monte Carlo assessment of the error propagation into hydrologic response. *Water Resources Research*, **42**, W08421

Hossain, F., Anagnostou, E. N., and Dinku, T., 2004. Sensitivity Analyses of Satellite Rainfall Retrieval and Sampling Error on Flood Prediction Uncertainty. *IEEE Transactions on Geoscience and Remote Sensing*, **42(1)**, 130-139

Hossain, F., and Anagnostou, E. N., 2004. Assessment of current passive-microwave- and infrared-based satellite remote sensing for flood prediction. *Journal of Geophysical Research*, **109**, D07102, doi:10.1029/2003JD002986

Hossain, F., and Anagnostou, E. N., 2006. Assessment of a multidimensional satellite rainfall error model for ensemble generation of satellite rainfall. *IEEE Geoscience and Remote Sensing Letters*, **3(3)**, 419-423

Huffman, G. J., Adler, R. F., Bolvin, D. T., and Nelkin, E. J., 2010. The TRMM Multi-Satellite Precipitation Analysis (TMPA). In: Gebremichael, M., and Hosain, F., eds. *Satellite Rainfall Applications for Surface Hydrology*. Springer. pp.3-22

Hughes, D. A., 1995. Monthly rainfall-runoff models applied to arid and semiarid catchments for water resource estimation purposes. *Hydrological Sciences Journal*, **40(6)**, 751-769

Hughes, D. A., Andersson, L., Wilk, J., and Savenije, H. H. G., 2006. Regional calibration of the Pitman model for the Okavango River. *Journal of Hydrology*, **331**, 30-42

Hut, R., and van der Giesen, N., 2010. The Trans-African Hydrometeorological Observation Project. *European Geosciences Union Grand Assembly 2010: Poster Presentation*. Delft University of Technology. Available: <http://www.tahmo.org/100424EGU2010TAHMOV2small.pdf> [accessed 24 March 2013]

IUCN, 2010. *Decision-making and dialogue relating to large dams and hydraulic infrastructures: Diversity of approaches; evolution of policies and practises applying to project preparation and implementation; case studies from Cameroon and Senegal. Report for the International Union for the Conservation of Nature*. International Union for the Conservation of Nature (IUCN). Available: http://cmsdata.iucn.org/downloads/decision_making_and_dialogue_relating_to_large_dams_and_hydraulic_infrastructure_1.pdf [Accessed 24 March 2013]

Jakeman, A. J., Littlewood, I. G., and Whitehead, P. G., 1990. Computation of the instantaneous unit hydrograph and indentifiable component flows with application to two small upland catchments. *Journal of Hydrology*, **117**, 275-300

Kebe, C. M. F., Sauvageot, H., and Nzeukou, A., The relationship between rainfall and area-time integrals at the transition from an arid to an equatorial climate. *Journal of Climate*, **18**, 3806-3819

Jeffrey, S. J., Carter, J. O., Moodie, K. B., and Beswick, A. R., 2001. Using spatial interpolation to construct a comprehensive archive of Australian climate data. *Environmental Modelling Software*, **16**, 309-330

Jones, M. J., and Wild, A., 1975. *Soils of the West African Savanna: Technical Communication No. 55, Commonwealth Bureau of Soils, Harpenden*. Farnham Royal: Commonwealth Agricultural Bureaux

Joyce, R. J., Janowiak, J. E., Arkin, P. A., and Xie, P., 2004. CMORPH: A Method that Produces Global Precipitation Estimates from Passive Microwave and Infrared Data at High Spatial and Temporal Resolution. *Journal of Hydrometeorology*, **5(3)**, 487-503

Kirstetter, P-E., Delrieu, G., Boudevillain, B., and Obled, C., 2010. Towards an error model for radar quantitative precipitation estimation in the Cevennes-Vivarais region, France. *Journal of Hydrology*, **394**, 28-41

Koechlin, J., 1997. Ecological conditions and degradation factors in the Sahel. In: Raynaut, C., ed. *Societies and Nature in the Sahel*. London: Routledge. pp.12-36

Lanza, L. G., 2000. A conditional simulation model of intermittent rain fields. *Hydrology and Earth System Sciences*, **4(1)**, 173-183

Lee, G., Tachikawa, Y., Sayama, T., and Takara, K., 2012. Catchment responses to plausible parameters and input data under equifinality in distributed rainfall-runoff modeling. *Hydrological Processes*, **26**, 893-906

Lorenz, E. N., 1963. Deterministic nonperiodic flow. *Journal of Atmospheric Science*, **20**, 130-141

Lorenz, E. N., 1969. The predictability of a flow which possesses many scale of motion. *Tellus*, **21**, 19

Madsen, H., 2003. Parameter estimation in distributed hydrological catchment modelling using automatic calibration with multiple objectives. *Advances in Water Resources*, **26**, 205-216

Maidment, R. I., Grimes, D. I. F., Allan, R. P., Greatrex, H., Rojas, O., and Leo, O., in press 2012. Evaluation of satellite-based and model re-analysis rainfall estimates for Uganda. *Meteorological Applications*. **IN PRESS**, Available: <http://onlinelibrary.wiley.com/doi/10.1002/met.1283/abstract> [Accessed 24 March 2013]

May, R. M., 2011. Science as organized scepticism. *Philosophical Transactions of the Royal Society A: Mathematical, Physical and Engineering Sciences*, **369**, 4685-4689

McMillan, H., Jackson, B., Clark, M., Kavetski, D., and Woods, R., 2011. Rainfall uncertainty in hydrological modelling: An evaluation of multiplicative error models. *Journal of Hydrology*, **400**, 83-94

Mellor, D., 1996. The Modified Turning Band (MTB) model for space-time rainfall. I. Model definition and properties. *Journal of Hydrology*, **175**, 113-127

Mellor, D., and O'Connell, P. E., 1996. The Modified Turning Bands (MTB) model for space-time rainfall. II. Estimation of raincell parameters. *Journal of Hydrology*, **175**, 129-159

Mellor, D., and Metcalfe, A. V., 1996. The Modified Turning Bands (MTB) model for space-time rainfall. III. Estimation of the storm/rainband profile and discussion of future model prospects. *Journal of Hydrology*, **175**, 161-180

Michaud, J., and Sorooshian, S., 1994a. Comparison of simple versus complex distributed runoff models on a midsized semi-arid watershed. *Water Resources Research*, **30(3)**, 593-605

Michaud, J., and Sorooshian, S., 1994b. Effects of rainfall-sampling on error simulations of desert flash floods. *Water Resources Research*, **30(10)**, 2765-2775

Middleton, B. J., Lorentz, S. A., Pitman, W. V., and Midgley, D. C., 1981. *Surface Water Resources of South Africa, Volume V, Drainage Regions MNPQRST, The Eastern Cape, Report no. 12/81*. Hydrological Research Unit, University of Witwatersrand, Johannesburg, South Africa. Available: http://iahs.info/hsj/280/hysj_28_01_0194.pdf [Accessed 24 March 2013]

Milford, J. R., and Dugdale, G., 1990. Estimations of rainfall using geostationary satellite data. *Applications of Remote Sensing in Agriculture, Butterworth, London. Proceedings of the 48th Easter School in Agricultural Science*. University of Nottingham. April 1989.

Montanari, A., and Di Baldassarre, G., 2013. Data errors and hydrological modelling: The role of model structure to propagate observation uncertainty. *Advances in Water Resources*, **51**, 498-504

Moradkhani, H., Sorooshian, S., Gupta, H. V., and Houser, P. R., 2005. Dual state-parameter estimation of hydrological models using ensemble Kalman filter. *Advances in Water Resources*, **28**, 135-147

Moradkhani, H., Hsu, K., Hong, Y., and Sorooshian, S., 2006. Investigating the impact of remotely sensed precipitation and hydrological model uncertainties on the ensemble streamflow forecasting. *Geophysical Research Letters*, **33(12)**, L12401

Morland, J. C., Grimes, D. I. F., and Hewison, T. J., 2001. Satellite observations of microwave emissivity of a semi-arid land surface. *Remote Sensing of Environment*, **77**, 149-164

Mulitza, S., Heslop, D., Pittauerova, D., Fischer, H. W., Meyer, I., Stuut, J-B., Zabel, M., Mollenhauer, G., Collins, J. A., Kuhnert, H., and Schulz, M., 2010. Increase in African dust flux at the onset of commercial agriculture in the Sahel region. *Nature*, **466**, 226-228

Mwakalila, S., Campling, P., Feyen, J., Wyseure, G., and Beven, K., 2001. Application of a data-based mechanistic modelling (DBM) approach for predicting runoff generation in semi-arid regions. *Hydrological Processes*, **15**, 2281-2295

NASA, 2013. *Precipitation Measurement Missions (PMM): Global Precipitation Measurement (GPM)*. National Aeronautics and Space Administration (NASA). Available: <http://pmm.nasa.gov/GPM> [Accessed 24 March 2013]

Nash, J. E., and Sutcliffe, J. V., 1970. River flow forecasting through conceptual models, Part 1 – A discussion of principles. *Journal of Hydrology*, **83**, 307-335

Nespor, V., and Sevruk, B., 1998. Estimation of wind-induced error of rainfall gauge measurements using a numerical simulation. *Journal of Atmospheric and Oceanic Technology*, **16**, 450-463

NGA, 2006. *National Geospatial-Intelligence Agency Raster Roam*. National Geospatial-Intelligence Agency. Available: http://geoengine.nima.mil/muse-cgi-bin/rast_roam.cgi [Accessed 24 March 2013]

Nikolopoulos, E. I., Anagnostou, E. N., and Hossain, F., 2010. Error propagation of satellite-rainfall in flood prediction applications over complex terrain: A case study in Northeastern Italy. In: Gebremichael, M., and Hosain, F., eds. *Satellite Rainfall Applications for Surface Hydrology*. Springer. pp.215-227

NOAA, 2010. *African Rainfall Estimation Algorithm Version 2.0*. The National Oceanic and Atmospheric Administration (NOAA) Climate Prediction Centre. Available: http://www.cpc.ncep.noaa.gov/products/fews/RFE2.0_tech.pdf [Accessed 24 March 2013]

Nicholson, S. E., 1993. An overview of African Rainfall fluctuations of the last decade. *Journal of Climate*, **6**, 1463-1466

Nicholson, S. E., 2005. On the question of the "recovery" of the rains in the West African Sahel. *Journal of Arid Environments*, **63**, 615-641

O'Connell, P. E., and Todini, E., 1996. Modelling of rainfall, flow and mass transport in hydrological systems: an overview. *Journal of Hydrology*, **175**, 3-16

Palmer, T. N., and Hardaker, T. N., 2011. Handling uncertainty in science. *Philosophical Transactions of the Royal Society A: Mathematical, Physical & Engineering Sciences*, **369**, 4681-4684

Pardo-Iguzquiza, E., 1998. Optimal selection of number and location of rainfall gauges for areal rainfall estimation using geostatistics and simulated annealing. *Journal of Hydrology*, **210**, 206-220

Pardo-Iguzquiza, E., Grimes, D. I. F., and Teo, C-K., 2006. Assessing the uncertainty associated with intermittent rainfall fields. *Water Resources Research*, **42**, W01412, doi:10.1029/2004WR003740

Pechlivanidis, I. G., Jackson, B. M., McIntyre, N. R., and Wheeler, H. S., 2011. Catchment scale hydrological modelling: A review of model types, calibration approaches and uncertainty analysis methods in the context of recent developments in technology and applications. *Global NEST Journal*, **13(3)**, 193-214

Perrin, C., Michel, C., and Andreassian, V., 2003. Improvement of a parsimonious model for streamflow simulation. *Journal of Hydrology*, **279**, 275-289

Pitman, W. V., 1973. *A Mathematical Model for Generating Monthly River Flows from Meteorological Data in South Africa*, A Ph.D Thesis, Hydrological Research Unit, University of Witwatersrand, South Africa.

Rain, D., 1999. *Eaters of the Dry Season: Circular Labor Migration in the West African Sahel*. Boulder, Colorado, USA: Westview Press

Refsgaard, J. C., and Abbott, M. B., 1996. The role of distributed hydrological modelling in water resources management. In: Abbott, M. B., and Refsgaard, J. C., eds. *Distributed Hydrological Modelling*. Dordrecht: Kluwer Academic Publishers. pp.1-16

Reynolds, C. A., Yitayew, M., Slack, D. C., Hutschinson, C. F., Huete, A., and Petersen, M. S., 2000. Estimating crop yields and production by integrating the FAO Crop specific Water Balance model with real-time satellite data and ground-based ancillary data. *International Journal of Remote Sensing*, **21**, 3487-3508

Schaake, J. C., Hamill, T. M., Buizza, R., and Clark, M., 2007. HEPEX – The Hydrological Ensemble Prediction Experiment. *Bulletin of the American Meteorological Society*, **88(10)**, 1541-1547

Seiller, G., Anctil, F., and Perrin, C., 2012. Multimodel evaluation of twenty lumped hydrological models under contrasted climate conditions. *Hydrology and Earth System Sciences*, **16**, 1171-1189

Seo, D. J., 1998. Real-time estimation of rainfall fields using rain gage data under fractional coverage conditions. *Journal of Hydrology*, **208**, 25-36

Sevenije, H. H. G., 2001. Equifinality, a blessing in disguise? *Hydrological Processes*, **15**, 2835-2838

Shaffii, M., and Smedt, F. De., 2009. Multi-objective calibration of a distributed hydrological model (WetSpa) using a genetic algorithm. *Hydrology and Earth System Sciences*, **13**, 2137-2149

Shah, S. M. S., O'Connell, P. E., and Hosking, J. R. M., 1996. Modelling the effects of spatial variability in rainfall in catchment response. 2. Experiments with distributed and lumped models. *Journal of Hydrology*, **175**, 89-111

Shen, Z., Chen, L., Liao, Q., Liu, R., and Hong, Q., 2012. Impact of spatial rainfall variability on hydrology and nonpoint source pollution modeling. *Journal of Hydrology*, **472-473**, 205-215

Sivaplan, M., Woods, R. A., and Kalma, J. D., 1997. Variable bucket representation of TOPMODEL and investigation of the effects of rainfall heterogeneity. *Hydrological Processes*, **11**, 1307-1330

Skees, J. R., and Collier, B., 2008. *The Potential of Weather Index Insurance for Spurring a Green Revolution in Africa*. GlobalAgRisk, Inc. Available: <https://www.agriskmanagementforum.org/doc/potential-weather-index-insurance-spurring-green-revolution-africa> [Accessed 24 March 2013]

Slingo, J., and Palmer, T., 2011. Uncertainty in weather and climate prediction. *Philosophical Transactions of the Royal Society A: Mathematical, Physical and Engineering Sciences*, **369**, 4751-4767

Smith, L. A., and Stern, N., 2011. Uncertainty in science and its role in climate policy. *Philosophical Transactions of the Royal Society A: Mathematical, Physical and Engineering Sciences*, **369**, 4818-4841

Stisen, S., Jensen, K. H., Sandholt, I., and Grimes, D., 2008. A remote sensing driven distributed hydrological model of the Senegal River basin. *Journal of Hydrology*, **354**, 131-148

Sugawara, M., 1979. Automatic calibration of the tank model. *Hydrological Sciences Bulletin*, **24(3)**, 375-388

Sultan, B., Baron, C., Dingkuhn, M., Sarr, B., and Janicot, S., 2005. Agricultural impacts of large-scale variability of the West African monsoon. *Agricultural and Forest Meteorology*, **128**, 93-110

Sun, X., Mein, R. G., Keenan, T. D., and Elliot, J. F., 2000. Flood estimation using radar and raingauge data. *Journal of Hydrology*, **271**, 1-21

Syed, K. H., Goodrich, D. C, Myers, D. E., and Sorooshian, S., 2003. Spatial characteristics of thunderstorm rainfall fields and their relation to runoff. *Journal of Hydrology*, **271**, 1-21

Symeonakis, E., Bonifacio, R., and Drake, N., 2009. A comparison of rainfall estimation techniques in sub-Saharan Africa. *Internatiional Journal of Applied Earth Observation and Geoinformation*, **11**, 15-26

Tadesse, A., and Anagnostou, E. N., 2009. The effect of storm life cycle on satellite rainfall estimation error. *Journal of Atmospheric and Oceanic Technology*, **26**, 769-777

TAHMO, 2012. *Trans-African Hydro-Meteorological Observatory*. Oregon State University. Available: <http://tahmo.info/> [Accessed 24 March 2013]

Taylor, C. M., and Lebel, T., 1998. Observational Evidence of Persistent Covective-Scale Rainfall Patterns. *Monthly Weather Review*, **126**, 1597-1607

Teo, C-K, 2006. *Application of satellite-based rainfall estimates to crop yield forecasting in Africa*. A Ph.D. diss., University of Reading, UK

Teo, C-K., and Grimes, D. I. F., 2007. Stochastic modelling of rainfall from satellite data. *Journal of Hydrology*, **346**, 33-50

Thiemann, M., Trosset, M., Guptam H., and Sorooshian, S., 2001. Bayesian recursive parameter estimation for hydrologic models. *Water Resources Research*, **37(10)**, 2521-2535

Todd, M. C., Barrett, E. C., Beaumont, M. J., and Bellerby, T. J., 1999. Estimation of daily rainfall over the upper Nile river basin using a continuously calibrated satellite infrared technique. *Meteorological Applications*, **6**, 201-210

Todd, M. C., Kidd, C., Bellerby, T. J., and Kniveton, D. R., 2001. A combined satellite infrared and passive microwave technique for estimation of small-scale rainfall. *Journal of Atmospheric and Oceanic Technology*, **18**, 742-755

Toth, Z., Talagrund, O., Candille, G., and Zhu, Y, 2003. Probability and Ensemble Forecasts. In: Jolliffe, I. T., and Stephenson, D. B., eds. *Forecast Verification: A Practitioner's Guide in Atmospheric Science*. Chichester, UK: John Wiley & Sons. pp.137-164

Tsai, M-J., Abrahart, R. J., Mount, N. J., and Chang, F-J., in press 2012. Including spatial distribution in a data-driven rainfall-runoff model to improve reservoir inflow forecasting in Taiwan. *Hydrological Processes*, **IN PRESS**, Available:

<http://onlinelibrary.wiley.com/doi/10.1002/hyp.9559/abstract> [Accessed 24 March 2013]

Vazquez, R. F., Beven, K., and Feyen, J., 2009. GLUE based assessment on the overall predictions of a MIKE SHE application. *Water Resources Management*, **23**, 1325-1349

Verdin, J., and Klaver, R., 2002. Grid-cell-based crop water accounting for the famine early warning system. *Hydrological Processes*, **16**, 1617-1630

Verdin, J., Funk, C., Senay, G., and Choularton, R., 2005. Climate science and famine early warning. *Philosophical Transactions of the Royal Society B*, **360**, 2155-2168

Vicente, G. A., Scofield, R. A., and Menzel, W. P., 1998. The Operational GOES Infrared Rainfall Estimation Technique. *Bulletin of the American Meteorological Society*. **79 no.9**, 1883-1898

Vorosmarty, C. J., McIntyre, P. B., Gessner, M. O., Dudgeon, D., Prusevich, A., Green, P., Glidden, S., Bunn, S. E., Sullivan, C. A., Reidy Liermann, C., and Davies, P. M., 2010. Global threats to human water security and river biodiversity. *Nature*, **467**, 555-561

Vrugt, J. A., Gupta, H. V., Bouten, W., and Sorooshian, S., 2003. A Shuffled Complex Evolution Metropolis algorithm for optimization and uncertainty assessment of hydrologic model parameters. *Water Resources Research*, **39(8)**, 1201, doi:10.1029/2002WR001642

Vrugt, J. A., ter Braak, C. J. F., Clark, M. P., Hyman, J. M., and Robinson, B. A., 2008. Treatment of input uncertainty in hydrologic modeling: Doing hydrology backward with Markov Monte Carlo simulation. *Water Resources Research*, **44**, W00B09

Wagener, T., Boyle, D. P., Lees, M. J., Wheater, H. S., Gupta, H. V., and Sorooshian, S., 2001. A framework for application and development of hydrological models. *Hydrology and Earth System Sciences*, **5(1)**, 13-26

Wagener, T., McIntyre, N., Lees, M. J., Wheater, H. S., and Gupta, H. V., 2003. Towards reduced uncertainty in conceptual rainfall-runoff modelling: Dynamic identifiability analysis. *Hydrological Processes*, **17**, 455-476

Wang, Y-C., Yu, P-S., and Yang, T-C., 2010. Comparison of genetic algorithms and shuffled complex evolution approach for calibrating distributed rainfall-runoff model. *Hydrological Processes*, **24**, 1015-1026

Washington, R., Harrison, M., Conway, D., Black, E., Challinor, A., Grimes, D., Jones, R., Morse, A., Kay, G., and Todd, M., 2006. African Climate Change: Taking the Shorter Route. In: *Bulletin of the American Meteorological Society*, **87(10)**, 1355-1366

Water Aid, 2012. *Horn of Africa Faces 'Worst Drought in 60 years'*. Water Aid. Available: <http://dev.wateraid.org/ethiopia/news/9894.asp> [Accessed 24 March 2013]

Webster, P. J., and Jian, J., 2011. Environmental Prediction, risk assessment and extreme events: adaption strategies for the developing world. *Philosophical Transactions of the Royal Society A: Mathematical, Physical and Engineering Sciences*, **369**, 4768-4797

Wheater, H. S., Jakeman, A. J., and Beven, K. J., 1993. Progress and directions in rainfall-runoff modelling. In: A. J. Jakeman, M. B. Beck, and M. J. McAleer, eds. *Modelling change in environmental systems*. Chichester, UK: Wiley. pp.101-132

Wheater, H. S., 2002. Progress in and prospects for fluvial flood modelling. *Philosophical Transactions of The Royal Society A: Mathematical, Physical and Engineering Sciences*, **360**, 1409-1431

Wilk, J., Kniveton, D., Andersson, L., Layberry, R., Todd, M. C., Hughes, D., Ringrose, S., and Vanderpost, C., 2006. Estimating rainfall and water balance over the Okavango River Basin for hydrological applications. *Journal of Hydrology*, **331**, 18-29

WMO, cited 2013. *Satellite Status*. World Meteorological Organization (WMO)
<http://www.wmo.int/pages/prog/sat/satellitestatus.php> [Accessed 24 March 2013]

Xuan, Y., Cluckie, I. D., and Wang, Y., 2009. Uncertainty analysis of hydrological ensemble forecasts in a distributed model utilising short-range rainfall prediction. *Hydrology and Earth System Sciences*, **13**, 293-303

Yapo, P. O., Gupta, H. V., and Sorooshian, S., 1998. Multi-objective global optimization for hydrologic models. *Journal of Hydrology*, **204**, 83-97

Zhao, R-J., 1992. The Xinanjiang model applied in China. *Journal in Hydrology*, **135**, 371-381